SECURITY CLASSIFICATION OF THIS PAGE (When Data Entered)

REPORT DOCUMENTATION PAGE

READ INSTRUCTIONS BEFORE COMPLETING FORM

1. REPORT NUMBER
NUREG/CR-1576
NRL Memorandum Report 4298

2. GOVT ACCESSION NO.

3. RECIPIENT'S CATALOG NUMBER

4. TITLE (and Subtitle)
A REVIEW OF FATIGUE CRACK GROWTH OF PRESSURE VESSEL AND PIPING STEELS IN HIGH-TEMPERATURE, PRESSURIZED REACTOR-GRADE WATER

5. TYPE OF REPORT & PERIOD COVERED
Interim report on a continuing NRL problem

6. PERFORMING ORG. REPORT NUMBER

7. AUTHOR(s)
W. H. Cullen and Kari Torronen*

8. CONTRACT OR GRANT NUMBER(s)
NRC-RES-79-103
NRC-FIN-B5528

9. PERFORMING ORGANIZATION NAME AND ADDRESS
Naval Research Laboratory
Washington, D.C. 20375

10. PROGRAM ELEMENT, PROJECT, TASK AREA & WORK UNIT NUMBERS
63-1065-0-0

11. CONTROLLING OFFICE NAME AND ADDRESS
U.S. Nuclear Regulatory Commission
Office of Nuclear Regulatory Research
Washington, D.C. 20555

12. REPORT DATE
September 19, 1980

13. NUMBER OF PAGES
126

14. MONITORING AGENCY NAME & ADDRESS(if different from Controlling Office)

15. SECURITY CLASS. (of this report)
UNCLASSIFIED

15a. DECLASSIFICATION/DOWNGRADING SCHEDULE

16. DISTRIBUTION STATEMENT (of this Report)
Approved for public release; distribution unlimited.

17. DISTRIBUTION STATEMENT (of the abstract entered in Block 20, if different from Report)

18. SUPPLEMENTARY NOTES
*Present address: Technical Research Centre of Finland, 02150 Espoo 15, Finland.

Prepared for the U.S. Nuclear Regulatory Commission, Office of Nuclear Regulatory Research, Reactor Safety Research Division under Interagency Agreement RES-79-103. NRC Distribution Category R5 and AN.

19. KEY WORDS (Continue on reverse side if necessary and identify by block number)
Fatigue crack propagation
Fractography
Hydrogen embrittlement
Nuclear pressure vessel steel

20. ABSTRACT (Continue on reverse side if necessary and identify by block number)
Fatigue crack growth data sets, for pressure vessel and piping steels, in reactor-grade water environment have appeared in various reports and publications since about 1972. All of the results which have been published from 1972 through 1979 have been plotted and are presented in this report. Beginning with a discussion of the need for these data, and an explanation of the laboratory facilities which are required for this research, this report goes on to describe the overall trends which have evolved through consideration of the data sets and the conditions under which they were generated. A model for hydrogen assisted fatigue crack growth is described and applied to the pressurized water reactor type of environment. A complete listing of references is included in the report.

DD FORM 1 JAN 73 1473 EDITION OF 1 NOV 65 IS OBSOLETE i
S/N 0102-LF-014-6601

SECURITY CLASSIFICATION OF THIS PAGE (When Data Entered)

CONTENTS

A REVIEW OF FATIGUE CRACK GROWTH OF PRESSURE VESSEL AND PIPING STEELS IN HIGH-TEMPERATURE, PRESSURIZED REACTOR-GRADE WATER

INTRODUCTION

The load-time characterization of nuclear reactor pressure vessels and primary loop piping can be described in terms of fatigue cycling due to numerous sources. During the lifetime of a typical reactor, start-up/shut-down procedures account for about 250 cycles, power loadings/unloadings ~50,000 cycles, step increases/decreases in output ~10,000 cycles, minor trips of reactor or turbine ~1000 cycles and deliberate hydro-leak tests ~20 cycles. Pump vibrations, although small in magnitude, account for the largest number of applied cycles $\sim 10^{10}$ to 10^{12} cycles. Under these conditions, it is reasonable to examine the possibility that small flaws could nucleate, if they do not already pre-exist, and achieve measureable and perhaps potentially hazardous amounts of growth. Hence, many nuclear reactor vendors, and other sponsors of nuclear materials related research have encouraged the measurement of fatigue crack growth rates in the high-temperature, pressurized reactor-grade water environment typical of the light water reactors.

Essentially, programs directed at evaluation of fatigue crack growth rates for use in light water reactor lifetime computations must address the following relevant areas:

a. Materials. Plates, forgings and welds of reactor pressure vessel materials, hot and cold leg piping materials and welds, and safe-end materials are all susceptible to fatigue failures. The effects of heat input during welding, and continued operation at 288°C (550°F), as well as thermal changes during annealing cycles must be acknowledged, and irradiation effects on reactor beltline materials must be accounted for.

b. Stresses. The loads, and the rates and waveforms associated with the application of those loads, should approximate or easily extrapolate to those of an operating power reactor. While in reality this is obviously a variable amplitude/variable frequency load sequence, the understanding of crack growth mechanisms is more easily attained through data from constant amplitude load (ΔP), or constant stress intensity factor (ΔK) types of tests. Once this understanding is attained, variable amplitude and random sequence loading tests can be carried out.

Manuscript submitted July 7, 1980

c. Environment. The tests must be conducted in high-temperature, pressurized reactor-grade water which simulates the operating reactor conditions. The water is either deoxygenated, to simulate pressurized water reactor (PWR) conditions, or a low, but constant concentration of oxygen ($\sim$200 ppb) is maintained to simulate boiling water reactor (BWR) conditions. In addition, a neutron moderator, boric acid, together with a small amount of lithium hydroxide, is added to the PWR coolant. Typical water chemistry specifications for the laboratory environment have been distilled from a number of vendor sources and other documents and are shown in Table 1.

Table 1 - Summary of Specifications for

Laboratory Simulated BWR and PWR Environments

	BWR	PWR
Boron	—	1000 ppm
Lithium	—	1 to 2 ppm
Dissolved Oxygen	200 ppb	1 to 2 ppb
Halides	0.2 max	0.2 max
Hydrogen	—	10-50 $cm^3/kg(H_2O)$
pH	6-7	4.5 - 10
Conductivity	0.5 μmho/cm	15-25 μmhos/cm

Electrochemical corrosion effects, which result from having different metallic species immersed in an electrolyte, are also a potential problem, although the intrinsically low conductivity of reactor grade water serves to minimize this difficulty. While the concern for this situation, and the demand for data extends back many years, the technology for performing this sort of research has developed over the last ten years or so, and it is only now (1980) that the laboratories engaged in this research number more than just a few.

On a laboratory scale, these tests are carried out in autoclaves, really small pressure vessels, which are implemented so as to pressurize and heat the reactor-grade water. Specimens are usually either compact tension (CT) or wedge-open-loaded (WOL) types. In many laboratory facilities, each specimen is instrumented with a displacement gage for measuring crack mouth opening and gripped in clevises mounted on load rods which pass through water-cooled sliding seals to the load cells and actuators which are generally external to the autoclaves.

The accurate measurement of the crack length has been a major factor in the slow development of this type of research. Direct observation of crack length, which is impossible while the test is on-going, has been achieved both by "beach-marking" the crack fracture surface by varying the load parameters, or by temporarily halting the test, removing the specimen, observing the crack traces on the surface and re-starting the test. However, as will be discussed in the section on graphical review of the data, varying loads and test interruptions may lead to non-steady state crack growth, and the resultant data will be difficult to either interpret, or reconcile, with data obtained using less perturbing techniques.

A preferred way of evaluating crack lengths without interrupting or perturbing the progress of the test is to measure the specimen compliance, which increases as the crack length increases. The exact relationship between compliance and crack length can be experimentally determined, or is readily available for specimens of standard geometry. This procedure requires the simultaneous measurement of displacement, usually normal to the crack plane, and load, and the referencing of this quotient, with appropriate normalizing terms, to the pre-existing relationship of crack length as a function of compliance. It has only been in the last few years that displacement gages, qualified for use in the high-temperature, pressurized water environment have become available. The two most prevelant devices are LVDT's (linear variable differential transformers) and clip gages implemented with weldable strain gages. Both of these have the sensitivity required and both can be designed for continuous and long-term use, enabling frequent measurement of crack length at any cyclic interval required.

Most laboratories are using specimens identical to, or nearly like those described in ASTM E647-78, Method of Test for Constant-Load-Amplitude Fatigue Crack Growth Rates Above 10^{-8} m/cycle. The size of these specimens varies, depending on the stress intensity factors to be applied, but the largest specimen tested to date has been ~100 mm thick (4T-CT). The general rule is to use the thickest specimen possible, both to better simulate the thickness of the pressure boundary components (up to ~ 300 mm) and to provide the elastic constraint necessary to support the higher stress intensity factors which may be studied. Most tests are performed using constant amplitude fatigue cycling, but as this data becomes better understood, some researchers are moving on to variable amplitude tests, and decreasing load tests in which ΔK is held constant as the crack extends.

Plots of da/dN vs ΔK indicate that crack growth data is subject to some variables which exert a major influence. Basic among these, all of which are being investigated at various laboratories are (a) load ratio (minimum load/maximum load, (= R)), (b) waveform, including ramp time, hold time, and frequency (of sinusoidal waveforms) (c) water chemistry, especially disslved oxygen content, and temperature, (d) materials variability, and (e) effects of irradiation. A number of other parameters, such as electrical potential, and load interactions are expected to have an effect, but the necessary research has not yet been undertaken, or is in its infant stages. Table 2 lists the laboratories which are actively engaged in this type of research, the references which contain their results to date, and an indication of the variables which have been explored most extensively. In addition to the entries in this table, it should be explained that a few other labs are performing this work and consider their results proprietary, or so preliminary that publication is not yet possible. Several research groups are currently establishing their autoclave facilities and expect to be generating fatigue crack growth data within a year.

The ASTM E647-Method of Test is a practical standard for fatigue crack growth tests which best pertains to situations in which the specimen loads can be carefully

Table 2 - Laboratories involved in high-temperature, pressurized water fatigue crack growth research.

Facility	References	Variables
Canada		
Ontario Hydro Toronto, Ontario, Canada	1	Steam environment, threshold studies, piping materials
Finland		
Technical Research Centre of Finland Espoo, Finland	—	Waveform and frequence, load ratio, materials, water chemistry, electrochemical effects, mechanisms
France		
Creusot-Loire Firminy, France	—	Waveform and frequence, temperature, load ratio, irradiation, materials
Germany		
Kraftwerk Union Erlangen, Germany	—	Materials, temperature, load ratio, frequency, electrochemical potential
Italy		
Centro Informazione Studie Esperienze Milano, Italy	—	Temperature, waveform, water chemistry
Japan		
Japan Atomic Energy Research Institute Ibaraki, Japan	2-8	Microstructure, waveform, BWR chemistry, materials
Sweden		
Studsvik Energiteknik AB Nyleoping, Sweden	9	Materials, rise time, water chemistry, temperature
United Kingdom		
Central Electricity Research Lab. Leatherhead, Surrey, UK	10-11	Frequency, temperature, steam environment, constant ΔK

Table 2 - continued

Laboratories involved in high-temperature pressurized water fatigue crack growth research.

Facility	References	Variables
Atomic Energy Research Establishment Harwell, UK	12-14	Frequency, waveform, temperature, load ratio, water chemistry
Atomic Energy Research Establishment Springfields, UK	15-16	Frequency, waveform water chemistry
Rolls Royce and Assoc. Ltd. Derby, UK	17	Load ratio
USA		
Babcock and Wilcox Alliance, OH	18	Waveform, constant ΔK, load ratio, water chemistry
General Electric Corp. San Jose, CA	19-30	Frequency, load ratio, materials
General Electric Corp. Schenectady, NY	31-32	Frequency, load ratio
Naval Research Lab. Washington, D. C.	33-41	Rise/hold time, temperature, materials, load ratio, mechanisms, irradiation, load interaction effects.
Westinghouse Corp. Pittsburgh, PA	42-68	Rise/hold time, temperature, materials, load ratio, size effects, starting ΔK, irradiation

**There are several other countries/laboratories which have only recently commissioned autoclaves, and have not yet published any results. Among these are Materialprufungsanstalt, Germany, two additional facilities in Japan, Technical Research Association for Integrity of Structures at Elevated Service Temperatures (ISES) which is sponsoring research at reactor systems vendors in Japan and Central Research Institute of the Electric Power Industry (CRIEPI) and labs in Australia, Netherlands and South Africa. The authors believe that this is a complete list of laboratories engaged in fatigue crack growth rate testing in a nuclear coolant environment. However, some laboratories just beginning such research, or those which have not published any results may have been inadvertantly overlooked.

regulated, and the crack extensions can be directly determined (e.g. by visual observation) while the test is on-going. A companion method of test for aqueous environments, utilizing compliance-based methods of crack extension determination, has not been developed, although such methods are under consideration. With special regard to the high-temperature, pressurized-water test practice, even the laboratories which are considered to be leaders in the field are constantly improving their facilities and upgrading their test practice to take advantage of the still-rapidly developing technology applicable to this work. At the present time, while a standard method of test would be desireable, it would be most difficult to write one which would be durable, or which would allow for the experimental ingenuity which often is a characteristic of this work.

In order to foster better cooperation and communication among the laboratories, vendors, and program sponsors either carrying out, or interested in these corrosion fatigue crack growth rate tests, a cooperative group was formally structured in 1978. The International Cyclic Crack Growth Rate (ICCGR) cooperative group now contains about thirty members representing twelve nations. Information on techniques, results and interpretation of the data is exchanged at the annual meetings of the full group. A series of round robin test programs has begun, and several laboratories have completed the first series of tests for which they are responsible. The results of these tests (with the exception of NRL and Westinghouse) are not published here, since they are considered privileged to the group itself. Future publication is anticipated.

With a significant amount of data now available, and with a sizeable number of laboratories now initiating their programs, it is worthwhile to examine the data which has been developed. We will show that there is a great deal of scatter in some of the results, but also that certain trends have been established. There are some regions (i. e. low ΔK) which need much more attention, and possibly some environmental effects, unique to these materials/environment combinations, which should be explored more fully. This data needs the organization provided by a review effort so that all the laboratories generating this data, and all the facilities making use of this data may better plan their programs to fill in the missing gaps, or to confirm or further explore those features most interesting to them.

One of the primary applications of this data is in the formation of Section XI-Rules for In-service Inspection of Nuclear Power Plant Components of the ASME Boiler and Pressure Code. Contained in the Appendix A of this code are two upper bound limits (for air and water environments) which are intended to reflect the rates of crack growth to be expected under reactor operating conditions. Constraints on temperature, waveforms, load ratio or materials are not applied since, in the words of the code, these default lines are "intended to be very conservative" and include "the effects of temperature, frequency and the pressurized water environment." Since these code limits were adopted, a large amount of research has been completed, and these lines are being re-evaluated in light of this and on-going research. Additionally, there is the possibility of a Section XI-like treatment of flaw growth being incorporated in Section III of the ASME code — Nuclear Power Plant Components: General Requirements, which is the guide for design of pressure vessel and piping components (among other facilities). Thus reliable and interpretable fatigue crack growth data may soon be required for design code purposes as well as for in-service inspection computations.

METHOD OF DATA ACQUISITION AND REPLOTTING

Perhaps the major component of the effort involved in producing such a review paper is the task of assembling and re-plotting the available data. All of the data

contained in this review is available in the open literature — that in fact was a primary criterion for inclusion. But beyond that, cognizant scientists at Westinghouse Nuclear Systems Division, General Electric Nuclear Power Division and Rolls Royce and Associates Ltd. have assisted us with valuable and helpful clarifications and explanations of their results.

As a general procedure, the individual data sets from laboratories other than the NRL were digitized on a computerized X-Y plotter, and the data points were correctly scaled and filed on magnetic disk for later plotting. The data was often digitized from the reports themselves, when available, or from photocopies, and as such, is subject to the vagaries of the various reproduction processes. The authors cannot attach any measure of precision with which the data is replotted and presented here, as compared to the original form. However, we are sure that the data is as accurately presented as is humanly and computationally possible, and that, at the very least, the character of the data has been accurately retained. It would seem prudent, however, not to redigitize the data as presented this review, creating results twice removed from the original. Future users should refer to the original references, which are noted in each figure caption.

Each data set has been replotted on exactly the same plotting grid and reduced to the same camera scale for inclusion in this report. This scale and format has been selected by the ICCGR Group in order to promote this uniformity. As originally plotted, each logarithmic decade was 62.5 mm in length; the figures have subsequently been reduced by the same camera scale factor (65%). In all cases, the ASME Section XI-Appendix A air and water default lines have been included on the individual plots to assist in referencing the data.

GRAPHICAL REVIEW OF DATA

The following graphical presentation contains only previously published data for ferritic reactor pressure vessel and piping steels mainly in high-temperature pressurized reactor grade water. Some data generated in ambient temperature water as well as high temperature air is also included when originally published in connection with high temperature water data or when used to serve as reference data. Some earlier data produced in high-temperature pressurized reactor grade water have not been included either due to the very high test frequencies used-preventing any environmental effects [42], or due to the absence of individual data points [19,20]. Additional ambient temperature data in pure water can be found in references 69-71 and in low temperature steam in Ref. 1. More air data has been published detailing for instance, the effect of temperature [69-75], frequency and load ratio [69-75], specimen size [69-73], specimen orientation and inclusion content [76-78], aging [79-80] and irradiation [81-87].

When comparing the data sets it is essential to keep in mind, in addition to the possible errors due to digitizing and replotting the data, the differences in data acquisition techniques used at various laboratories. The accuracy between techniques differs; some may even introduce artifacts to the test results as stated earlier. The older data sets were generally produced from a vs N data using the secant method; later the incremental second-order polynomial has been most commonly used; both methods are described in ASTM E647. For instance, much of the older Westinghouse data, as published originally, was computed using the secant method. With the help of W. Bamford, that data is presented here after having been recomputed using the incremental polynomial methods.

The plotting grid used for all data sets in this review is given in Fig. 1. Depending

on waveform and temperature, the NRL results, generated with low load ratio, have appeared in one of the two appropriate ($R < 0.5$) growth rate regimes shown in Fig. 1. These regions have been somewhat modified from the original NRL presentation [40] and a regime for high load ratio test results has been added to give three growth rate regimes inside which almost all the results presented in this review can be fitted.

The graphical data is presented in the following with the pressurized water reactor results first, followed by the boiling water reactor results. The first group contains NRL and Westinghouse results followed by UK data. The second group is comprised of General Electric, Westinghouse and JAERI data. As the majority of data is appropriate to PWR water chemistry, only other environments are indicated in the figure legends. The data sets are further grouped, as well as possible, according to load ratio, followed by waveform, particularly frequency, or period.

The individual data sets are given in Figs. 2 to 89. No attempt is made here to discuss each data set in turn. Instead the general trends will be evaluated and the apparent discrepancies will be discussed. The classification into low and high growth rate categories has been in some cases rather difficult due to large scatter and abrupt crack growth retardations and accelerations. In these cases the general trend of the data set was deduced and that has been used as a guide. In a few cases, when it is evident that several interruptions of the test or other test device malfunctions have considerably affected the results, the data has not been used in the evaluation of general trends.

In the following, the basic variables, according to which the data has been grouped, are (a) water chemistry (PWR and BWR),(b) load ratio R (high implies $R > 0.5$, low $R \sim 0.20$), (c) temperature (high implies 288°C, low 93°C), (d) waveform (ramp-type waveforms with no hold, short hold (<60 secs) or long hold (>60 secs), sinewave and triangular), (e) rise time or frequency (a short ramp is of the order of 1 sec, long > 60 secs), a high frequency is of the order of 1 Hz, or more, intermediate ~17 mHz (1 cpm), and low is of the order of 8 mHz or less), (f) materials,and (g) testing laboratory. The summary of the general trends as a function of these variables (except materials) is given in Table 3. The air data is not included as it always resides close to the air default line regardless of the testing variables (Figs. 10, 82,84). Table 4 gives a summary of the serialization of the figures in terms of their content.

Based on the data in Table 3, only a relative few of all the possible combinations of the variables listed above have been tested. There are also some discrepancies between the individual results obtained using the same combination of variables. In some cases these discrepancies are interlaboratory, but intralaboratory differences may also be seen indicating the existence of some variables not considered in Table 3 (e.g., materials variability or slight difference in water chemistry, especially in dissolved oxygen content). However, several conclusions can be drawn from the results presented in Table 3.

To produce an accelerated crack growth rate (above the air results), a sufficiently long rising part of the load cycle is needed, i. e., the ramp time must exceed 1 sec. or the frequency be lower than 1 Hz. However, in high temperature PWR water, with a high load ratio, even 1 Hz sinewave loading produces an initial acceleration of the cyclic crack growth, followed by a bendover to the low category occurring at rather low ΔK values (Fig. 14, 15, Refs. 46, 48). At low load ratios a slight difference between 1 Hz and 10 Hz has been reported-the latter giving somewhat smaller crack growth rate values [42]. At lower temperatures, in water containing 8 ppm dissolved oxygen, an accelerated crack growth rate has been reported for 1 Hz triangular wave loading [10].

Table 3-A Summary of General Trends in CCGR

Water Chemistry			PWR			BWR		
			Rise Time/Frequency			Rise Time/Frequency		
R	Temp	Waveform	Short/High	Intermediate	Long/Low	Short/High	Intermediate	Long/Low
	Low	Ramp/No Hold			High (3 NRL) Low (1 W)			
		Ramp/Short Hold						
		Ramp/Long Hold	Low (4 NRL)		High (3 NRL) (2 W)			
		Sinewave					High (2 JAERI)	
		Triangular				High (1 CEGB)	High (1 CEGB)	High (1 CEGB)
Low	High	Ramp/No Hold		Low (1 NRL) High (1 W)	Low (3 NRL, 3 W) High (1 NRL, 3 W)		High (1 GE)	High (1 GE)
		Ramp/Short Hold		Low (1 NRL)				
		Ramp/Long Hold	Low (2 NRL, 2 W)		Low (4 NRL, 2 W) High (2 W)			High (1 GE)
		Sinewave	Low (1 W)	High (2 NRL, 6 W) Low (2 W)	High (3 W)	Low (5 JAERI)	High (5 JAERI) (1 W)	High (1 JAERI)
		Triangular			Low (1 NRL)	Low (1 GE)	High (3 JAERI) Low (2 JAERI)	
High	High	Ramp/No Hold			High (5 W)		High (2 GE)	High (9 GE)
		Ramp/Short Hold						
		Ramp/Long Hold						Low (2 GE)
		Sinewave	High to Low (1 W)	High (11 W) Low (2 RR)	High (1 W)		High (1 GE)	High (2 GE)
		Triangular					High (6 GE)	

NRL-Naval Research Laboratory
W-Westinghouse Nuclear Power Systems Division
GE-General Electric Nuclear Systems Division

JAERI-Japan Atomic Energy Research Institute
CEGB-Central Electricity Generating Board
RR-Rolls Royce and Associates

Table 4 - Summary of Figure Serialization

Laboratory	Conditions	Figure Number
NRL Washington, DC	93°and 288°C, PWR conditions ramp/hold waveforms, R=0.2 sinusoidal waveforms, R=0.2	2-9
Westinghouse Pittsburgh, PA	288°C, PWR conditions sinusoidal waveforms, R=0.2	11-13 18-20 27, 32,33 41-42, 58
	288°C, PWR conditions sinusoidal waveforms, R=0.7	14-17 21-23 48-50, 54
	288°C, PWR conditions ramp/hold waveforms, R=0.2	24-25 28-31 34-40 43-47 56-57
	288°C conditions ramp/hold waveforms, R=0.7	51-53 55,59
Rolls Royce Derby, UK	288°C, PWR conditions sinusoidal waveforms, R=0.7	60-61
UKAEA Springfields, UK	25°C, PWR conditions triangular waveforms, R=0.0, 0.5 variable pH	62-63 65
CEGB Surrey, UK	90°C, PWR conditions triangular waveforms, R=0.5	64

Table 4 - continued

Summary of Figure Serialization

Laboratory	Conditions	Figure Number
General Electric Co.	260-288°C, BWR conditions triangular or sawtooth waveforms, R=.05	66, 72-73 75
	288°C, BWR conditions triangular, sawtooth or ramp/hold waveforms, R=0.5, 0.6, 0.78	67-71, 74 76-80
	288°C, BWR conditions sinusoidal waveforms, R=0.16	81
JAERI	260°C, BWR conditions sinusoidal or triangular waveforms, R=0.25	84-89

The most obvious reason for this exception to the majority of results is the higher oxygen content.

In almost all cases, for lower temperatures, when the length of the rising part of the load cycle exceeds some limiting value between 1 and 60 secs an environment assisted crack growth acceleration is seen. The reason for the only exception (Fig. 36, Ref. 58) showing low crack growth rate with a 60 sec ramp is not known; the authors of Ref. 58 speculate that the explanation can be found in the higher than typical initial ΔK value and subsequent crack growth reversals. According to results summarized in Table 3, increasing ramp times or decreasing frequencies do not decrease the enhancement of the crack growth rates in the PWR (low-oxygen) environment at the low temperature. However, Atkinson and Lindley [10,11] report that a peak enhancement occurs between 0.1 and 0.01 Hz in 3 ppm O_2 containing water. The reason for this behavior will be discussed in the section on models for environment assisted cyclic crack growth.

The test results produced at the reactor operating temperature using low load ratios (less than 0.22) show rather controversial behavior. It is evident that the sinewave loading with intermediate frequency ($\sim$ 17 mHz) produces the most accelerated data. Two exceptions are Westinghouse 4T-CT specimens (Figs. 32 and 33, Ref. 53,57). The Westinghouse authors speculate that the thickness of the specimen results in crack tip environments of substantially different character from those of thinner specimens. Also, during the testing of the second 4T-CT specimen several test interruptions occured, introducing crack growth retardations, which might confuse the results. The results with lower frequencies, although still in the high regime, appear to be less accelerated than 17 mHz results, indicating the trend that rising parts of the load cycle which are longer than some critical value of about 17 mHz allow less environmental assistance.

This is not true for the BWR water chemistry, however. The early General Electric [19,20] and JAERI [3,6,7] results show increasing crack growth rates with decreasing frequency, the lowest test frequency applied being 0.62 mHz and 1.7 mHz respectively. The obvious variable accounting for this behavior is the higher oxygen content of BWR water chemistry and subsequent change in the corrosion fatigue mechanisms. This will be discussed in the following section.

The use of trapezoidal waveforms produces the most controversial results. At NRL, intermediate ramp times which are roughly equivalent to the rising part of the 17 mHz sinewave have produced, with one exception, crack growth rates in the low regime (Fig. 5b and c, refs. 35,36), but at Westinghouse some results of similar tests are in the high regime (Fig. 47, Ref. 62). The NRL specimens are A508-2 steel whereas the Westinghouse results are from a weld metal. Generally a tendency toward slightly higher cyclic crack growth rates in welds can be seen throughout the results.

The long ramp times ($\geq$60 secs) with and without hold time produce some data sets in both the low and high category. Even crack growth rates starting definitely in the high regime and then reversing to the lower category, or totally arresting, are also seen (Figs. 30, 34, and 38, Refs. 58-61). With these ramp times no definite pattern between materials is evident: base metal of different heats, HAZ and weld metal tests all produce results in both regimes. An interlaboratory difference seems to exist: only one of the nine such data sets generated at NRL belongs to the high regime whereas the Westinghouse results belong about evenly in both categories; the previously mentioned three widely varying data sets (Figs. 30, 34 and 38) are all Westinghouse results.

An explanation for this behavior may be sought from the water chemistry,

particularly from the dissolved oxygen content. An indication of this explanation is seen in the BWR results, where both intermediate and long ramp times produce data in the high region, i. e. when dissolved oxygen is present, no depression of crack growth rates back to the air line has occurred even with increasing ramp times plus the addition of long hold times (Fig. 77 (GE spec. CP-2), Ref. 29). Thus it is possible that in some cases the water used at Westinghouse initially has had relatively high dissolved oxygen content (hundreds of ppbs), which has produced the initially high crack growth rates. The dissolved oxygen is usually consumed gradually by oxidation reactions, thus during the longer tests a decrease back to the lower regime will occur. However, no water chemistry data to support this speculation has been published.

However, the above considerations do not explain all the discrepancies seen in the long ramp data. Three NRL specimens showing different behavior for a 60 sec ramp/reset waveform were tested in a multispecimen assembly i.e., they were tested simultaneously and their testing conditions were equal (Figs. 6, 7 and 8, Ref. 36). Weld metal and plate specimens in this test assembly produced data in the low regime, but a forging steel specimen (A508-2) exhibits data in the upper bound of the high category. It is important to note that this base metal specimen was from a different heat of A508-2 than those previously tested (Fig. 46, Ref. 34,40), which produced data in the low regime. In this case a possible explanation is that the particular heat of A508-2 was more susceptible to the environmental effect, possibly for reasons such as larger impurity content or other metallurgical factors.

If, for PWR water chemistry, the sinewave and trapezoidal loading conditions are compared, it is evident that sinewave testing produces more acceleration in the cyclic crack growth rate. An NRL test involving 22 sec ramp 4 sec hold was intended to simulate the sinewave, but the results definitely belong in the low regime (Fig. 5c, Ref. 36). One possible explanation for this difference may be the varying rate of change of crack tip opening in the sinewave loading as compared to the monotonic change produced by ramp time tests. This will be further discussed in the mechanisms section. For BWR water conditions only very few data sets are available for comparison, but obviously any diffrences are less pronounced than those for PWR conditions.

Results from tests utilizing high load ratio (>0.5) are only available at high temperatures. If the rising part of the load cycle is sufficiently long (frequency >1 Hz), the resulting crack growth behavior resides in the high category, above the ASME Code Section XI water default line, within the range of the other variables investigated. The general trend of this data is also shown in Fig. 1. The crack growth rate increases drastically at small ΔK values (around 10 MPa$\sqrt{m}$) but bends over towards the air line after reaching crack growth rate values greater than about 10^{-3} mm/cycle. There are, however, exceptions to this general behavior, although most of the data resides in the shaded area shown in Fig. 1. In the case of PWR environment these exceptions are generated in weld metal or HAZ testing. In three cases the test results started along the general trend, but an abrupt reversal soon occured, leading to obvious crack arrest (Figs. 49, 51, and 52, Refs. 50, 55 and 62). In three other cases the converse behavior is seen: the crack growth started with a very high crack growth rate value, showed a strong retardation and then increaseed rapidly (Figs. 52, 53 and 57, Ref. 62). As all these data sets are either from weld metal or HAZ, it seems possible that that the observed behavior is due to the inhomogeneous structure seen by the advancing crack tip. The Rolls-Royce data (Figs. 60 and 61, Ref. 17), which differs considerably from the Westinghouse data, was acquired in tests which involved several changes in test frequency and load. This is known to cause transients and crack growth retardations [88], which is probably the reason for this discrepancy.

For the higher load ratios, the behavior in the BWR environment does not differ from that in the PWR environment. However, an additional feature pertaining to the BWR environment is worth reemphasizing. When, in the later stages of a ramp time test, an extended hold period was introduced, a rapid retardation and subsequent arrest of the crack growth occured (Fig. 77, Ref. 29). Those authors (Ref. 29) could not suggest any explanation for the behavior.

The few room temperature water data sets included in this review follow the same general trends as the higher temperature data. Increasing the load ratio introduces the environmental effect, but the crack growth enhancement is much smaller than at higher temperatures (Fig. 62-63, Ref. 15). An increased pH also causes an accelerated crack growth rate (Fig. 65, Ref. 16).

In the preceding presentation of the data the main effects of the principal variables have been discussed. Some additional information can be obtained in the published literature. A few results have been published detailing the effect of temperatures between the two considered here (93°C and 288°C). According to these, the greatest enhancement in cyclic crack growth in water environment occurs around 200°C, i. e. between the cool-down and operating temperatures [2,7]. This is consistent with the general corrosion behavior of the steels in question [2]. The effect of the dissolved oxygen content in the BWR environment has been studied (200 ppb versus 7 ppm). the results indicating no significant difference [29]. However, studies concerning the effect of lower oxygen contents (5-200 ppb) have not been conducted. Some tests utilizing two superposed waveforms have been conducted, but their results have not been published in the da/dN vs ΔK form [68]. Two variables which are not very often mentioned are the effect of the specimen orientation and the inclusion content of the material. As these are known to affect the air results [76-78] and the stress corrosion behavior [80], it seems likely that they will influence also the environmentally assisted cyclic crack growth rates.

It is also apparent that microstructure has some effect on the environmental cyclic crack growth rate enhancement. This is seen especially in the weld metal and HAZ samples, as stated previously, which have inhomogeneous microstructure and consequently show transients in the crack growth results. The BWR environment, together with high ΔK values, exhibits results showing a considerable influence of microstructure [7,8]. In coarse grain, as opposed to fine-grain HAZ structure, an enhancement of the crack growth rate occurs whereas in untempered martensitic structure a relative retardation is evident (Fig. 88, Refs. 7, 8).

The observed trends which have been described in this section can be summarized as follows:

(a) For low-temperature, deoxygenated water (PWR conditions), high-frequency ($\gtrsim$1 Hz) or short rise time ($\sim$1 sec) waveforms and low load ratios, produce data on or near the ASME air default line. Longer rise time ($\gtrsim$60 sec) components lead to higher crack growth rates, approaching, but seldom exceeding the ASME water default line.

(b) For high-temperature, deoxygenated water (PWR conditions), high-frequency ($\gtrsim$ 1 Hz) or short rise time ($\sim$ 1 sec) waveforms, and low load ratios, produce data on or near the ASME air default line. Mid-range frequency ($\sim$ 17 mHz ($\sim$ 1 cpm)) sinusoidal waveforms result in higher crack growth rates, which bend over toward the air line at higher ΔK, or higher growth rate values. Waveforms with long ramp times ($\geq$ 300 secs)

produce data on the air default line. There appears to be a tendency for long-period sinusoidal waveforms ($\gtrsim$ 1.7 mHz) to also depress the growth rates, but this trend is not as clear-cut as the companion trend for ramp-hold type waveforms.

(c) For high-temperature, deoxygenated water and high load ratios, the data trends or functions of waveform and frequency are not as well developed as for low load ratios. The bulk of the data clusters just above the water default line. Due to the large scatter in data due to start-up transients, the lower ΔK data is rather poorly defined. Data for sinusoidal waveforms exhibits the same bend-over phenomenon as did similar data at low load ratios, trending, in this case, toward the water default line. On the average, sawtooth waveforms produce data residing slightly below sinusoidal data of equivalent period.

(d) For high-temperature, oxygenated-water (BWR conditions), the data are more monotonically dependent on load ratio and cycle time. For higher frequencies and low load ratios (1 Hz and 0.2, resp.) the data resides between the ASME air and water default lines, and increase, with decreasing frequency, to reach the water line. For high load ratios, the test frequencies near 1 Hz yield data on or near the water line, and lower frequencies, or comparably longer ramp times yield data which increases from that trend.

(e) Within the above trends for BWR tests (Item (d)), the effect of increased dissolved oxygen content seems to be to increase crack growth rates. The reader should be aware that adequately controlling and monitoring higher dissolved oxygen contents ($\gtrsim$ 100 ppb) is somewhat difficult in small laboratory test systems, and the dependence of the data on oxygen content should be considered in light of this possible variability.

As stated in the introduction, the majority of these data sets have been published after the adoption of the ASME Code Section XI upper bound limits. It is now evident that virtually all the high load ratio data resides above, i. e. on the unconservative side of the water default line. The low load ratio data, with a few exceptions, (for example-Figs. 18, 57 and 70) resides under that limit. Thus a definite need for re-evaluation of the code limits has arisen [12, 65, 68]. Whether this re-evaluation will adopt limits based on the upper bound or the mean of the data remains to be seen. The current absence of low ΔK data will also introduce difficulties in the re-evaluation. In addition it should be kept in mind that the present results are based on tests conducted with rather small test specimens. Whether the electrochemical conditions are the same inside a flaw in the real structure is an open question.

MODELS FOR ENVIRONMENT ASSISTED CYCLIC CRACK GROWTH

Two basic mechanisms, dissolution assistance and hydrogen assistance, have generally been proposed to explain environmentally enhanced crack growth in simulated PWR and BWR environments [16,40,41,67]. In the former process the advancement of the crack is assisted by removal (dissolution) of the metal at the crack tip whereas in the latter process the mechanical separation at the crack tip is facilatated by hydrogen embrittlement.

In aqueous environments, the electrochemical conditions at the crack tip during both sustained and cyclic loading have been shown to be independent of the bulk

electrochemistry. Under a free corrosion potential, the pH is found to be in the acidic regime, regardless of the bulk dissolved oxygen content [90-93]. Under these circumstances an anodic reaction involving metal-surface dissolution occurs at the crack tip. This must be balanced by a corresponding cathodic reaction, and this reaction takes place either on the crack sides or on the external surface. In the absence of dissolved oxygen the cathodic reaction involves the reduction of hydrogen ions to atomic hydrogen, which can then enter the metal. When dissolved oxygen is present in the bulk water, another cathodic reaction can occur on the external surface, i. e. the reduction of dissolved oxygen to hydroxyl ions. This reaction cannot occur, or occurs to a lesser degree, near the crack tip, where the solution is nearly, or totally deoxygenated.

Thus two processes can enhance the crack growth: anodic dissolution at the crack tip and/or hydrogen embrittlement of the metal in front of the advancing crack. The authors of this review favor the latter mechanism, and our opinion is based primarily on the copious fractographic evidence [43,45,67,93,94,95,96]. In the following, the hydrogen assistance mechanism is briefly reviewed and adapted to the general trends of the environmental enhancement in cyclic crack growth rate.

Hydrogen evolution occurs only during rise time of the fatigue cycles as fresh metal surface at the advancing crack tip is exposed to the environment. Hydrogen can subsequently enter the metal provided certain requirements, concerning adequate surface reaction time, competing repassivation and possibly adequate fresh surface area, are met. Once the hydrogen has entered the metal, it diffuses along the stress gradient towards the region of high triaxial stress just ahead of the crack tip. The bulk diffusion rate at the elevated temperatures in question is high enough to allow, within seconds, an excess concentration of hydrogen in the plastic enclave [120].

The presence of hydrogen in the plastic enclave introduces a macroscopic embrittling effect and a subsequent increase in cyclic crack growth rate. Considering the basic mechanisms of the microscopic hydrogen effects [see reviews -Refs. 97-101], a great controversy is, however, apparent. In his recent review Thompson concludes that hydrogen can affect fracture when its concentration in a certain volume reaches a critical level, and that all the fracture modes can be affected.

At the present time no preference to the various hydrogen assistance models can be expressed. The following text presents some proposed mechanisms, which appear to be relevant when considering the explanation of the observed behaviorism. It has been shown that hydrogen impedes the dislocation motion, i. e., increases the flow stress in the plastic zone [97-100,102]. This in turn results in a smaller plastic zone size [103-104] and in a lower crack closure load, i. e. larger effective ΔK (at least in the lower ΔK region); producing an accelerated crack growth rate [105-106]. On the other hand, Beachem [107,108] has suggested a contradictory model according to which hydrogen reduces the local stress required for dislocation motion. Also, Hirth and Johnson [97] have stated that in the case of void coalescence and a fixed plastic zone size such a lower local yield stress would indeed give a lower stress intensity for crack propagation.

Another approach, based on continuum mechanics models, states that a delicate balance exists at a crack tip between cleavage and plastic deformation in ferritic iron alloys [109-111]. Hydrogen may, by forming surface hydrides [109,110], or by lowering the surface energy [112], or the cohesive energy [113-116], suppress plastic deformation and hence favor cleavage fracture.

Hydrogen Embrittlement Mechanism at 93°C

The results presented earlier show that a waveform composed of a fast rise time (of the order of 1 second) followed by a hold time does not accelerate the crack growth rate significantly above the ASME Section XI air line (see Table 3). The explanation for the general absence of environmental effect at such comparatively high frequencies may be sought from the passivation behavior of the fresh metal surface at the crack tip and the subsequent possibilities of hydrogen absorption and transport. Using a slow strain rate test method, it has been shown that a maximum influence of the environment is observed over a critical range, and the susceptibility decreases at faster and slower strain rates [117-119]. For a corrosion fatigue test at high frequencies, corresponding to larger strain rates in constant strain rate testing, the interaction of the exposed metal with the environment is of no consequence, because the rate at which the metal fails by ductile fracture exceeds the rate at which the environment can affect fracture via any of the possible mechanisms (dissolution, hydrogen embittlement or absorption of damaging species).

Because there is opportunity for hydrogen generation and subsequent entry into the metal, a long rise time, with or without a hold time, produces an accelerated growth rate. The passivation at the frequencies used is not rapid enough to prevent this hydrogen entry. The contradictory behavior observed by Atkinson and Lindley [10,11] showing retardation of crack growth rate enhancement with extensive ramp times is difficult to explain. The relatively high dissolved oxygen content in their water environment may be of some consequence, however, as will be discussed later, this normally leads to the opposite effect. Another possibility is that at this temperature range the presence of oxygen accelerates the cathodic reaction based on the reduction of dissolved oxygen. This has to subsequently accelerate the corresponding anodic reaction, i. e. more pronounced dissolution at the crack tip may occur causing crack tip blunting and crack growth rate retardation. This kind of behavior has been suggested by Kondo and co-workers [2-7] and Radon and co-workers [121].

Hydrogen Embrittlement at 288°C

As in the case at 93°C, high frequencies, i. e. short rise times (of the order of 1 sec), do not allow the accelerating effect of environment. At lower frequencies, the formation of a passivating film can inhibit the entry of hydrogen at the crack tip. This film can be formed provided the rates of the anodic and cathodic reactions are sufficiently slow, as would be the case in completely deoxygenated water (PWR conditions) and provided that the crack tip straining rate is rather monotonic, as in trapezoidal load waveform testing. On the contrary, in the sinewave load testing, the continuous changes in the crack tip straining rate may prevent the passive film formation and hence facilitate the hydrogen entry and subsequent crack growth enhancement. If the frequency is lowered sufficiently, however, the film formation may occur, thus preventing the hydrogen entry.

As stated earlier, in the presence of dissolved oxygen (BWR conditions) the reaction rates may again be higher. This may facilitate pronounced hydrogen evolution even with longer ramp times, which in turn will result in the accelerated crack growth rates seen in BWR results at these frequencies. As the dissolution rate increases it is, however, difficult to understand why no crack tip blunting and subsequent lowering of the crack growth rates will occur, as was discussed in connection with the lower temperature results.

As the graphical presentation of the data shows, the applied ΔK values

considerably influence the environmental enhancement of the crack growth. The results generated so far indicate crack growth rates at low ΔK values reside near the ASME Section XI air default line, but this behavior may be connected with the start-up of the test only. The formation of a stable, and more acidic environment in the crack tip may require a prolonged time, after which the environmental influence may be seen.

At intermediate ΔK levels for which the acidic crack tip environment has been established, enough hydrogen is generated and absorbed to produce crack growth enhancement. This enhancement is related to the plastic zone size. In the high load ratio tests the acceleration starts with lower ΔK values, but at comparable crack growth rate values for both high and low load ratio tests showing accelerated crack growth rates, the plastic zone sizes are roughly equal.

At higher ΔK values, depending again on the load ratio, a bendover or plateau, i.e., a retardation of the environmental influence is seen when a comparable plastic zone size is achieved. This apparently occurs because at this stage the crack growth rate exceeds the rate of evolution of hydrogen and therefore the critical hydrogen content needed for the embrittling effect cannot be achieved [67]. Also, the altered electrochemical conditions associated with the increased surface area generated during the higher crack growth rate might change the potential, causing a more anodic state [90], with the consequence that the level of surface hydrogen release decreases [121]. Thus, at higher ΔK values the crack growth rate is so fast that it overcomes the hydrogen generation and absorption into the plastic enclave [57].

Fractography and Metallography

The fractography and metallography performed strongly supports the hydrogen embrittlement model [16, 40, 41, 67]. Typical features of specimens showing no environmental influence in water as well as in air are a transgranular fracture path, coupled with ductile striations and dense microcracking or branching. When accelerated crack growth rates are observed, the fracture mode changes at the lower temperatures to cleavage-like with no striations. Some intergranular fracturing is seen and branching is not evident [40,41]. At the higher temperature the striations are of the brittle type [16, 40, 41, 122] and features typical of hydrogen assisted stress corrosion cracking can be seen [40,41]. When the bendover occurs, the fracture mode transforms or reverts to a more ductile type and extensive branching is observed [40].

Reportedly, the fractographic features also depend on the material being tested. Contrary to the features reviewed above, the mechanism of fatigue crack growth in the weld specimens is void coalescence, independent of the environmental influence [67]. The large number of coarse carbides in the weld specimens is suggested to be sufficient to influence the void nucleation process and explain the occurrence of this mechanism of crack propagation. As discussed by Thompson [99], hydrogen may enhance the rate of microvoid formation and growth and thus introduce the crack growth rate acceleration.

When test interruptions or other abrupt changes in applied load or frequency have occurred, this can be readily seen in the fractography. These occurrences introduce major crack branches, which can explain the observed transients and reversals in the crack propagation data [26-28]. The crack growth retardation after long test interruptions, when the specimen has been taken out of water, are perhaps due to the long period required to re-establish the acidic crack tip environment necessary for hydrogen evolution.

AREAS OF FUTURE WORK

With the consideration of this report in mind, there are a number of areas which will require research in order to provide mechanistic understanding of the phenomena, or to assist in providing engineering applicability for this data. Tests with higher load ratios (> 0.7) and applied ΔK values approaching threshold will need to be carried out, especially for piping materials, and, based on these results, tests with complex load spectra may follow. The effects of neutron irradiation damage have not been ascertained. If studies of irradiated pressure vessel steels indicate that the useful life of reactors may be extended, by annealing the vessel so as to recover some of the properties degraded by irradiation, then FCGR tests of irradiated, annealed and reirradiated steels will have to be conducted. The interrelationship of stress-corrosion cracking under static load and corrosion fatigue crack growth needs to be better understood. In order to better understand the mechanistic basis, tests involving measurement of electrochemical potential changes during fatigue cycling may lead to an understanding of the corrosion kinetics. The clear delineation of the micro-mechanistic differences arising from boiling water reactor chemistry as opposed to pressurized water reactor chemistry has not yet been accomplished. Similarly tests at intermediate temperatures (between 100 and 300°C), or with dissolved oxygen contents somewhere between PWR and BWR conditions (2 to 200 ppb) may also assist in the mechanistic evaluation.

When collected together, this seems like a rather significant quantity of data. However, much of it is somewhat preliminary in nature, having been produced at laboratories just beginning high-temperature, pressurized water FCGR research. Even among those laboratories with a significant amount of experience in this field, many of the data sets are fraught with difficulties--servo-hydraulic and mechanical problems, temperature and pressure control outages and interruptions for data acquisition purposes or other, often unexpected transients. As with most scientific endeavors, there will come a time when successful completion of these experiments will become commonplace and data can be considered to be far more reliable and reactor-typical.

We authors do caution against unadvised use of this data. In each case, it would seem appropriate and prudent to make a judgement about the integrity of a particular data set before using it in calculations, or for modeling purposes or other types of sensitive analysis. Some key points to check for would be:

(a) The accuracy of crack length determination, coupled with the practice and accuracy of any post-test corrections to the crack length.

(b) The practice of correcting the applied load for seal friction losses and changes in the internal water pressure.

(c) The care and accuracy with which the water chemistry was regulated. Especially important is the accuracy of the dissolved oxygen content regulation and measurement.

(d) The material parameters and their effect on the data. A sensitive study of heat-to-heat differences has not been undertaken, but as pointed out in the text, microstructure is known to have an effect on FCGR.

CONCLUSIONS

Although it is extremely difficult to assimilate the significance of each one of

these data sets, some overall trends and conclusions have emerged as we have gathered together these data.

1. For the lower load ratios ($R \leq 0.2$) the FCGR data resides below the ASME water default line, with only minor exceptions in which some data acquired just after test start-up has briefly surmounted the water default line.

2. For the higher load ratios ($R > 0.5$) most of the data lies above the ASME water default line.

3. As a category, the 17 mHz (1 cpm) sinewave tests reside consistently higher than tests of other frequencies and other waveforms, for both low and high load ratios.

4. For the PWR (low-oxygen) environment, long-period waveforms apparently depress crack growth rates. For BWR (higher oxygen) environments, the crack growth rates monotonically increase with increasing cycle period. This suggests a basic micromechanistic difference attributable to the two environments.

5. There are some important areas for future research. FCGR for threshold, or near-threshold ΔK values, as a function of load ratio, need to be determined. Along with this, the effects of start-up and thermal cycling transients need also to be established. since many of the data sets included in this report exhibit what appear to be growth rate transients, especially at the beginning of the test, when the ΔK is lower, the effect of these transients, and whether they would recur for successive start-ups should be determined. Testing with combined waveforms, (i.e. variable amplitude, variable frequency tests) will result in a data generated under more realistic conditions; the interrelationship, if any, between fatigue, and stress corrosion cracking should be established, and fatigue tests at intermediate temperatures should be carried out to better address the question of the effects of thermal transients.

ACKNOWLEDGMENT

This research was sponsored by the Reactor Safety Research Division of the U. S. Nuclear Regulatory Commission. The continuing support of this agency is appreciated.

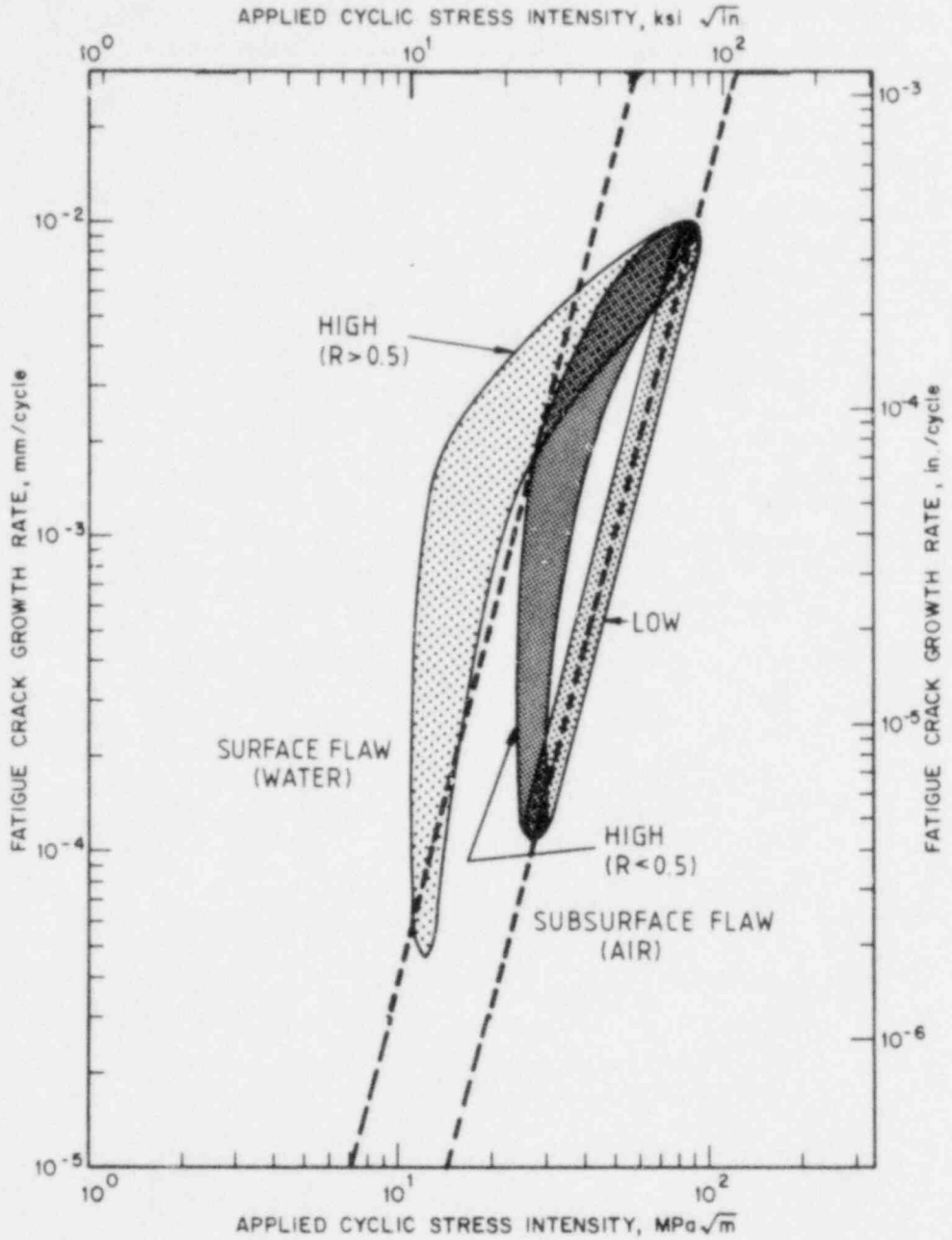

Fig. 1. The plotting grid used for all data sets in this review. The dashed lines are taken from the ASME Boiler and Pressure Vessel Code-Section XI. Shown on the grid are the three basic growth rate regimes inside which almost all the results presented in this report reside. The high and low categories for $R < 0.5$ are generalizaions of the same nomenclature introduced in Ref. 40.

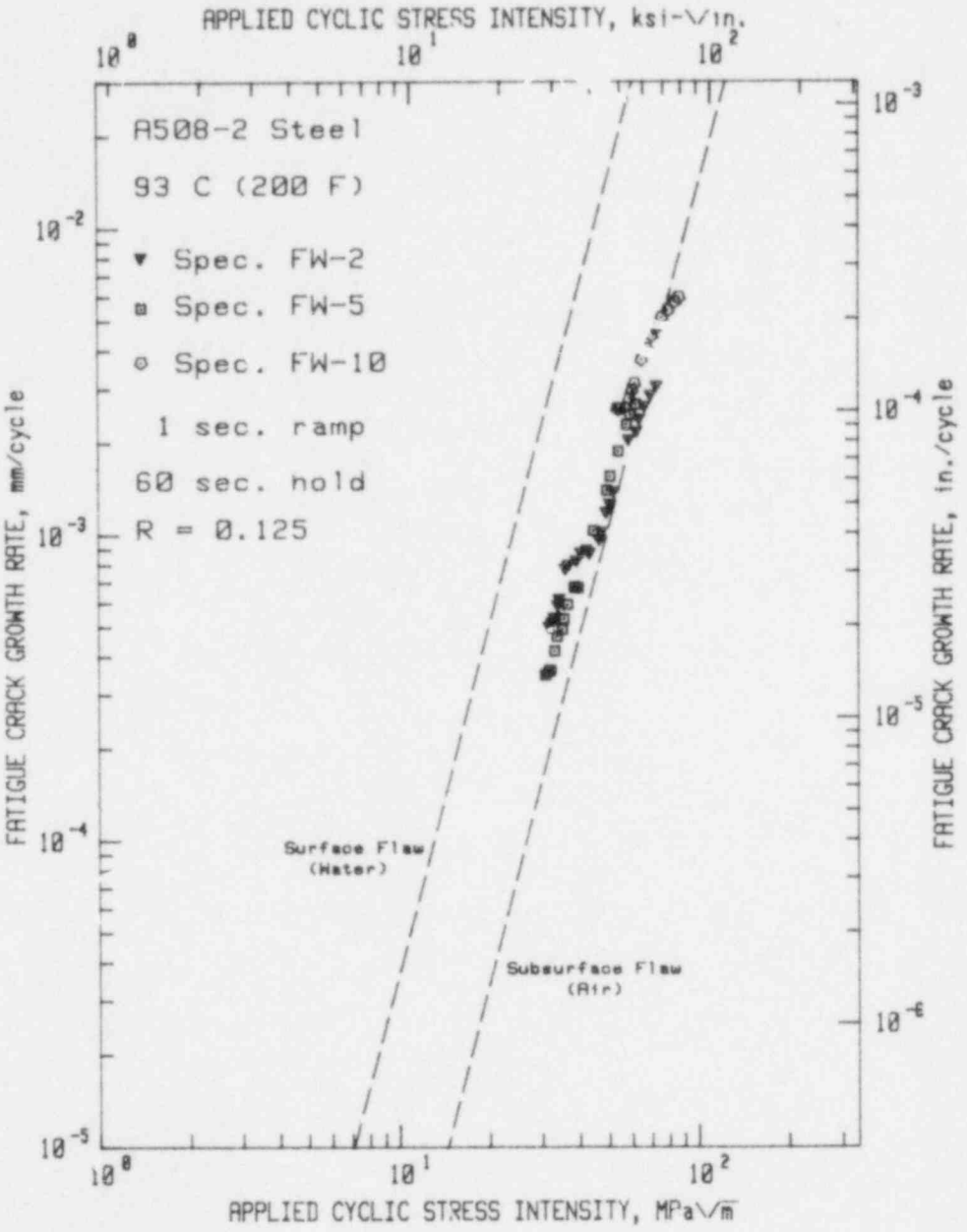

Fig. 2a. Fatigue crack growth rate vs applied cyclic stress intensity factor for A508-2 steel in 93°C reactor-grade water-PWR conditions. The short rise time component results in data residing in the low growth rate category. References 34,40.

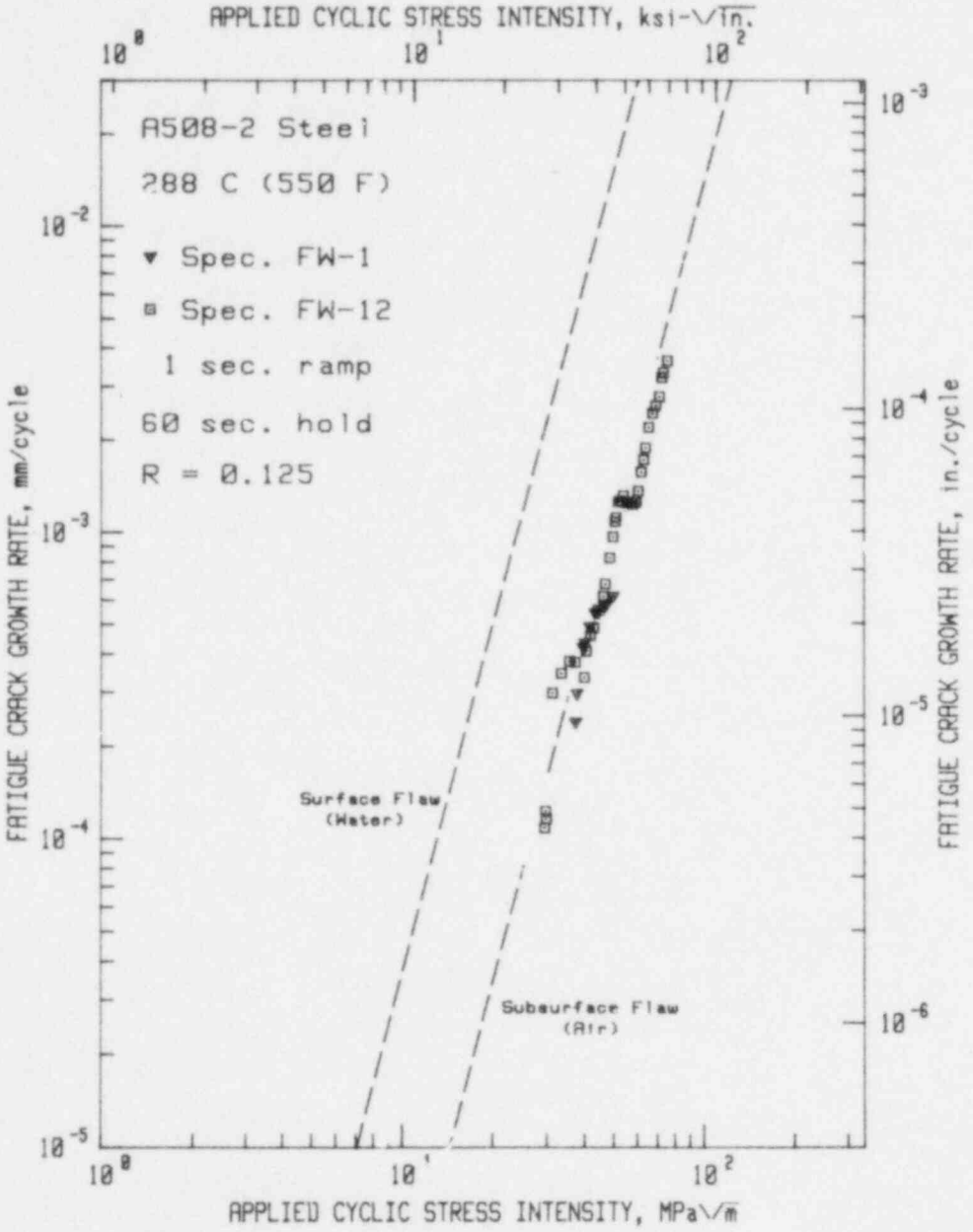

Fig. 2b. Fatigue crack growth rate vs applied cyclic stress intensity factor for A508-2 steel in pressurized, high-temperature, reactor-grade water --PWR conditions. As in the lower temperature analogous waveform results of Fig. 2a., the short rise time results in data residing in the low growth rate category. References 34,40.

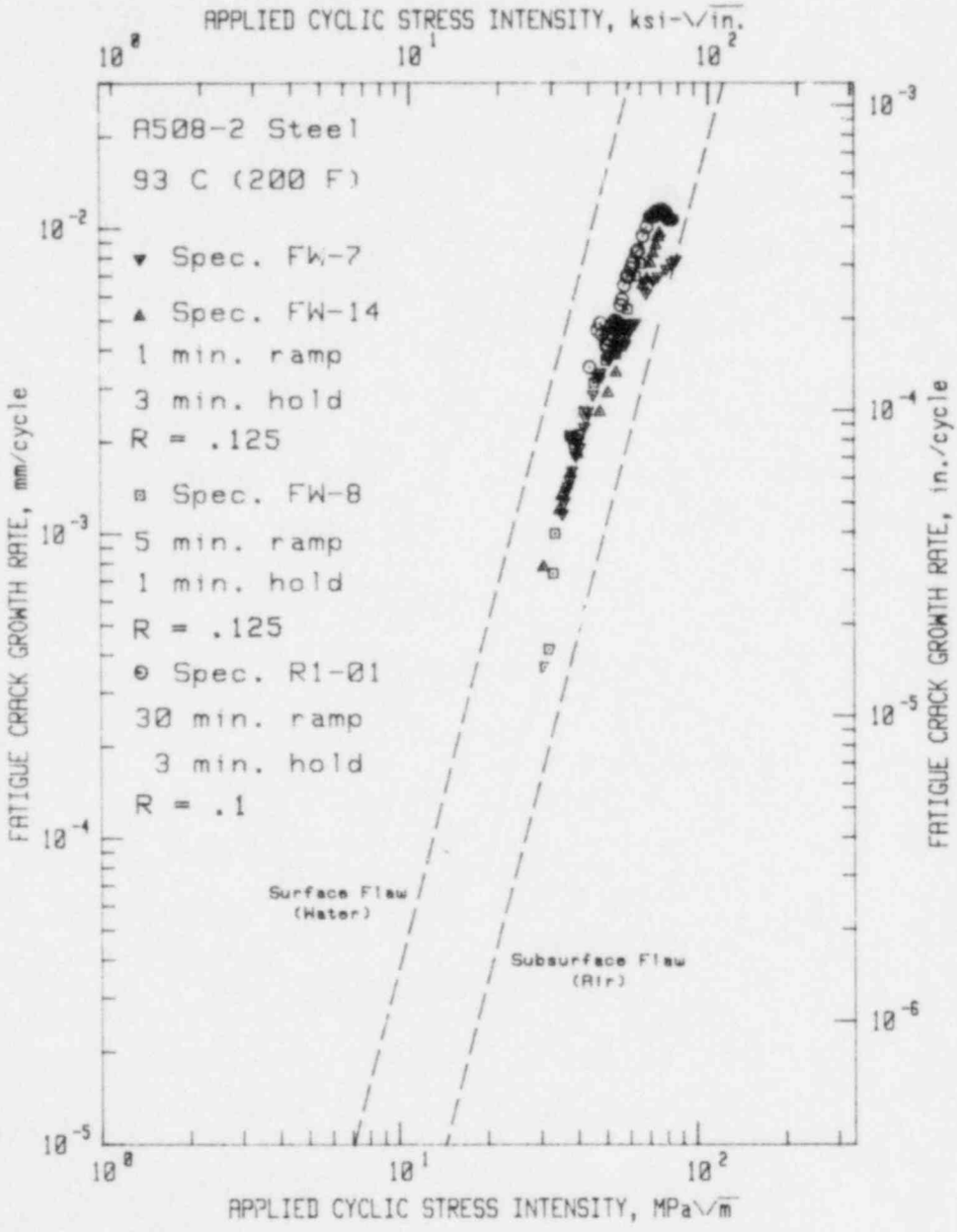

Fig. 3a. Fatigue crack growth rate vs applied cyclic stress intensity factor for A508-2 steel in 93°C reactor-grade water--PWR conditions. These long-rise-time waveforms all result in data in the high growth rate category. References 34-40.

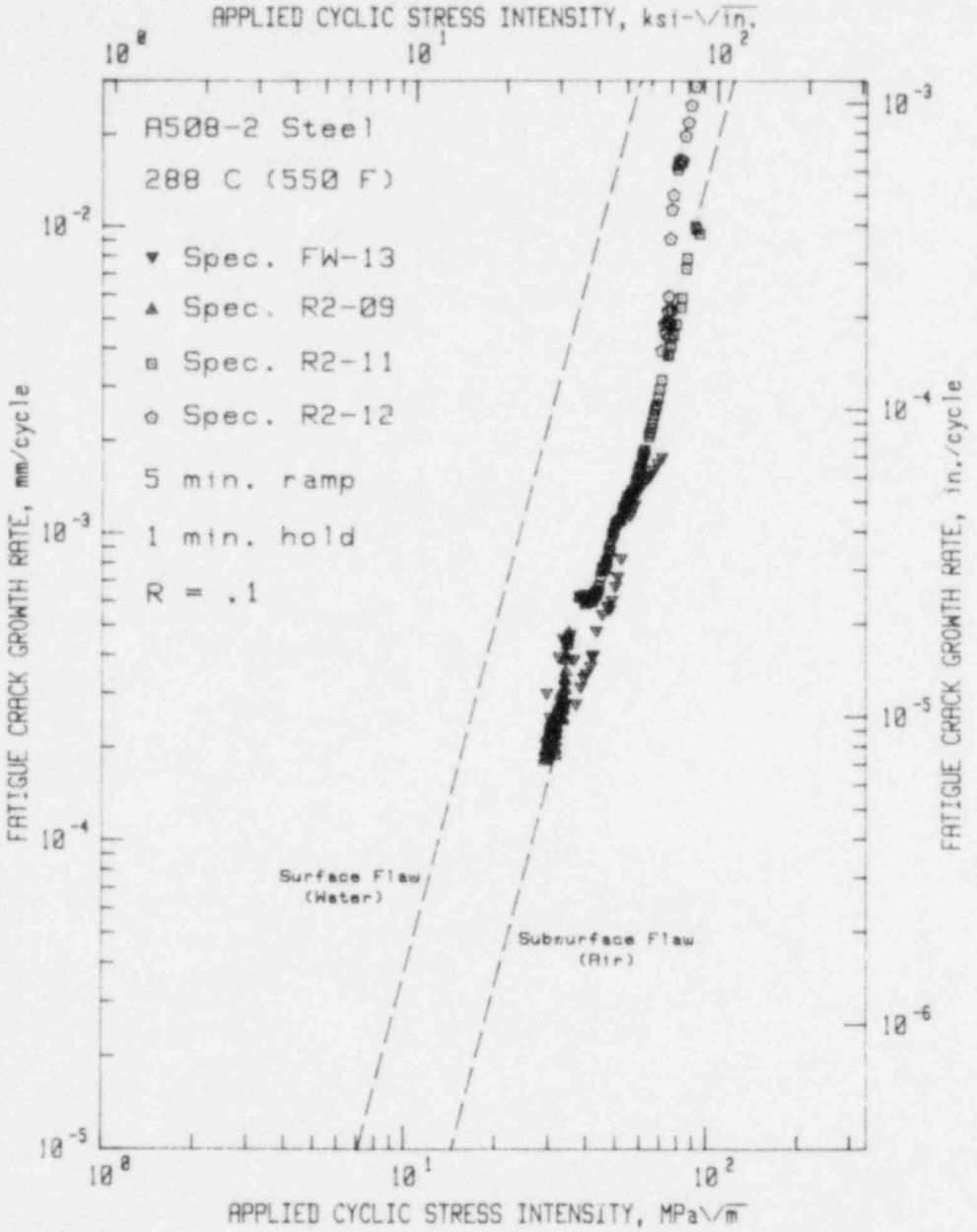

Fig. 3b. Fatigue crack growth rate vs applied cyclic stress intensity factor for A508-2 steel in pressurized, high-temperature reactor-grade water--PWR conditions. These data sets do not show the acceleration of crack growth rates due to the increased ramp time component. References 34,40.

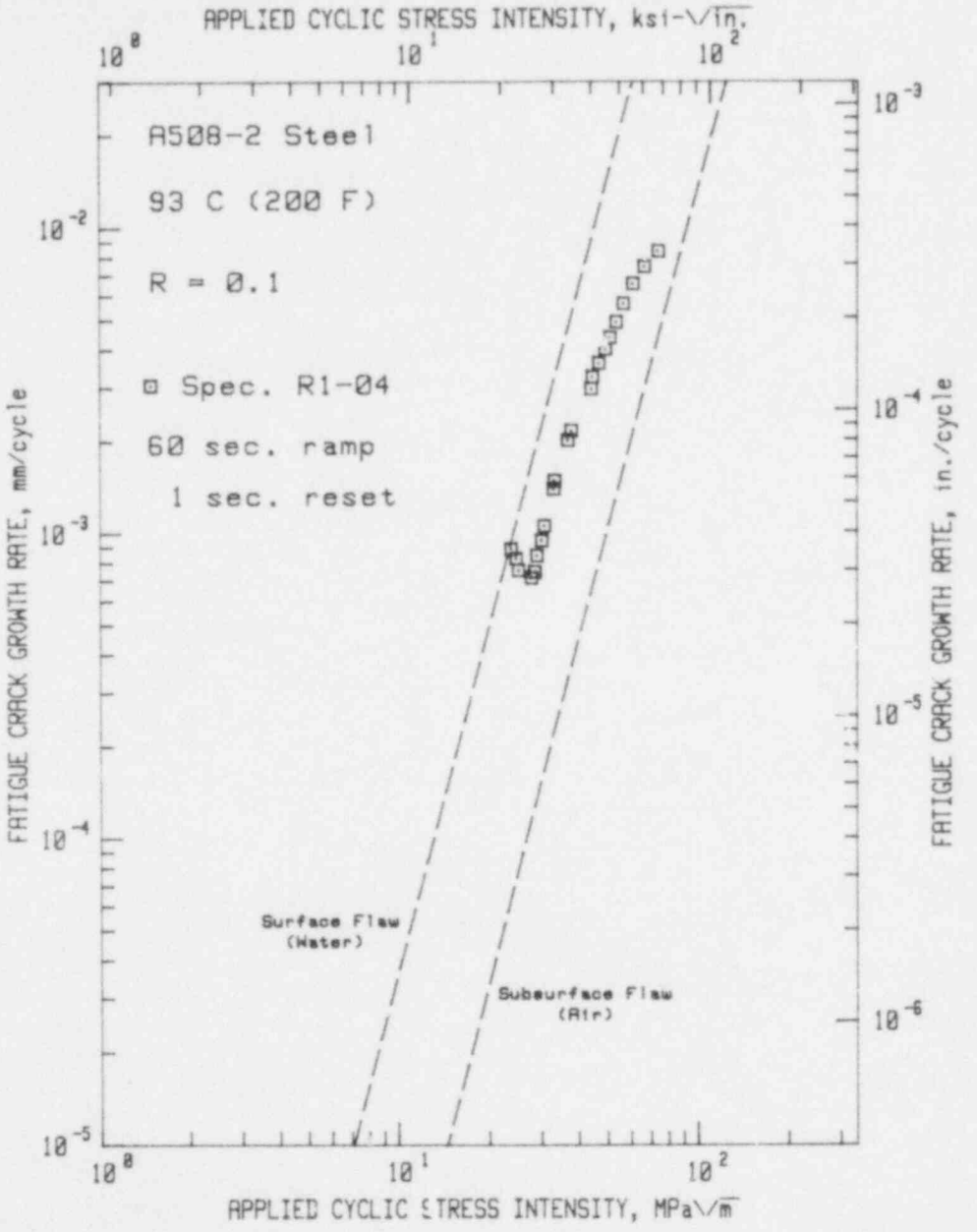

Fig. 4a. Fatigue crack growth rate vs applied cyclic stress intensity factor for A508-2 steel in 93°C reactor-grade water--PWR conditions. Compared with Fig. 3a., this result clearly indicates that a hold time component is not necessary to produce data in the high growth rate category at this temperature. The longer ramp times are by themselves sufficient. References 34-40.

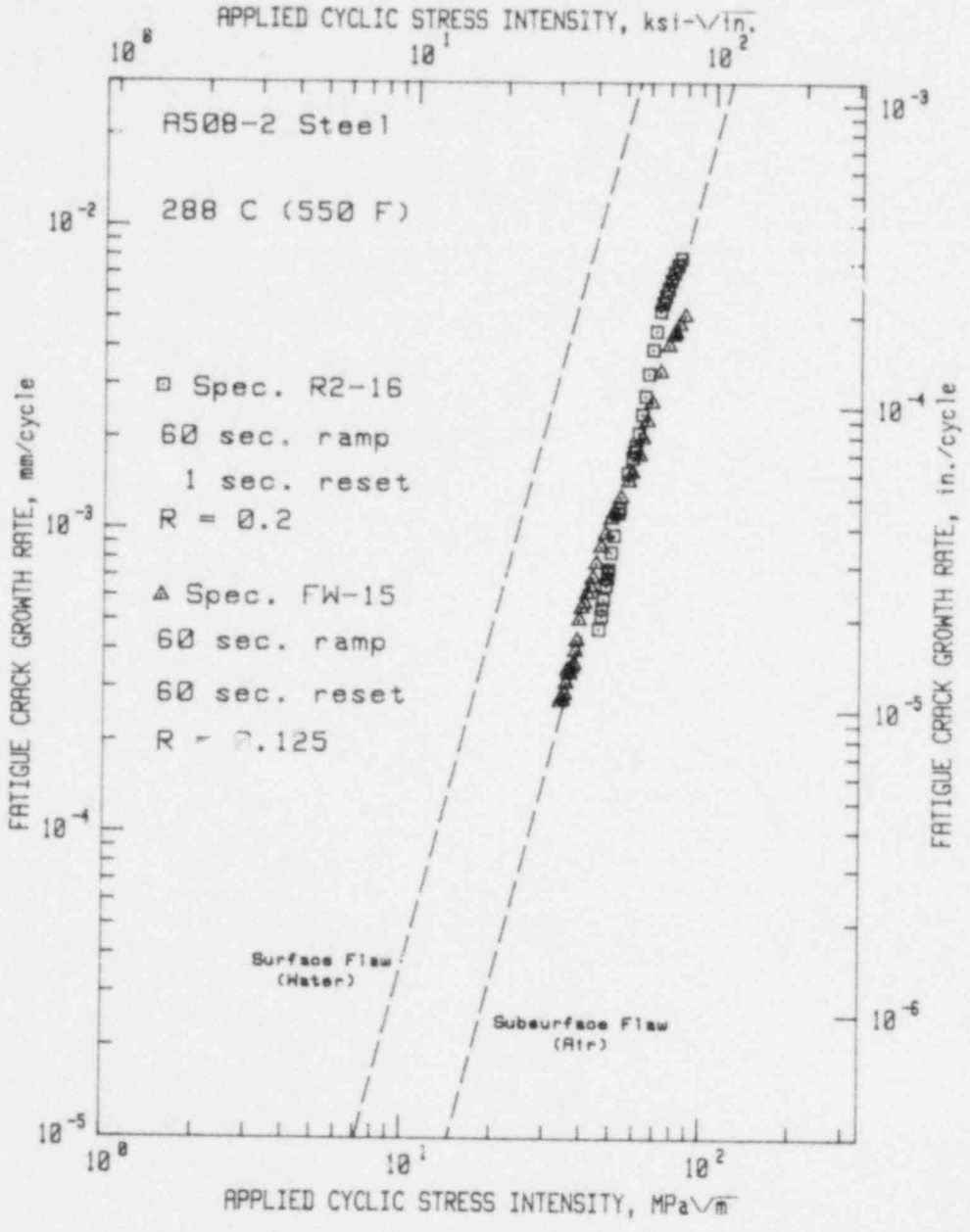

Fig. 4b. Fatigue crack growth rate vs applied cyclic stress intensity factor for A508-2 steel in pressurized, high-temperature reactor-grade water--PWR conditions. For the high temperature, waveforms with ramp time only components do not exhibit accelerated crack growth rates. References 34-40.

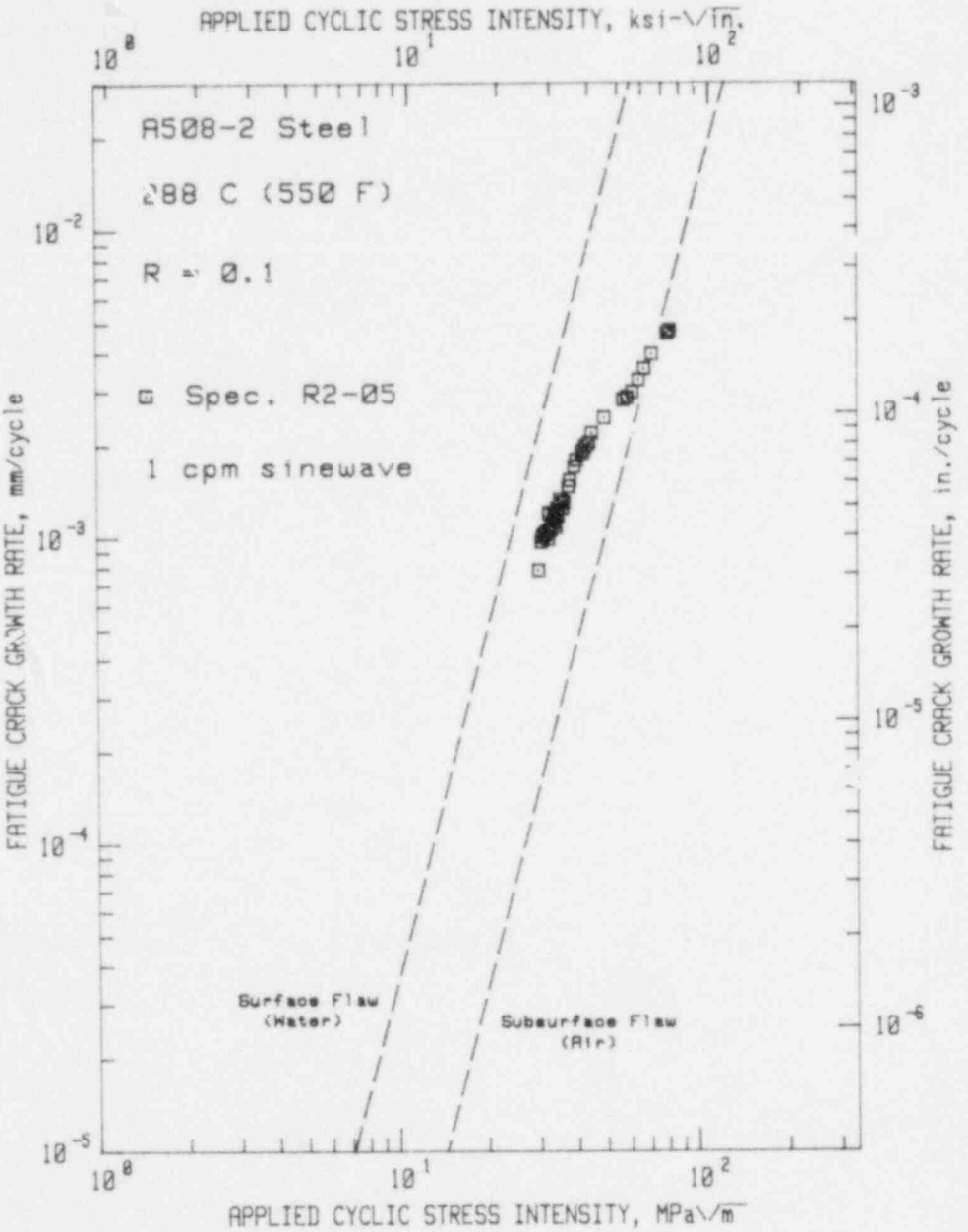

Fig. 5a. Fatigue crack growth rate vs applied cyclic stress intensity factor for A508-2 steel in pressurized, high-temperature reactor-grade water--PWR conditions. The 17 mHz (1 cpm) sinusoidal waveform consistently produces data sets residing in the high growth rate category. See Figs.11-13, 19-20. References 34-40.

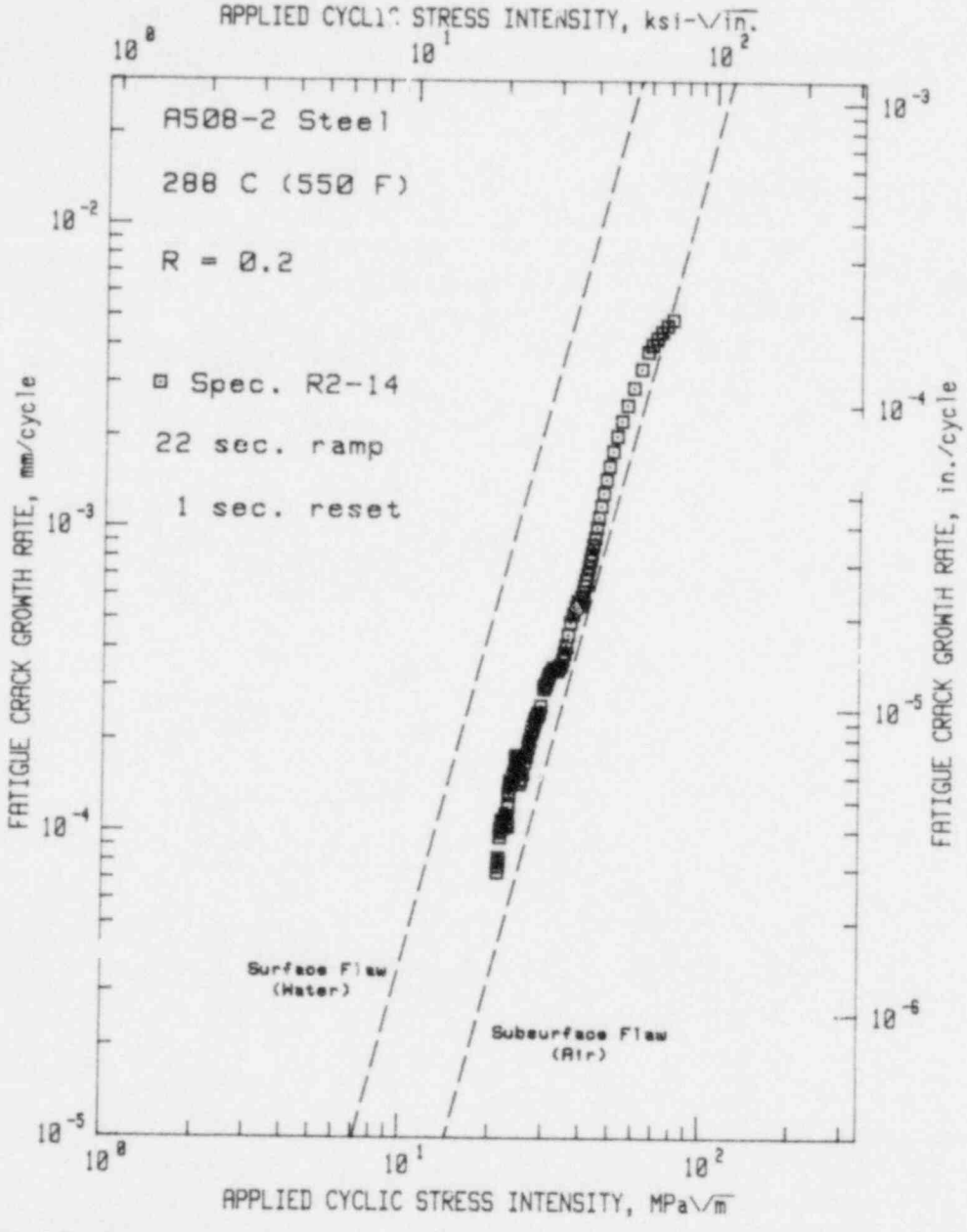

Fig. 5b. Fatigue crack growth rate vs applied cyclic stress intensity factor for A508-2 steel in pressurized, high-temperature reactor-grade water--PWR conditions. This test represents an attempt to model the high growth rate sinewave results with a waveform with a ramp time only component. Obviously, additional components are necessary, as these results are substantially lower than those of Fig. 5a. Reference 35.

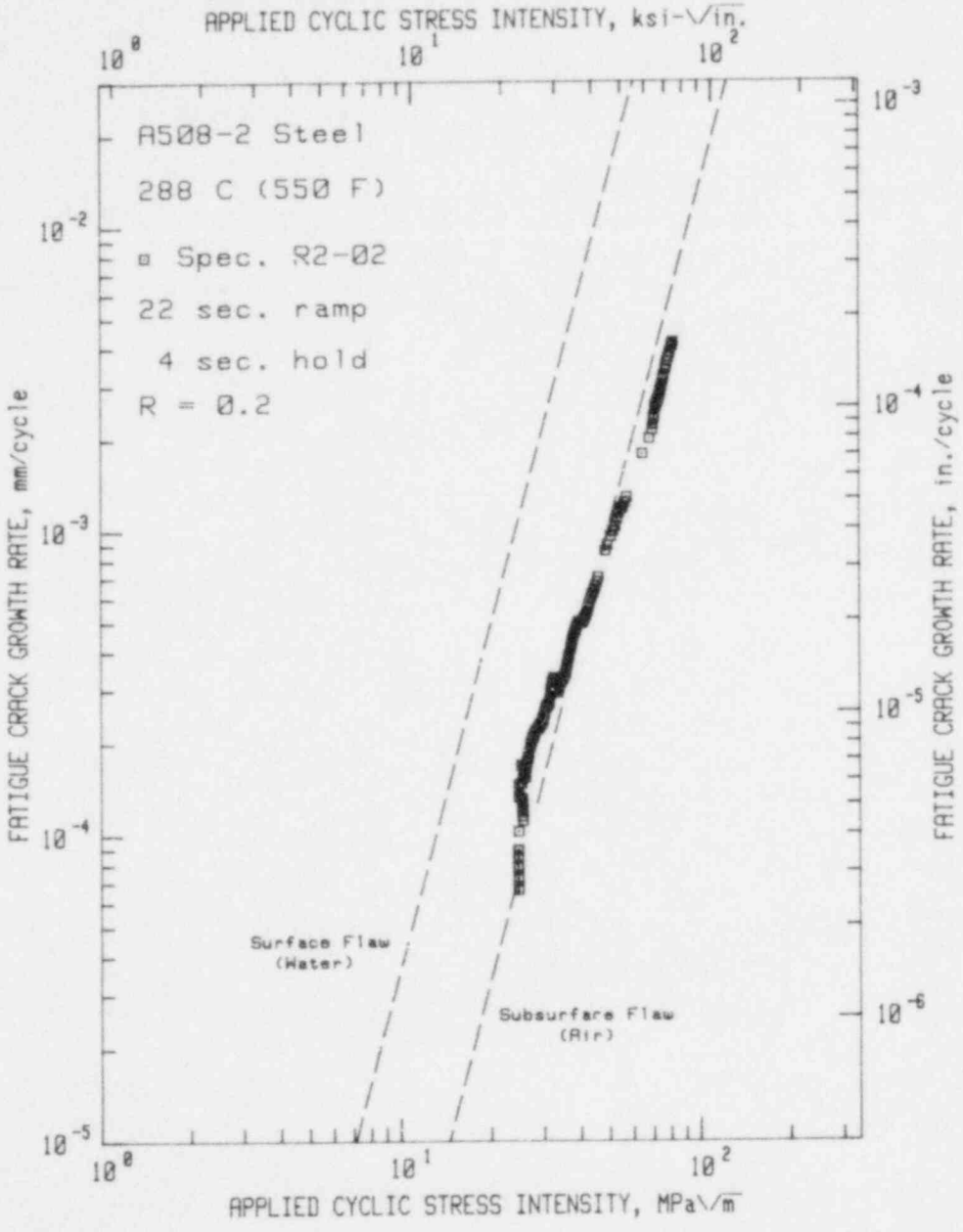

Fig. 5c. Fatigue crack growth rate vs applied cyclic stress intensity factor for A508-2 steel in pressurized, high-temperature reactor-grade water—PWR conditions. This test was the second in the series aimed at representing sinusoidal waveform behavior with various ramp time/hold time combinations. The combination above does not result in accelerated crack growth rates. Reference 36.

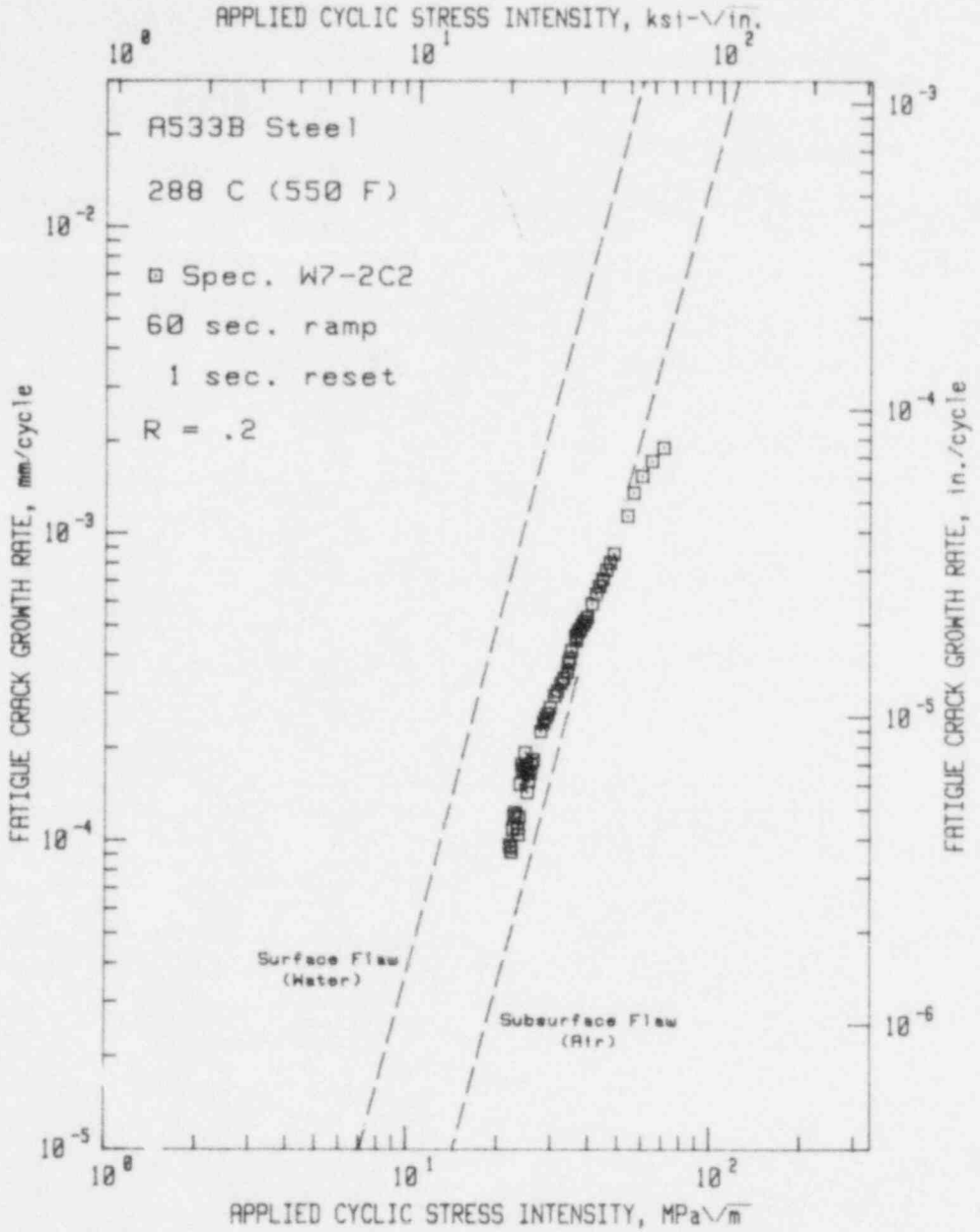

Fig. 6. Fatigue crack growth rate vs applied cyclic stress intensity factor for A533B-1 steel in high-temperature, pressurized reactor-grade water--PWR conditions. This data set resides in the low crack growth rate category, as expected from previous tests (see Fig. 4b.) Reference 36.

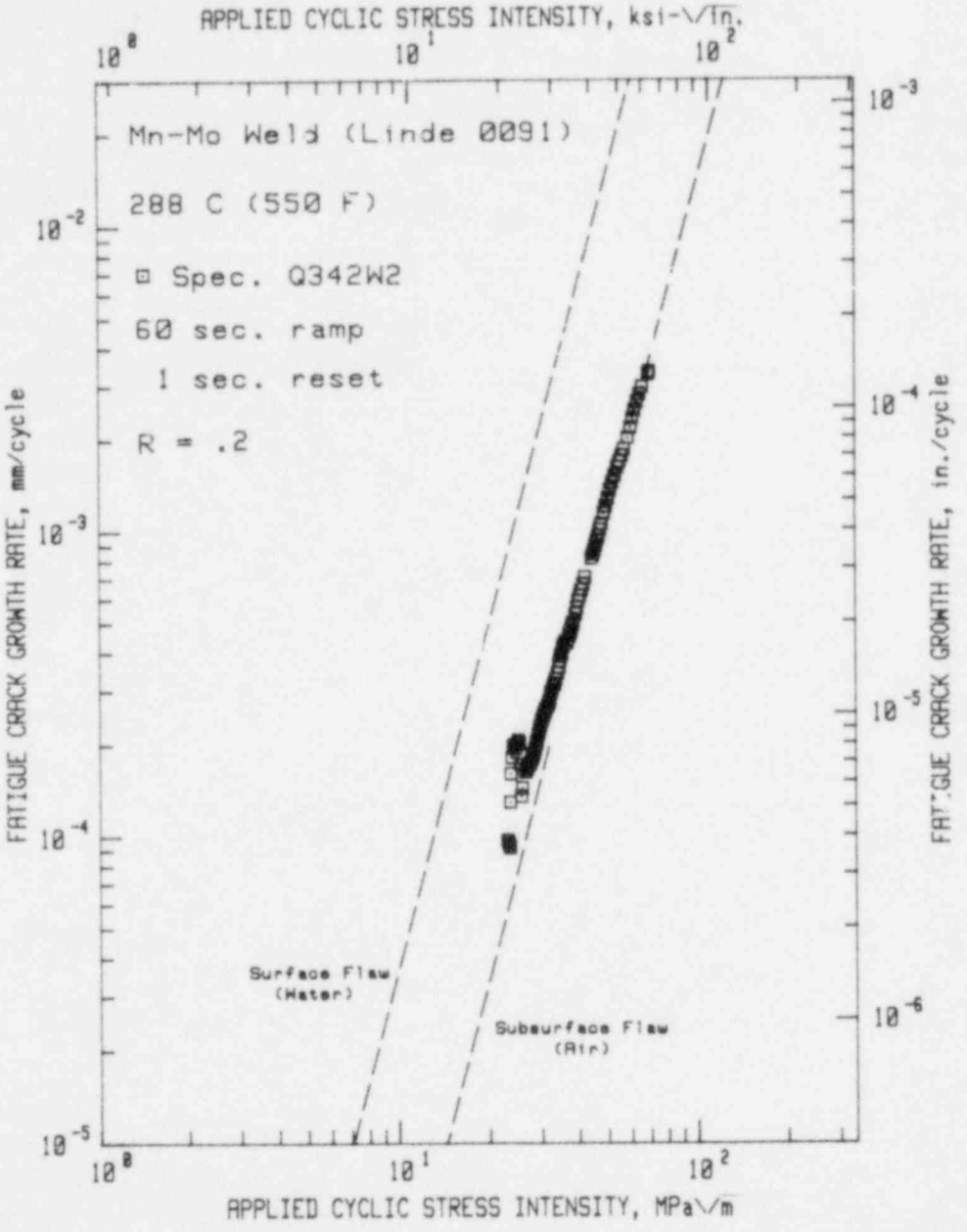

Fig. 7. Fatigue crack growth rate vs applied cyclic stress intensity factor for submerged arc deposited weld metal with Linde 0091 flux in the high-temperature, pressurized, reactor grade water-PWR conditions. As in the previous figure, the crack growth rates are quite low. Reference 36.

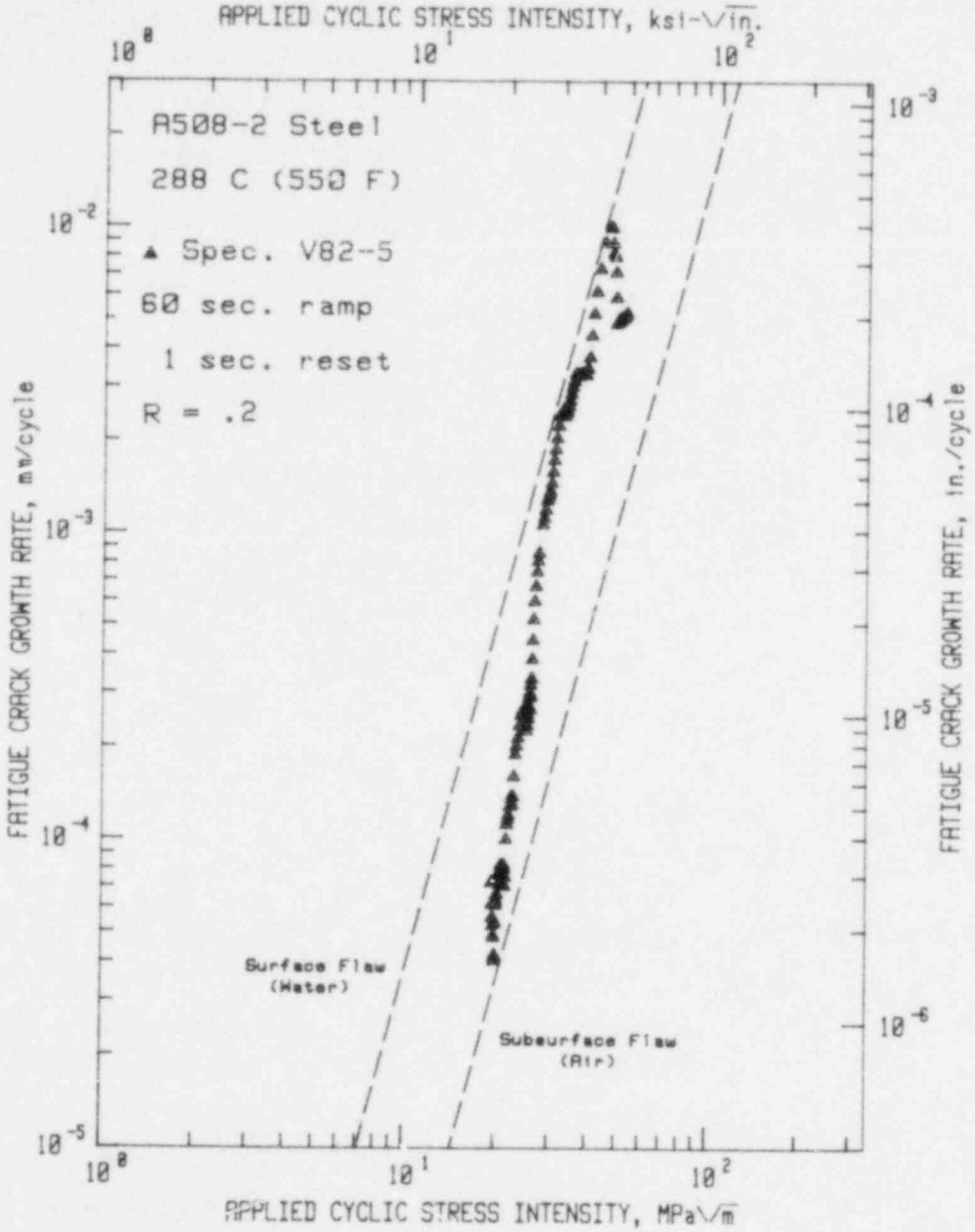

Fig. 8. Fatigue crack growth rate vs applied cyclic stress intensity factor for A508-2 forging steel in the high-temperature, pressurized, reactor-grade water environment --PWR conditions. Unlike the results for a different heat of A508-2, Fig. 4b, these data points reside near the top of the band defined by the ASME limits. Reference 36.

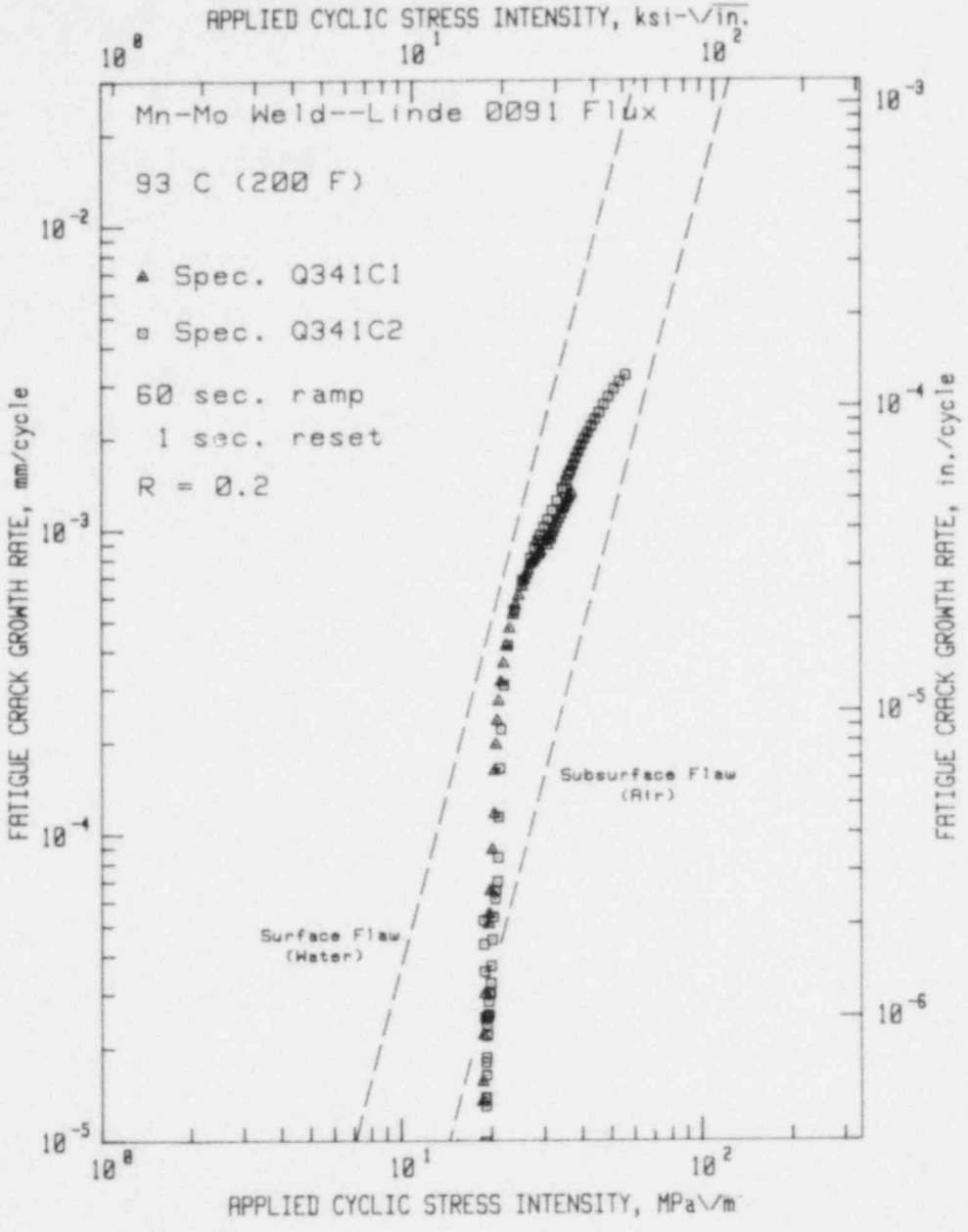

Fig. 9. Fatigue crack growth rate vs applied cyclic stress intensity factor for submerged arc weld metal with Linde 0091 flux in the high-temperature pressurized reactor-grade water - PWR conditions. These data sets reside in the high growth rate category as expected for longer ramp time waveforms at the lower temperature. Reference 34.

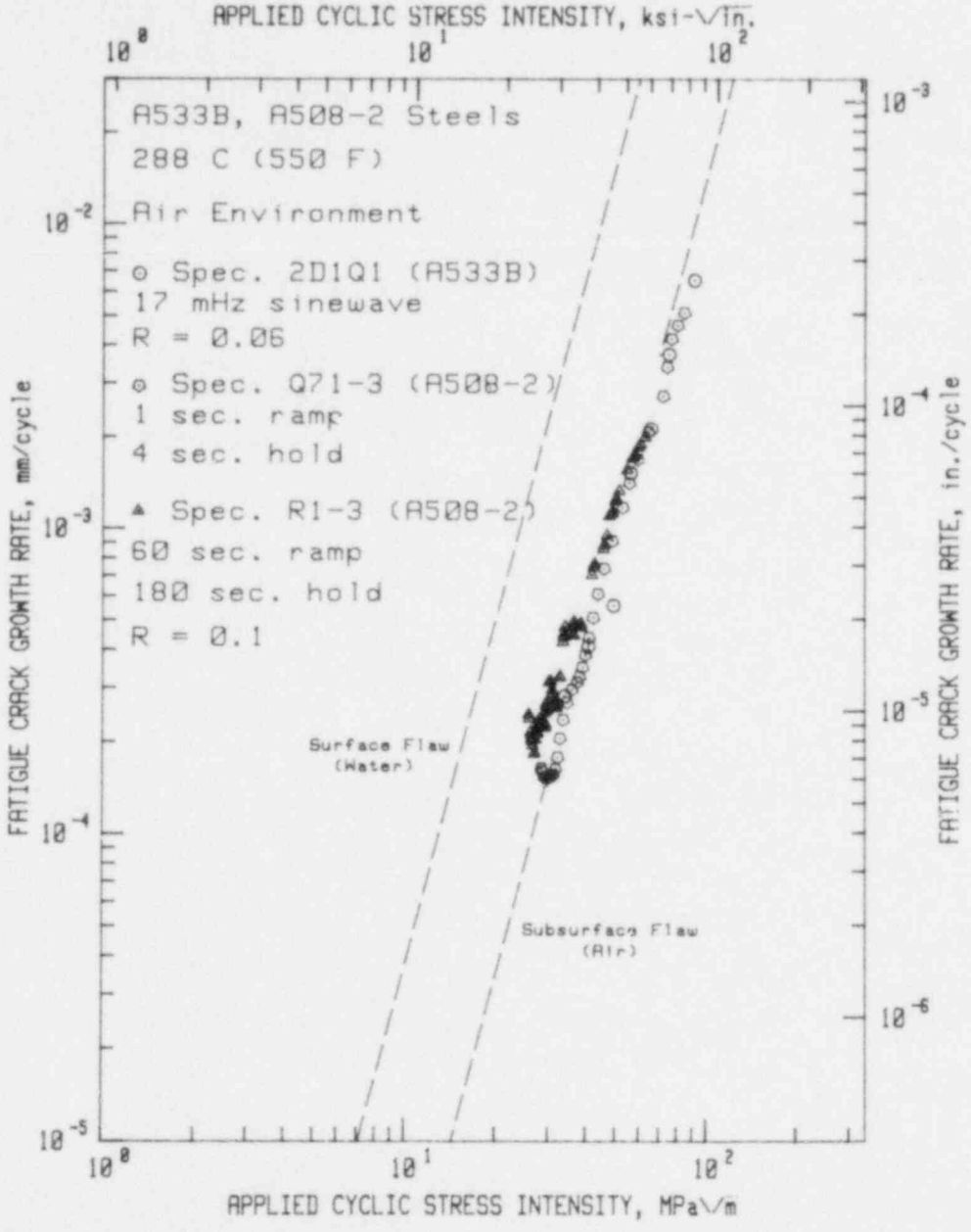

Fig. 10. Fatigue crack growth rate vs applied cyclic stress in a high-temperature air environment. These represent baseline data sets, and a reference for much of the data that follows. When the corrosive environment is not present, the data reside on or near the ASME air default line. References 40,44.

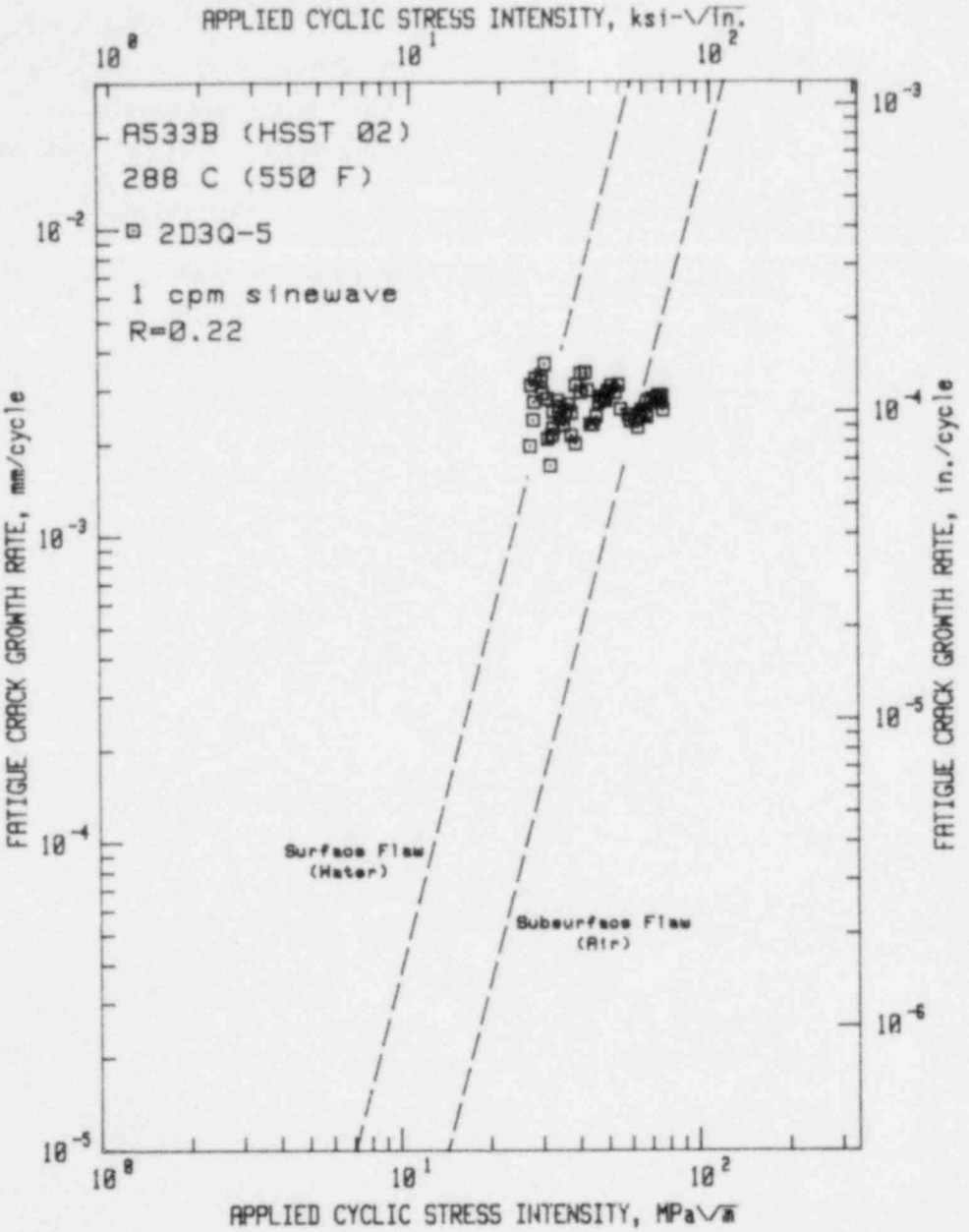

Fig. 11. Fatigue crack growth rate vs applied cyclic stress intensity factor for A533B steel in high-temperature, pressurized, reactor-grade water--PWR conditions. This data basically agrees with most of the 17 mHz sinewave tests in that it resides rather high for lower ΔK values, and trends toward the ASME air line for higher values. References 43,47.

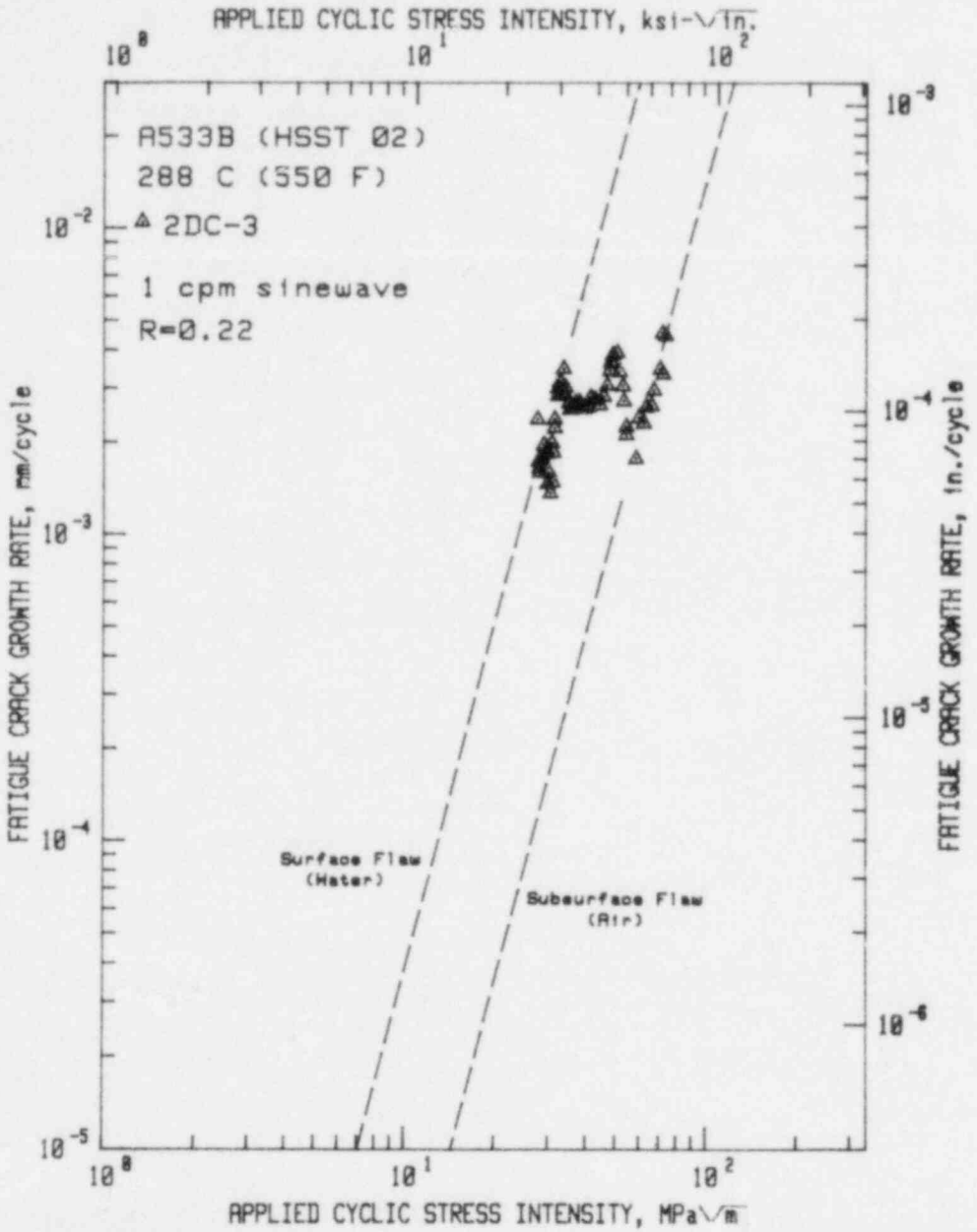

Fig. 12. Fatigue crack growth rate vs applied cyclic stress intensity factor for A533B steel in high-temperature, pressurized, reactor-grade water--PWR conditions. See Fig. 11. References 44,45.

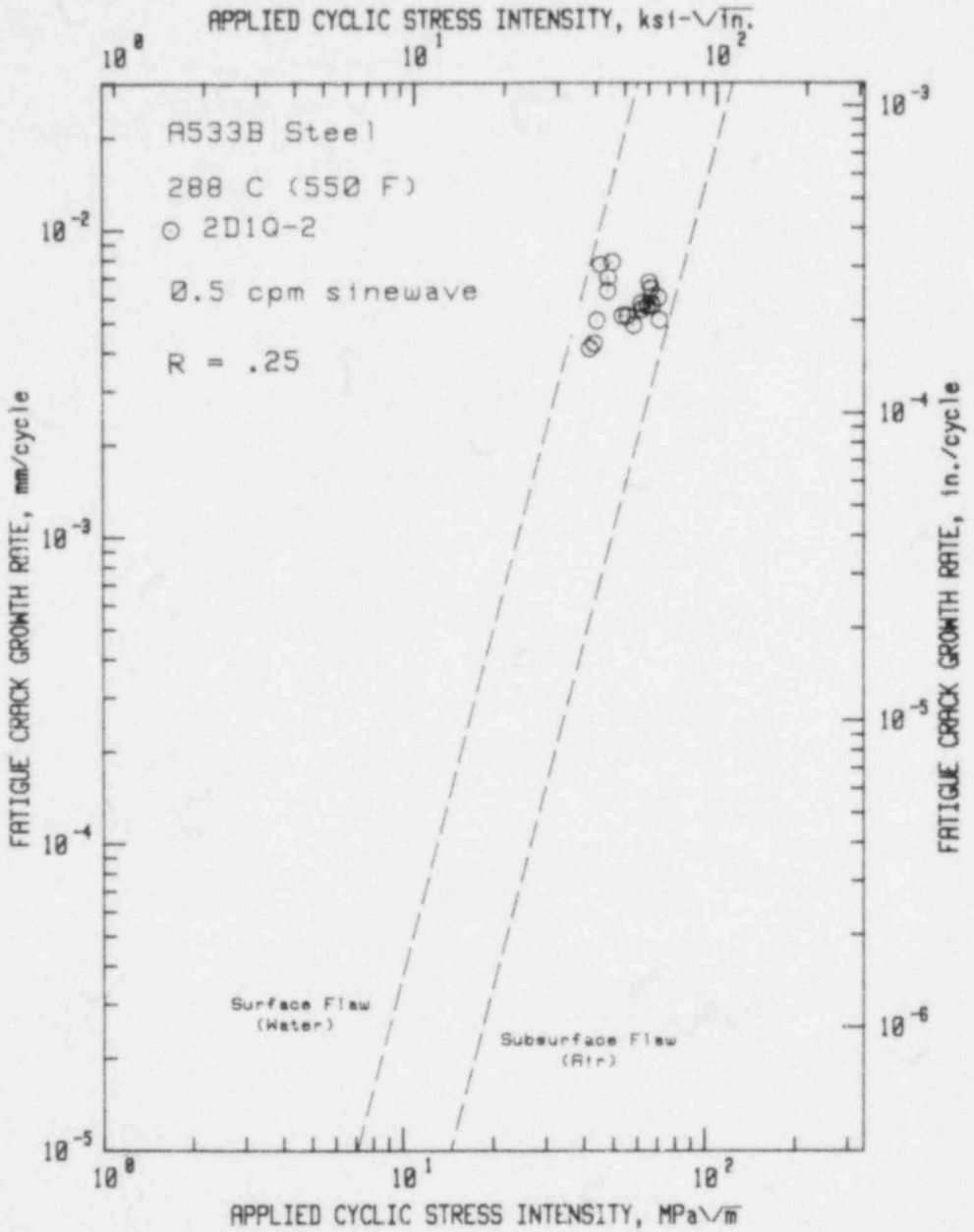

Fig. 13. Fatigue crack growth rate vs applied cyclic stress intensity factor for A533B steel in high-temperature, pressurized, reactor-grade water--PWR conditions. This sinewave period, twice that of the data in Figs. 11 and 12, results in somewhat higher crack growth rates, but essentially the same trends in other respects. Reference 63.

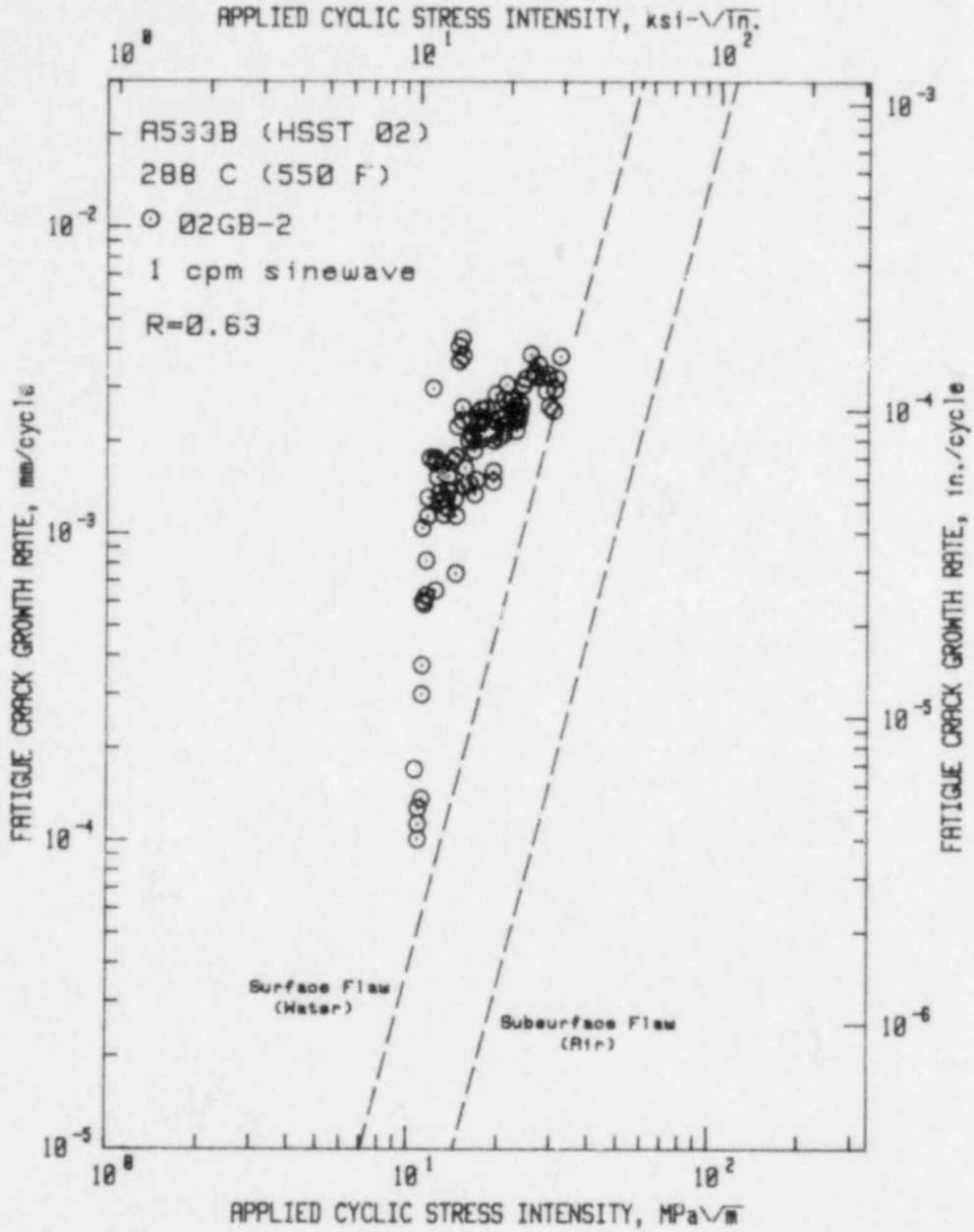

Fig. 14. Fatigue crack growth rate vs applied cyclic stress intensity factor for A533B steel in high-temperature, pressurized, reactor-grade water--PWR conditions. The high load ratio (0.63) coupled with the low frequency (17 mHz) resulted in some of the highest crack growth rates ever observed for these materials. See also Figs. 16 and 17. References 46-48.

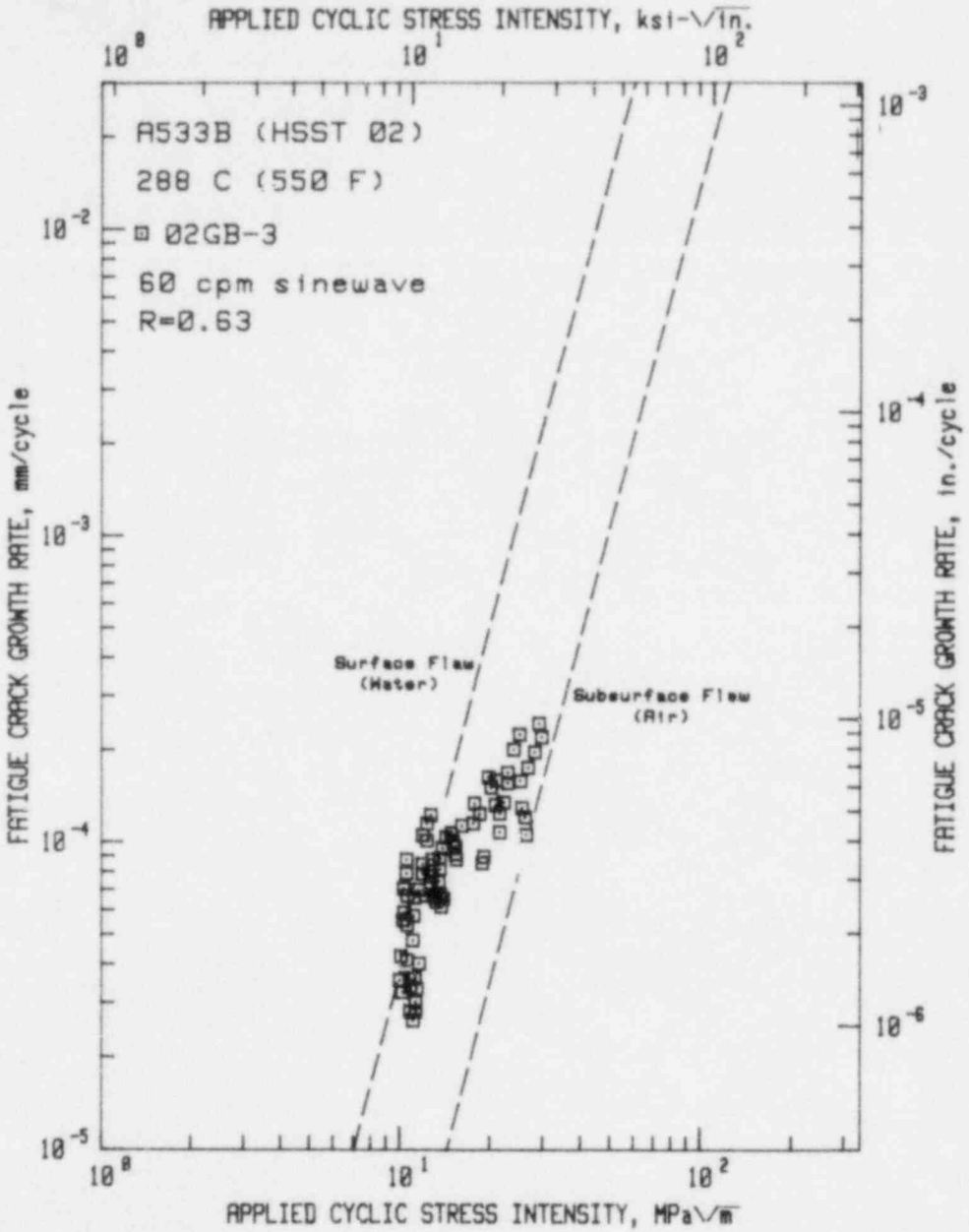

Fig. 15. Fatigue crack growth rate vs applied cyclic stress intensity factor for A533B steel in high-temperature, pressurized, reactor-grade water—PWR conditions. In comparison with Figs. 14, 16, and 17, the relatively lower crack growth rate is due to the higher test frequency. (1 Hz) References 46-48.

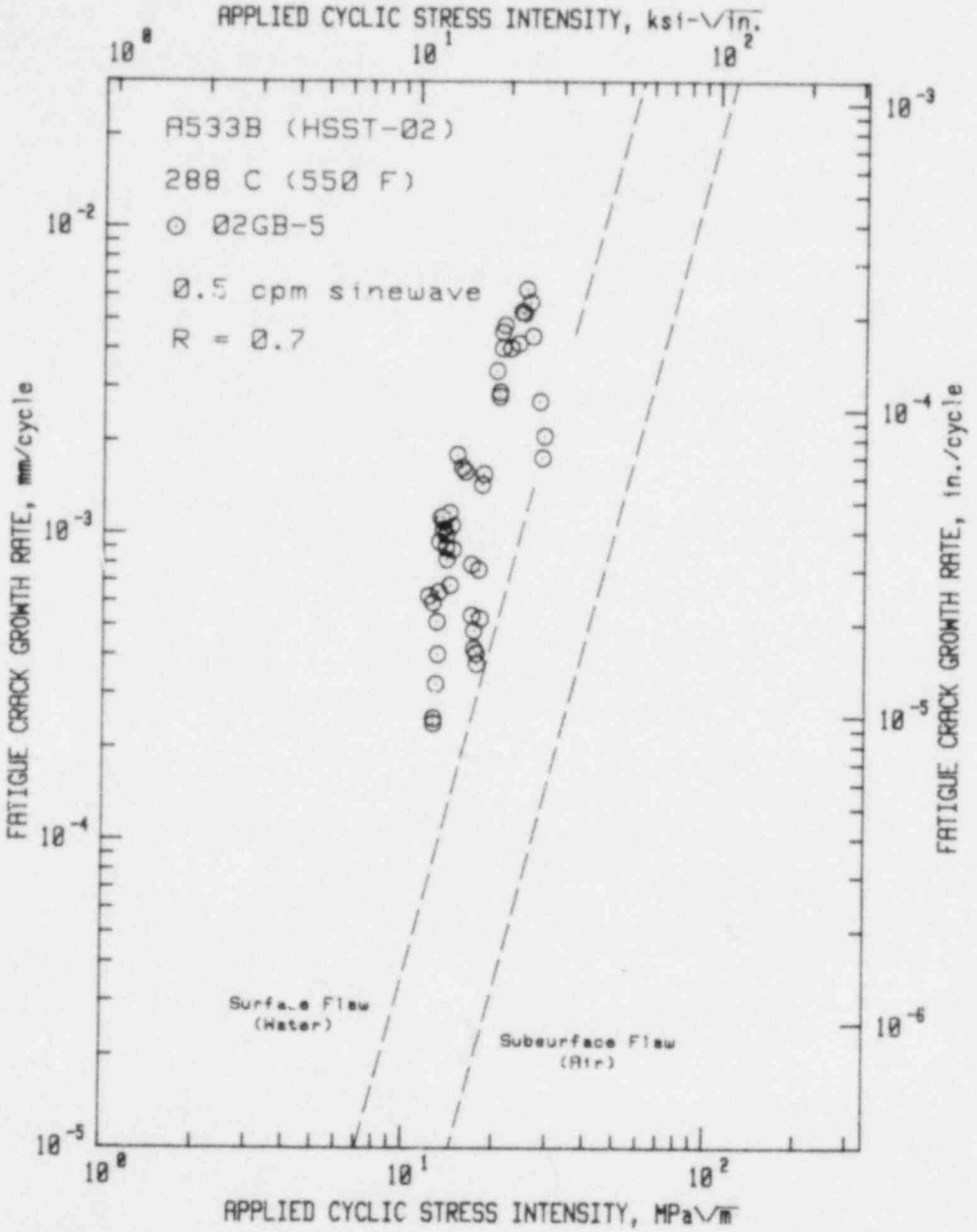

Fig. 16. Fatigue crack growth rate vs applied cyclic stress intensity factor for A533B steel in the high-temperature, pressurized reactor-grade water environment-PWR conditions. As in Figs. 14 and 17, the low frequency and high load ratio lead to relatively high crack growth rates. Reference 49.

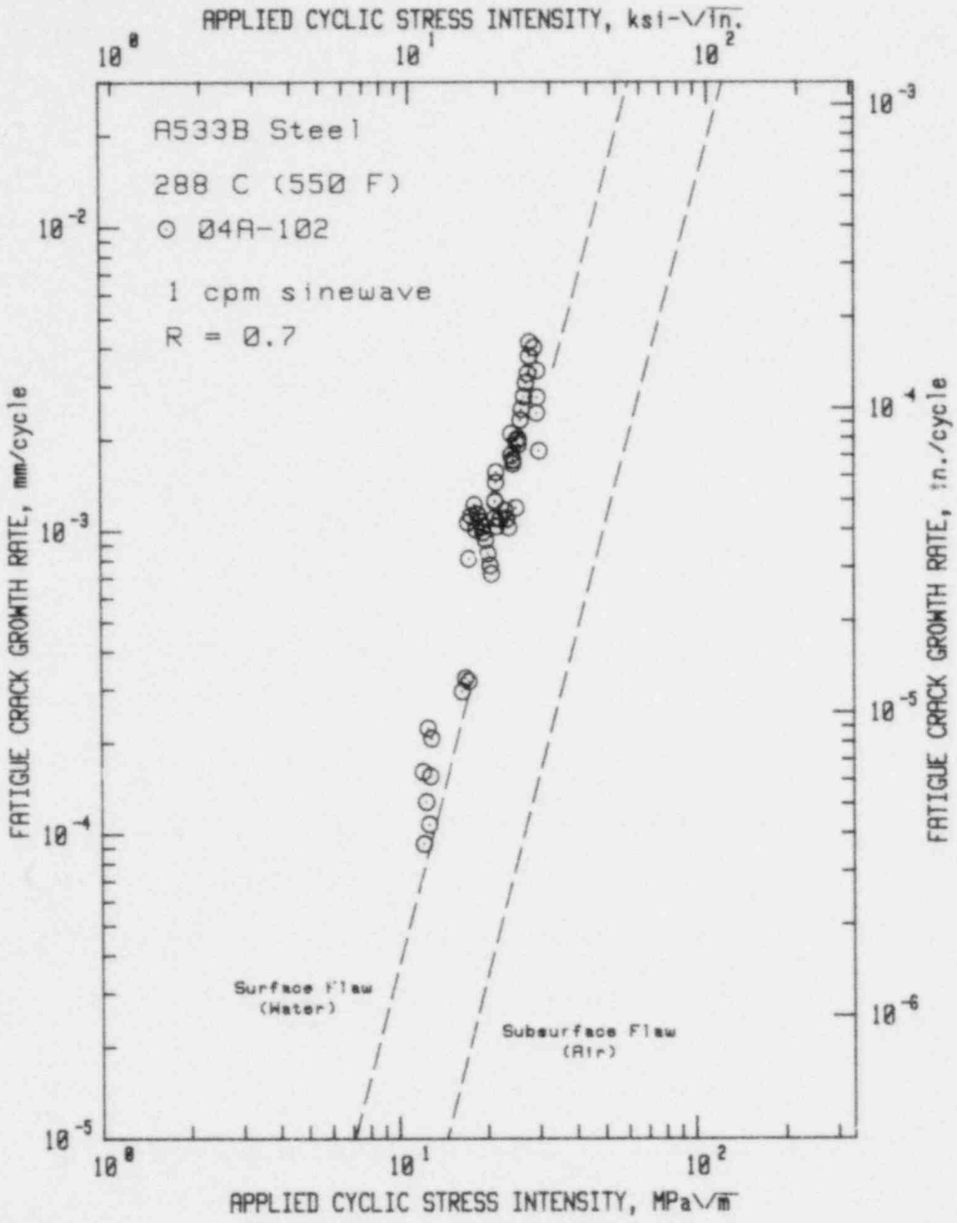

Fig. 17. Fatigue crack growth rate vs applied cyclic stress intensity factor for A533B steel in the high-temperature pressurized reactor-grade water environment-PWR conditions. As in Figs. 14 and 16, the crack growth rates are relatively high. References 49,67.

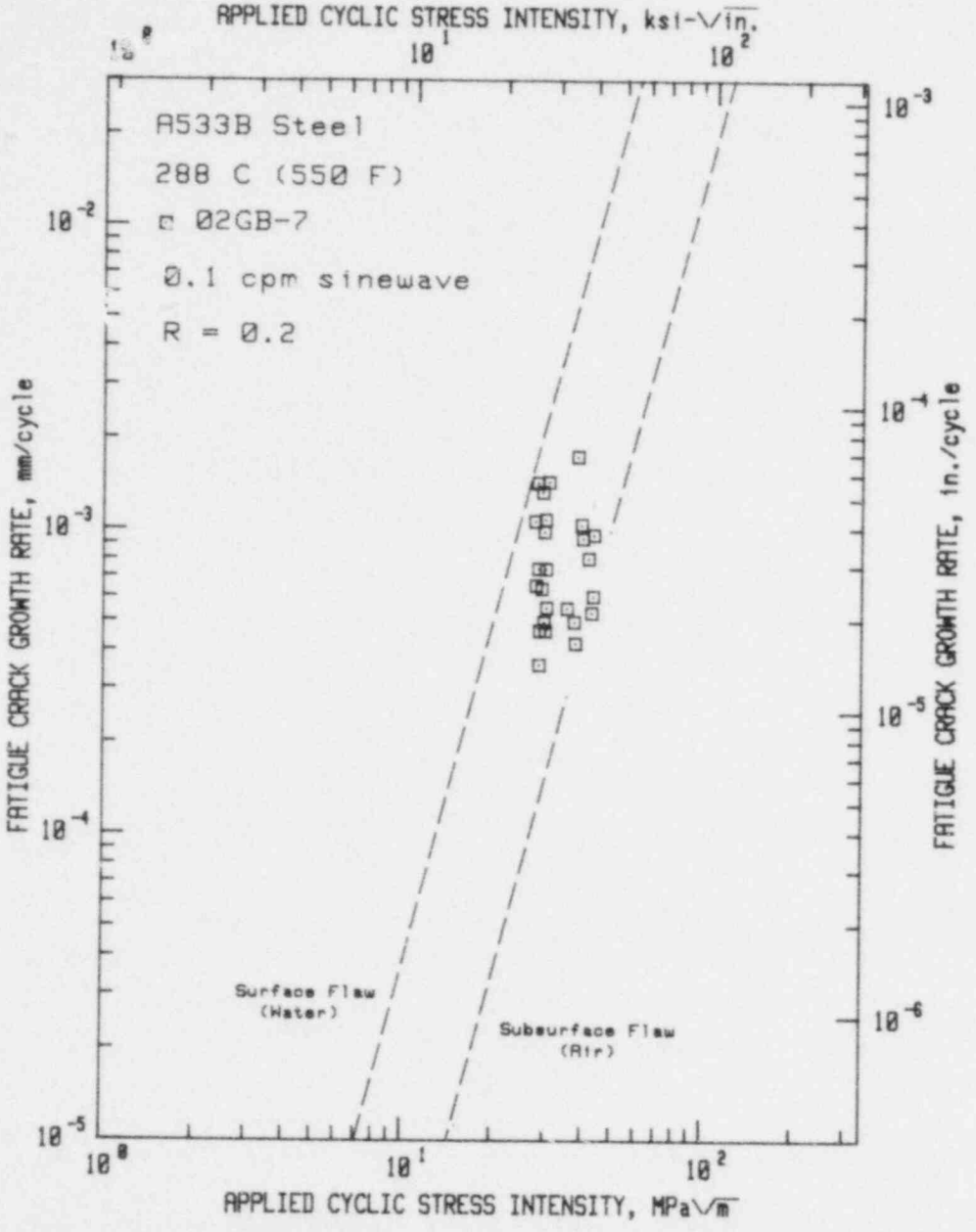

Fig. 18. Fatigue crack growth rate vs applied cyclic stress intensity factor for A533B steel in the high-temperature pressurized reactor grade water environment-PWR conditions. Although the test frequency is quite low (1.7 mHz) the low load ratio (0.2) results in crack growth rates somewhat below the ASME water default line. References 49-63.

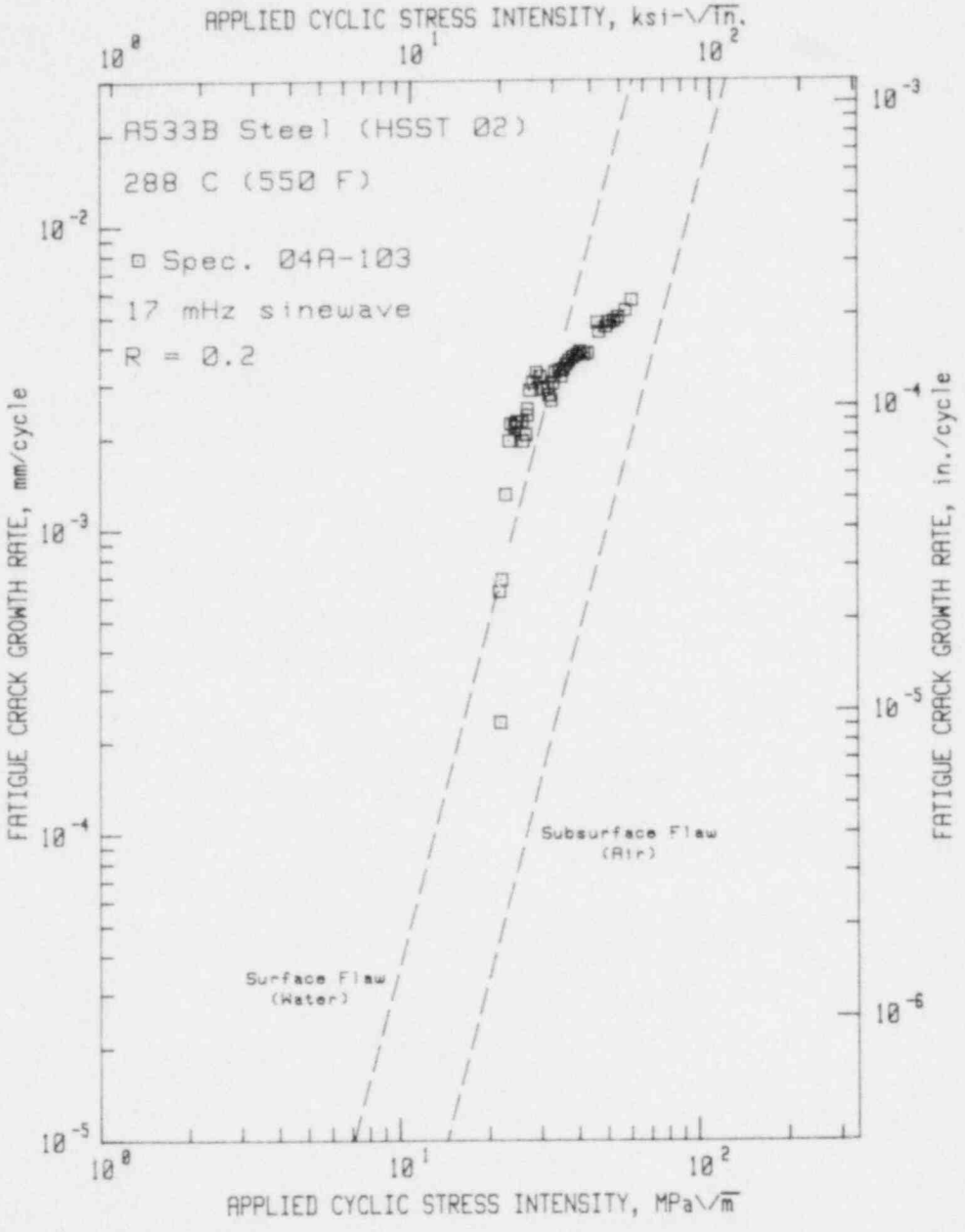

Fig. 19. Fatigue crack growth rate vs applied cyclic stress intensity factor for A533B steel in high-temperature, pressurized reactor-grade water environment-PWR conditions. For low load ratios (~0.2), this frequency and waveform (17 mHz sinusoidal) consistently produces the highest crack growth rates. This particular data set is, however, the most accelerated of the class of tests. Reference 51.

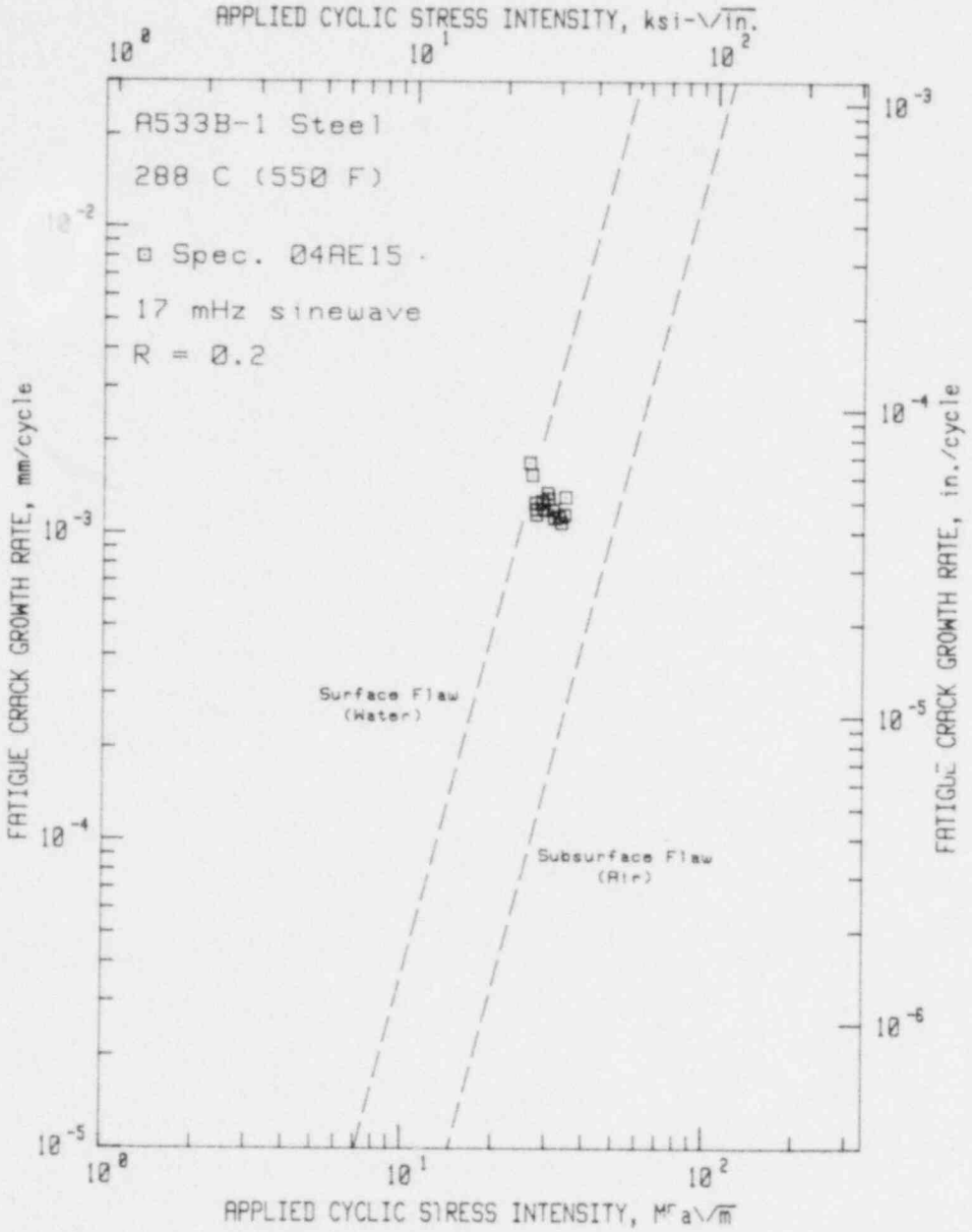

Fig. 20. Fatigue crack growth rate vs applied cyclic stress intensity factor for A533B steel in high-temperature, pressurized reactor-grade water--PWR environment. This cluster of data is consistent with the data set on the previous page, also of A533B of the same heat.Reference 62.

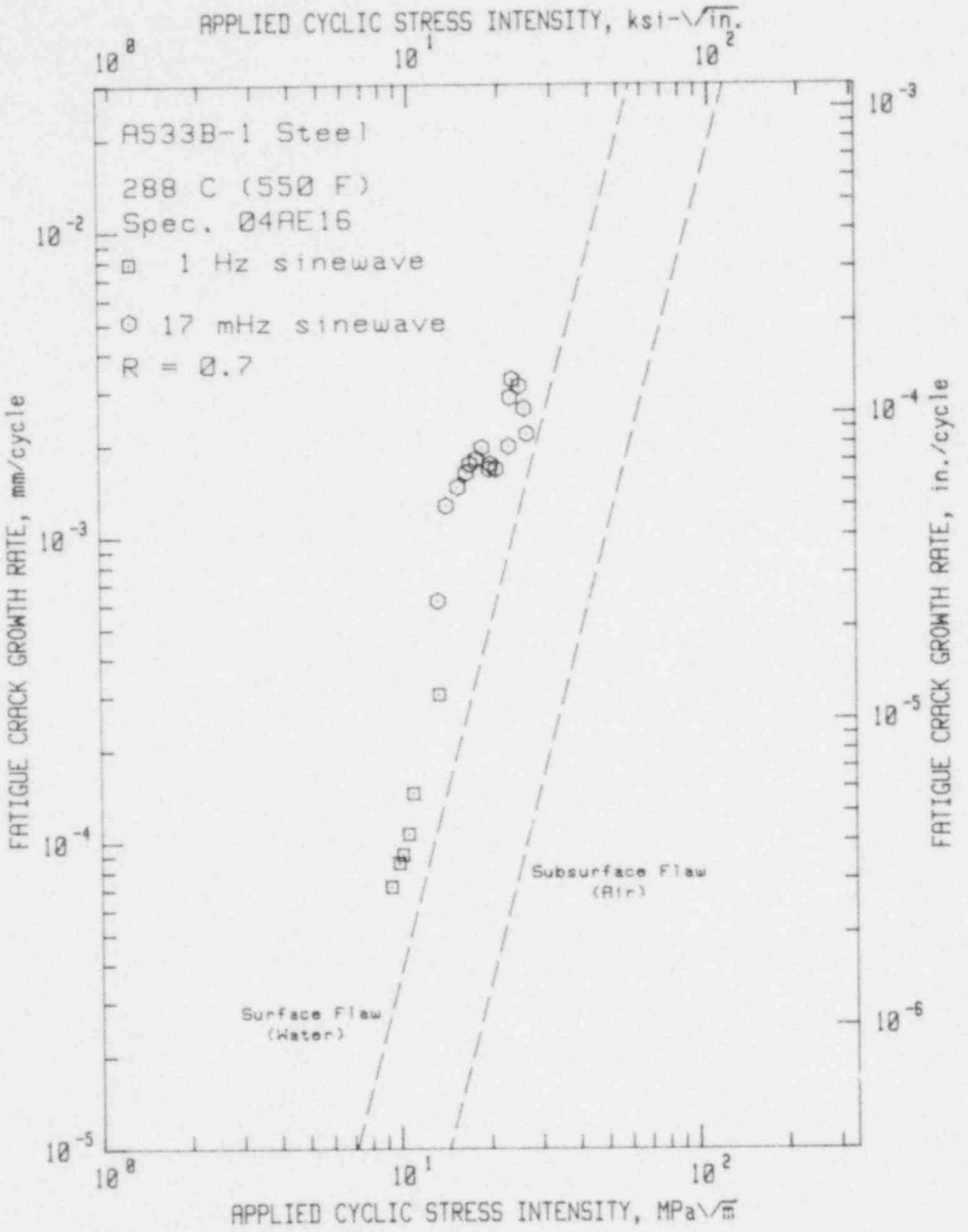

Fig. 21. Fatigue crack growth rate vs applied cyclic stress intensity factor for A533B-1 steel in high-temperature, pressurized reactor-grade water-PWR conditions. This and the following data set were produced by beginning with a few millimeters of crack extension with a relatively short period sinewave, followed by the actual test at the period (17 mHz) desired. The data agree, in most respects, with other similar data sets. Reference 62.

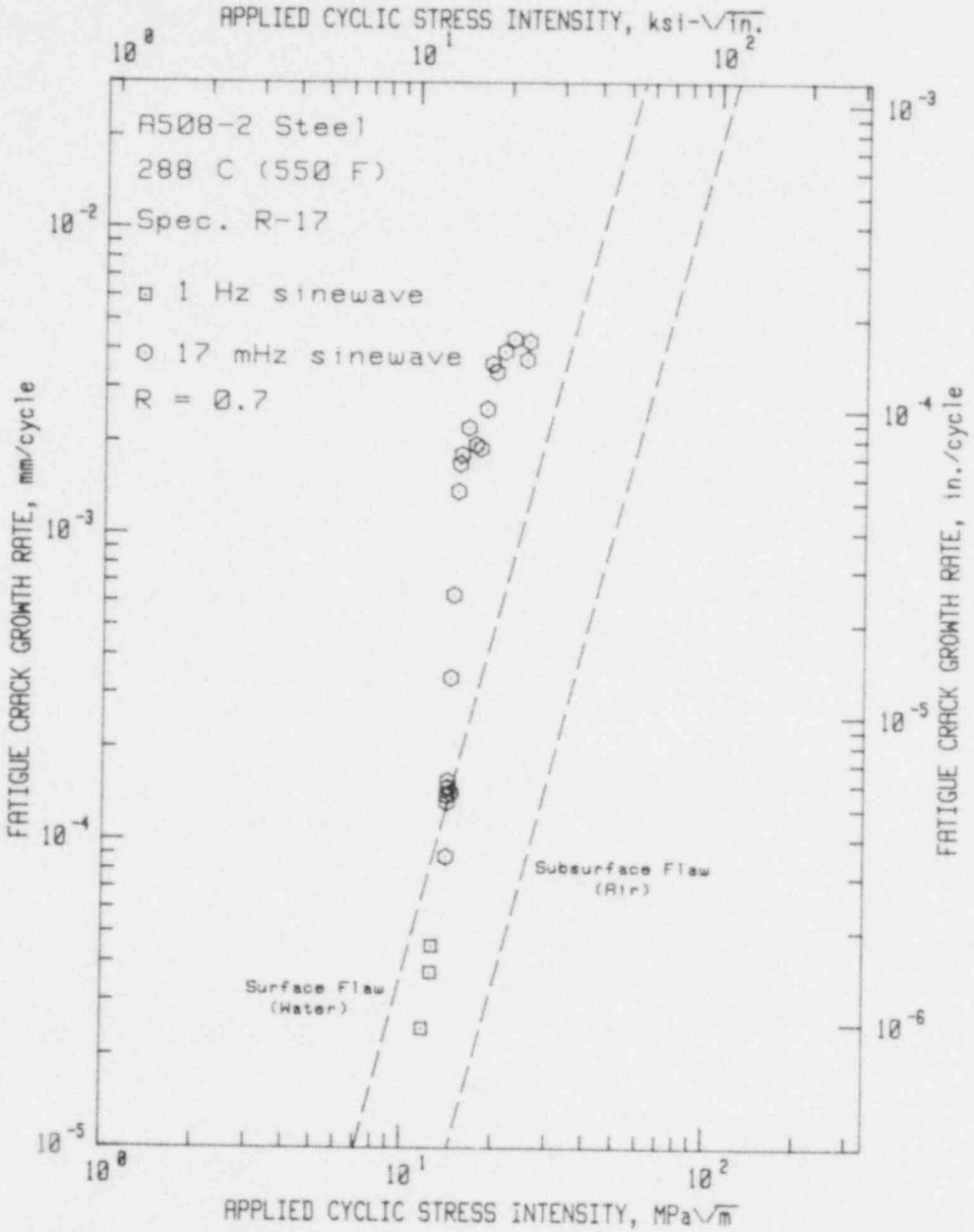

Fig. 22. Fatigue crack growth rate vs applied cyclic stress intensity factor for A508-2 steel in high-temperature, pressurized reactor-grade water—PWR conditions. See Fig. 21. Reference 62.

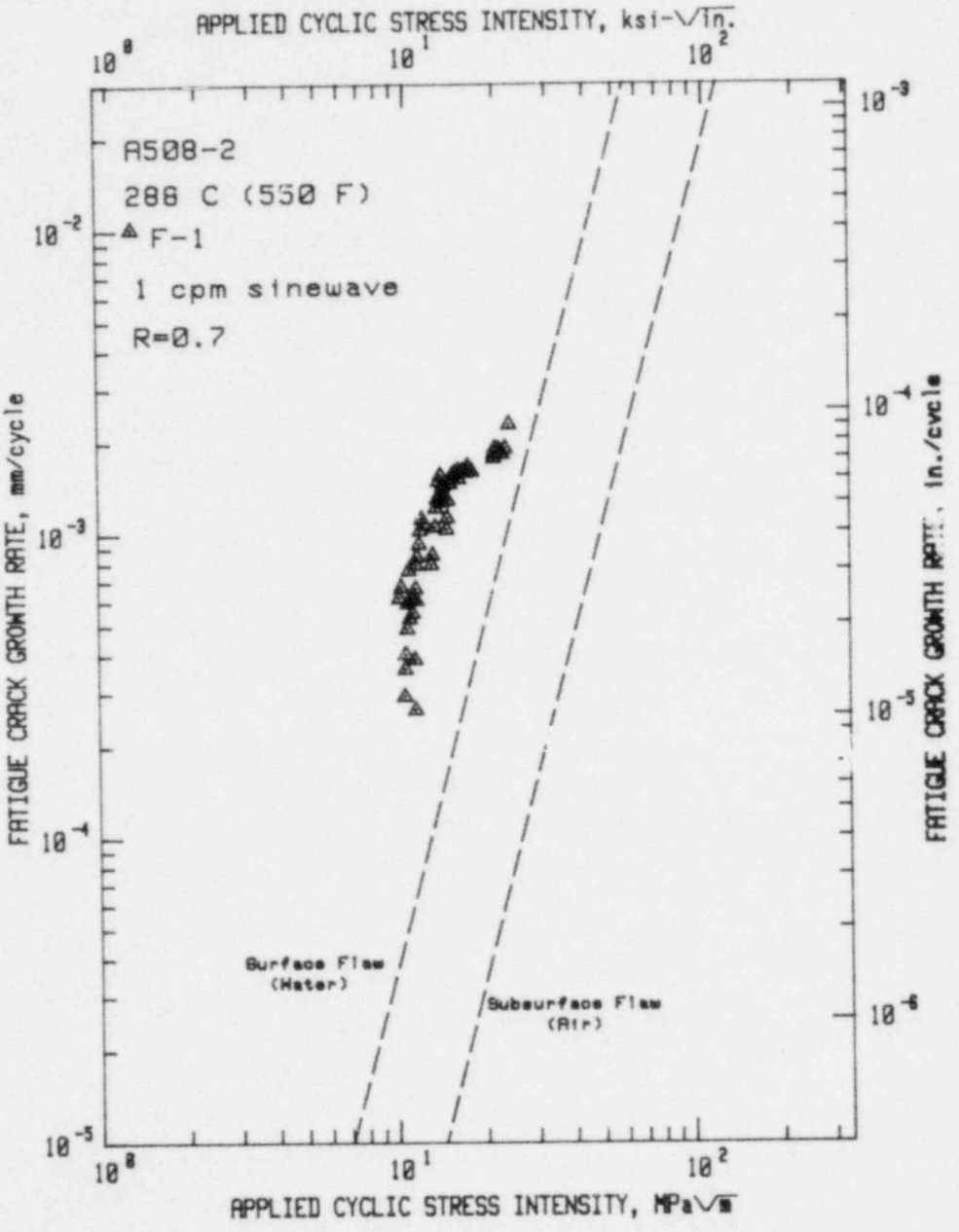

Fig. 23. Fatigue crack growth rate vs applied cyclic stress intensity factor for A508-2 forging steel in high-temperature, pressurized reactor-grade water—PWR conditions. This data set is equivalent to Fig. 14 in conditions and results. Reference 50.

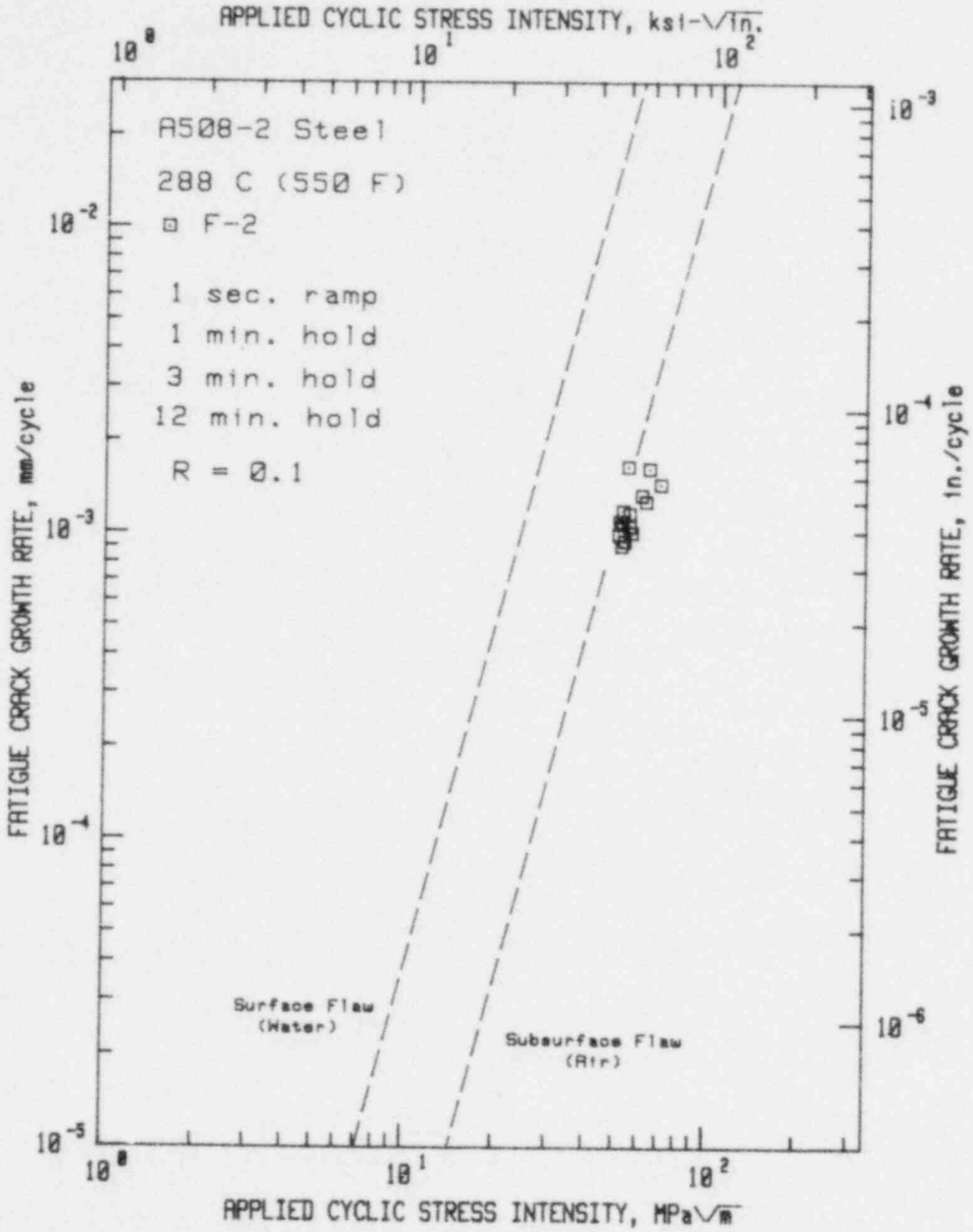

Fig. 24. Fatigue crack growth rate vs applied cyclic stress intensity factor fo A508-2 forging steel in high-temperature, pressurized reactor-grade water—PWR conditions. Most of the F-and R-series of specimen code (both A508-2 steel) in this and the following figures (25-38) resulted from tests under the NRC sponsored preliminary test matrix program carried out by NRL and Westinghouse. The crack growth rates situated near the ASME air default line, are rather low, and result from the short ramp time component. Reference 54.

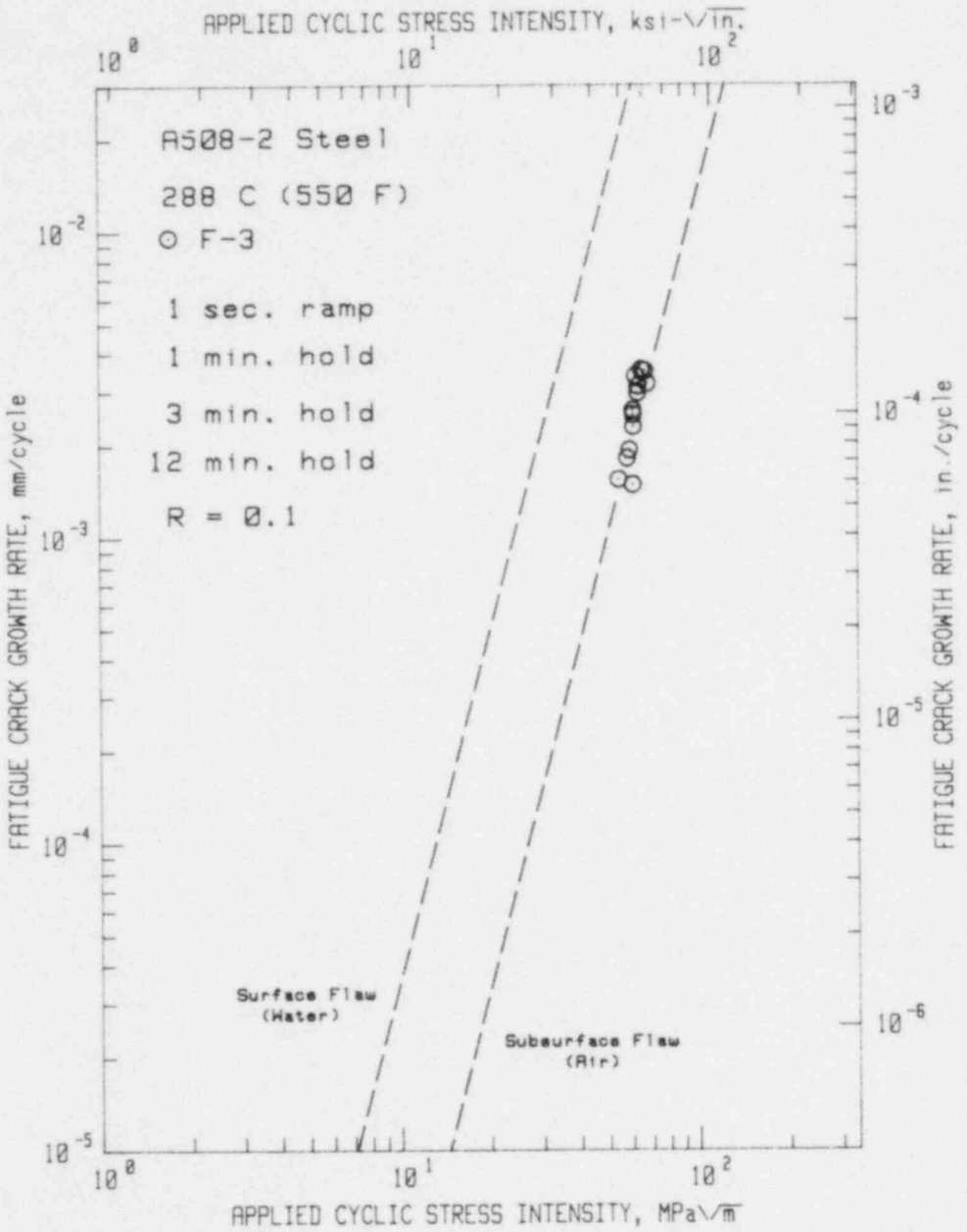

Fig. 25. Fatigue crack growth rate vs applied cyclic stress intensity factor for A508-2 forging steel in high-temperature, pressurized reactor-grade water--PWR conditions. As in Fig. 24, the short ramp time component results in relatively low crack growth rates. Reference 54.

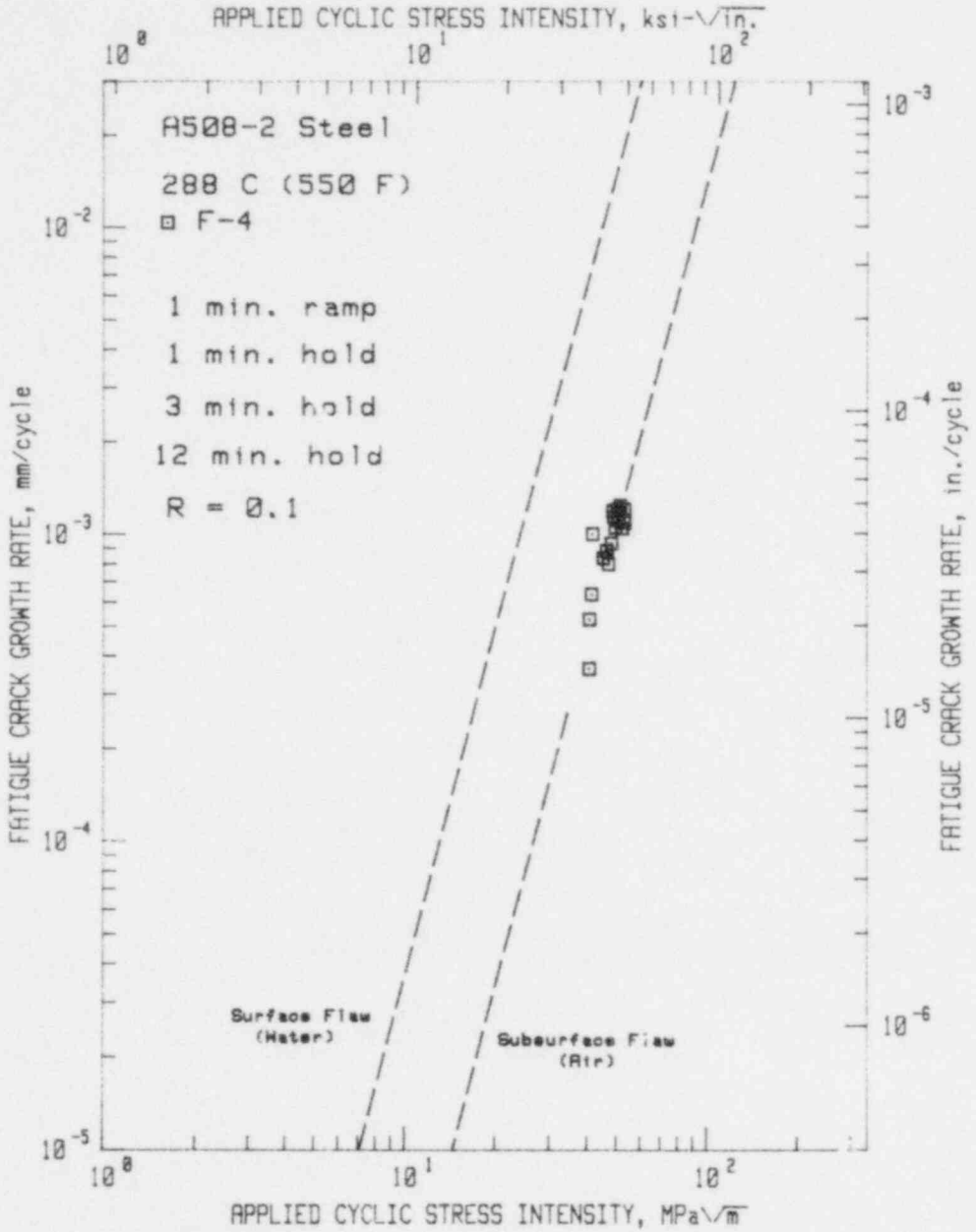

Fig. 26. Fatigue crack growth rates vs applied cyclic stress intensity factor for A508-2 forging steel in high-temperature, pressurized reactor-grade water - PWR conditions. In this figure, the growth rates are depressed to this relatively low level by oxide formation at the crack tip, or by diffusion of the hydrogen out of the plastic enclave, or both. Reference 54.

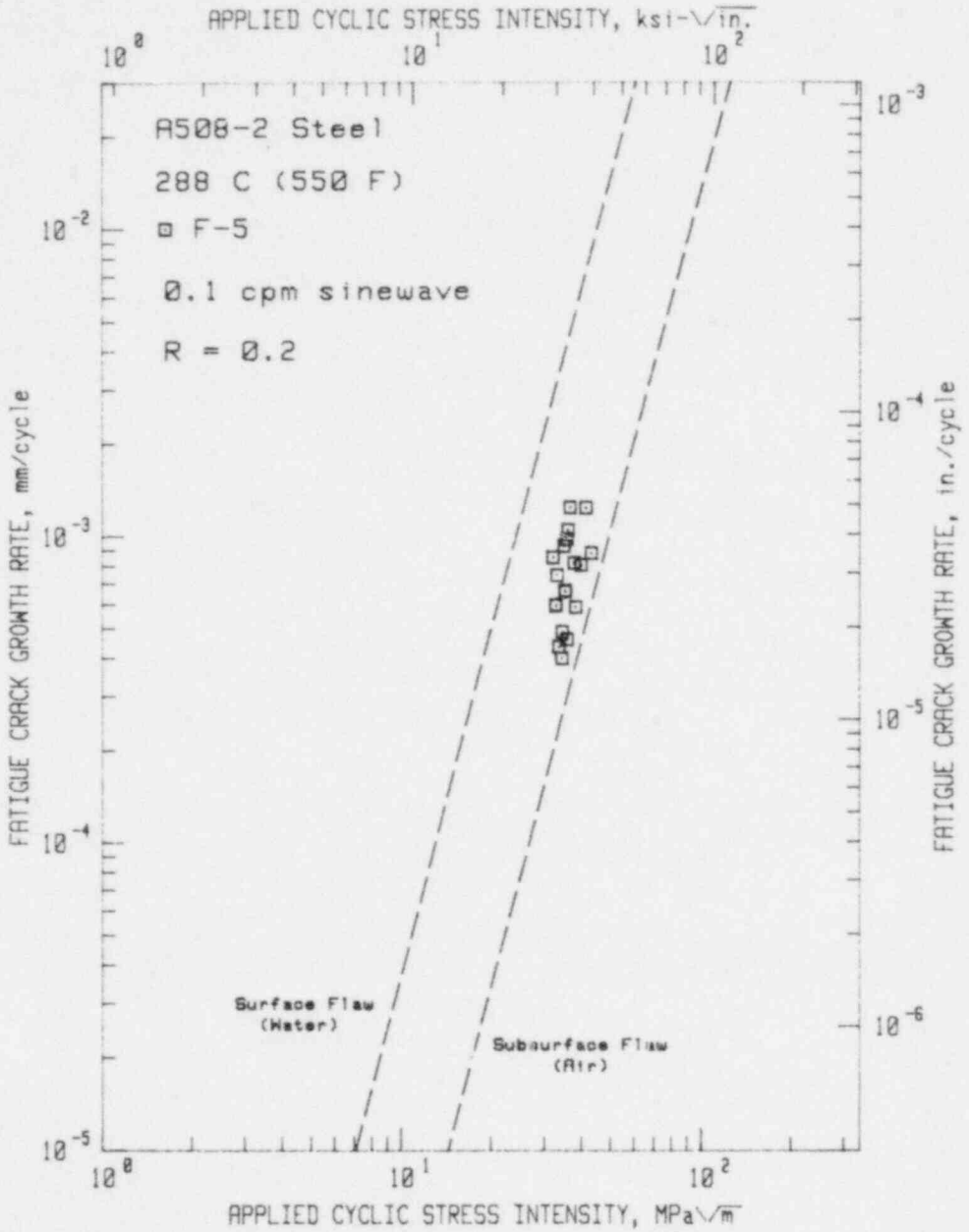

Fig. 27. Fatigue crack growth rate vs applied cyclic stress intensity factor for A508-2 forging steel in high-temperature, pressurized, reactor-grade water—PWR conditions. This data, developed for a very low frequency sinusoidal waveform (1.7 mHz) is not as accelerated as data for a 17 mHz frequency. Reference 53.

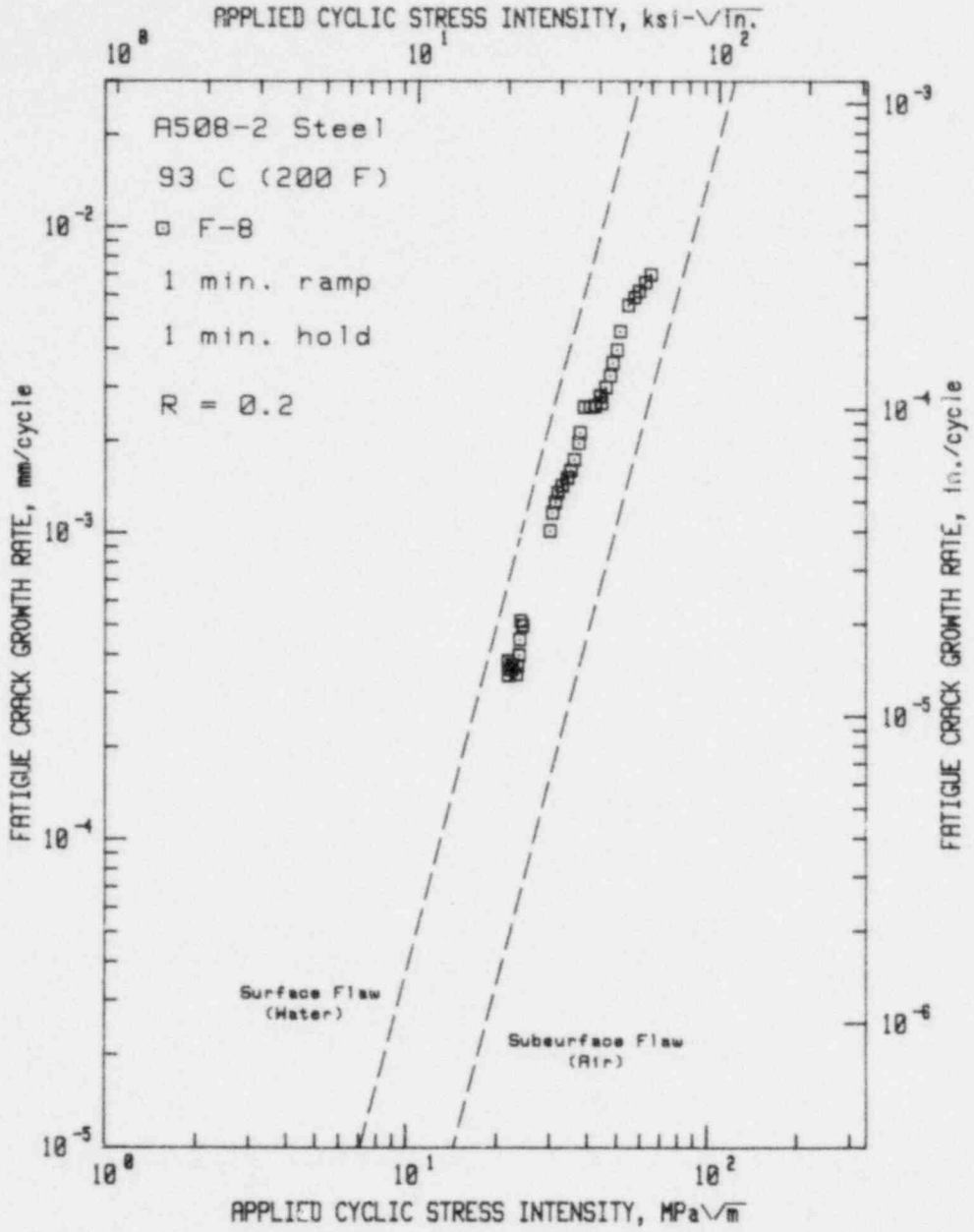

Fig. 28. Fatigue crack growth rate vs applied cyclic stress intensity factor for A508-2 forging steel in low temperature, reactor-grade water—PWR conditions. For this temperature, the 60 sec. ramp time results in a substantial acceleration of growth rates. It is likely that hydrogen accumulates in the plastic enclave and cannot diffuse away at this relatively low temperature. Reference 54.

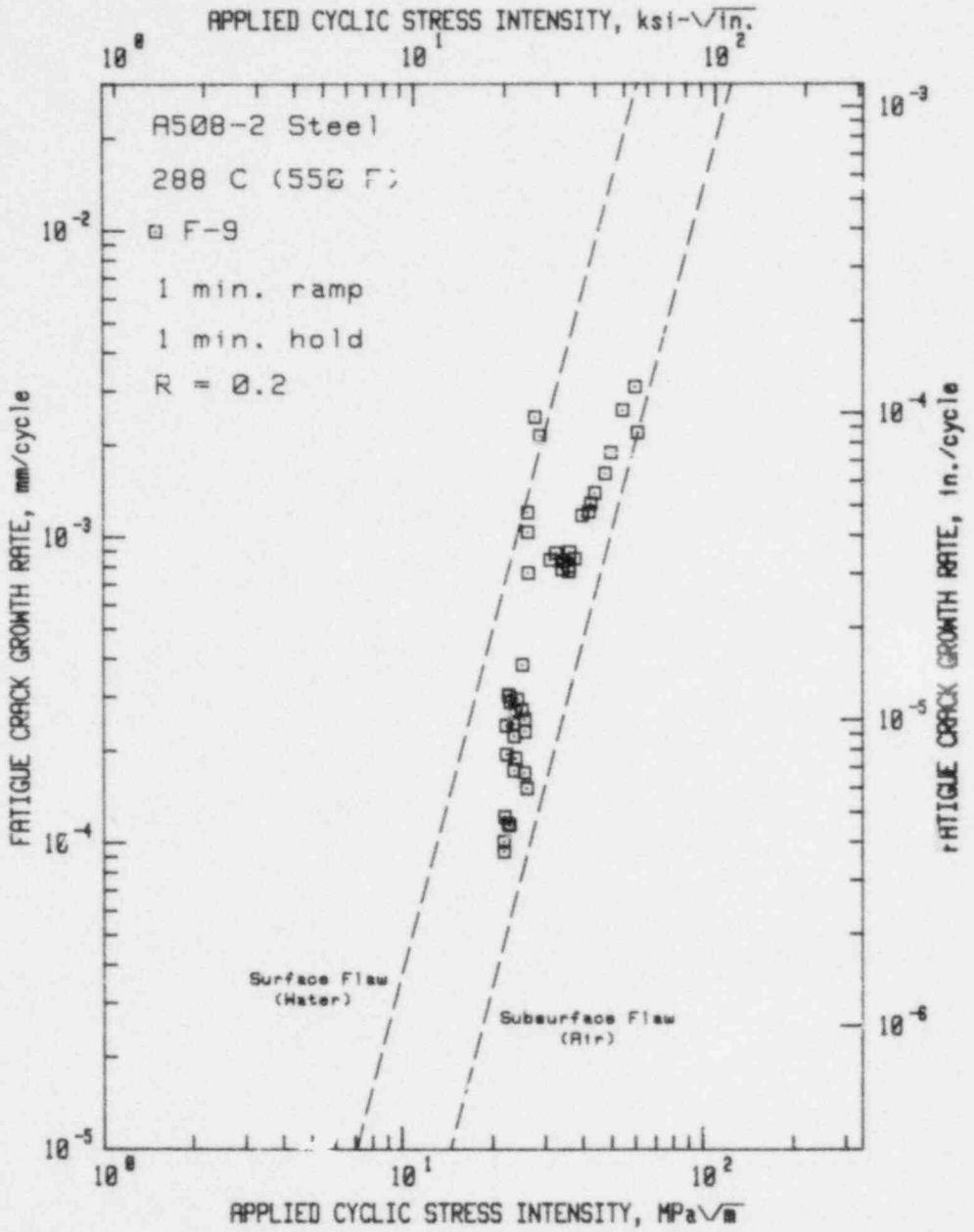

Fig. 29. Fatigue crack growth rate vs applied cyclic stress intensity factor for A508-2 forging steel in high-temperature, pressurized reactor-grade water—PWR conditions. According to the model proposed in section III, these growth rates would be expected to reside on the ASME air default line. This is not quite the case, however they are, on the average, a factor of two above this level, which is generally considered within the scatter band for FCGR tests. References 55,59.

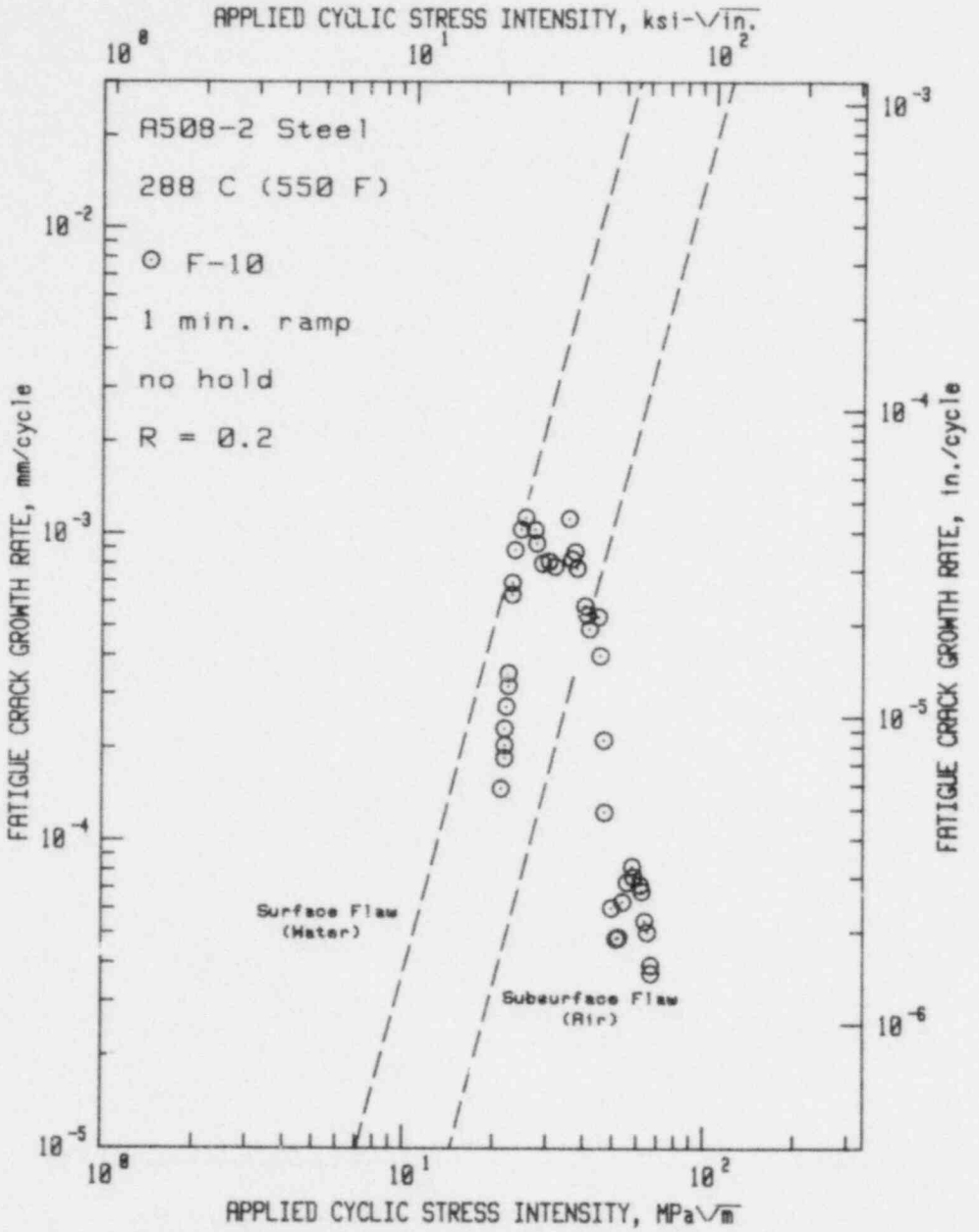

Fig. 30. Fatigue crack growth rate vs applied cyclic stress intensity factor for A508-2 forging steel in high-temperature, pressurized, reactor-grade water--PWR conditions. The large acceleration at the beginning of the test, and the large retardation of growth rates for values of 35-65 MPa m are both unusual charcteristics of these tests. In this case the data are well-supported by microscopic da/dN examination (striation measurements) and the correlation was found to be excellent. References 58 and 59.

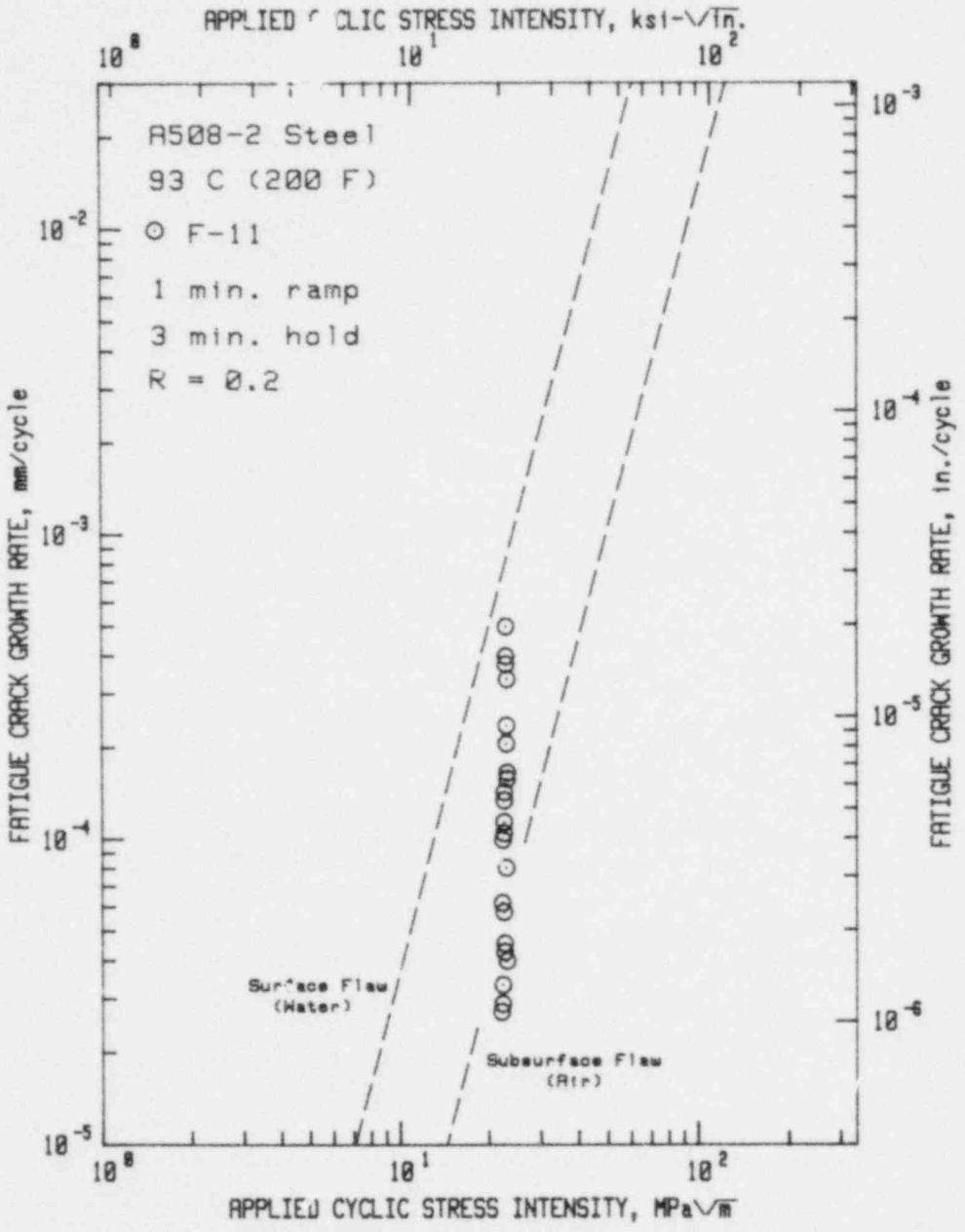

Fig. 31. Fatigue crack growth rate vs applied cyclic stress intensity factor for A508-2 forging steel in high-temperature, pressurized reactor-grade water—PWR conditions. This test was terminated prematurely due to equipment malfunction. Reference 58.

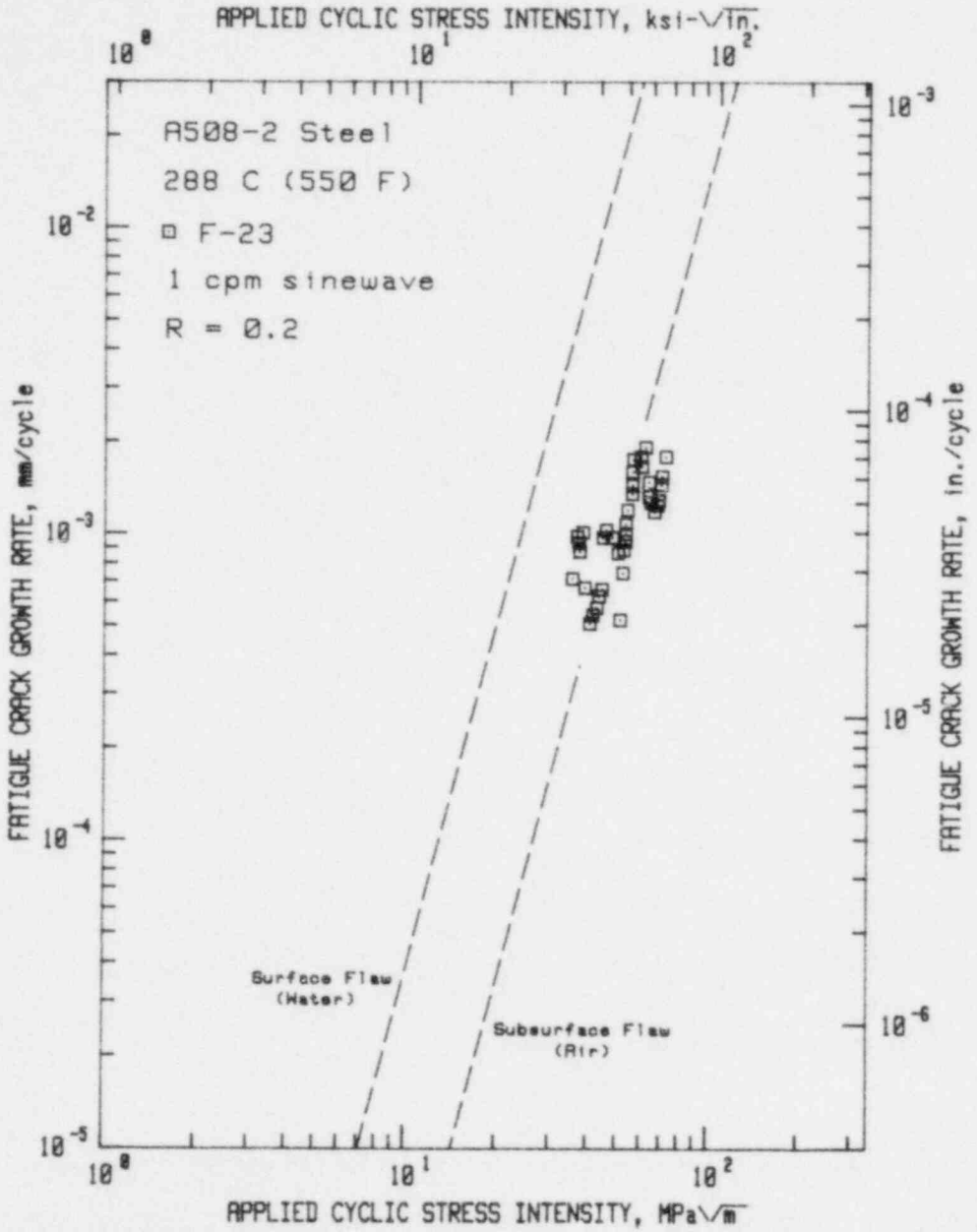

Fig. 32. Fatigue crack growth rate vs applied cyclic stress intensity factor for A508-2 forging steel in high-temperature, pressurized reactor-grade water—PWR conditions. Data for a 100 mm thick specimen (4T-CT). This waveform results in rather high growth rates for 25 and 50 mm thick specimens. The autho speculate that the thickness of the specimen results in crack tip envi ments of a substantially different character. Reference 53.

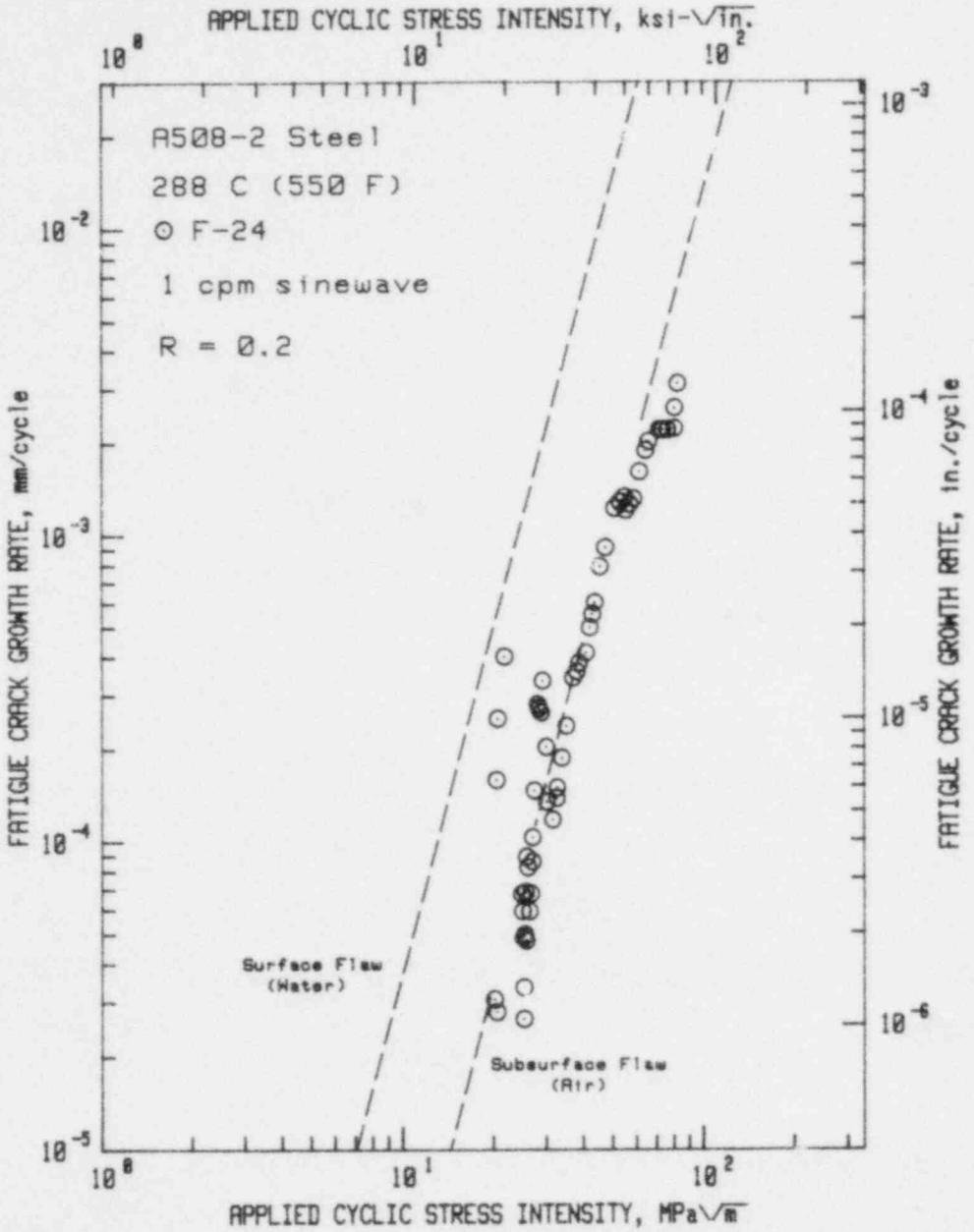

Fig. 33. Fatigue crack growth rate vs applied cyclic stress intensity factor for A508-2 forging steel in high-temperature, pressurized reactor-grade water--PWR conditions. Same test parameters as for Fig. 32. Reference 57.

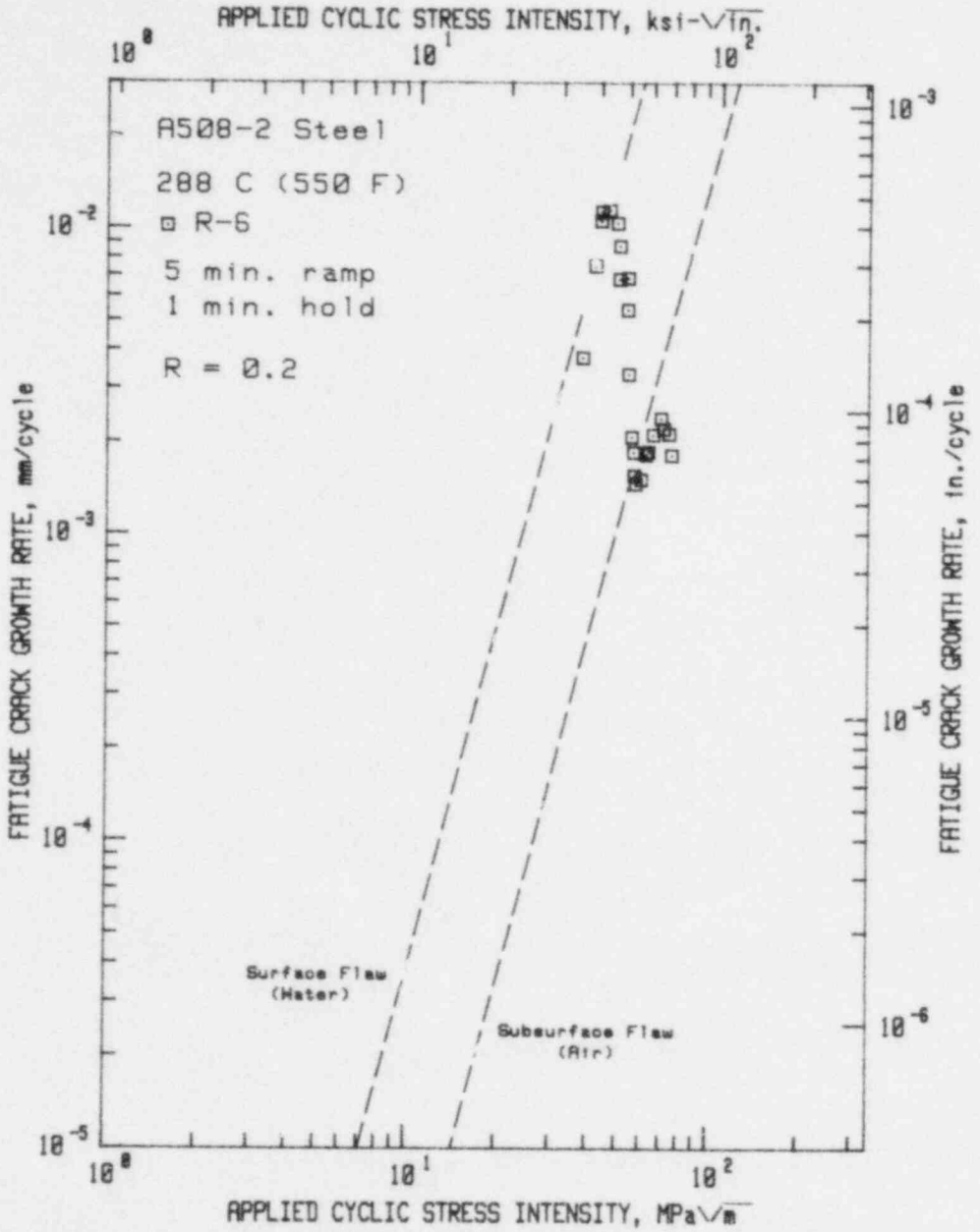

Fig. 34. Fatigue crack growth rate vs applied cyclic stress intensity factor for A508-2 forging steel in high-temperature, pressurized reactor-grade water--PWR conditions. The NRL data for this same waveform/material/temperature combination is decidedly in the low growth rate category. See Fig. 4. References 58 and 59.

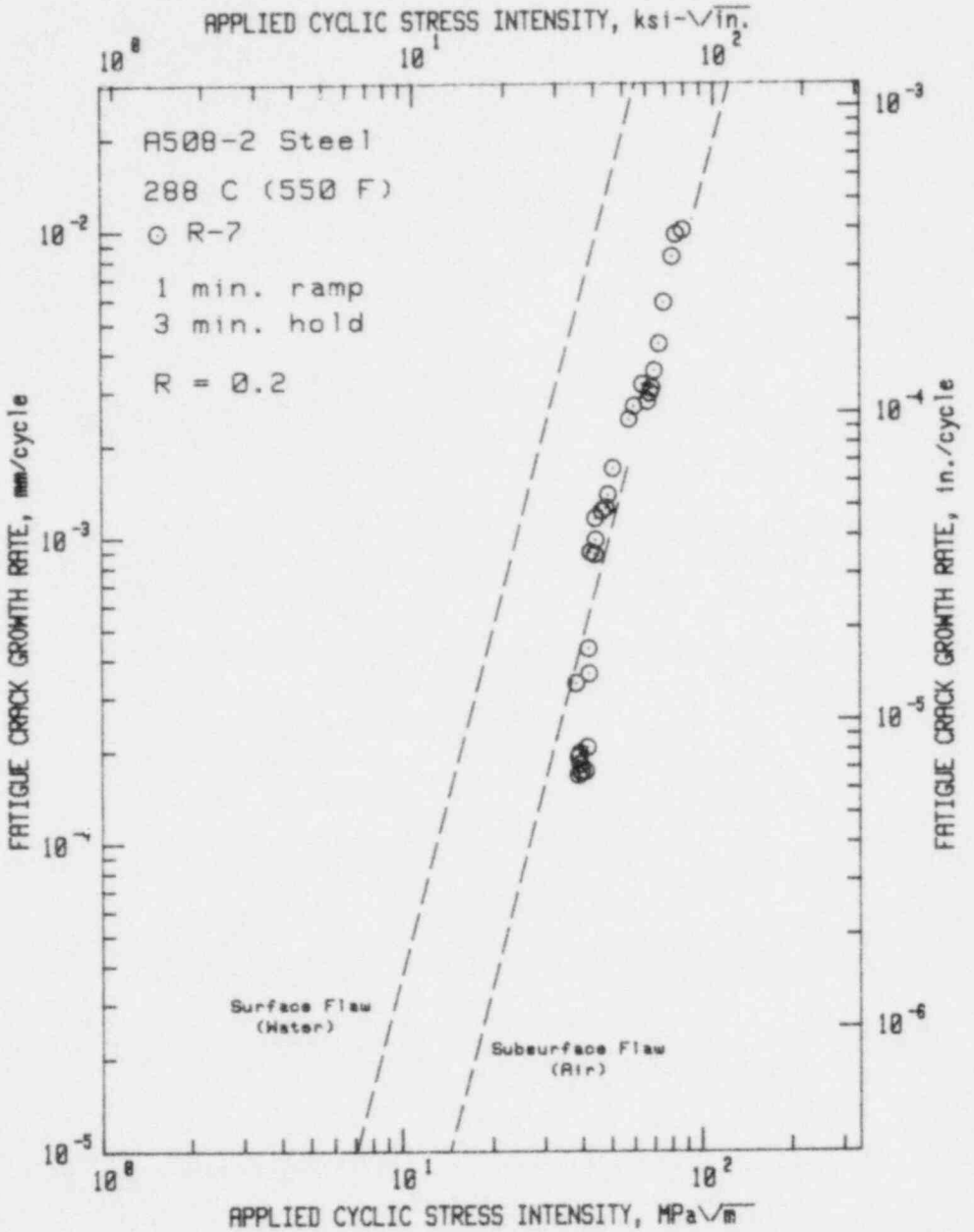

Fig. 35. Fatigue crack growth rate vs applied cyclic stress intensity factor for A508-2 forging steel in high-temperature, pressurized reactor-grade water—PWR conditions. In accordance with the proposed model, these growth rates should be, and are, in the low growth rate category. Reference 59.

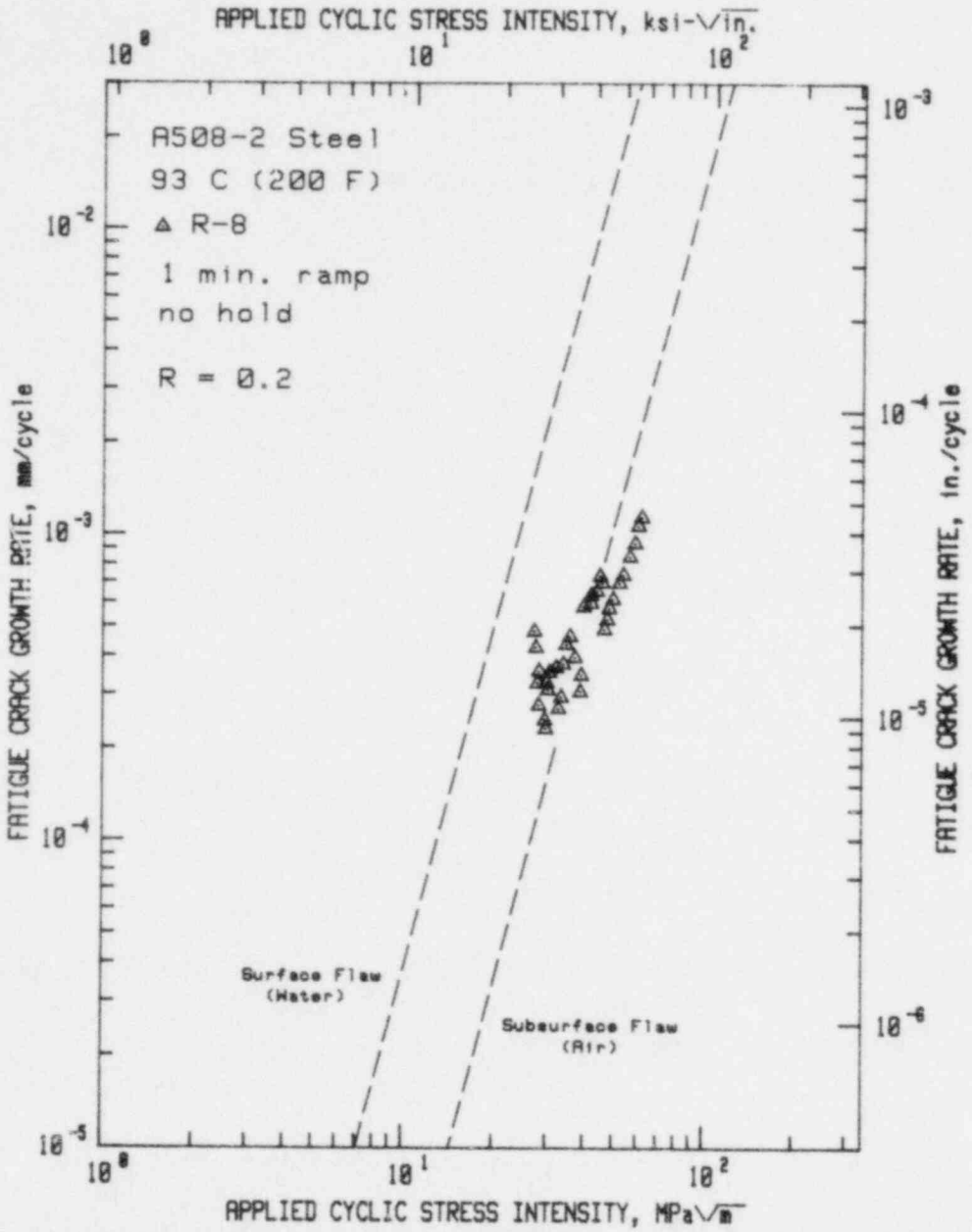

Fig. 36. Fatigue crack growth rate vs applied cyclic stress intensity factor for A508-2 forging steel in low-temperature, reactor-grade water—PWR conditions. An NRL test for the same material/temperature/environment combination resulted in fairly high growth rates. Reference 58.

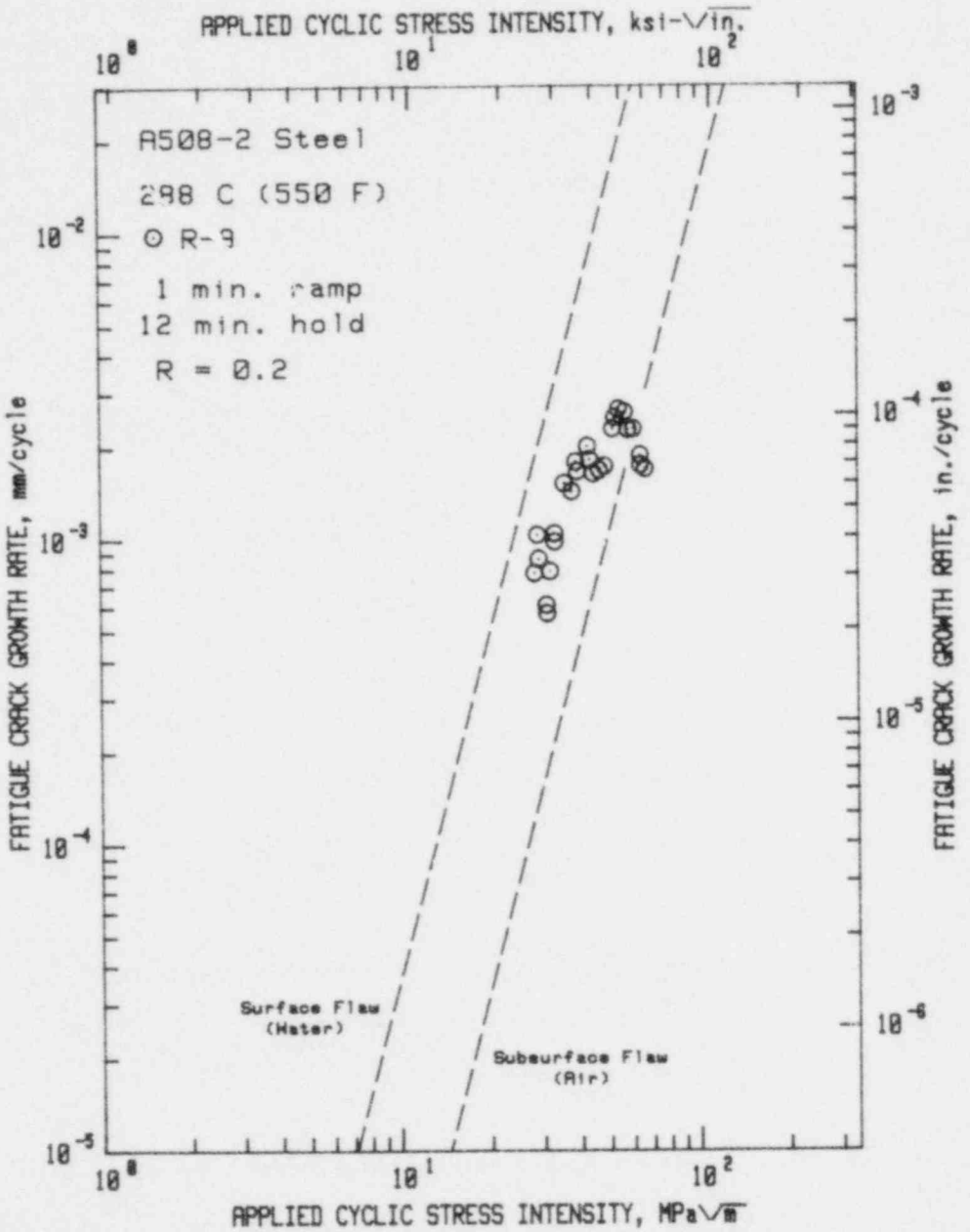

Fig. 37. Fatigue crack growth rate vs applied cyclic stress intensity factor for A508-2 forging steel in the high temperature pressurized reactor-grade water--PWR conditions. Based on the proposed model, these FCGR's would be expected to reside in the low growth rate category. This data does not appear to agree with that hypothesis or with the data from Fig. 26, for this identical waveform, and nearly equal load ratios. Reference 61.

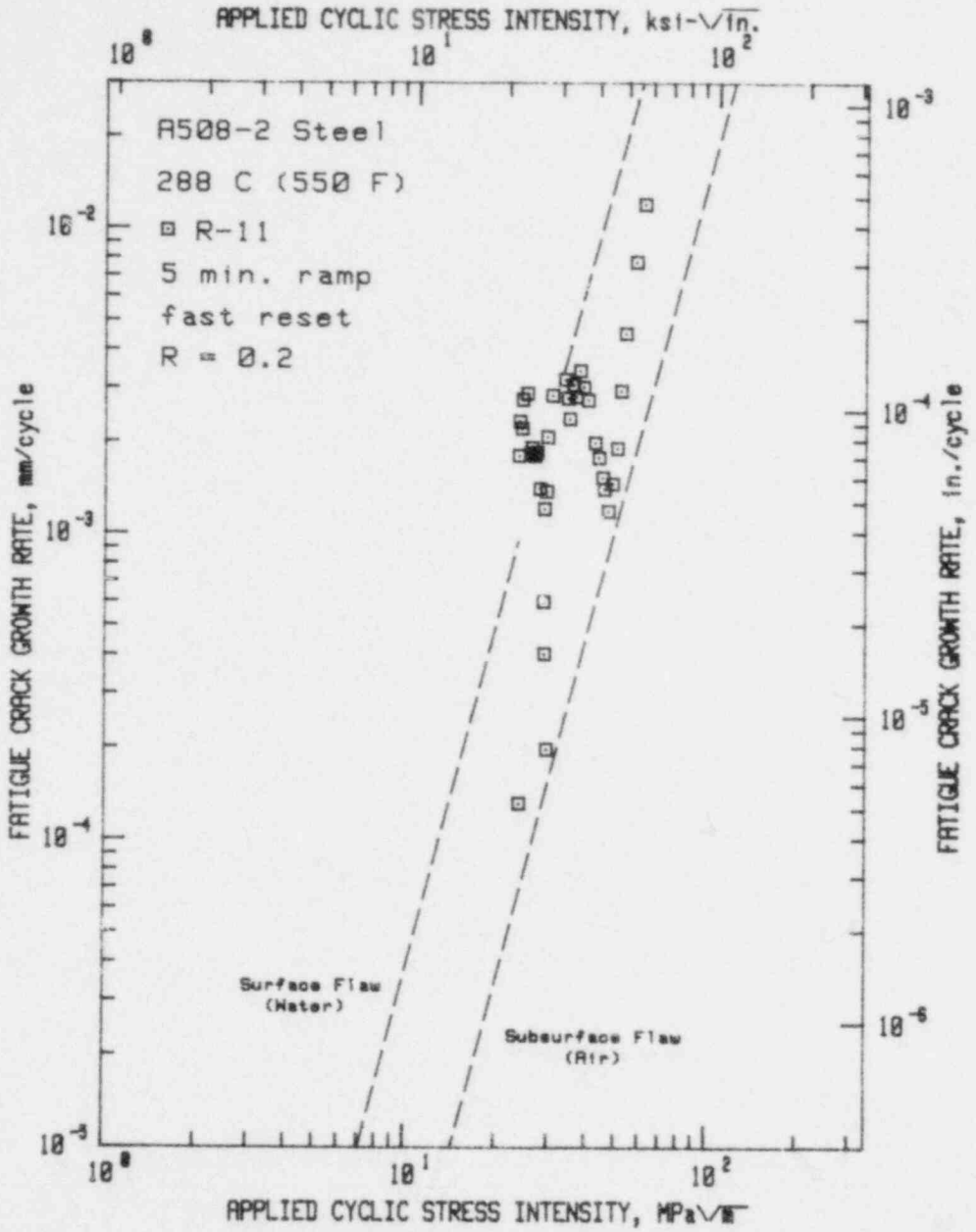

Fig. 38. Fatigue crack growth rate vs applied cyclic stress intensity factor for A508-2 forging steel in the high-temperature pressurized reactor-grade water--PWR conditions. FCGR data for this long ramp time would be expected to fall in the low growth rate category over the entire ΔK range. References 60,61.

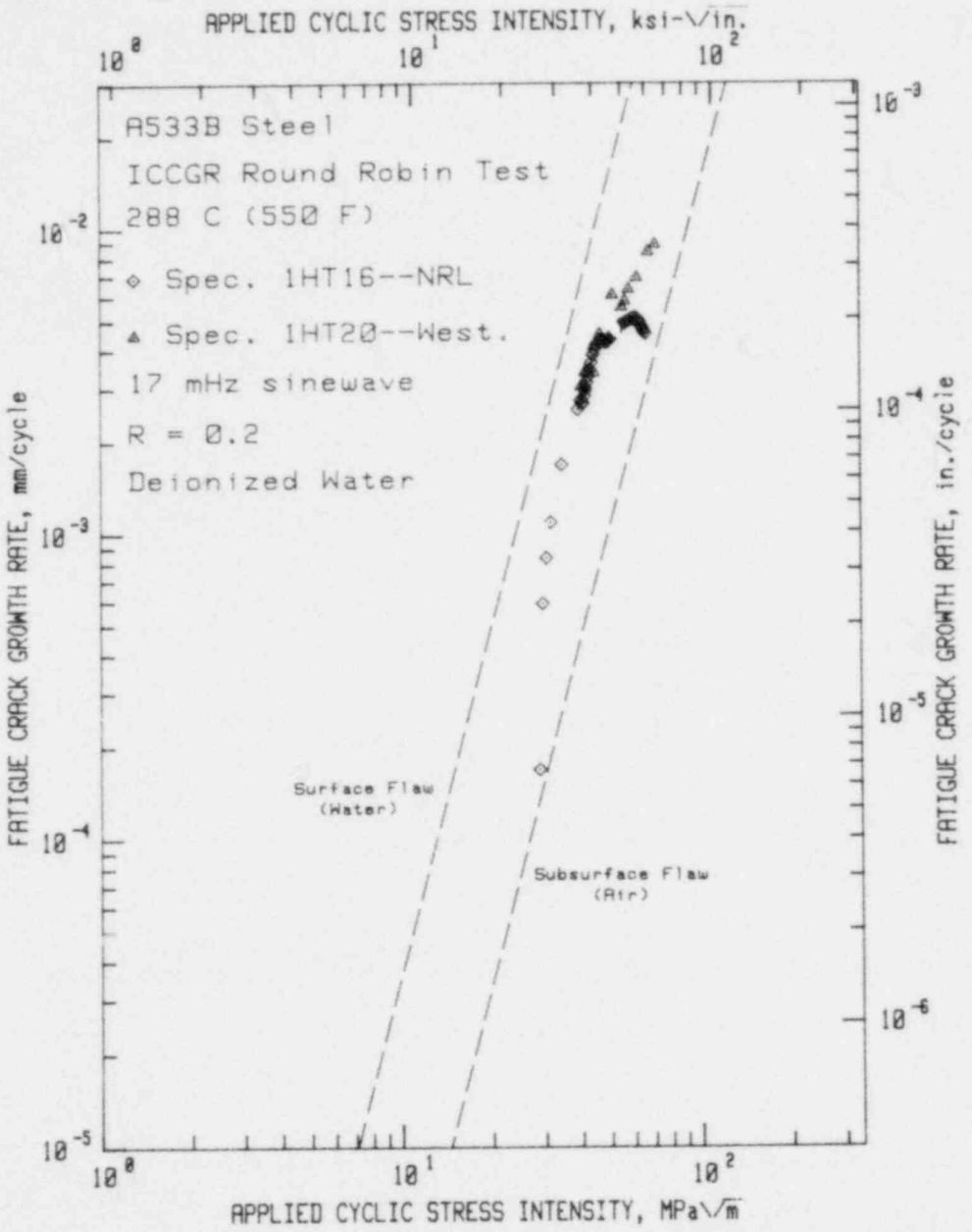

Fig. 39. Fatigue crack growth rate vs applied cyclic stress intensity factor for A533B steel in high-temperature, pressurized, reactor-grade water. These results represent NRL and Westinghouse data from the first round robin test of the International Cyclic Crack Growth Rate (ICCGR) cooperative group. This data compares very well with other 17 mHz data found in Figs. 11, 12, 19, 20, 40 and 58.

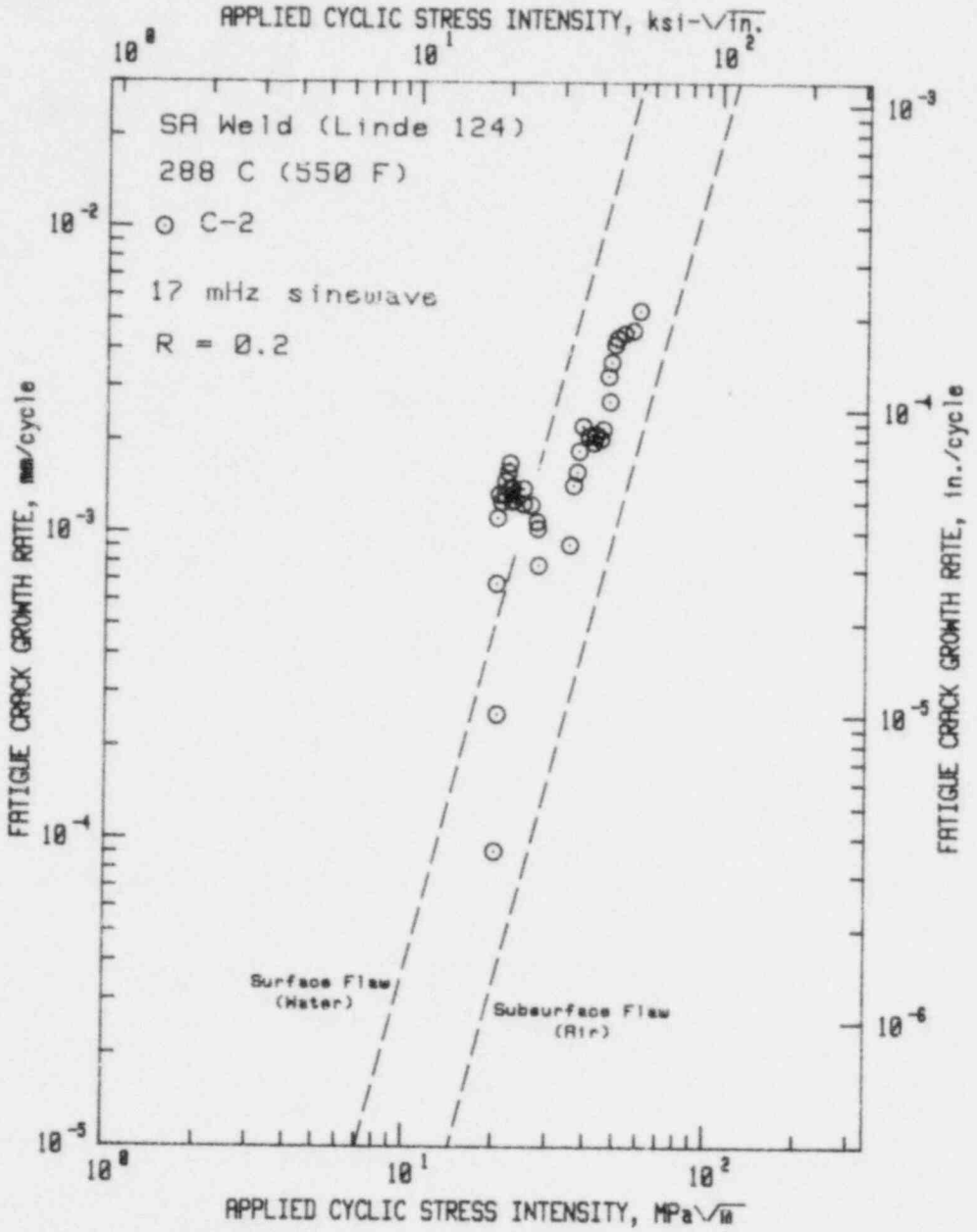

Fig. 40. Fatigue crack growth rate vs applied cyclic stress intensity factor for submerged arc deposited weld metal with Linde 124 flux in high-temperature, pressurized reactor-grade water environment—PWR conditions. This figure, Figs. 43 and 44, and 46 all exhibit a strong acceleration at start-up, followed by a decay to a more or less power law crack growth relationship. Reference 51.

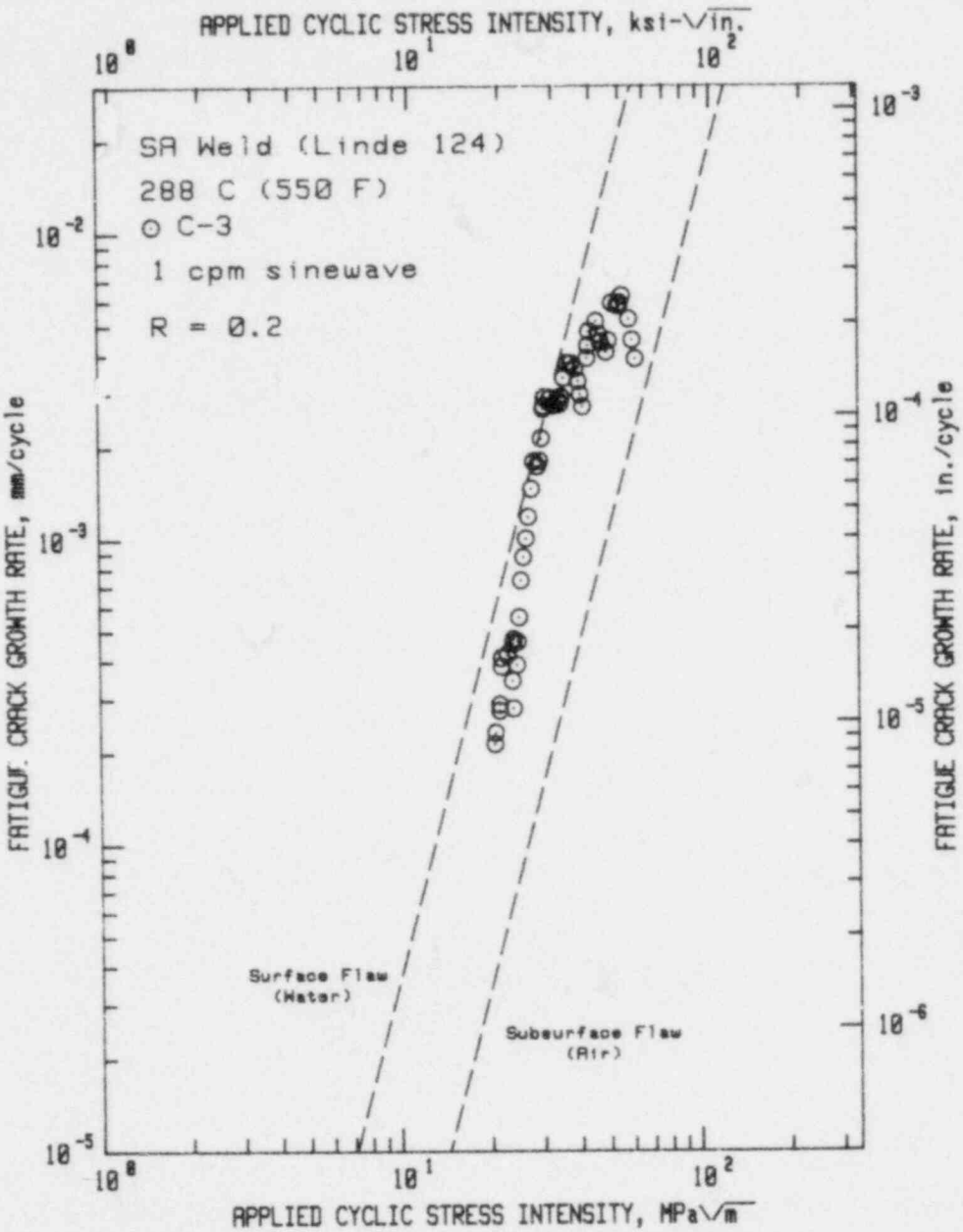

Fig. 41. Fatigue crack growth rate vs applied cyclic stress intensity factor for submerged arc deposited weld metal with Linde 124 flux in the high-temperature, pressurized reactor-grade water--PWR conditions. As for other 17 mHz sinewave tests, this data resides fairly high as compared with other tests for similarly low load ratios (R=0.2). Reference 52.

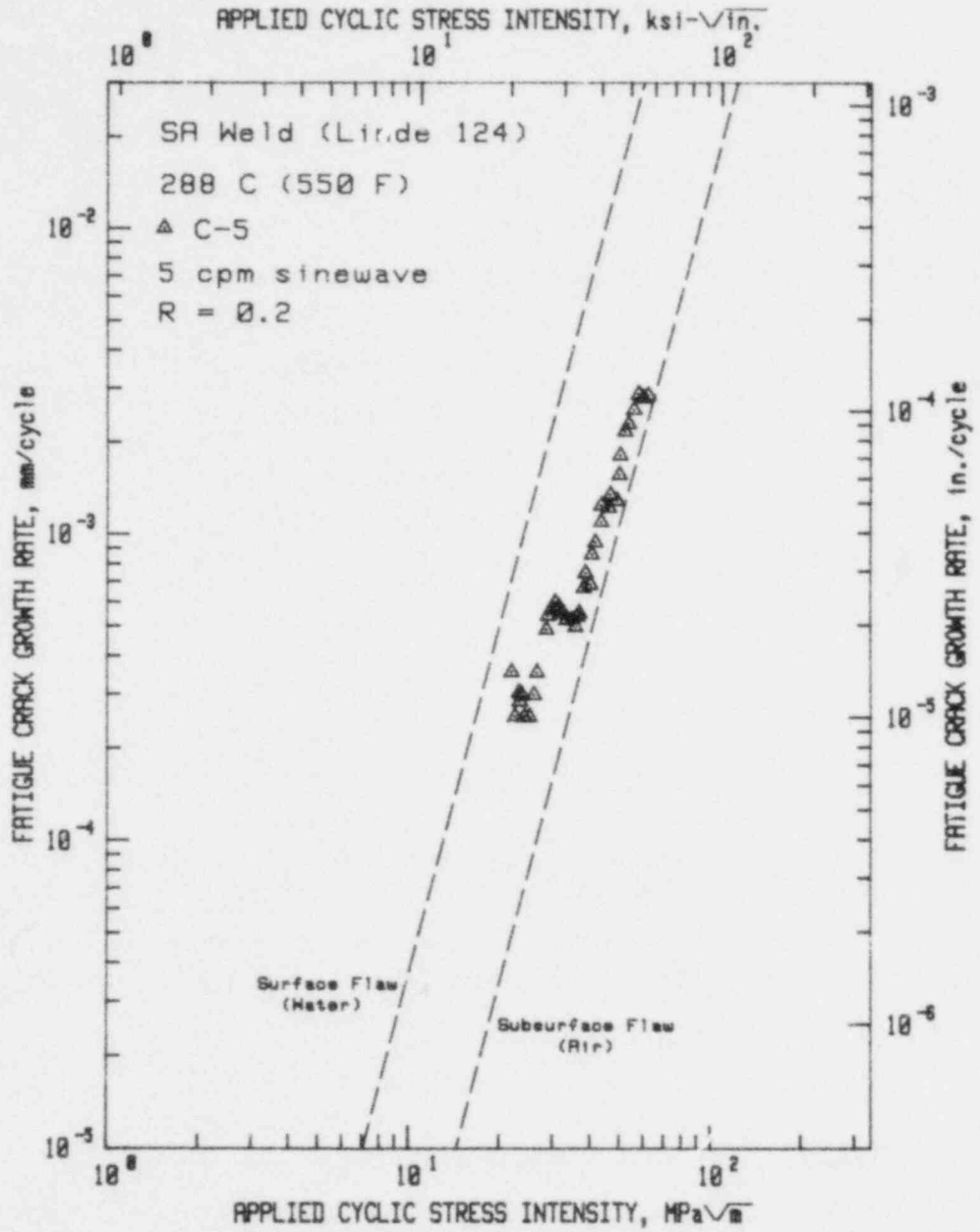

Fig. 42. Fatigue crack growth rate vs applied cyclic stress intensity factor for submerged arc deposited weld metal with Linde 124 flux in the high-temperature, pressurized reactor-grade water—PWR conditions. Compared with the previous figure, this higher frequency results in a lower crack growth rate. Reference 53.

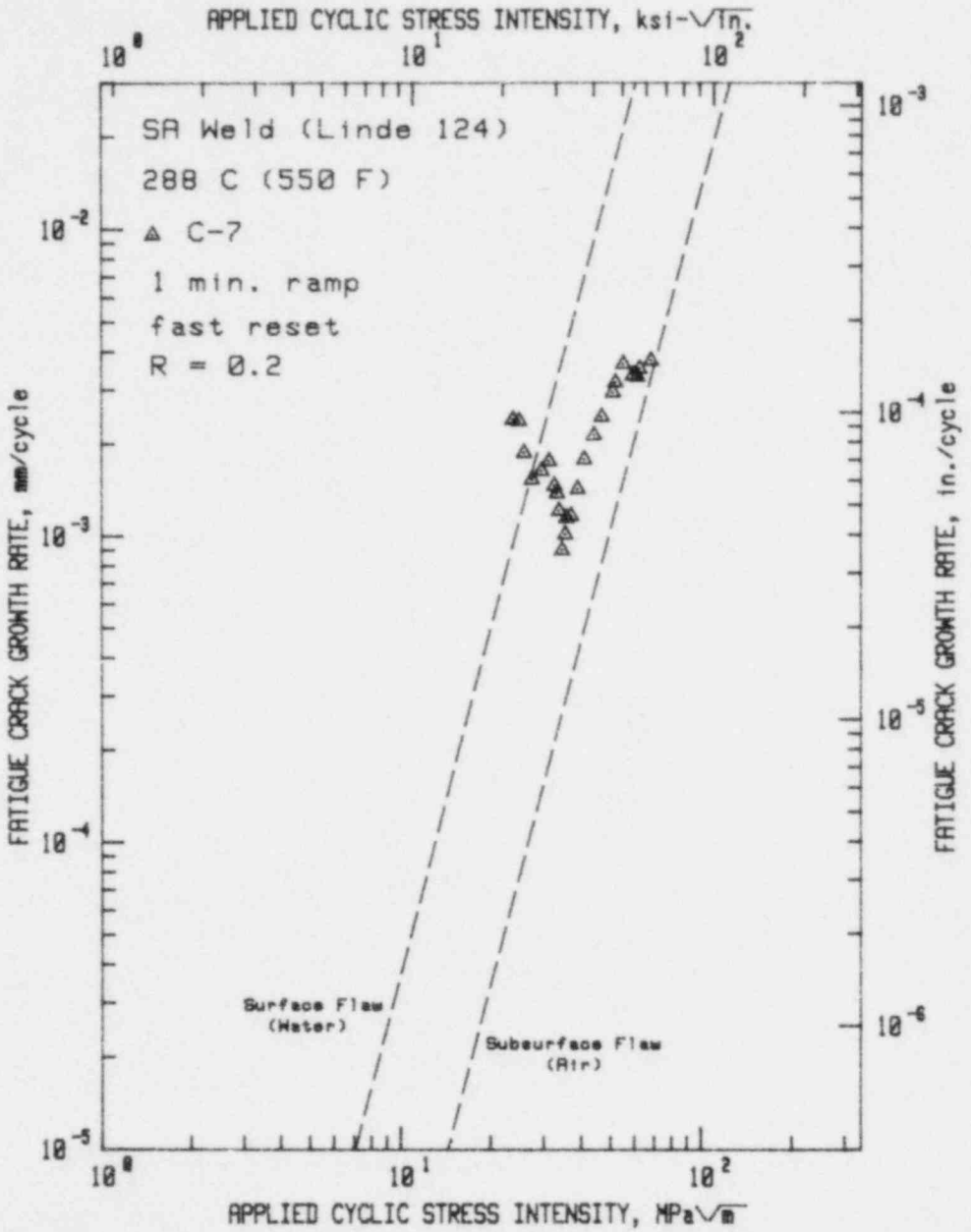

Fig. 43. Fatigue crack growth rate vs applied cyclic stress intensity factor for submerged arc deposited weld metal with Linde 124 flux in the high-temperature, pressurized reactor-grade water environment—PWR conditions. Reference 61.

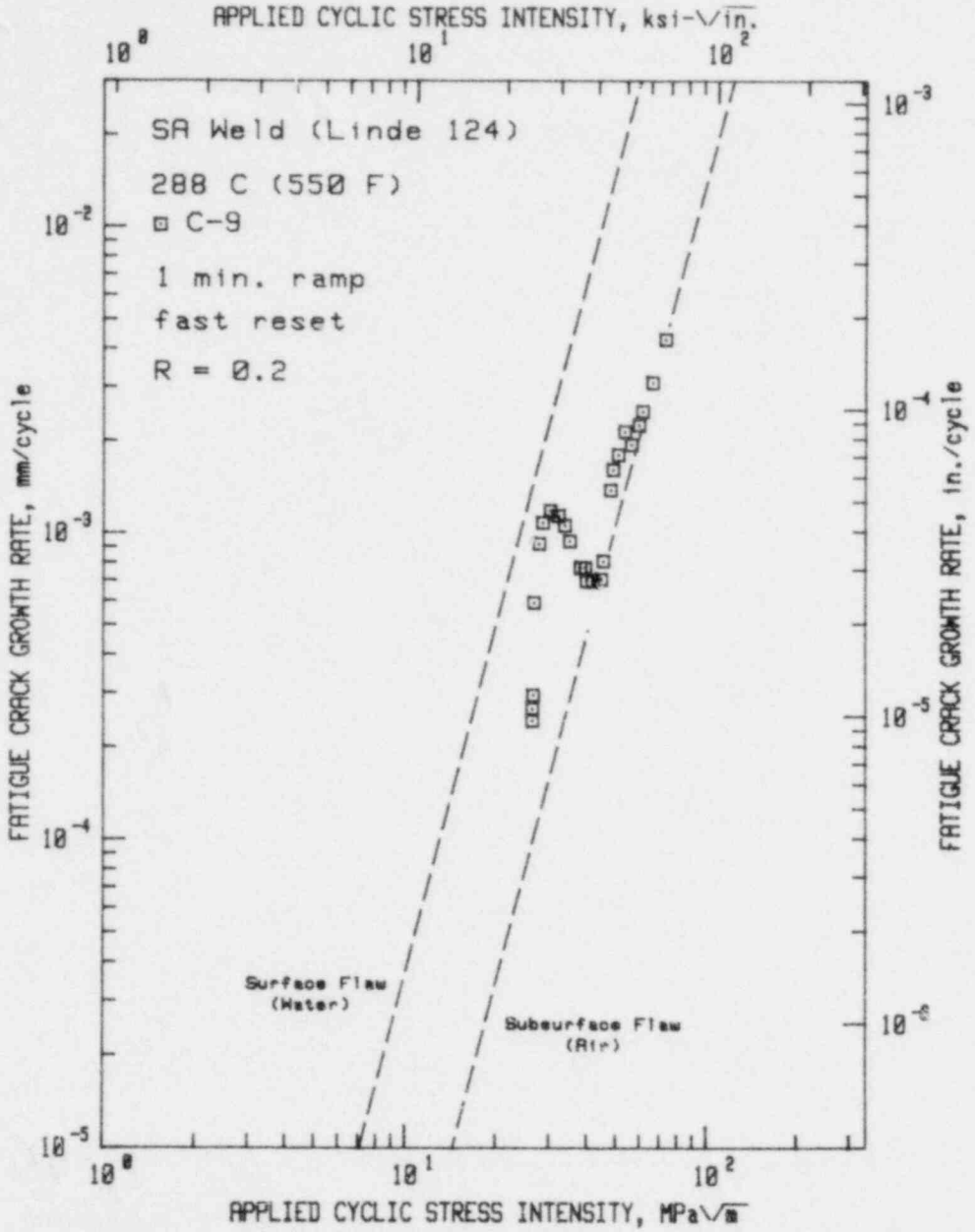

Fig. 44. Fatigue crack growth rate vs applied cyclic stress intensity factor for submerged arc deposited weld metal with Linde 124 flux in the high-temperature, pressurized reactor-grade water environment--PWR conditions. Reference 61.

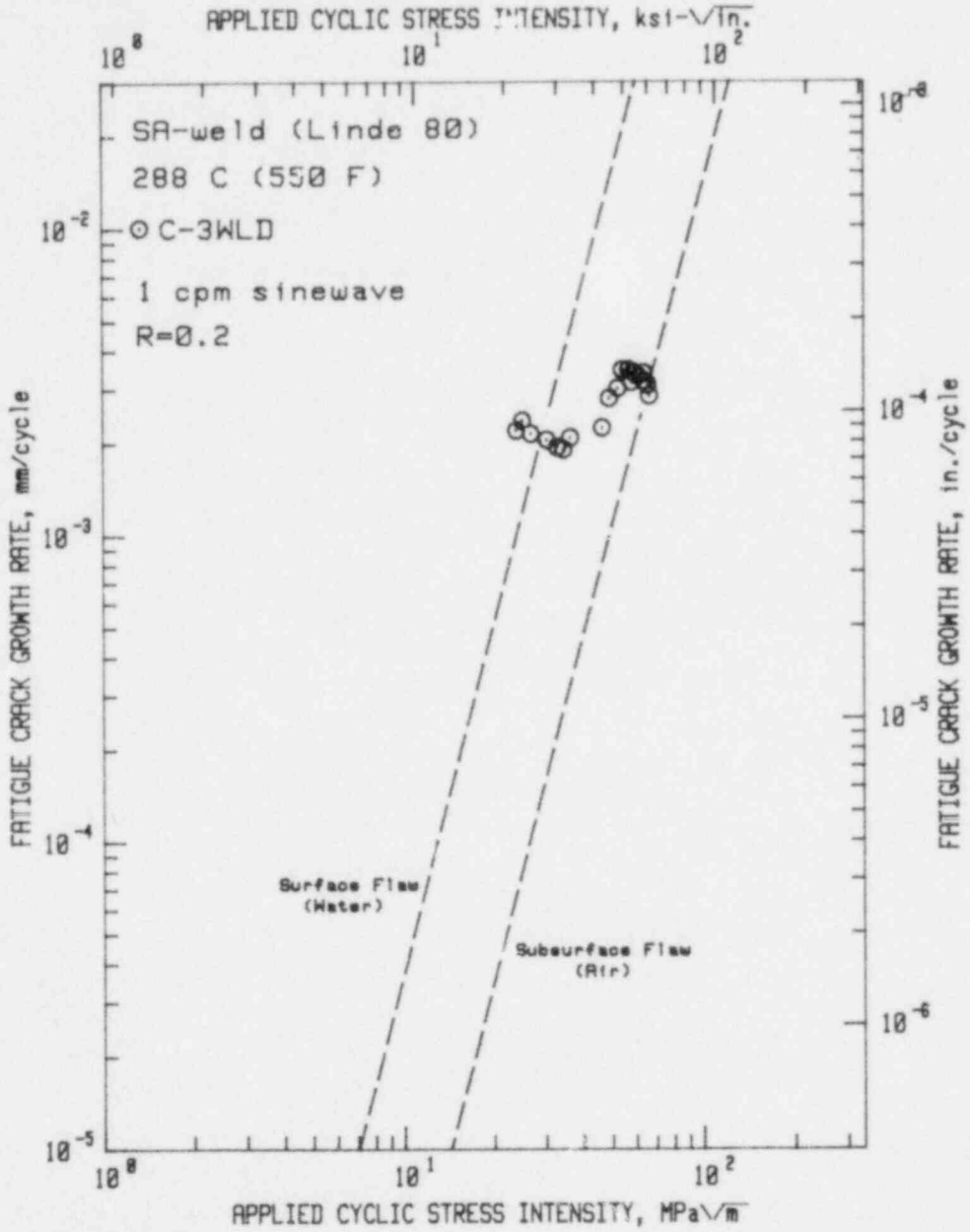

Fig. 45. Fatigue crack growth rate vs applied cyclic stress intensity factor for submerged arc deposited weld metal with Linde 80 flux in the high-temperature, pressurized reactor-grade water environment--PWR conditions. As for other 17 mHz sinewave tests, this data is rather high, but draws toward the ASME air default line at larger values of ΔK. Reference 62.

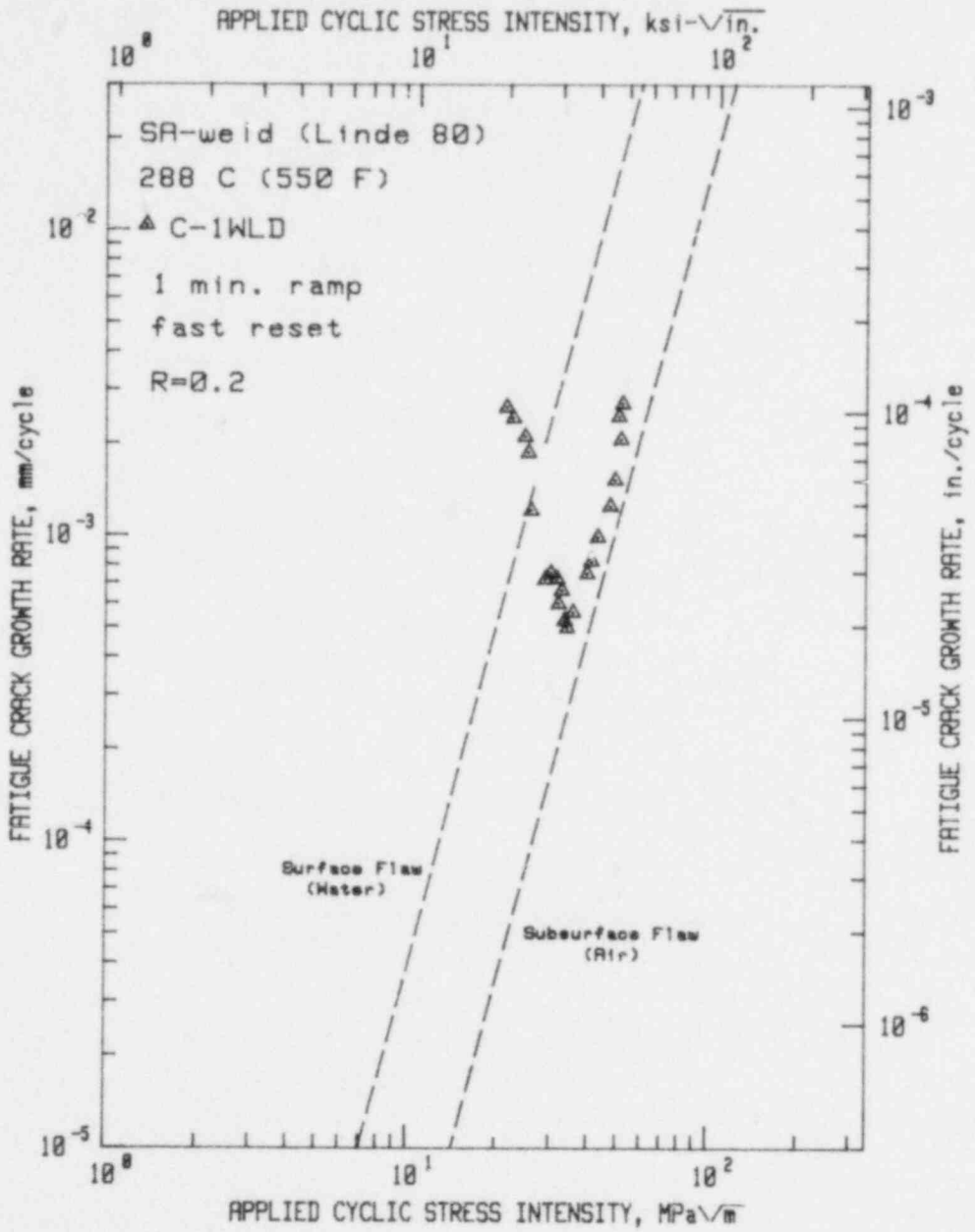

Fig. 46. Fatigue crack growth rate vs applied cyclic stress intensity factor for submerged arc deposited weld metal with Linde 80 flux in high-temperature, pressurized reactor-grade water environment--PWR conditions. See Fig. 42. Reference 62.

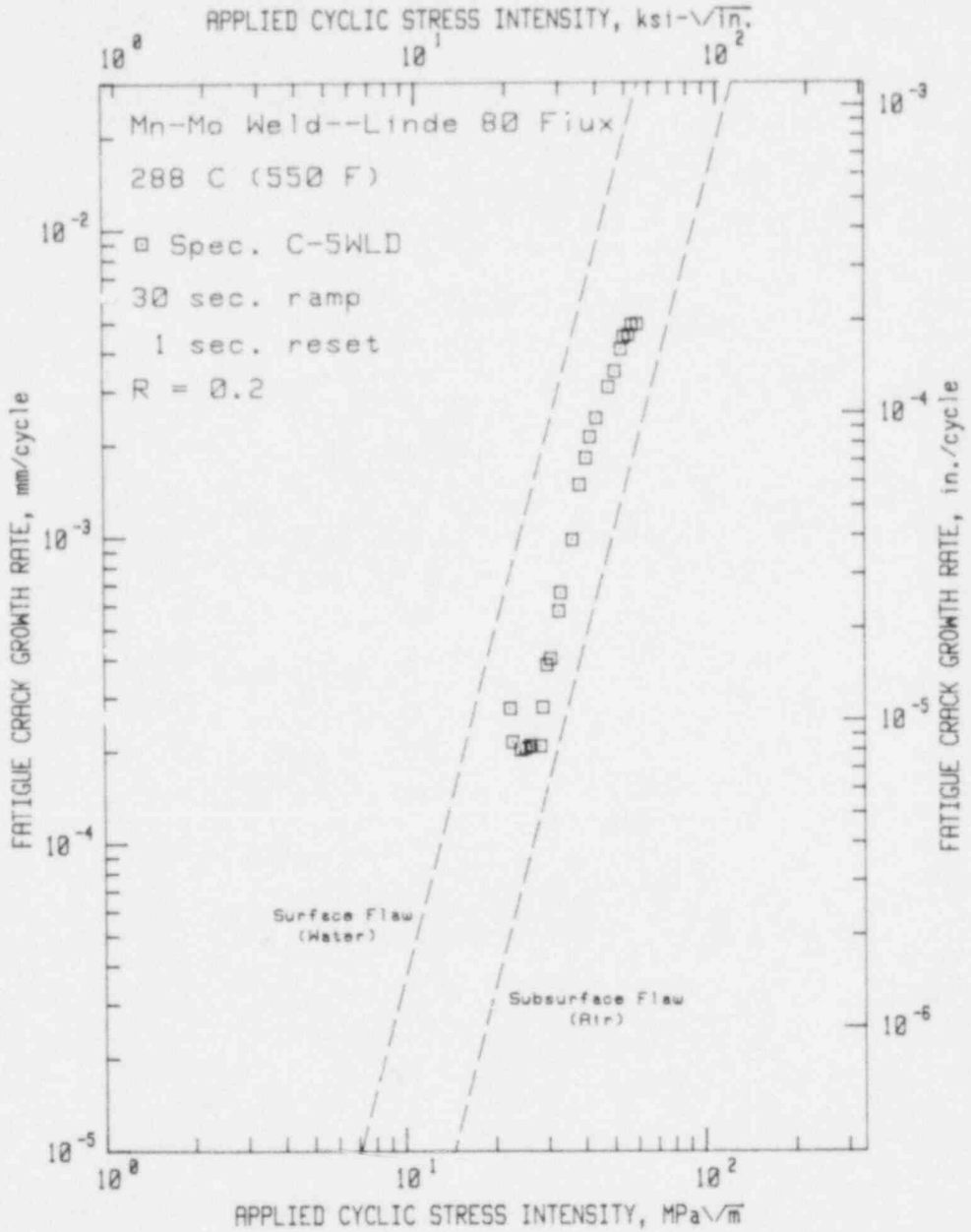

Fig. 47. Fatigue crack growth rate vs applied cyclic stress intensity factor for submerged arc weld metal deposit with Linde 80 flux in the high-temperature, pressurized reactor-grade water environment—PWR conditions. For the larger values of ΔK, this data set resides slightly higher than that in the previous figure. This tends to support the possibility that waveforms involving a 30 sec rise time component are somewhat more aggressive. Reference 62.

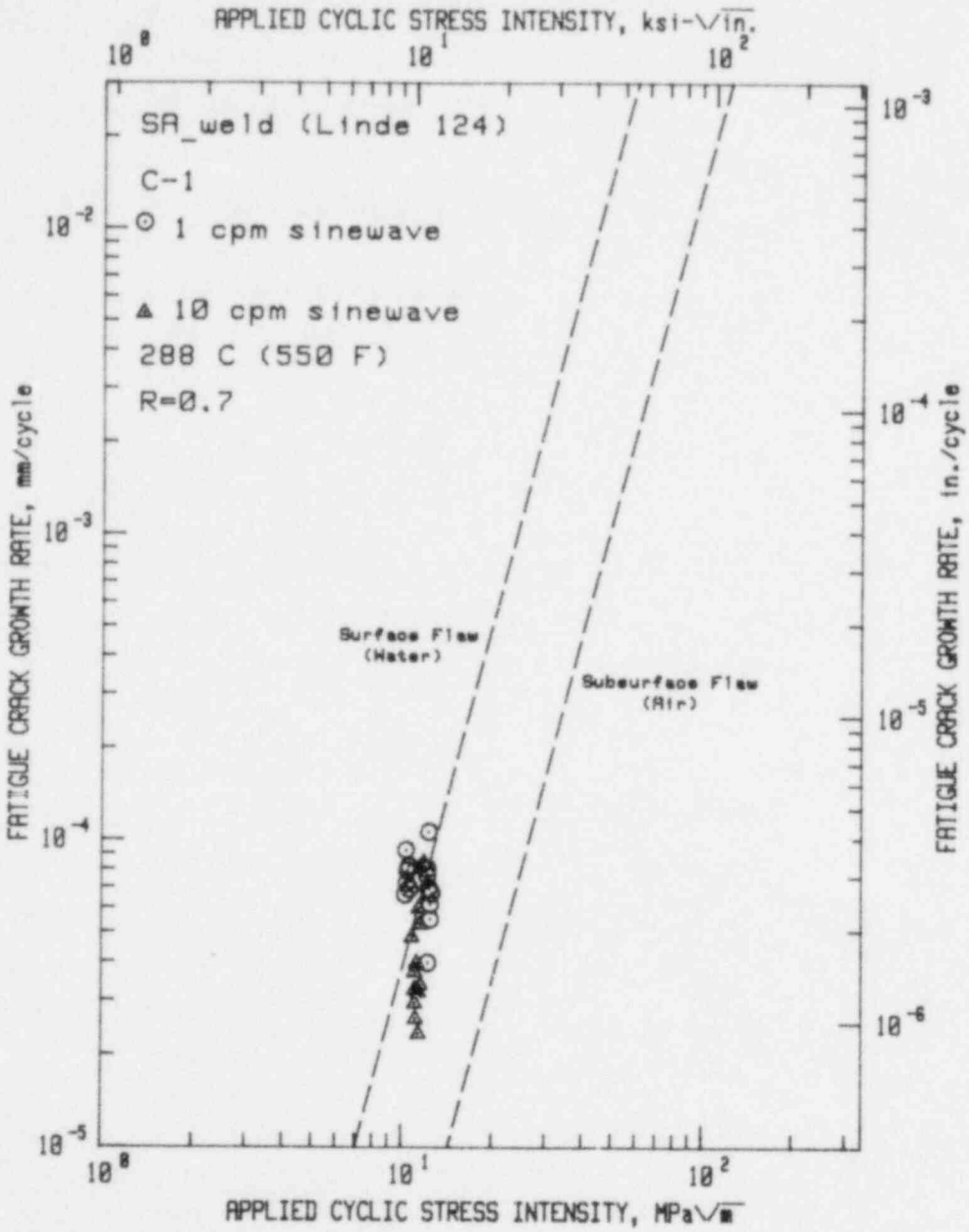

Fig. 48. Fatigue crack growth rate vs applied cyclic stress intensity factor for submerged arc deposited weld metal with Linde 124 flux in the high-temperature, pressurized reactor-grade environment--PWR conditions. This data, while spanning a small ΔK range, resides on or above the ASME water default line, typical of R=0.7 FCGR data. Reference 50.

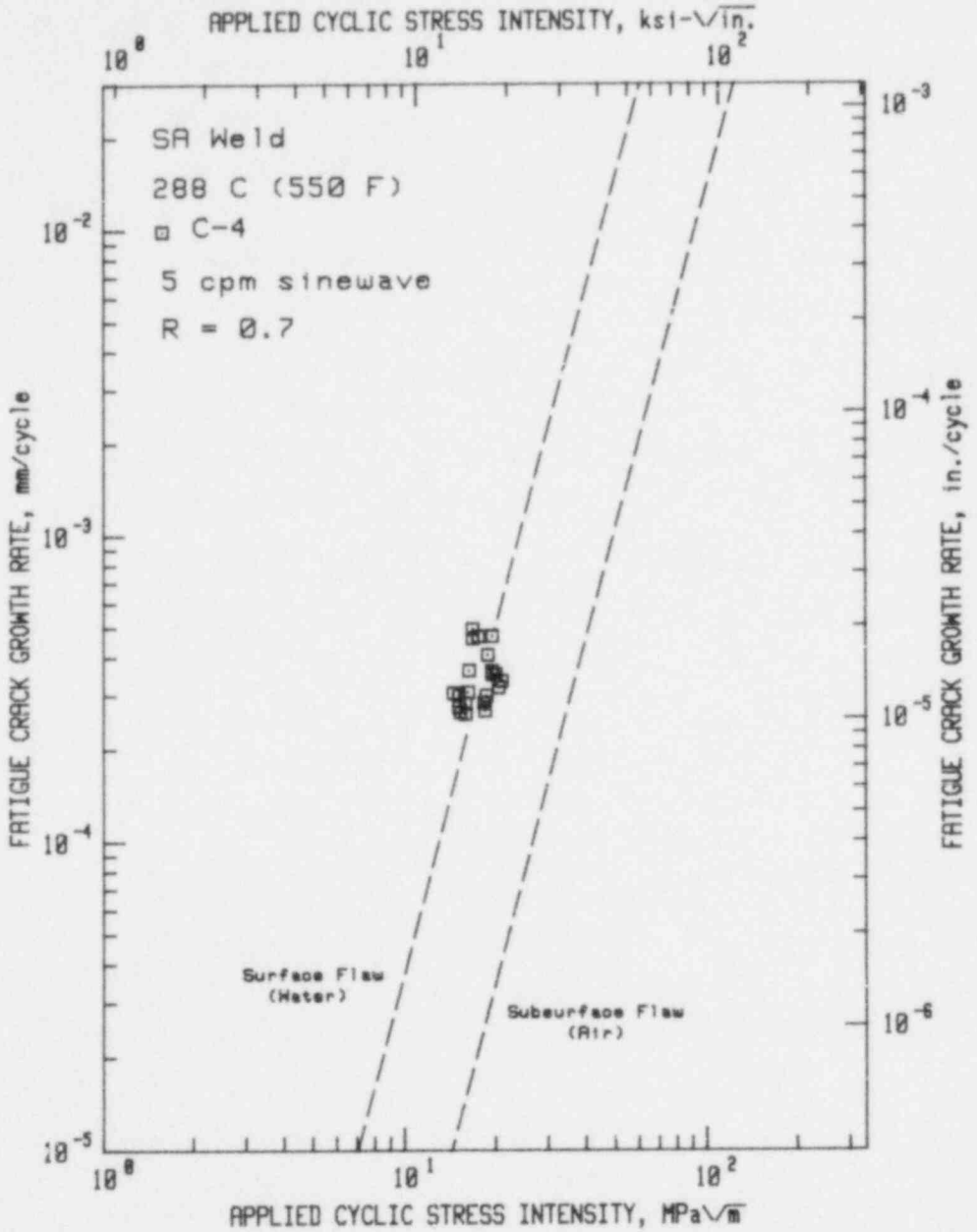

Fig. 49. Fatigue crack growth rate vs applied cyclic stress intensity factor for submerged arc deposited weld metal with Linde 124 flux in the high-temperature, pressurized reactor-grade water environment--PWR conditions. As expected for a 105 mHz, R=0.7 test, this data resides on, or slightly above the ASME water default line. Reference 52.

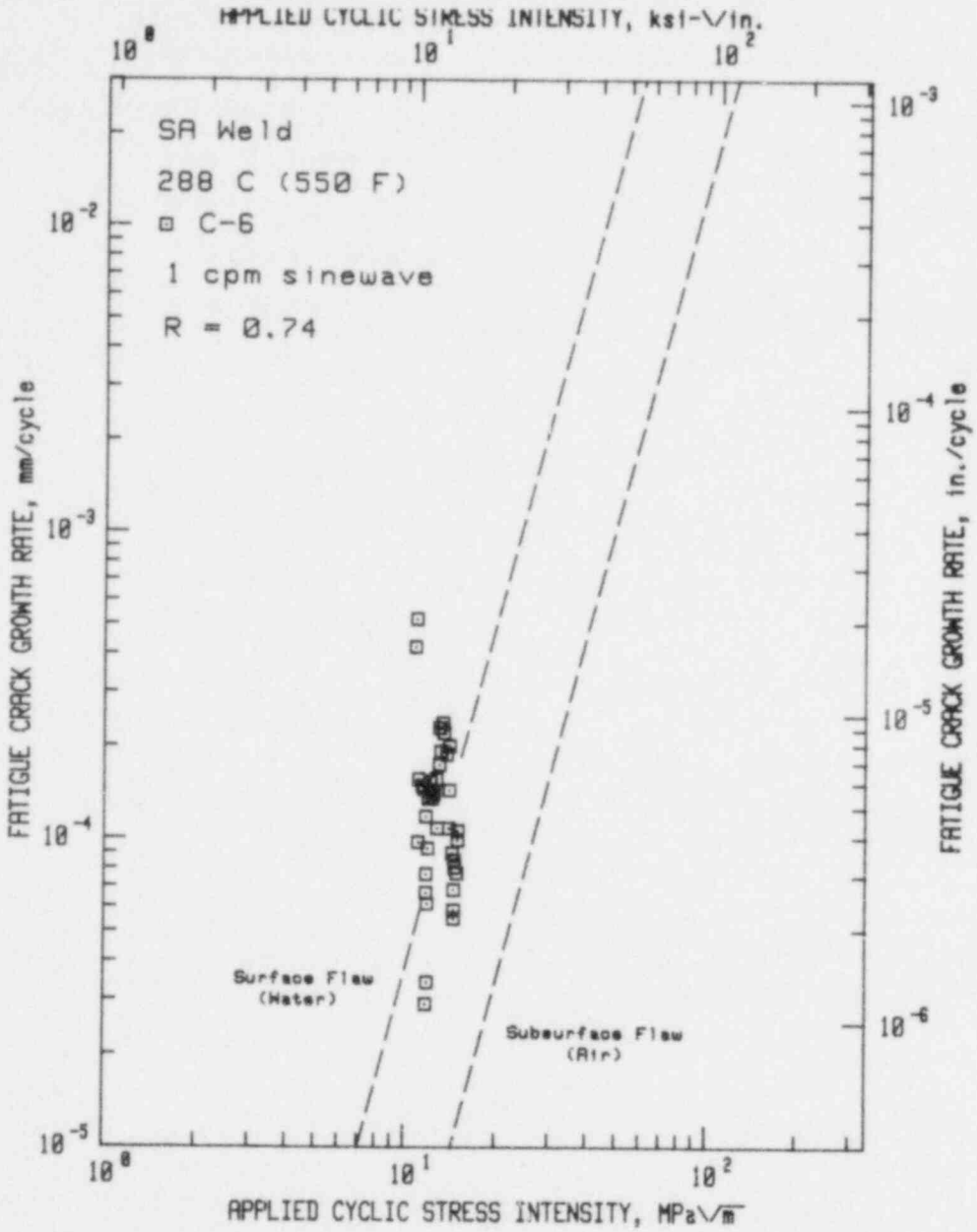

Fig. 50. Fatigue crack growth rate vs applied cyclic stress intensity factor for submerged arc deposited weld metal with Linde 124 flux in the high-temperature, pressurized reactor-grade water environment—PWR conditions. This data is for a slightly higher load ratio than other tests in this series, and was terminated after 6.5 months of testing "because crack growth had nearly stopped." Reference 55.

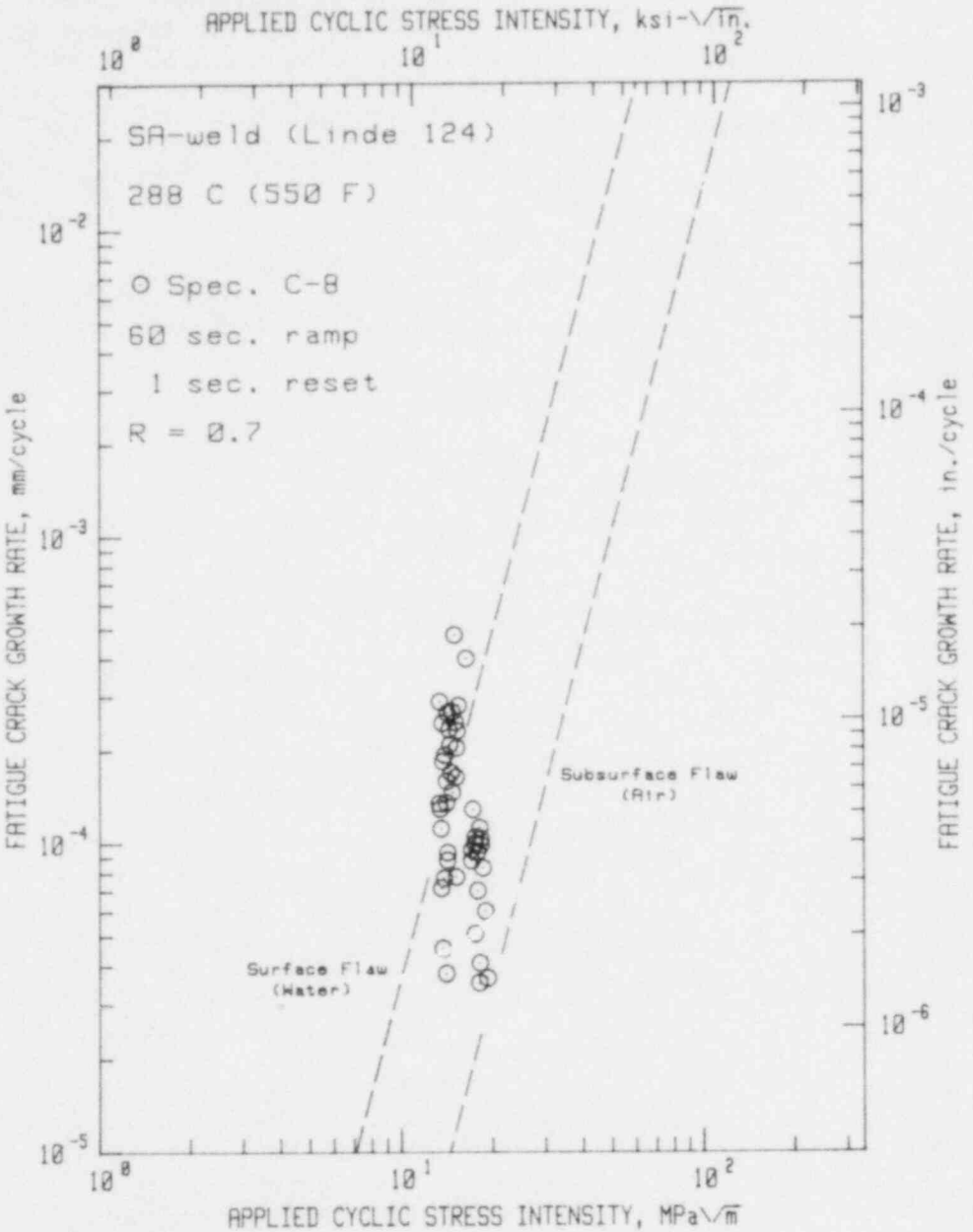

Fig. 51. Fatigue crack growth rate vs applied cyclic stress intensity factor for submerged arc deposited weld metal with Linde 124 flux in the high-temperature, pressurized reactor-grade water environment--PWR conditions. This data resides rather low compared with other high load ratio data, a fact which is not clearly attributable to the waveform (see next figure). Reference 62.

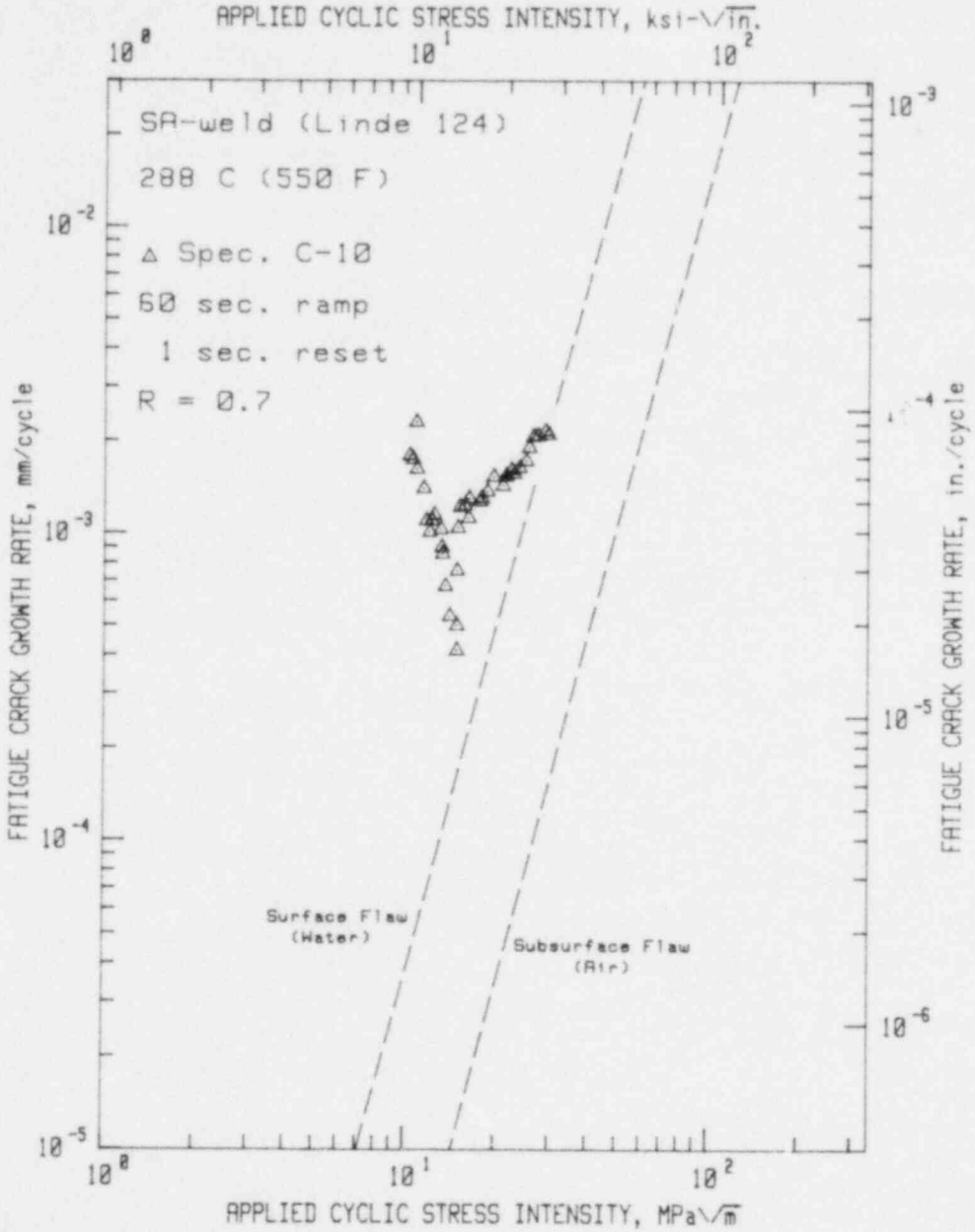

Fig. 52. Fatigue crack growth rate vs applied cyclic stress intensity factor for submerged arc deposited weld metal with Linde 124 flux in the high-temperature, pressurized reactor-grade water environment--PWR conditions. This data resembles that of two similar tests in the following figures, and is quite similar to 17 mHz sinewave data of the same load ratio. Reference 62.

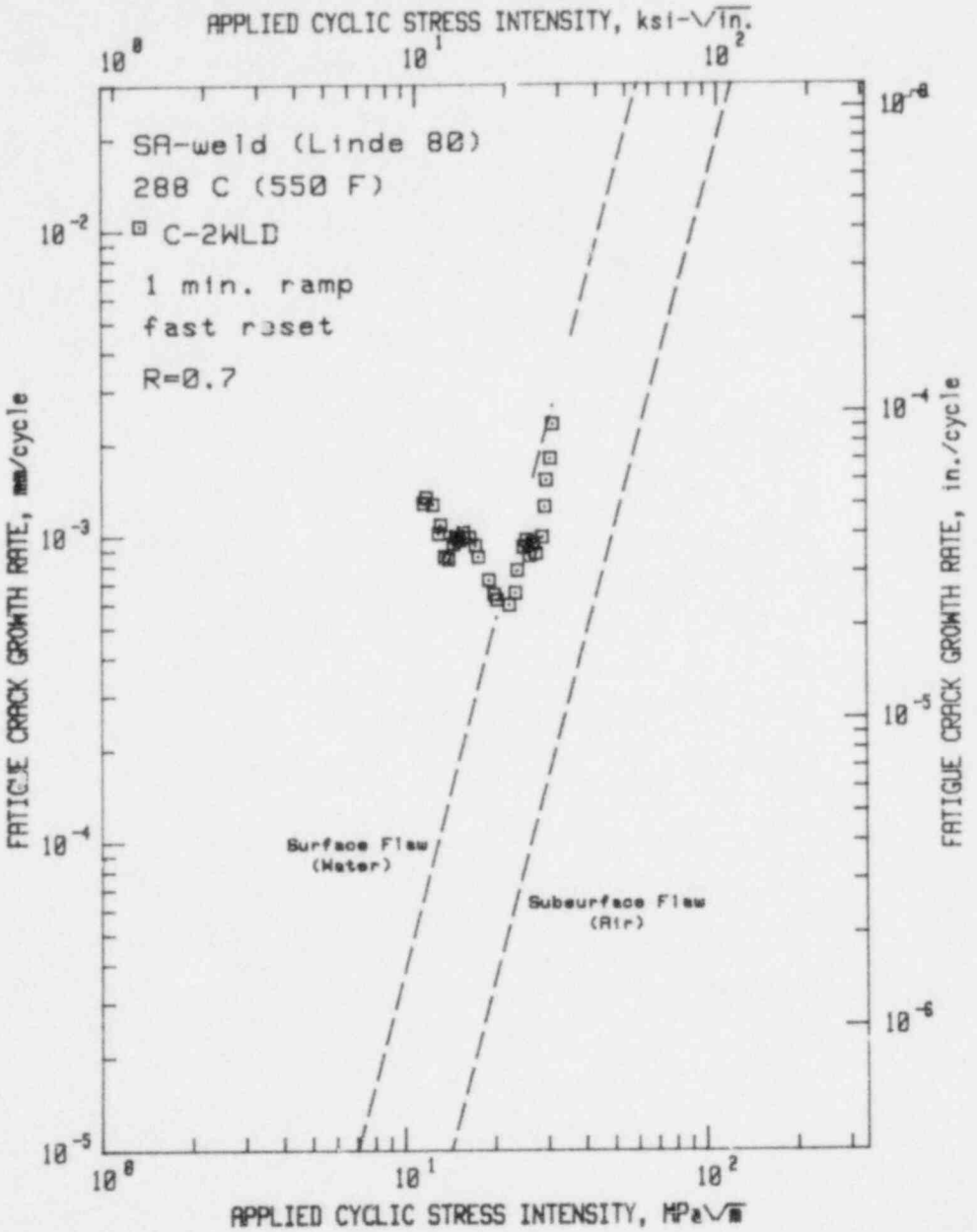

Fig. 53. Fatigue crack growth rate vs applied cyclic stress intensity factor for submerged arc deposited weld metal with Linde 80 flux in high-temperature, pressurized reactor-grade water environment--PWR conditions. See previous Fig. 51. Reference 62.

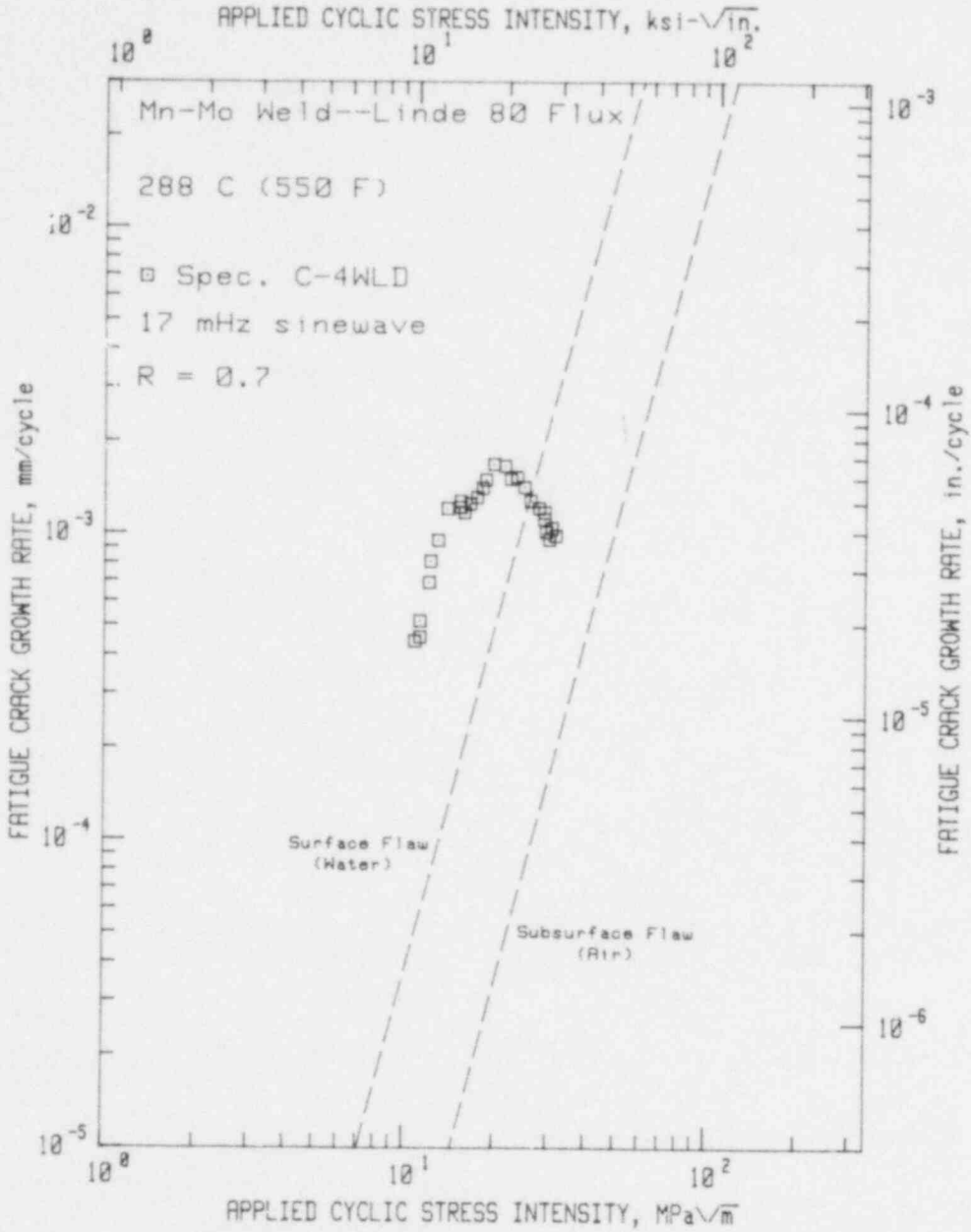

Fig. 54. Fatigue crack growth rate vs applied cyclic stress intensity factor for submerged arc weld metal deposit with Linde 80 flux in high-temperature, pressurized reactor-grade water environment--PWR conditions. This data set begins well to the left of the ASME water default line, as expected for the higher load ratio tests, and exhibits the trend toward the ASME air default line for higher ΔK values. Reference 62.

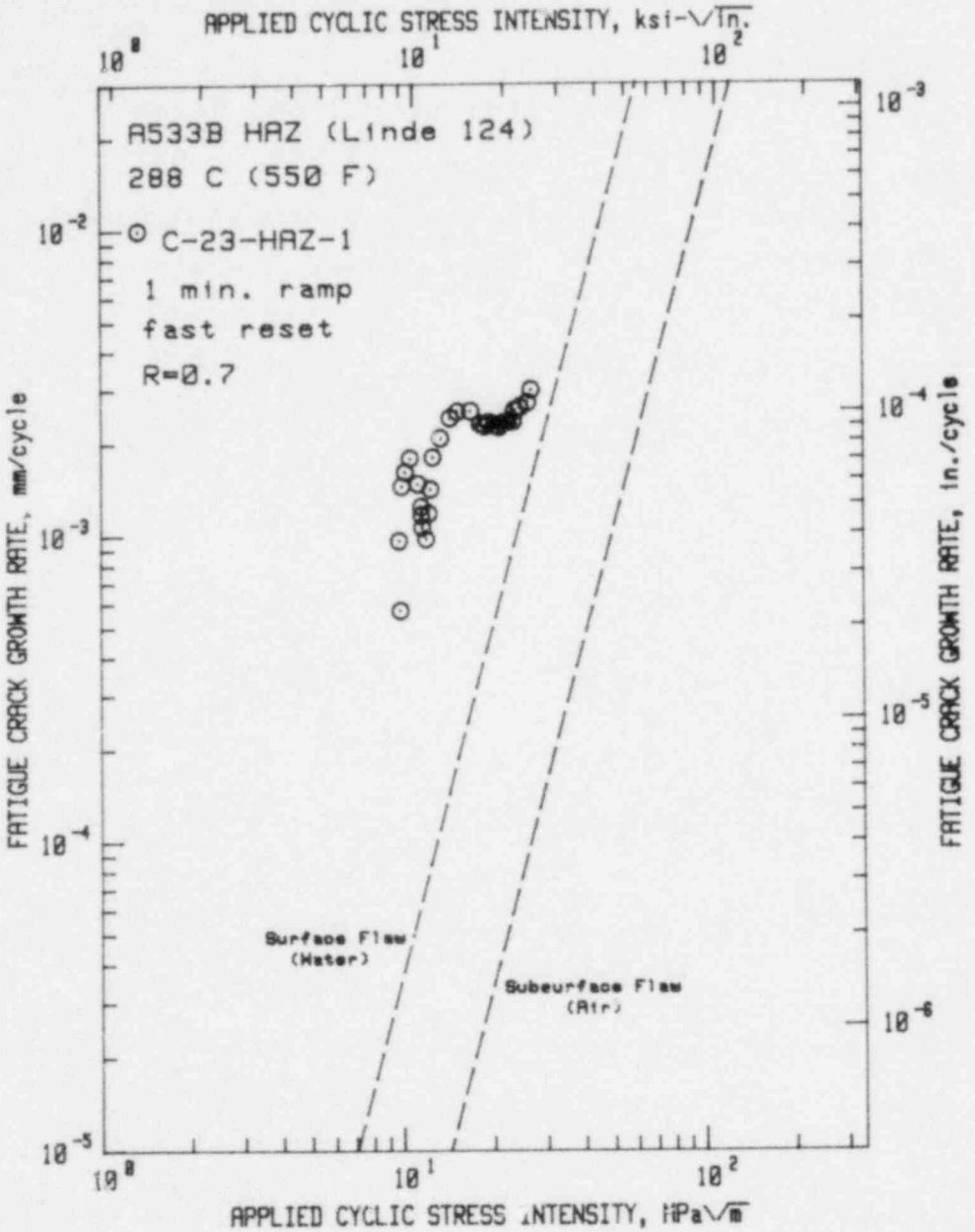

Fig. 55. Fatigue crack growth rate vs applied cyclic stress intensity factor for submerged arc deposited weld metal with Linde 124 flux in high-temperature, pressurized reactor-grade water environment—PWR conditions. See Fig. 53. Reference 62.

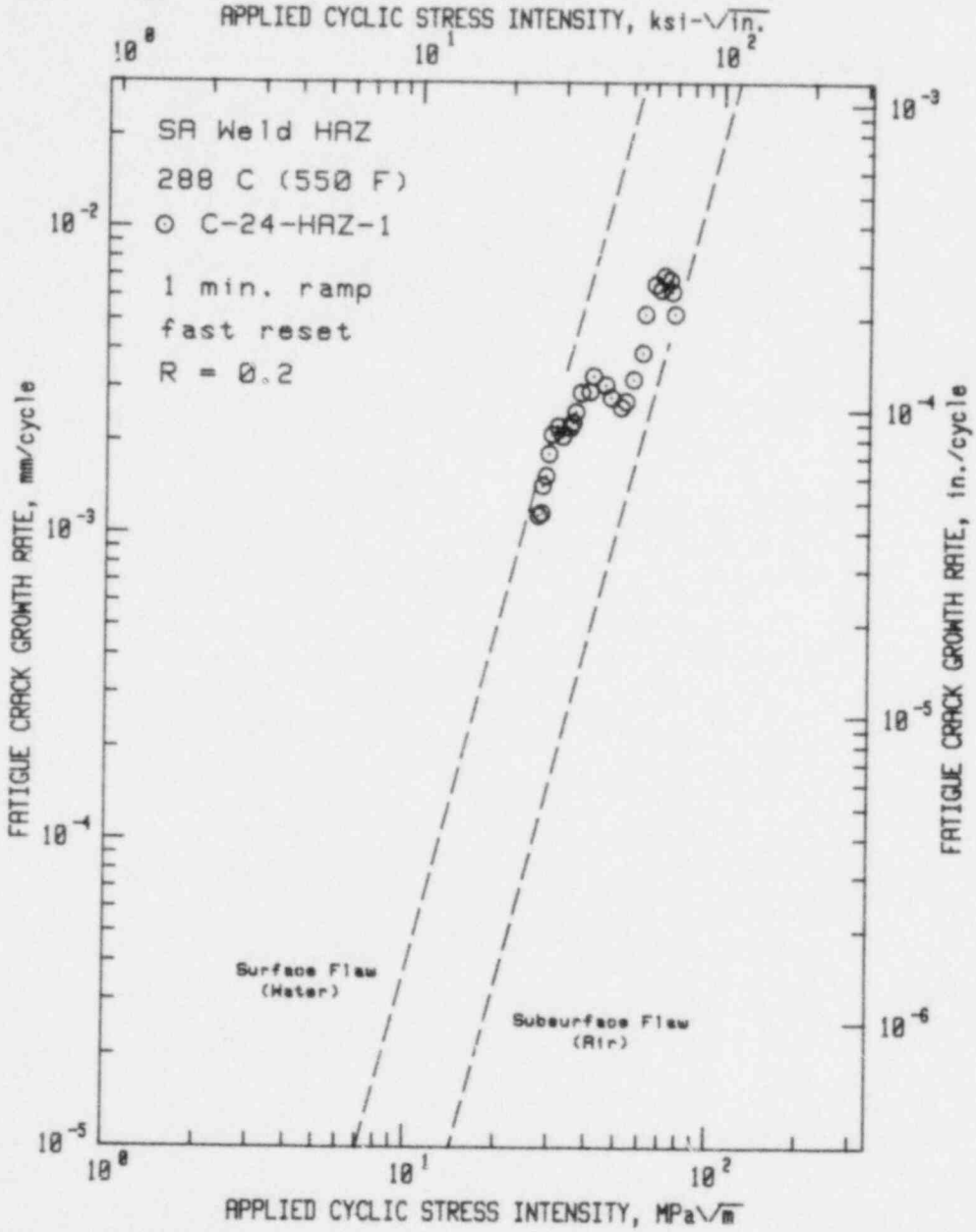

Fig. 56. Fatigue crack growth rate vs applied cyclic stress intensity factor for heat-affected zone of a submerged arc weld deposit in high-temperature, pressurized reactor-grade water environment—PWR conditions. This data, in its initial stage, is significantly more accelerated than that from other tests of the same waveform. Note that the trend is toward the ASME air default line, much like 17 mHz sinewave data. Reference 61.

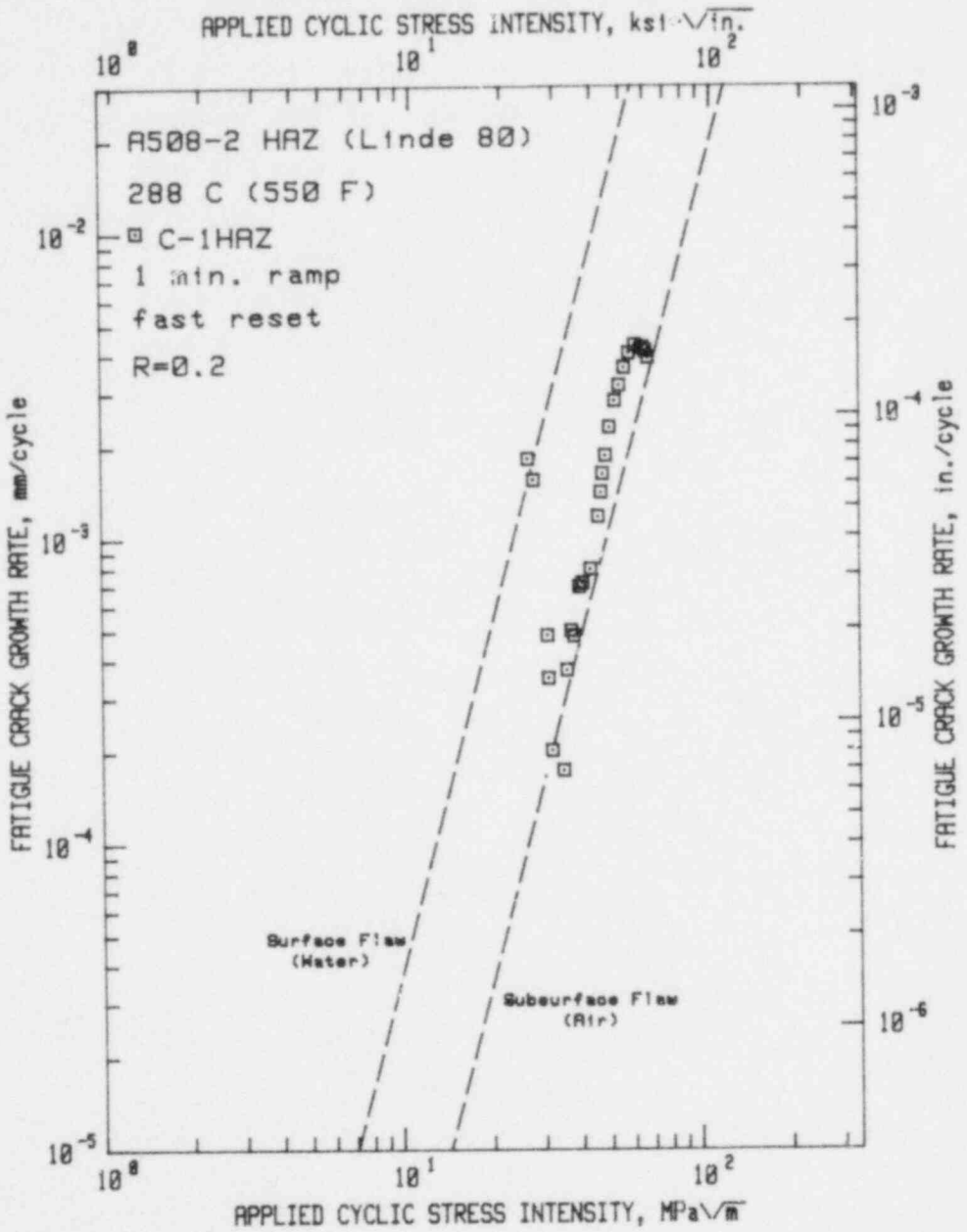

Fig. 57. Fatigue crack growth rate vs applied cyclic stress intensity factor for the heat-affected zone of a submerged arc weld deposit in high-temperature, pressurized reactor-grade water environment--PWR conditions. This data, also begins with rather high growth rates, as in the previous figure, but quickly returns to the low growth rate category and basically resides near the ASME air default line. Reference 62.

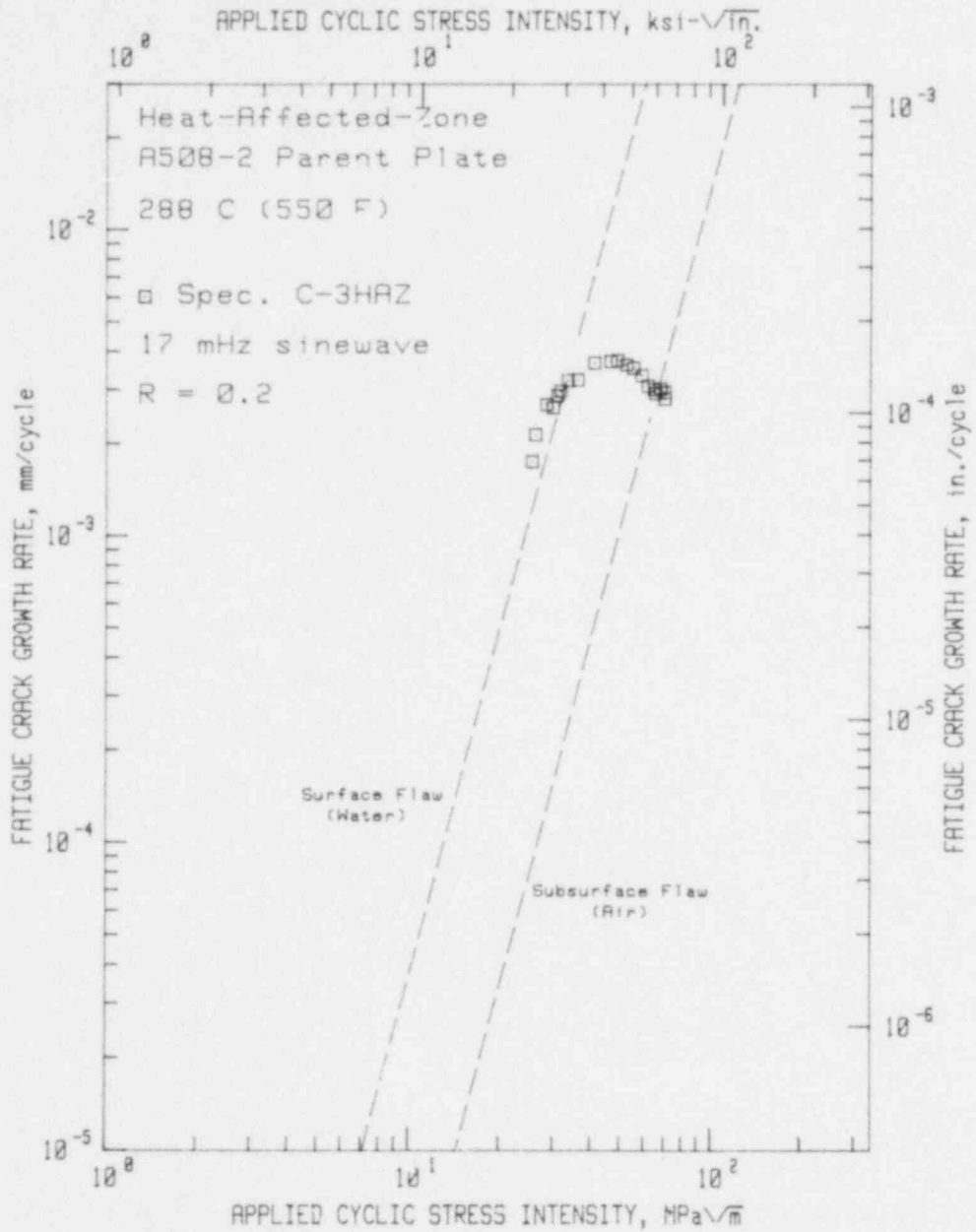

Fig. 58. Fatigue crack growth rate vs applied cyclic stress intensity factor for the heat-affected zone of a submerged arc weld deposit in high-temperature, pressurized reactor-grade water environment—PWR conditions. This data appears at quite high growth rates, and exhibits the expected trend toward the ASME air default line at higher values of ΔK. Reference 62.

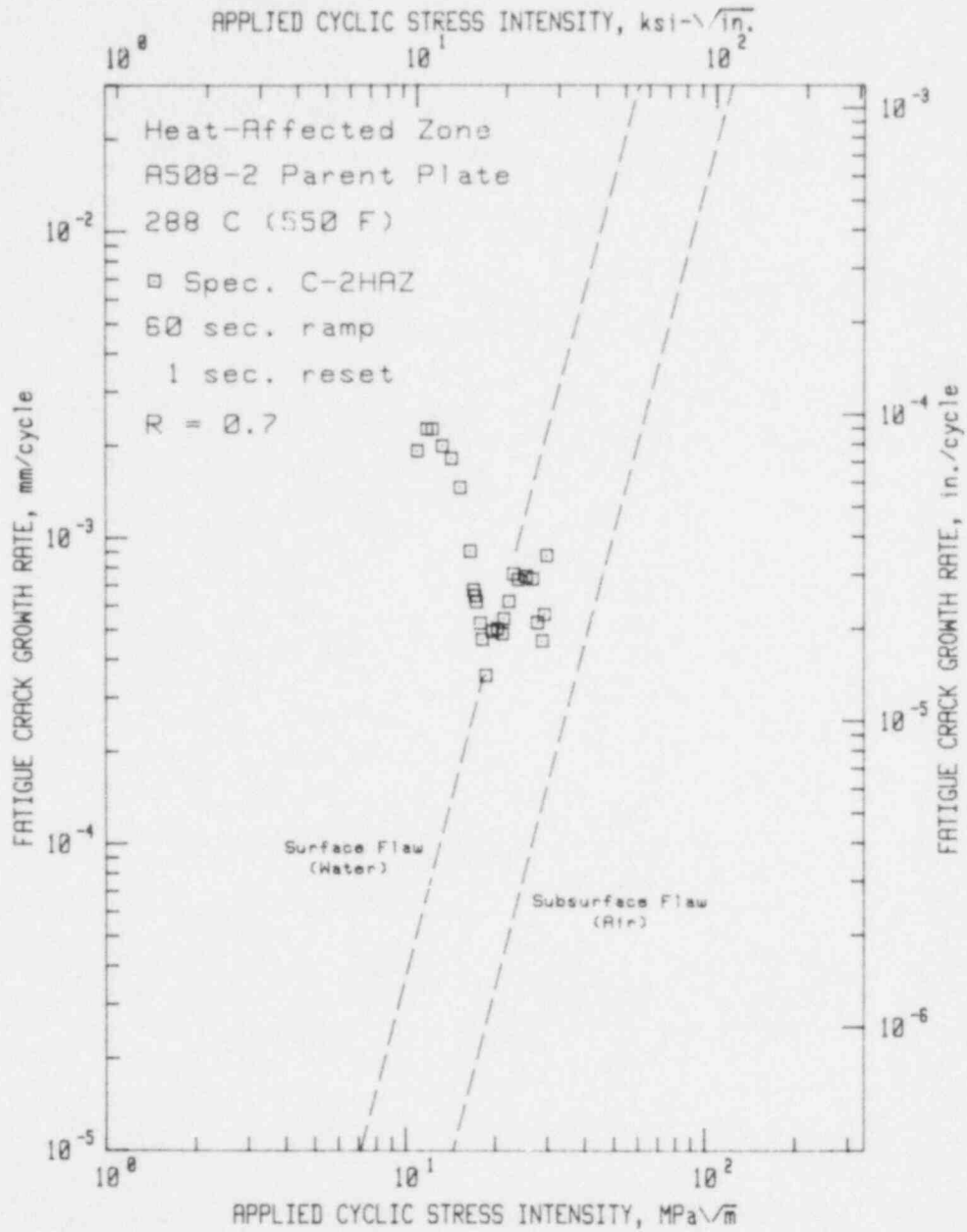

Fig. 59. Fatigue crack growth rate vs applied cyclic stress intensity factor for the heat-affected zone of a submerged arc weld deposit in high-temperature, pressurized reactor-grade water environment--PWR conditions. This data begins well to the left of the ASME water default line, as expected for a high load ratio test, then trends to rather low growth rate values. Reference 62.

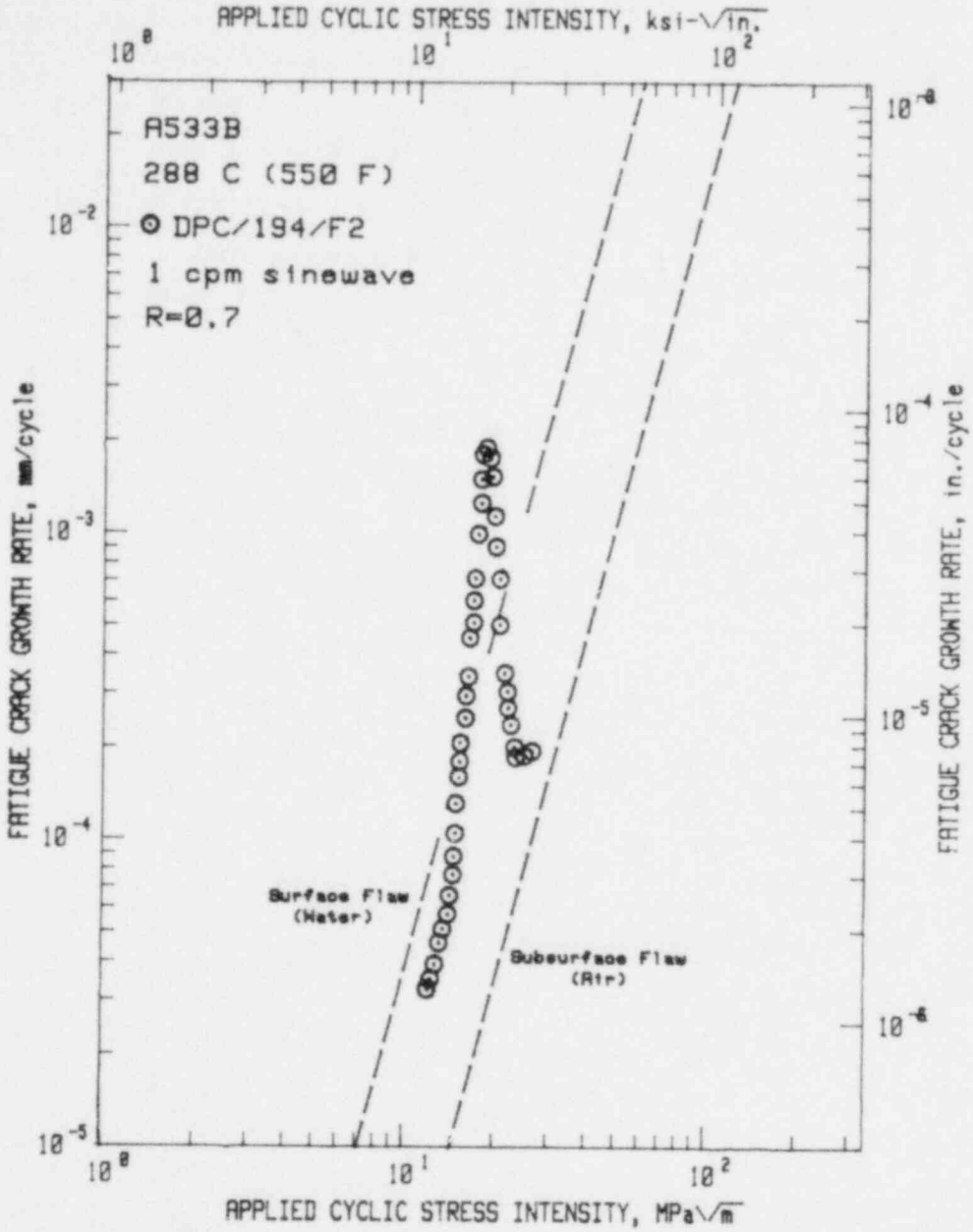

Fig. 60. Fatigue crack growth rate vs applied cyclic stress intensity factor for A533B steel in high-temperature, pressurized reactor-grade water—PWR conditions. This data was acquired during a test which involved several changes in test frequency and load performed so as to extend the crack and obtain data over a larger span of ΔK in a shorter total test time. Reference 17.

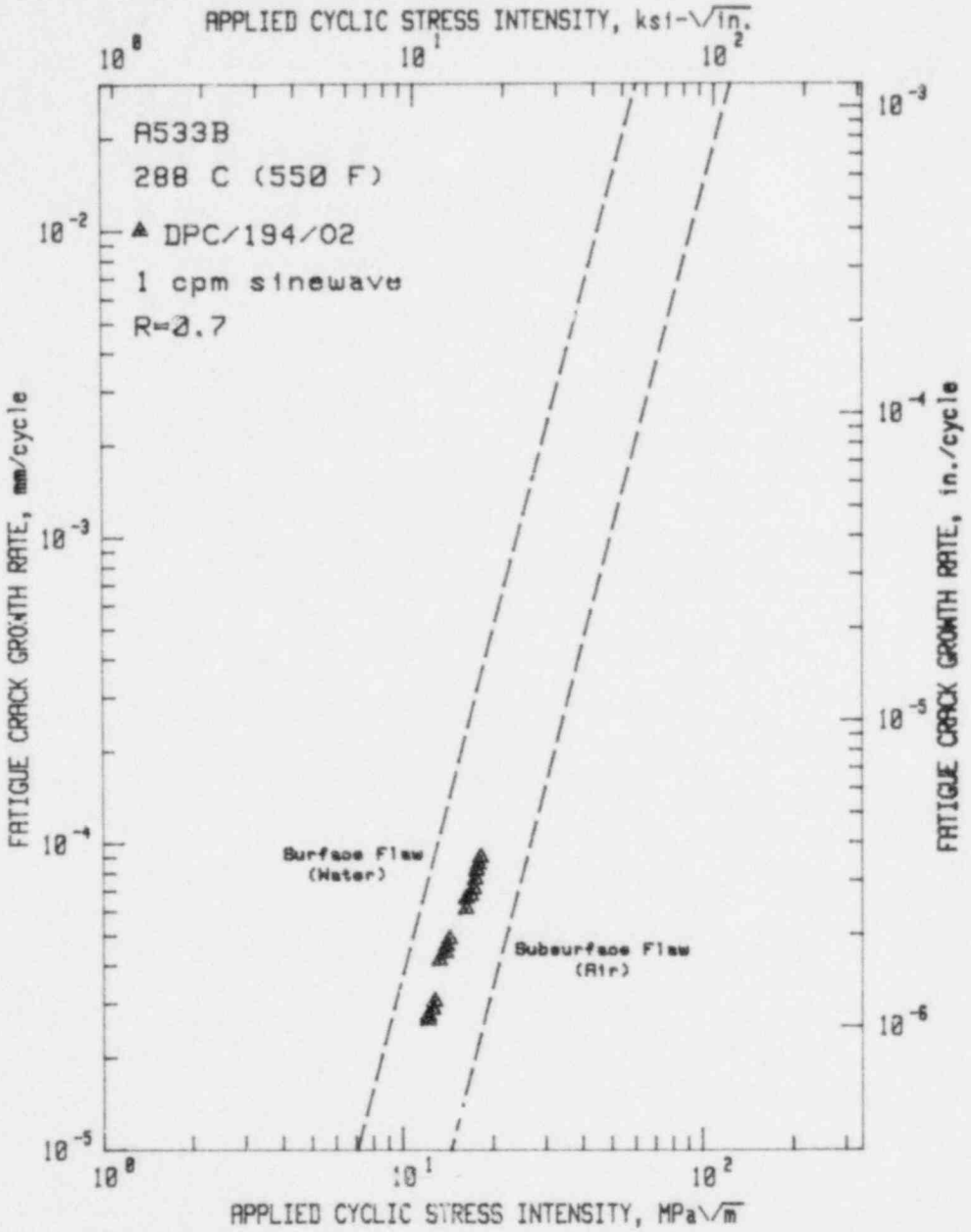

Fig. 61. Fatigue crack growth rate vs applied cyclic stress intensity factor for A533B steel in high-temperature, pressurized reactor-grade water—PWR conditions. As in the above figure, this data was produced using a test procedure involving changes of frequency, but in this case, the load was not changed. Reference 17.

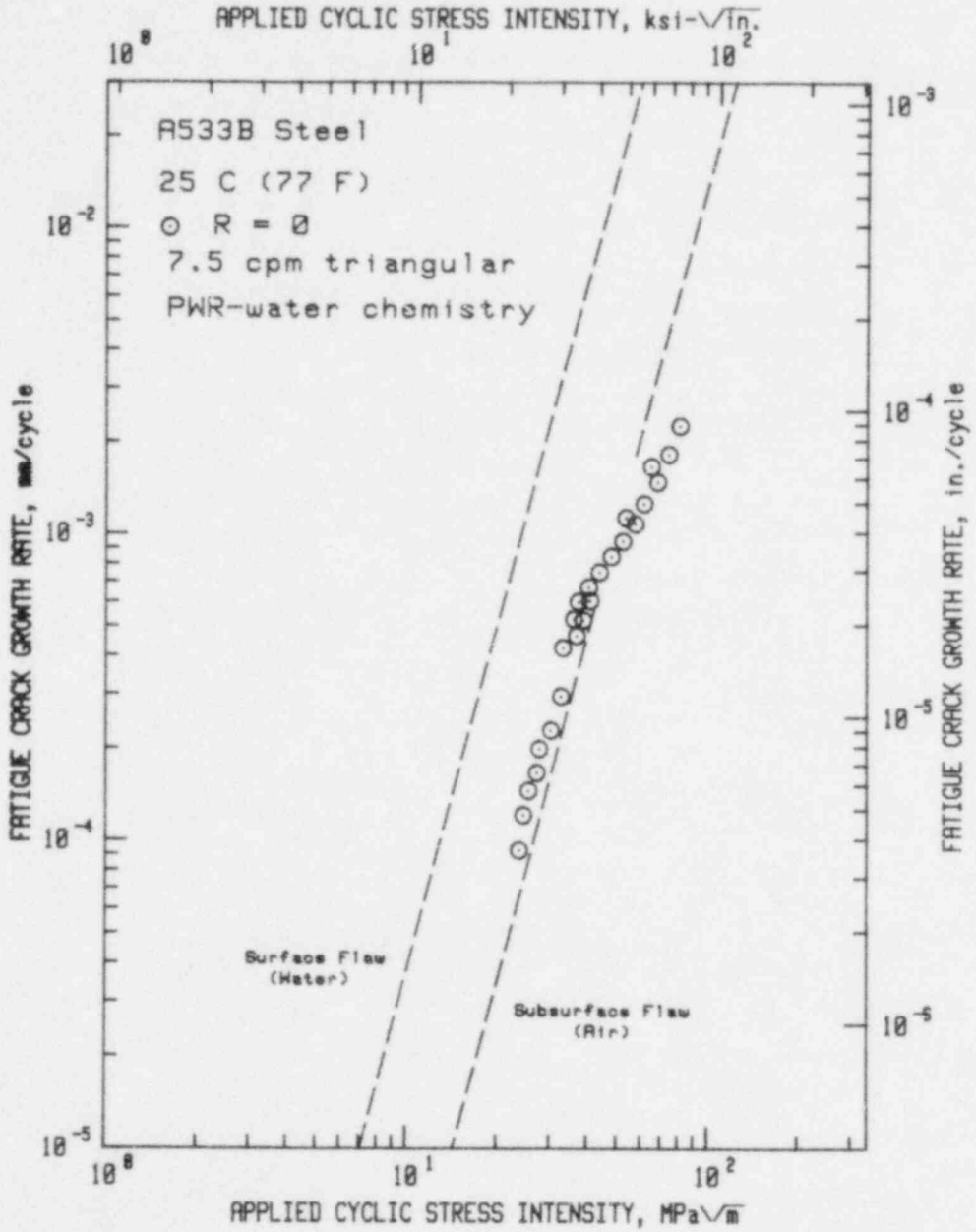

Fig. 62. Fatigue crack growth rate vs applied cyclic stress intensity factor for A533B steel in reactor-grade water. For this low load ratio, the data reside essentially on or near the ASME air default line. Reference 15.

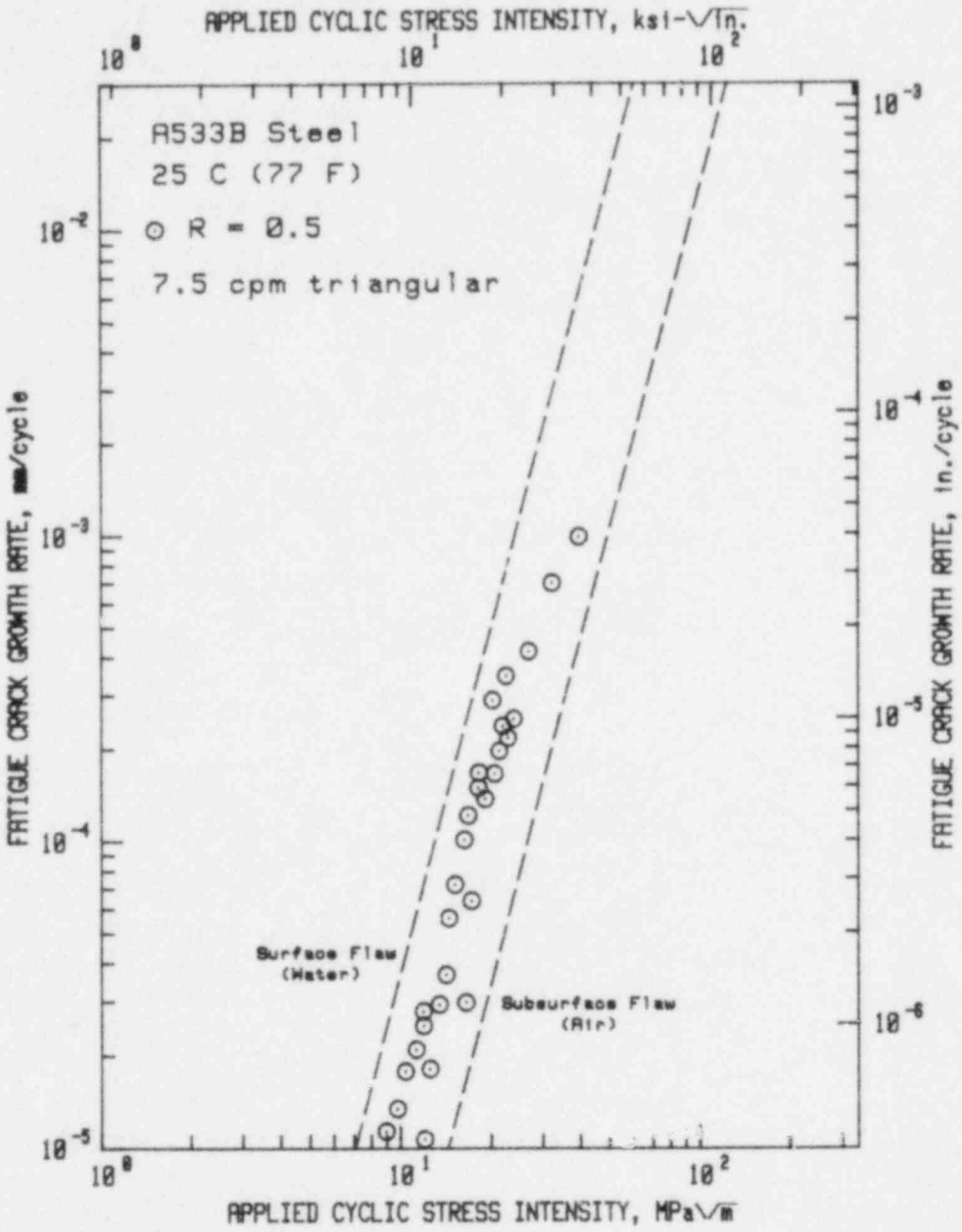

Fig. 63. Fatigue crack growth rate vs applied cyclic stress intensity factor for A533B steel in reactor-grade water. Compared with the previous figure, the higher load ratio results in higher crack growth rates for a given ΔK value. Reference 15.

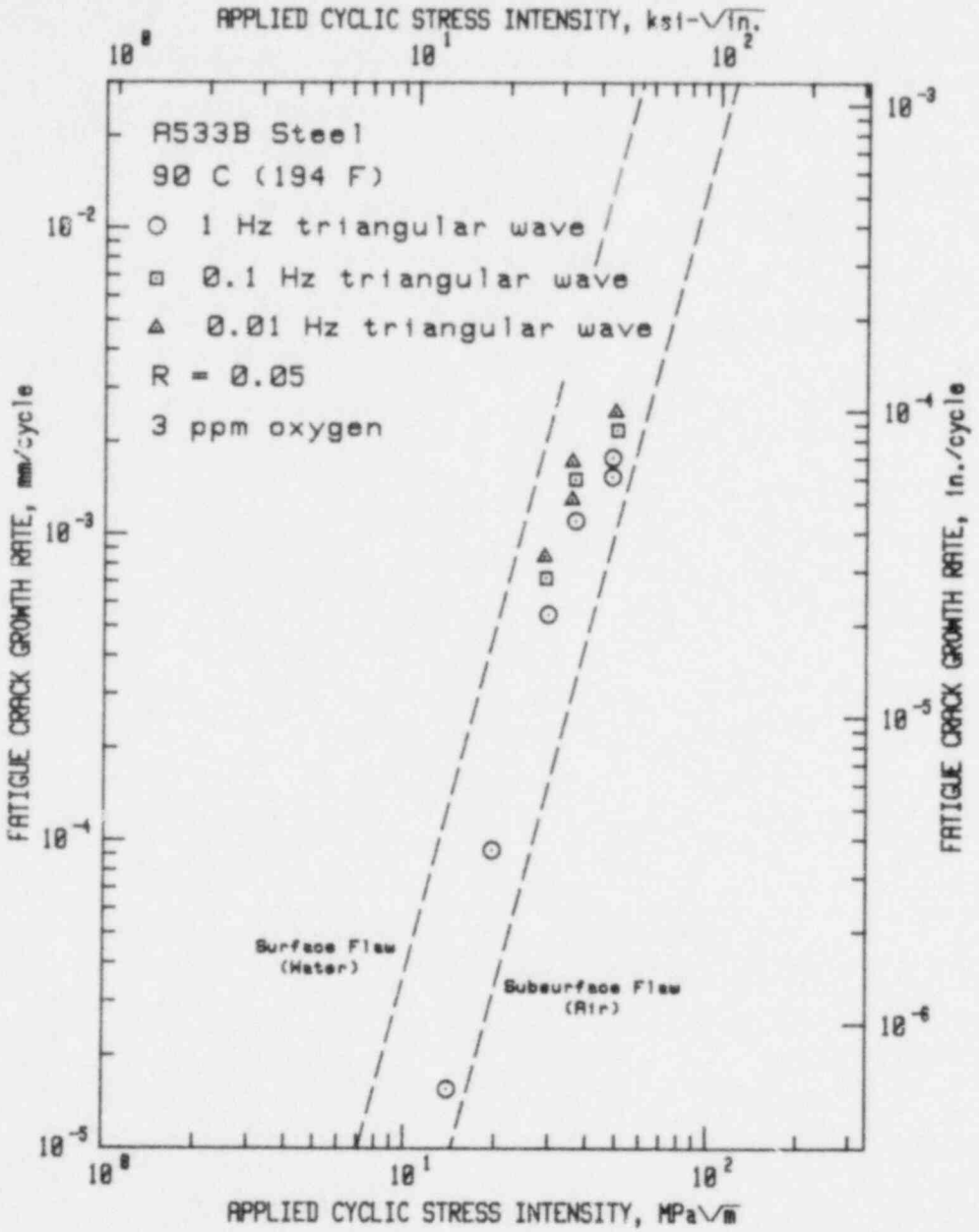

Fig. 64. Fatigue crack growth rate vs applied cyclic stress intensity factor for A533B steel in reactor-grade water. The expected increase in fatigue crack growth rates with increasing cyclic period is clearly realized in this data. Reference 10.

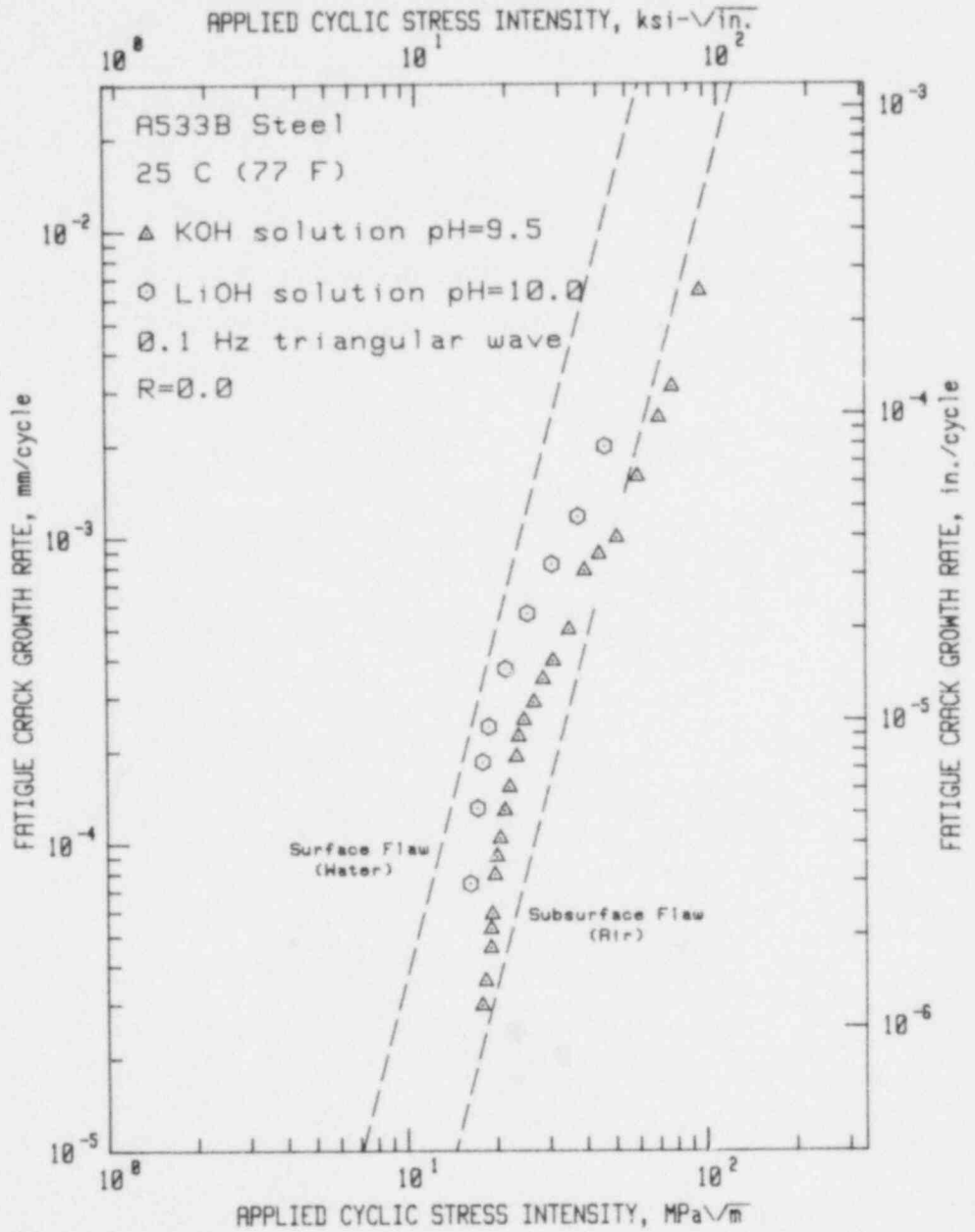

Fig. 65. Fatigue crack growth rate vs applied cyclic stress intensity factor for A533B steel in aqueous solutions of varying pH. The more basic solution depresses the fatigue crack growth rates. Reference 16.

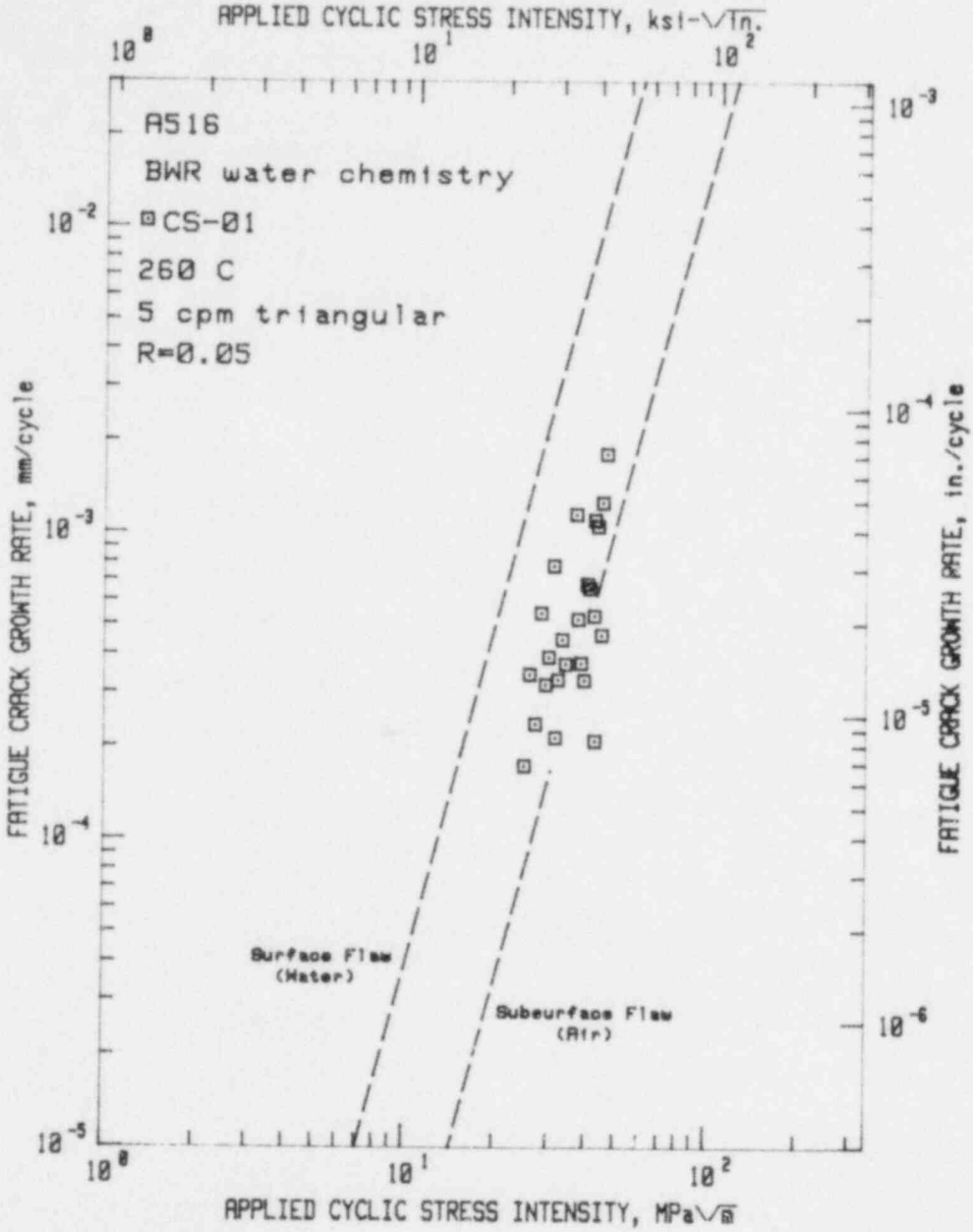

Fig. 66. Fatigue crack growth rate vs applied cyclic stress intensity factor for A516 steel in high-temperature, pressurized reactor-grade water—BWR conditions. For the most part, this data resides on or near the ASME air default line, as expected for this short period, low load ratio test. References 21, 23.

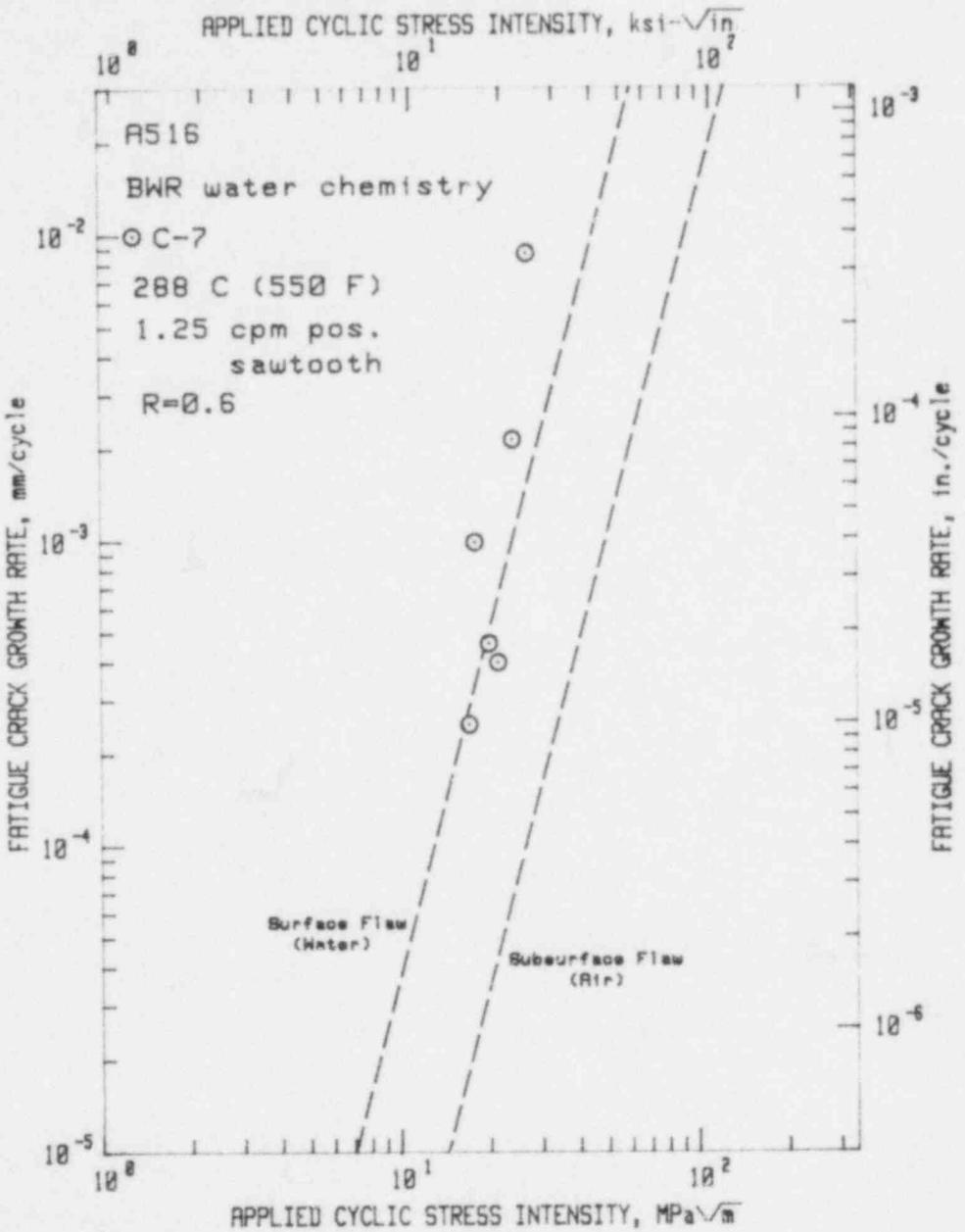

Fig. 67. Fatigue crack growth rate vs applied cyclic stress intensity factor for A516 steel in high-temperature, pressurized reactor-grade water—BWR conditions. Compared with the previous figure, this data set resides higher due to both the higher load ratio, and the longer cyclic period. Reference 24.

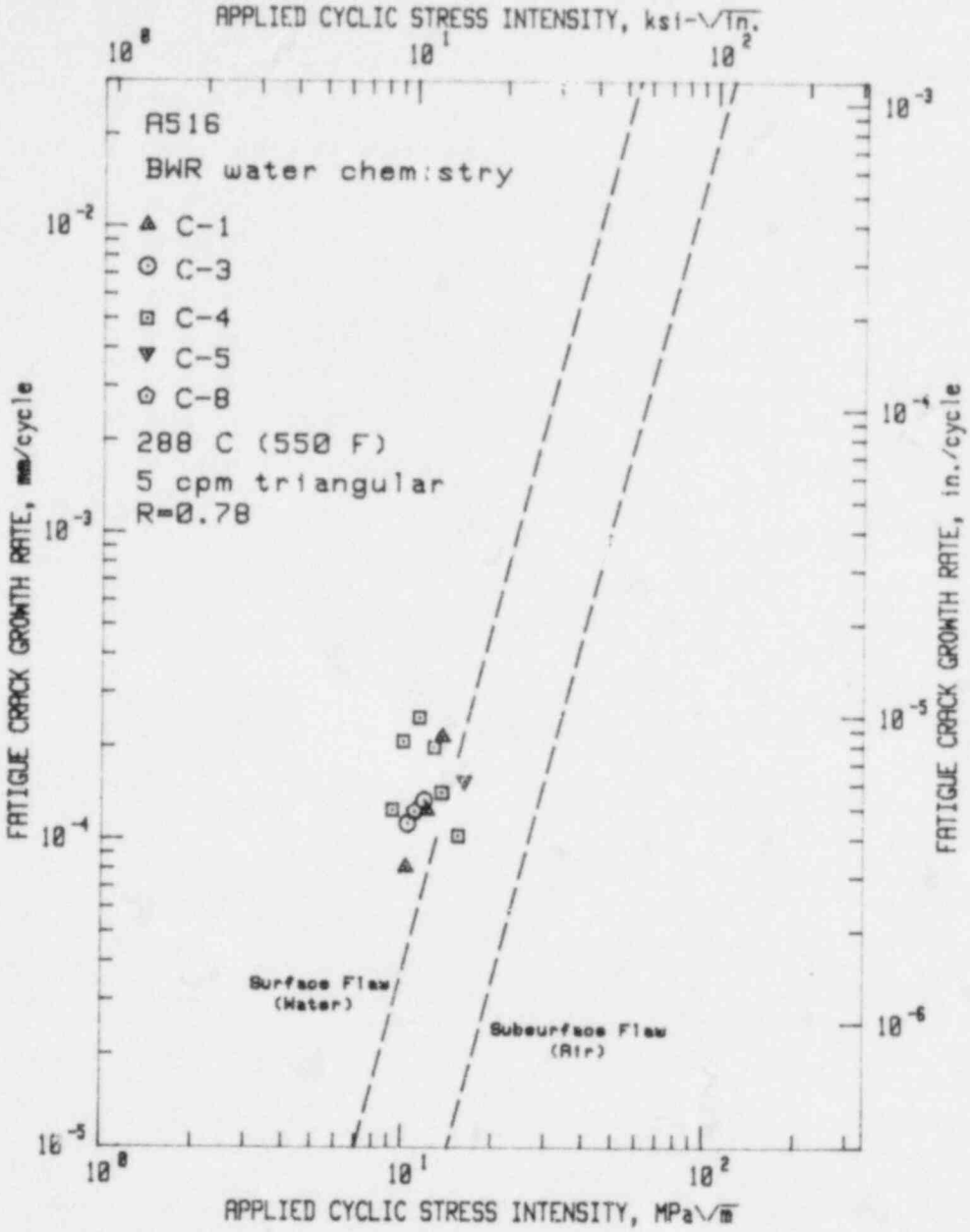

Fig. 68. Fatigue crack growth rate vs applied cyclic stress intensity factor for A516 steel in high-temperature, pressurized reactor-grade water—BWR conditions. This high load ratio results in data that is well to the right of the ASME water line, even for the relatively short cyclic period of the test. References 22, 23.

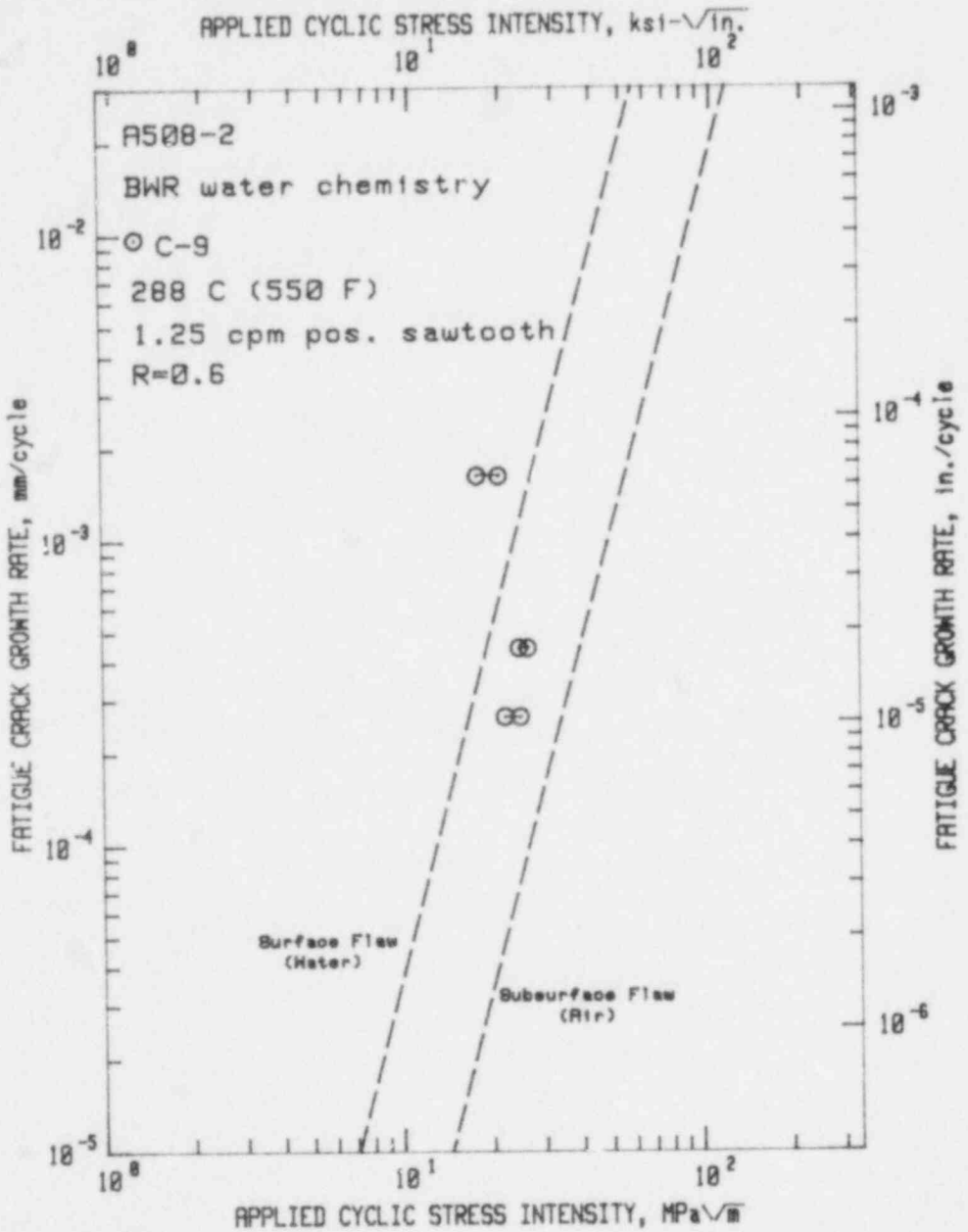

Fig. 69. Fatigue crack growth rate vs applied cyclic stress intensity factor for A508-2 steel in high-temperature, pressurized reactor-grade water—BWR conditions. The pairs of data points represent initial and final ΔK values for the increment of crack extension for which the rate was measured. The data agrees with the trends of the A516 data in the previous figures. Reference 24.

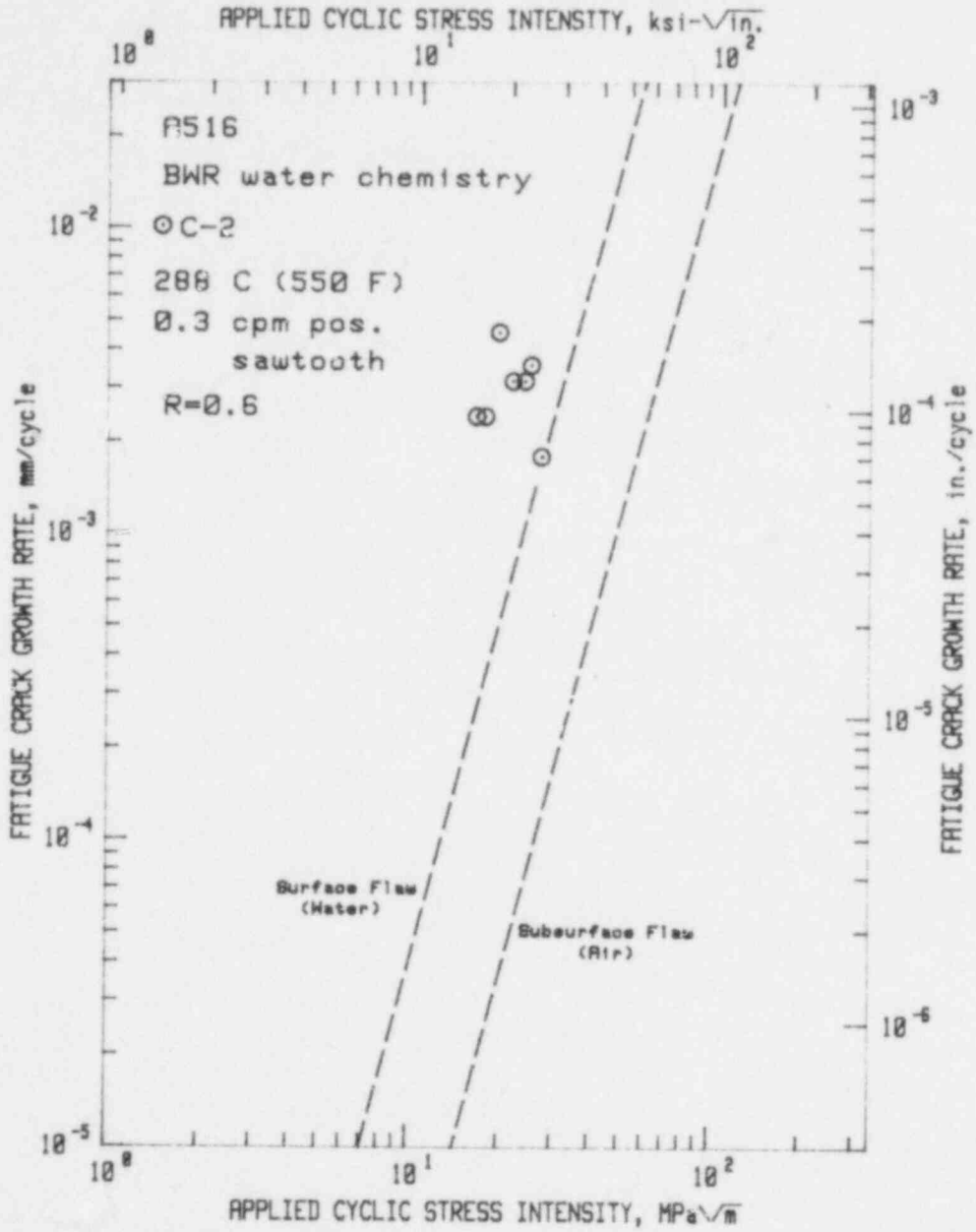

Fig. 70. Fatigue crack growth rate vs applied cyclic stress intensity factor for A516 steel in high-temperature pressurized reactor-grade water--BWR conditions. For this relatively long period waveform and high load ratio, this data lies substantially to the left of the ASME water default line. Reference 24.

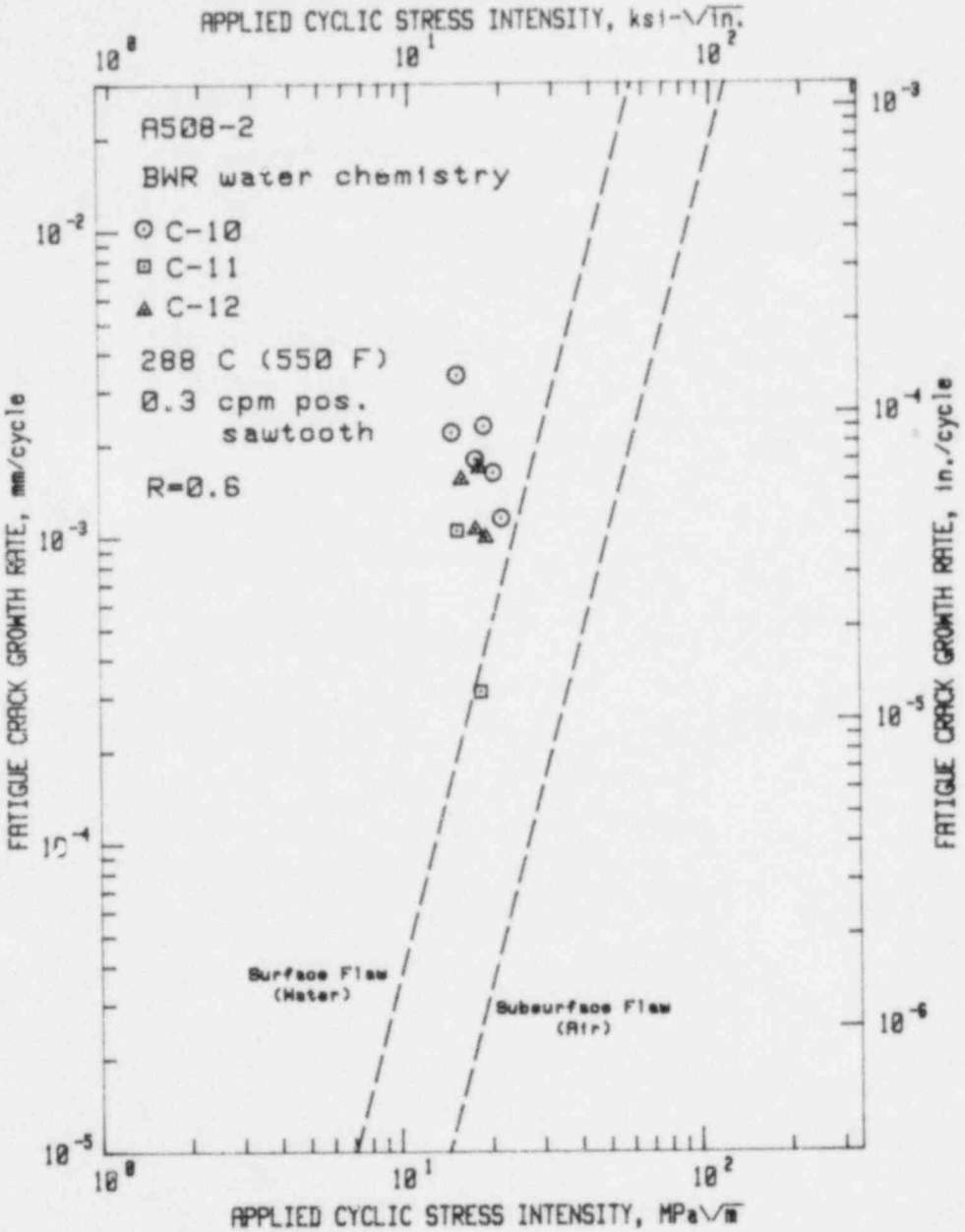

Fig. 71. Fatigue crack growth rate vs applied cyclic stress intensity factor for A508-2 steel in high-temperature, pressurized reactor-grade water--BWR conditions. This data agrees with the data of the previous figure. Reference 24.

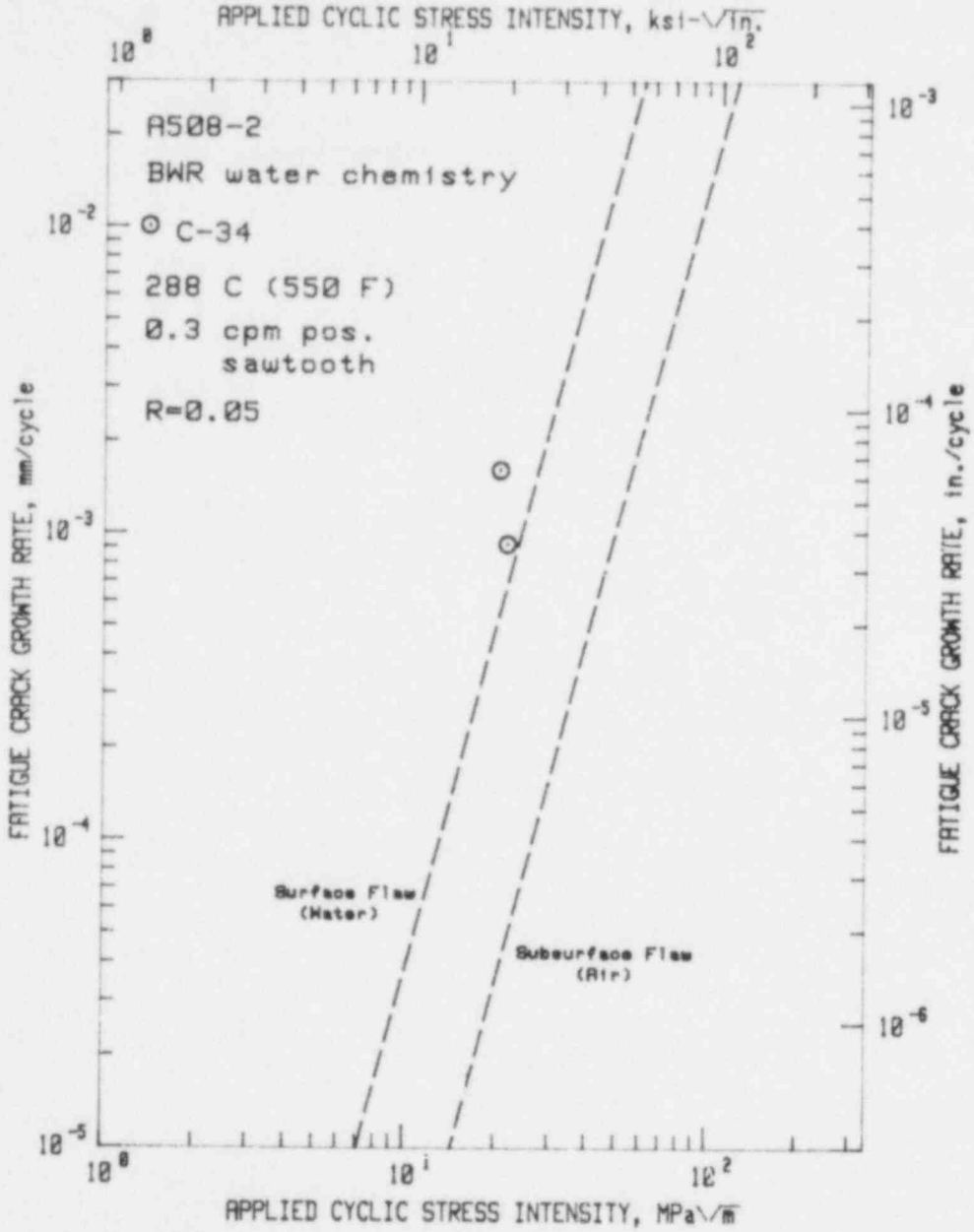

Fig. 72. Fatigue crack growth rate vs applied cyclic stress intensity factor for A508-2 steel in high-temperature, pressurized reactor-grade water--BWR conditions. For the low load ratio involved, these are rather high crack growth rates. Reference 25.

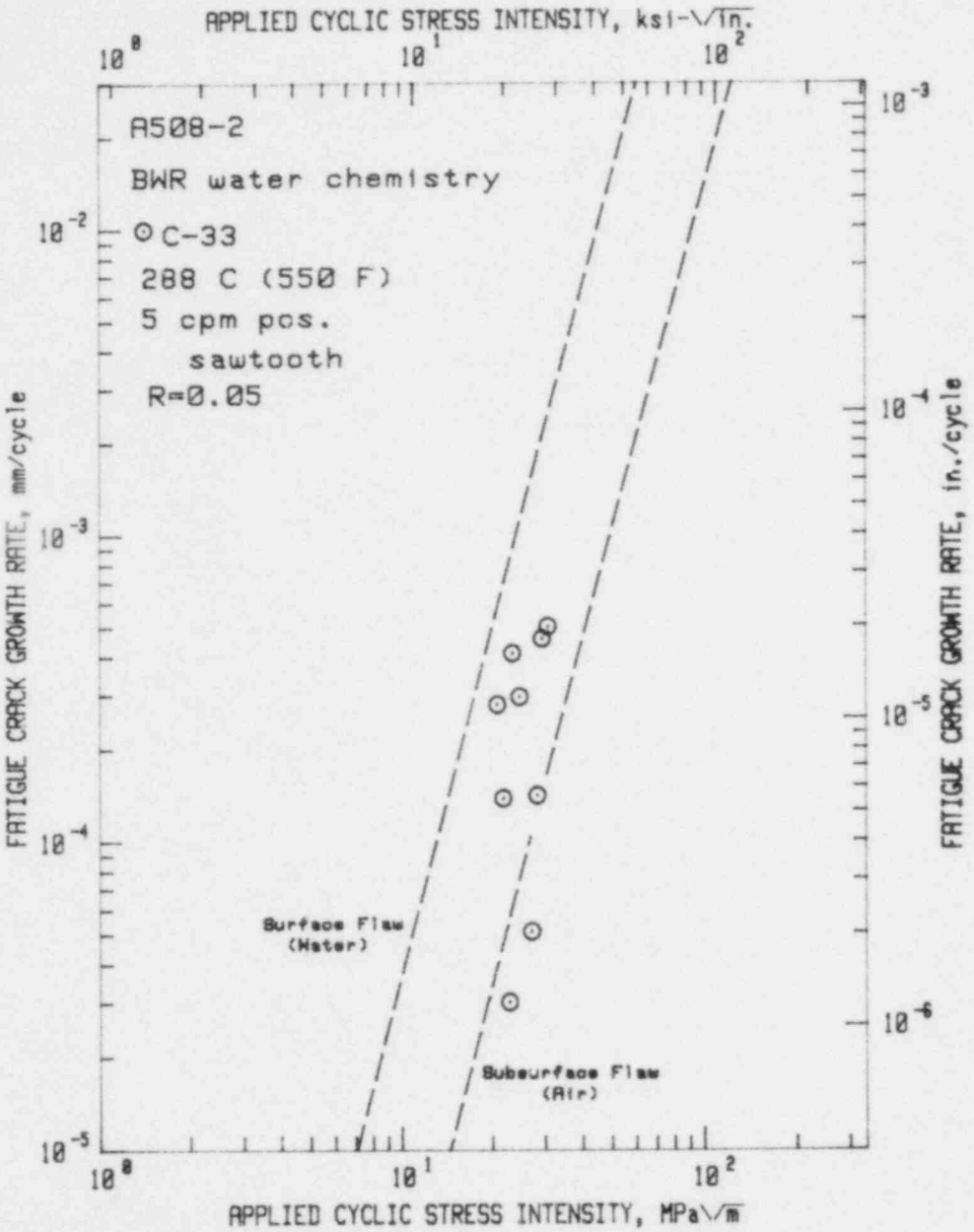

Fig. 73. Fatigue crack growth rate vs applied cyclic stress intensity factor for A508-2 steel in high-temperature, pressurized, reactor-grade water--BWR conditions. Relative to the data set in the previous figure, these results are lower due to the higher test frequency leading to reduced time for the environmental assistance to develop. Reference 25.

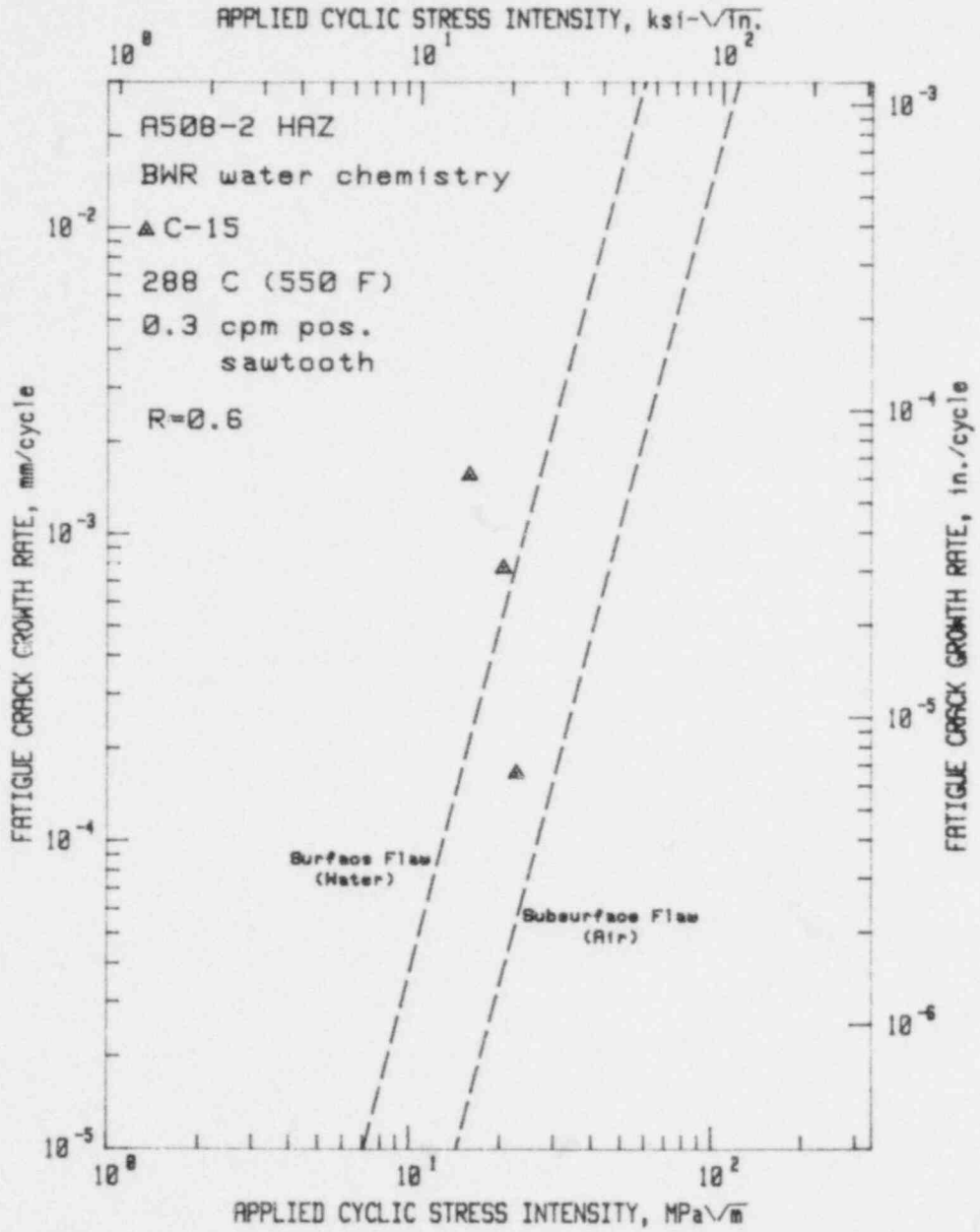

Fig. 74. Fatigue crack growth rate vs applied cyclic stress intensity factor for the heat-affected zone of an A508-2 parent plate in the high-temperature, pressurized reactor-grade water—BWR conditions. The strong downward trend of this data is difficult to rationalize, but the initial values agree well with other data for this waveform/frequency/load ratio combination. Reference 24.

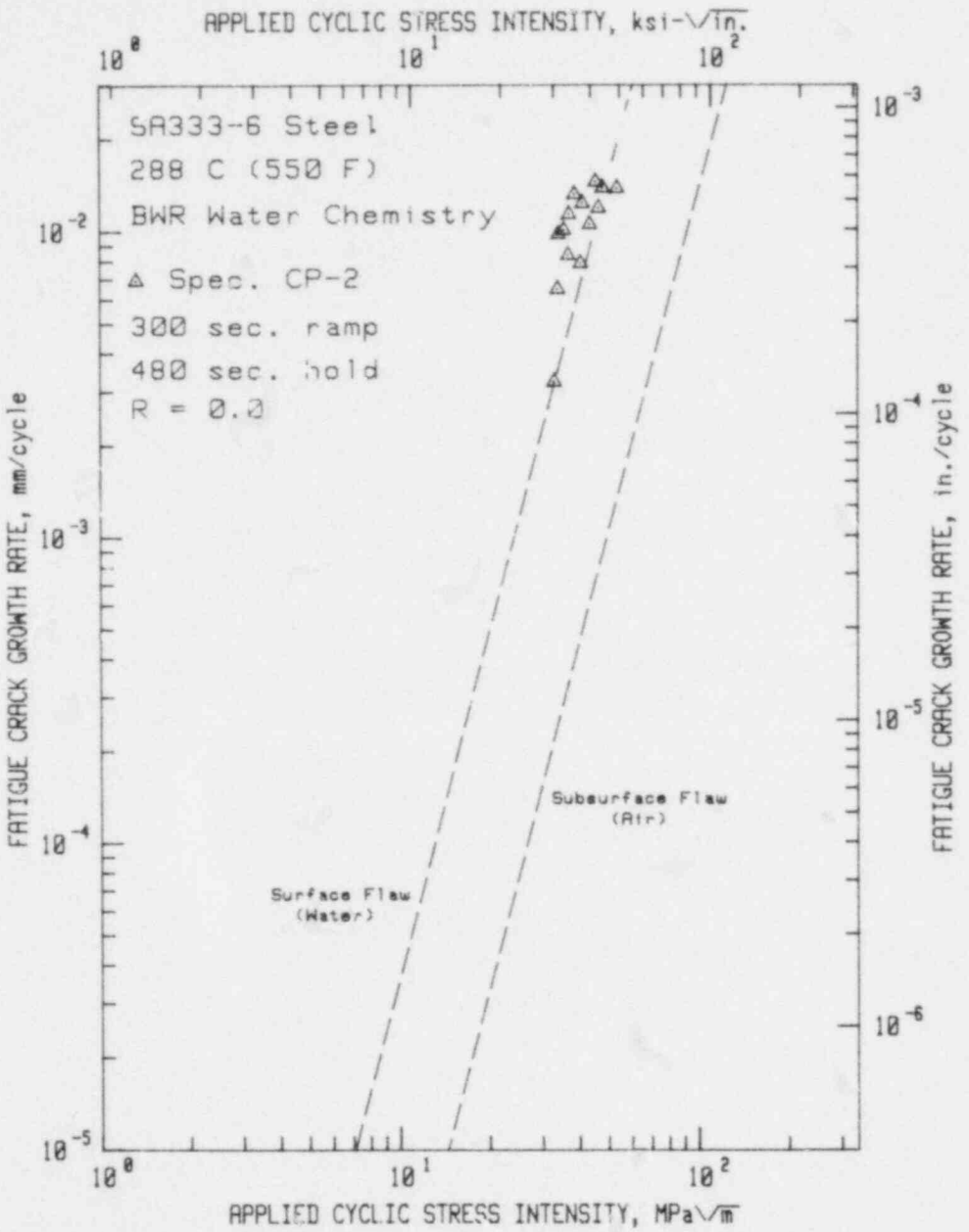

Fig. 75. Fatigue crack growth rate vs applied cyclic stress intensity factor for SA333-6 steel in the high-temperature, pressurized water environment--BWR conditions, 6 ppm dissolved oxygen. In spite of the low load ratio, the high dissolved oxygen content, coupled with the long period waveform results in high crack growth rates. Reference 29.

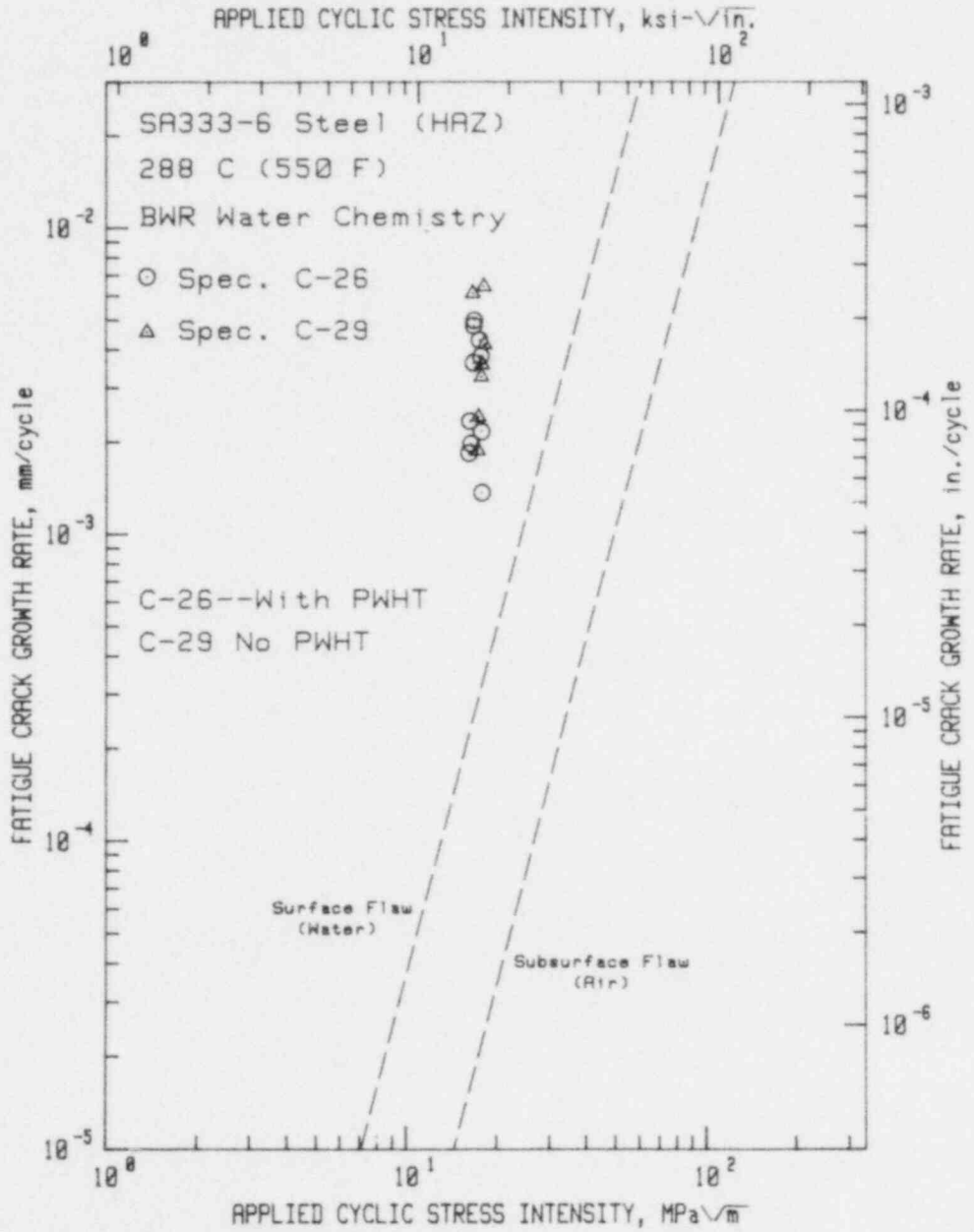

Fig. 76. Fatigue crack growth rate vs applied cyclic stress intensity factor for heat affected zone of SA333-6 in high-temperature, pressurized reactor-grade water--BWR conditions, 0.2 ppm dissolved oxygen. The application of a post-weld heat treatment does not seem to have an effect on the crack growth rate results. Reference 29.

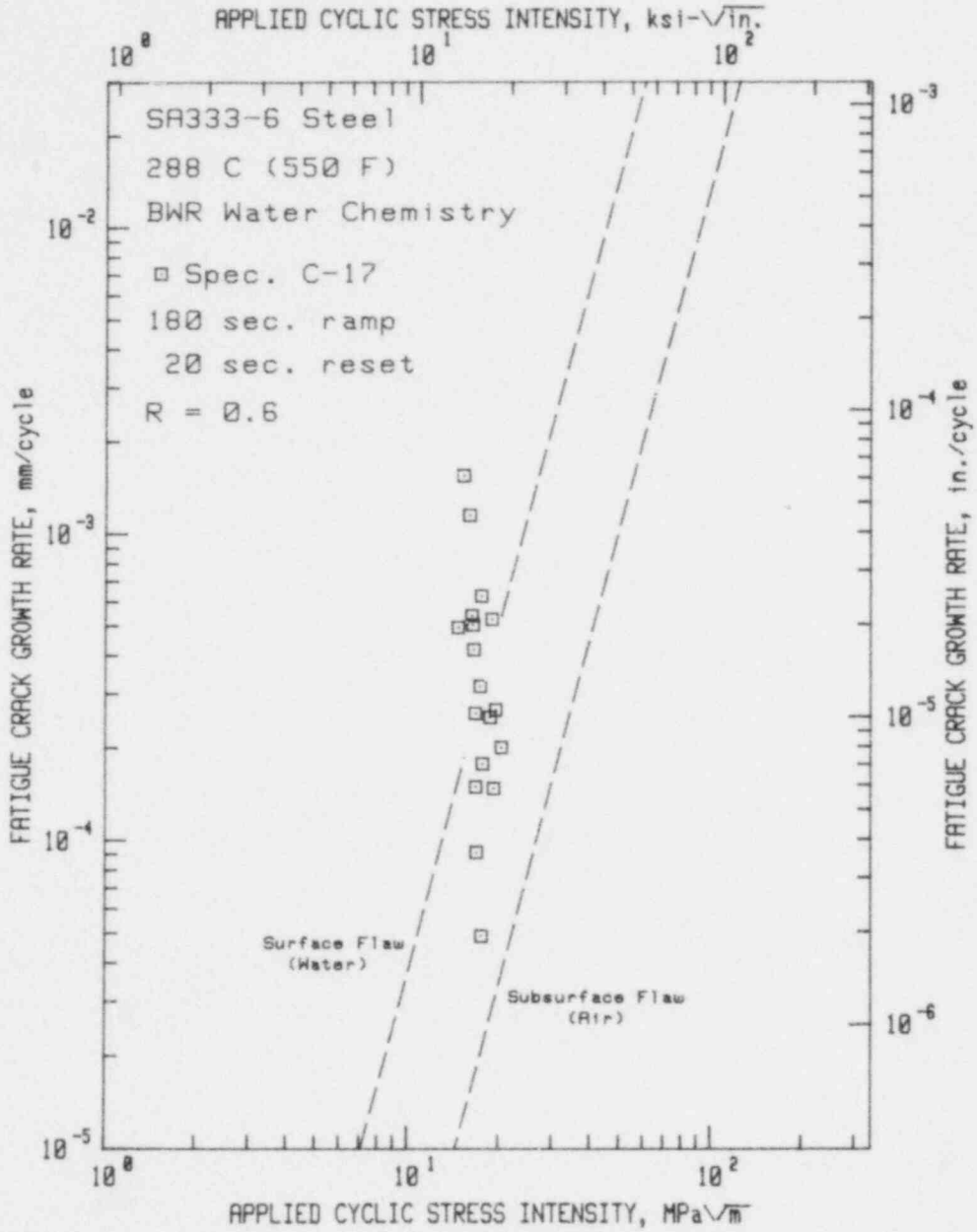

Fig. 77. Fatigue crack growth rates vs applied cyclic stress intensity factor for SA333-6 steel in high-temperature, pressurized reactor-grade water--BWR conditions. This data set shows an unusually strong deceleration at the higher ΔK values, considering the load ratio. Reference 29.

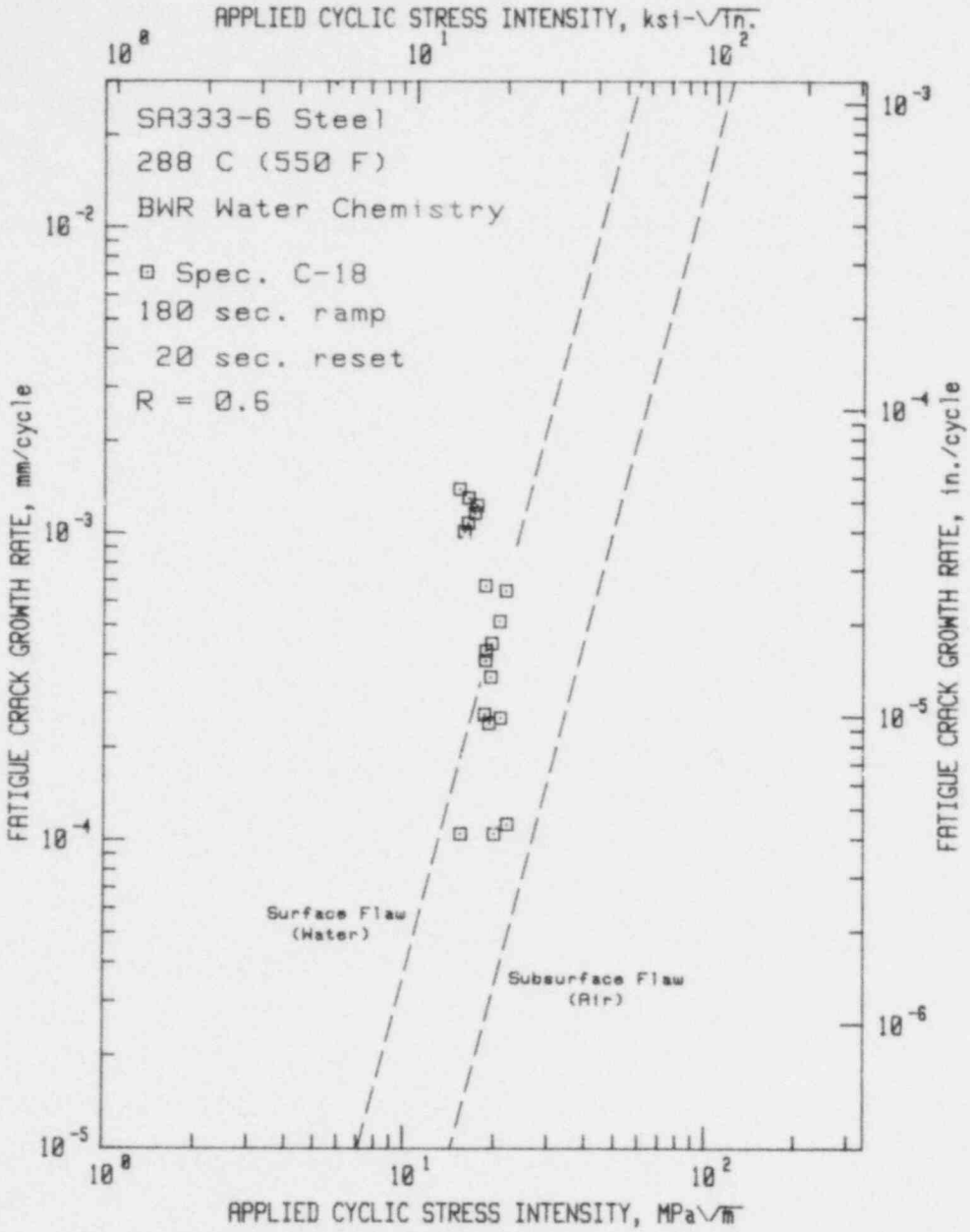

Fig. 78. Fatigue crack growth rates vs applied cyclic stress intensity factor for SA333-6 steel in high-temperature, pressurized reactor-grade water--BWR conditions. This data set reflect the same overall deceleration as in the previous figure, with increasing ΔK, which runs counter to the expected trend. Reference 29.

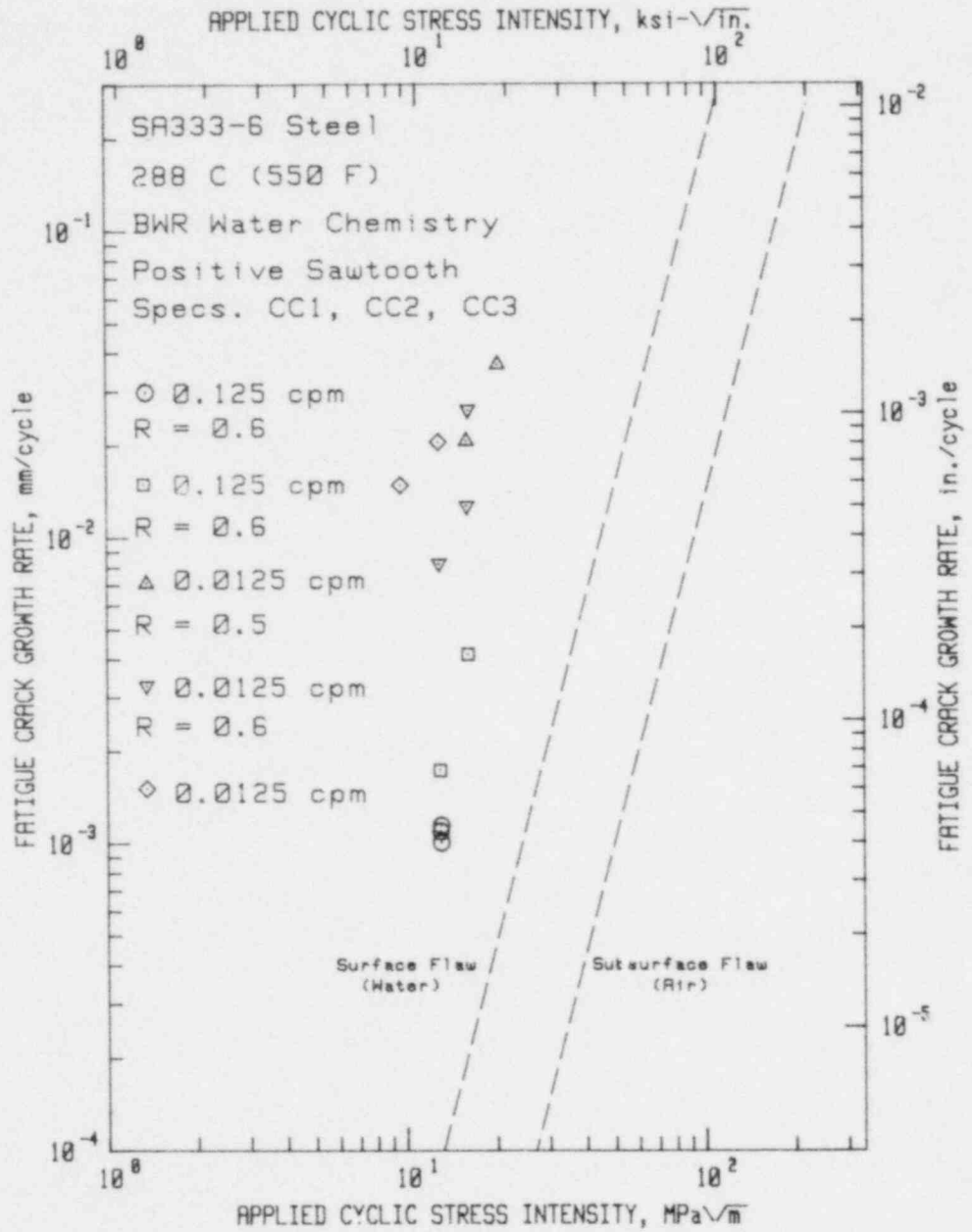

Fig. 79. Fatigue crack growth rates vs applied cyclic stress intensity factor for SA333-6 steel in high-temperature, pressurized reactor-grade water--BWR conditions. This data shows the expected trends of increased growth rates with increased cycle time. Reference 29.

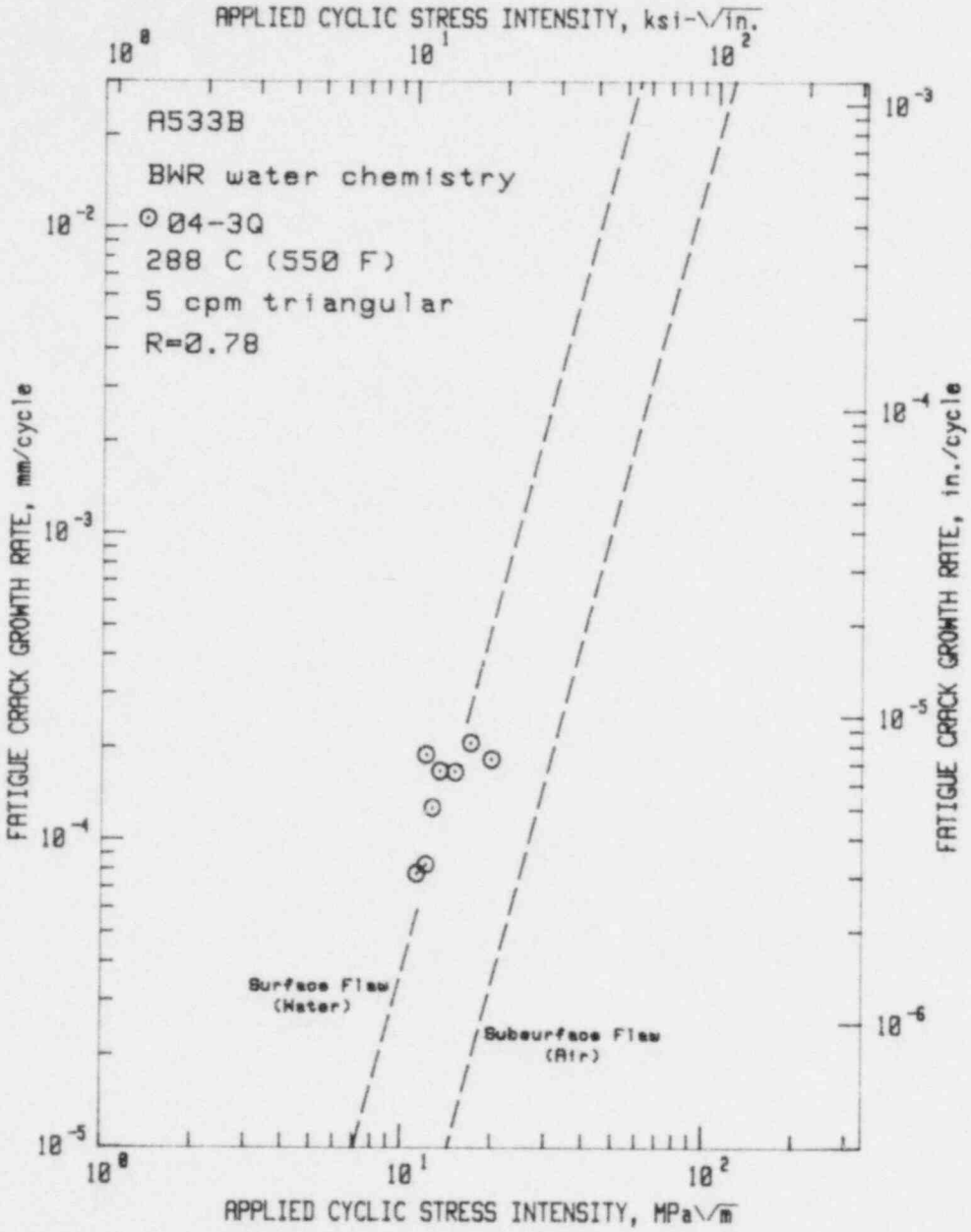

Fig. 80. Fatigue crack growth rate vs applied cyclic stress intensity factor for A533B steel in high-temperature, pressurized reactor-grade water--PWR conditions. This data compares well with other high load ratio tests with waveforms in this frequency range. References 22,23.

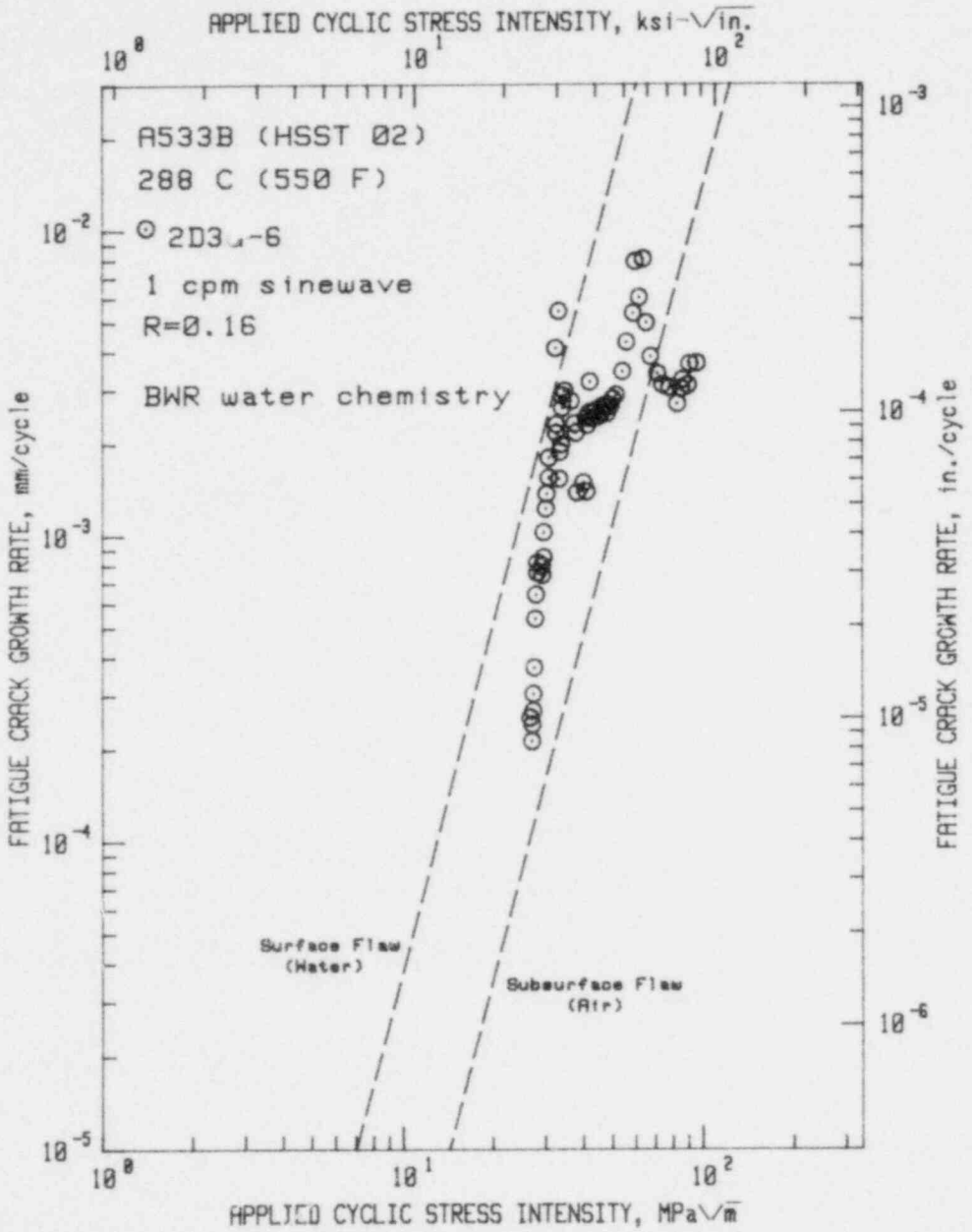

Fig. 81. Fatigue crack growth rate vs applied cyclic stress intensity factor for A533B steel in high-temperature, pressurized reactor-grade water--BWR conditions. For this relatively low load ratio, this data compares with other data for this material in both PWR and BWR environments. References 43,47.

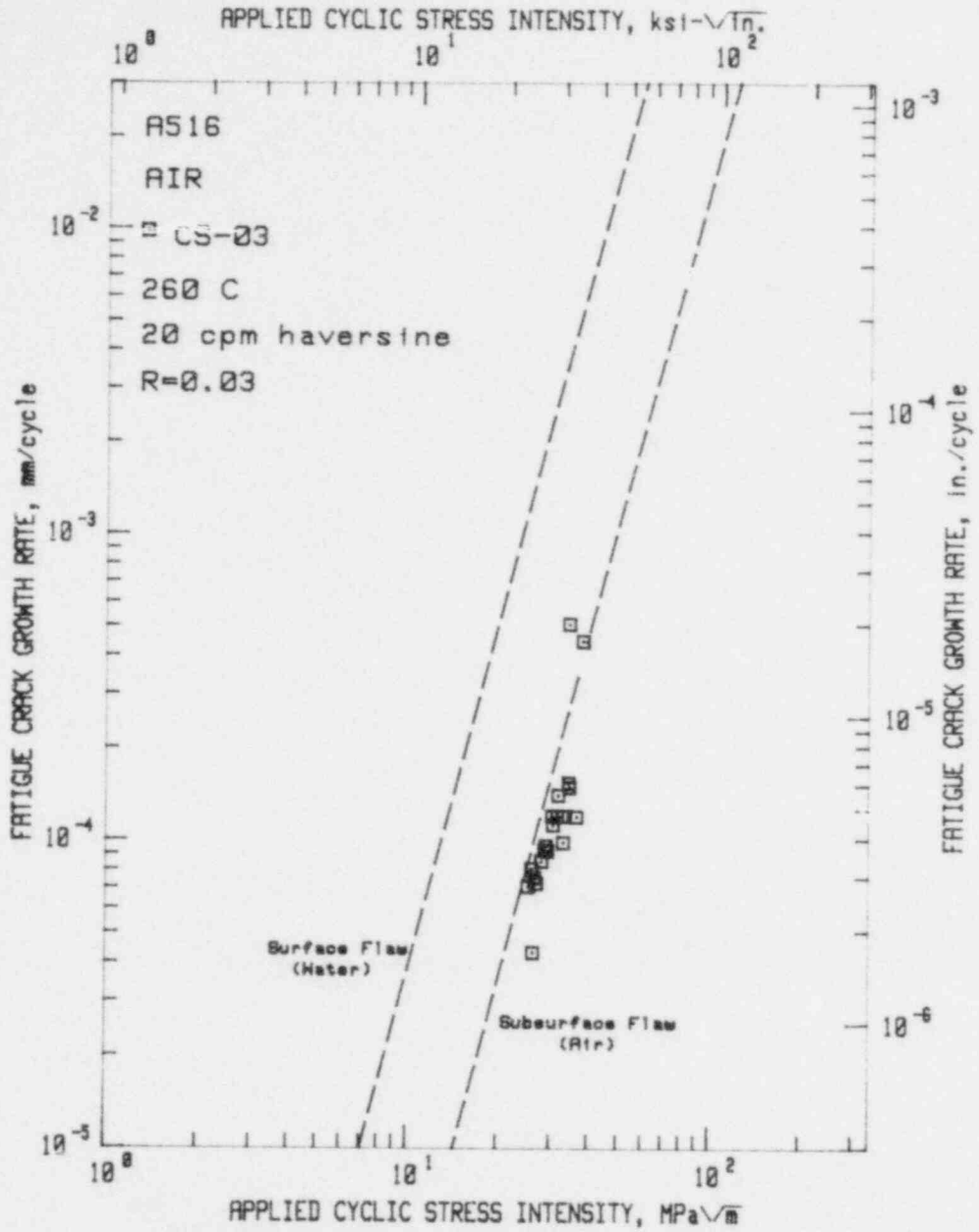

Fig. 82. Fatigue crack growth rate vs applied cyclic stress intensity factor for A516 steel in a high-temperature air environment. This data set represents baseline behavior for this material. Reference 21.

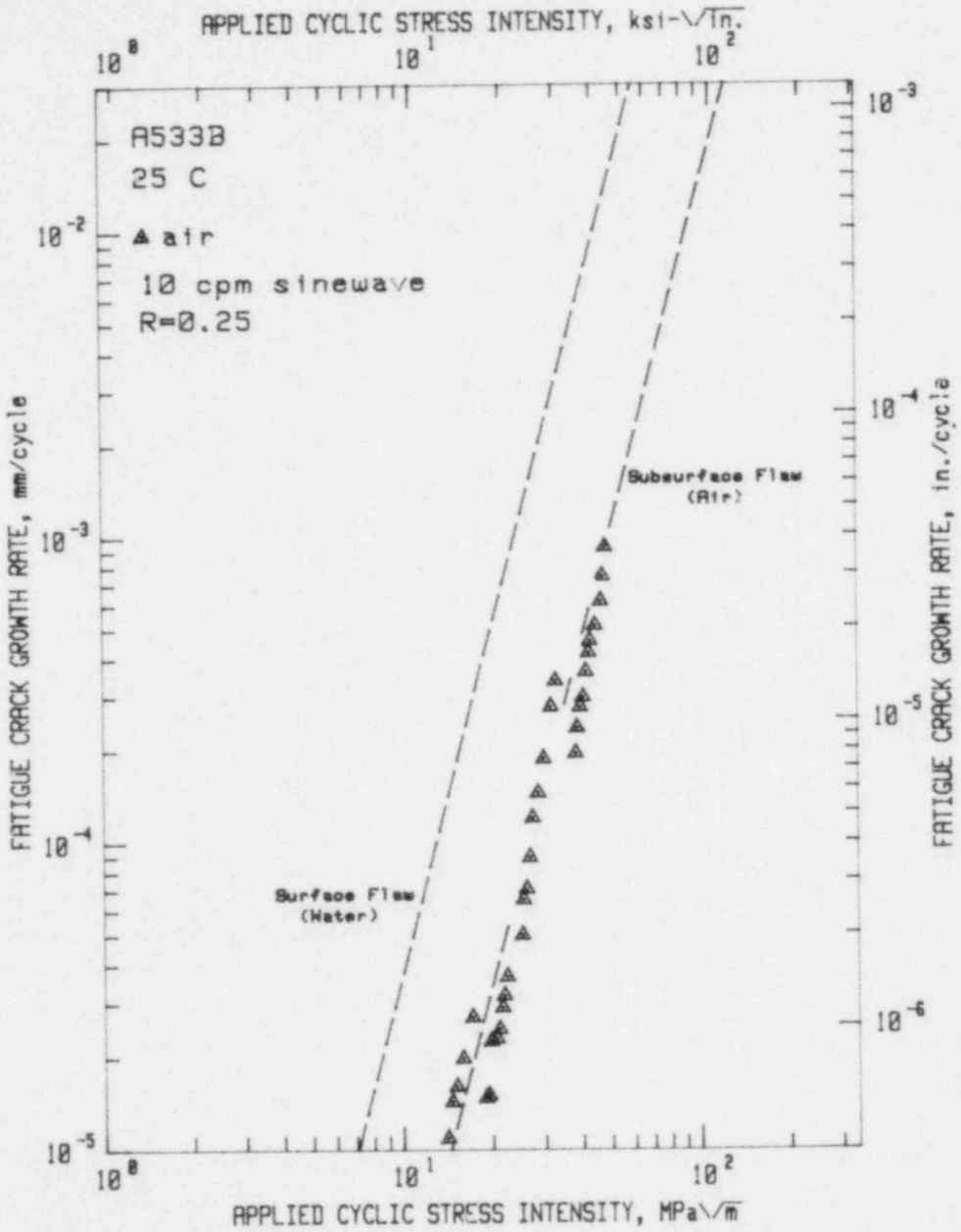

Fig. 83. Fatigue crack growth rate vs applied cyclic stress intensity factor for A533B steel in a room temperature air environment. This represents baseline data for the bulk of the work by Kondo and associates. References 3,4.

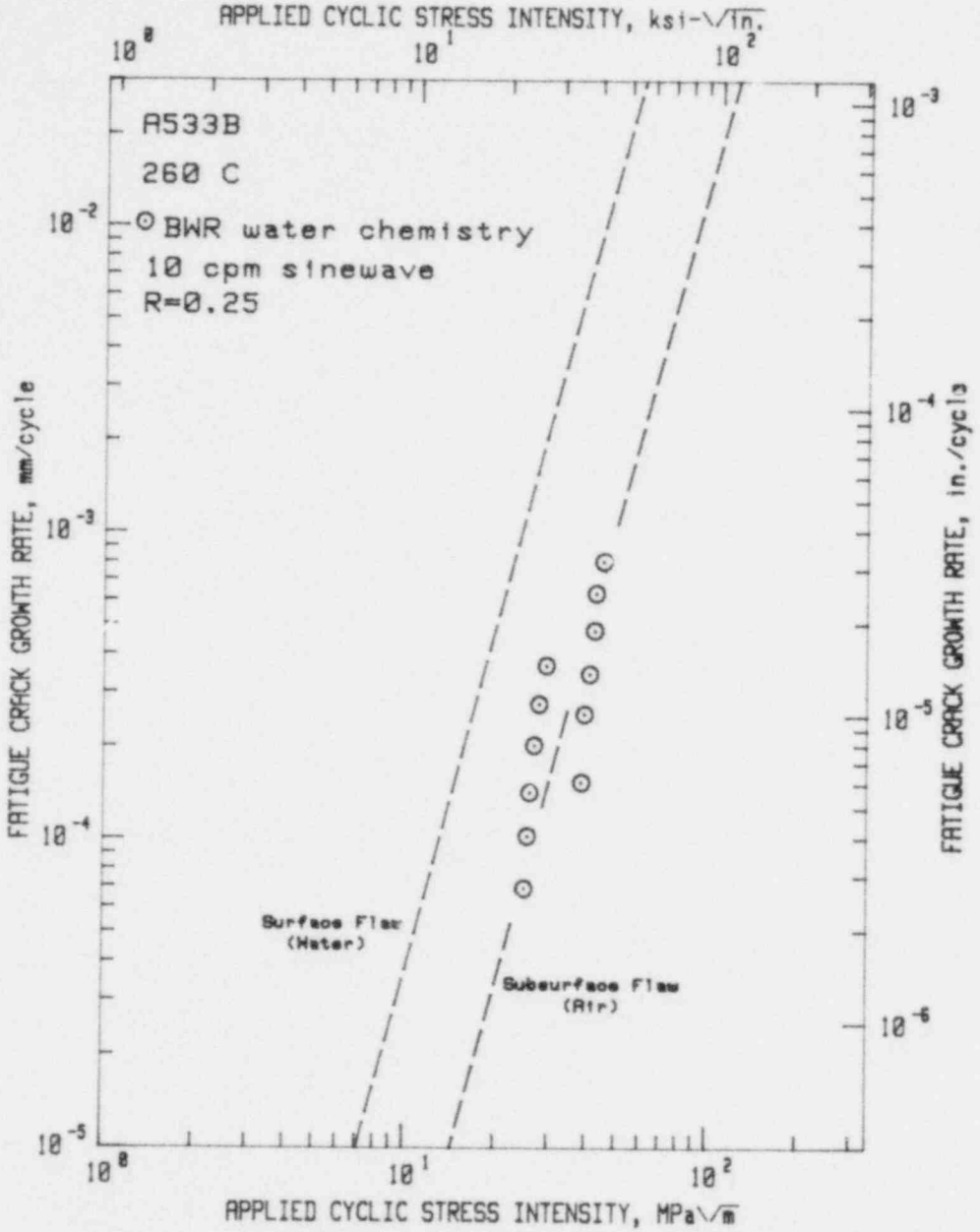

Fig. 84. Fatigue crack growth rate vs applied cyclic stress intensity factor for stainless-clad A302B steel in air, and in high-temperature, pressurized reactor grade water—BWR conditions. The rather low growth rates indicate that the clad has no adverse effect. It is difficult to assert that the clad has a positive effect, since growth rates for a 170 mHz (10 cpm) waveform would be quite low anyway. References 2,3,4.

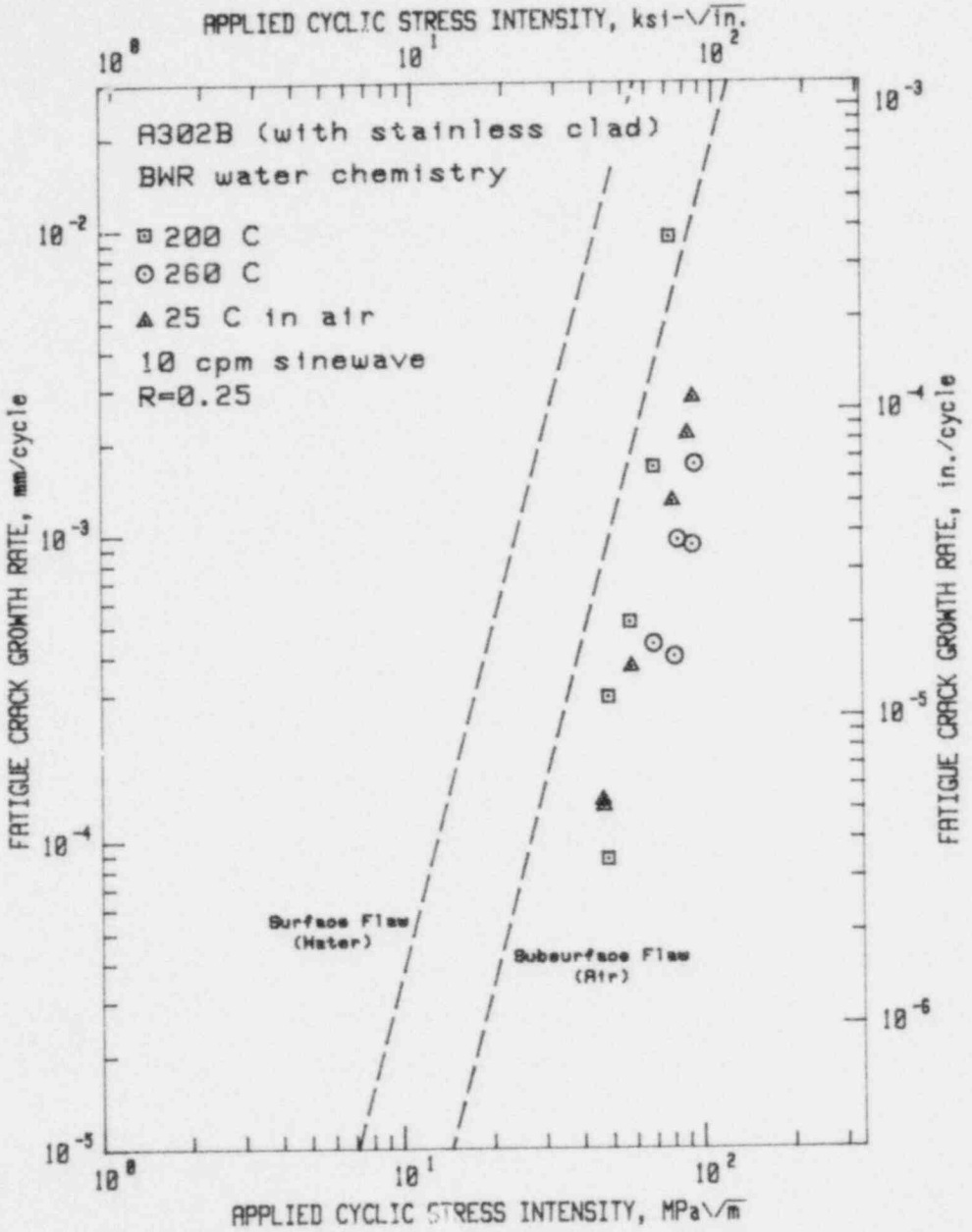

Fig. 85. Fatigue crack growth rate vs applied cyclic stress intensity factor for A533B steel in high-temperature, pressurized reactor-grade water--BWR conditions. These results, when compared with those of Fig. 86, indicate that the environment has little effect for these loading conditions. References 3,4.

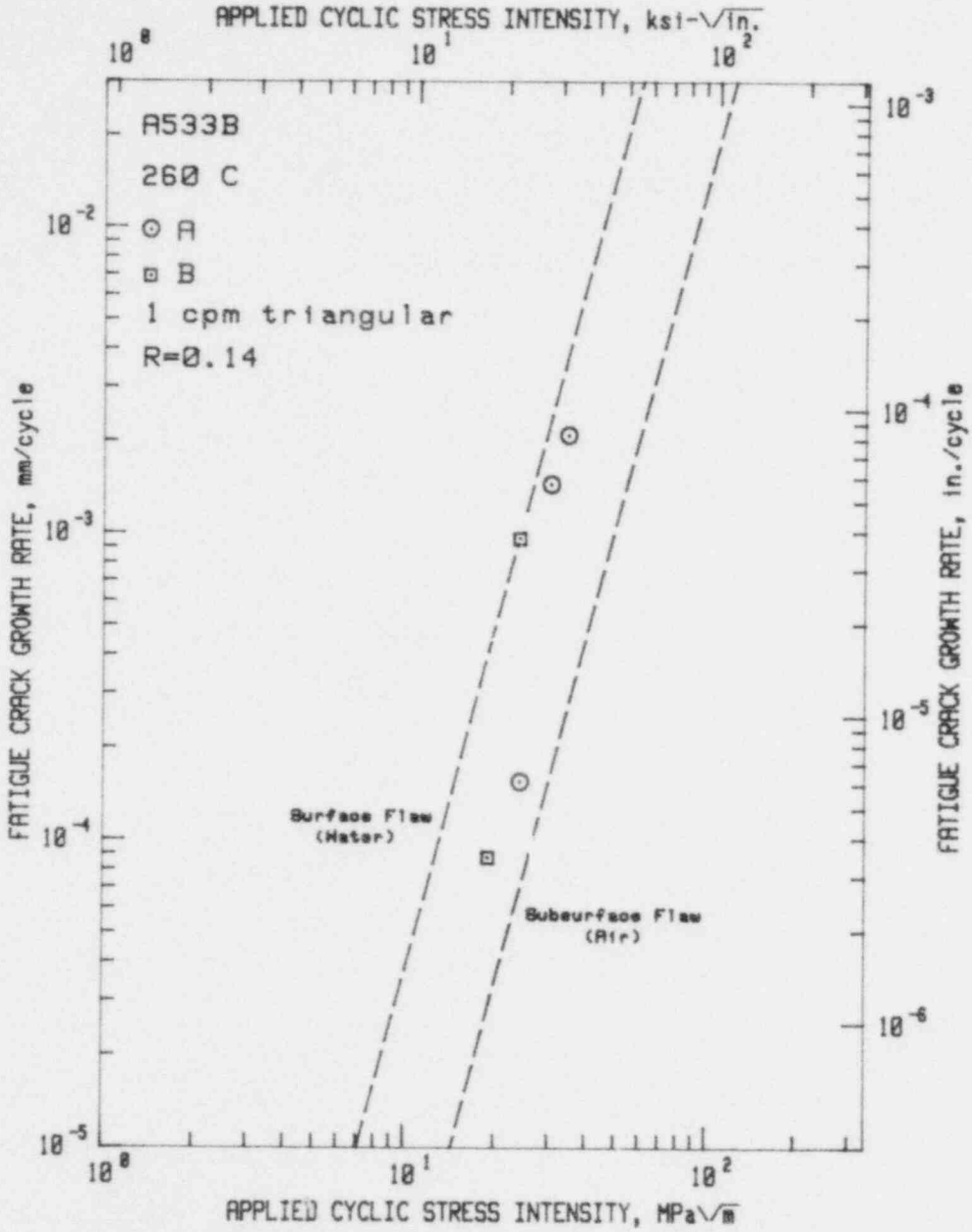

Fig. 86. Fatigue crack growth rate vs applied cyclic stress intensity factor for A533B steel in high-temperature, pressurized, reactor-grade water--BWR conditions. Materials A and B represent two different heats of A533B. Reference 7.

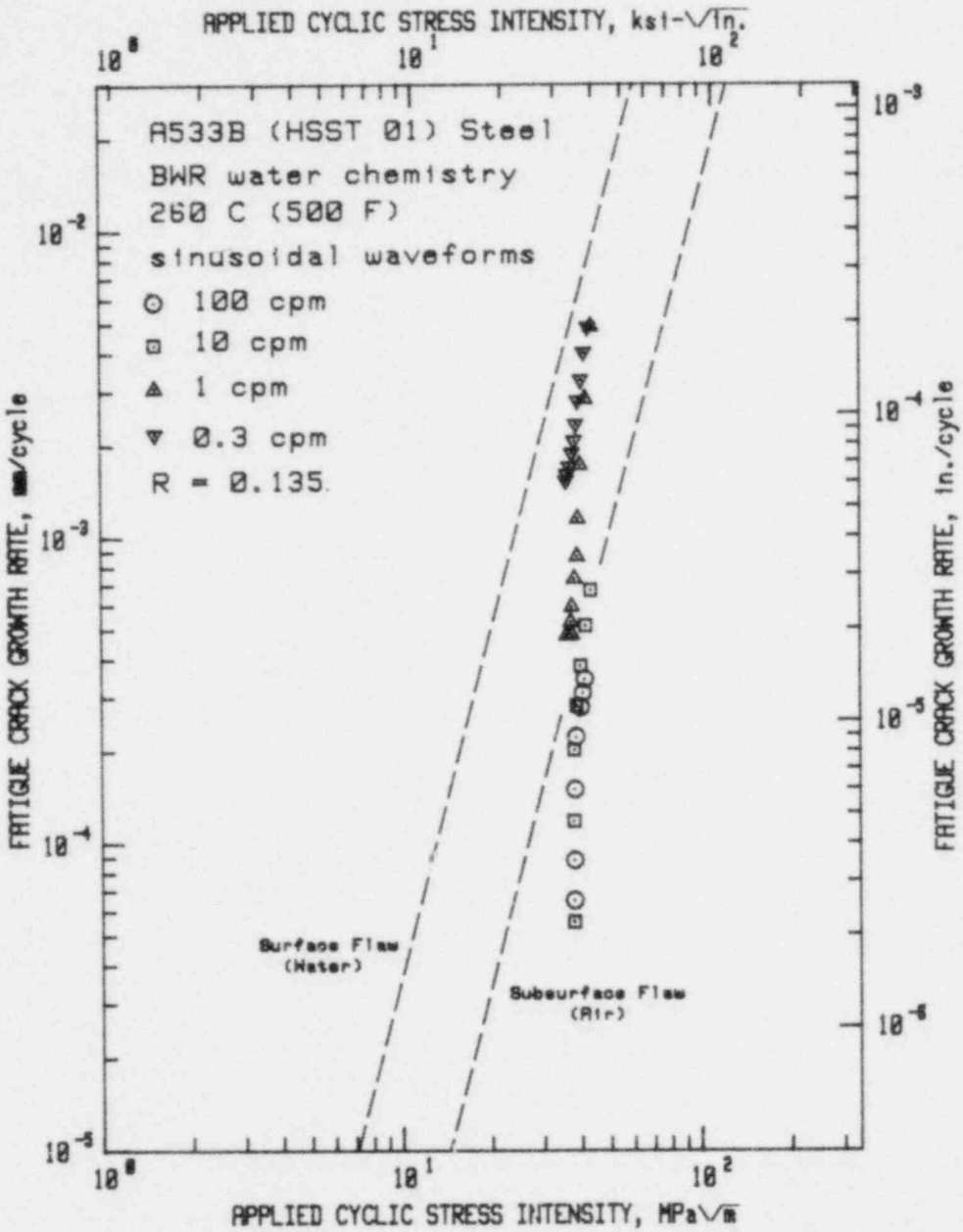

Fig. 87. Fatigue crack growth rate vs applied cyclic stress intensity factor for A533B steel in high-temperature, pressurized reactor-grade water—BWR conditions. Specimens in Figs. 84-89 were double edge notched tension specimens, with crack extensions determined by beach marks. Reference 3.

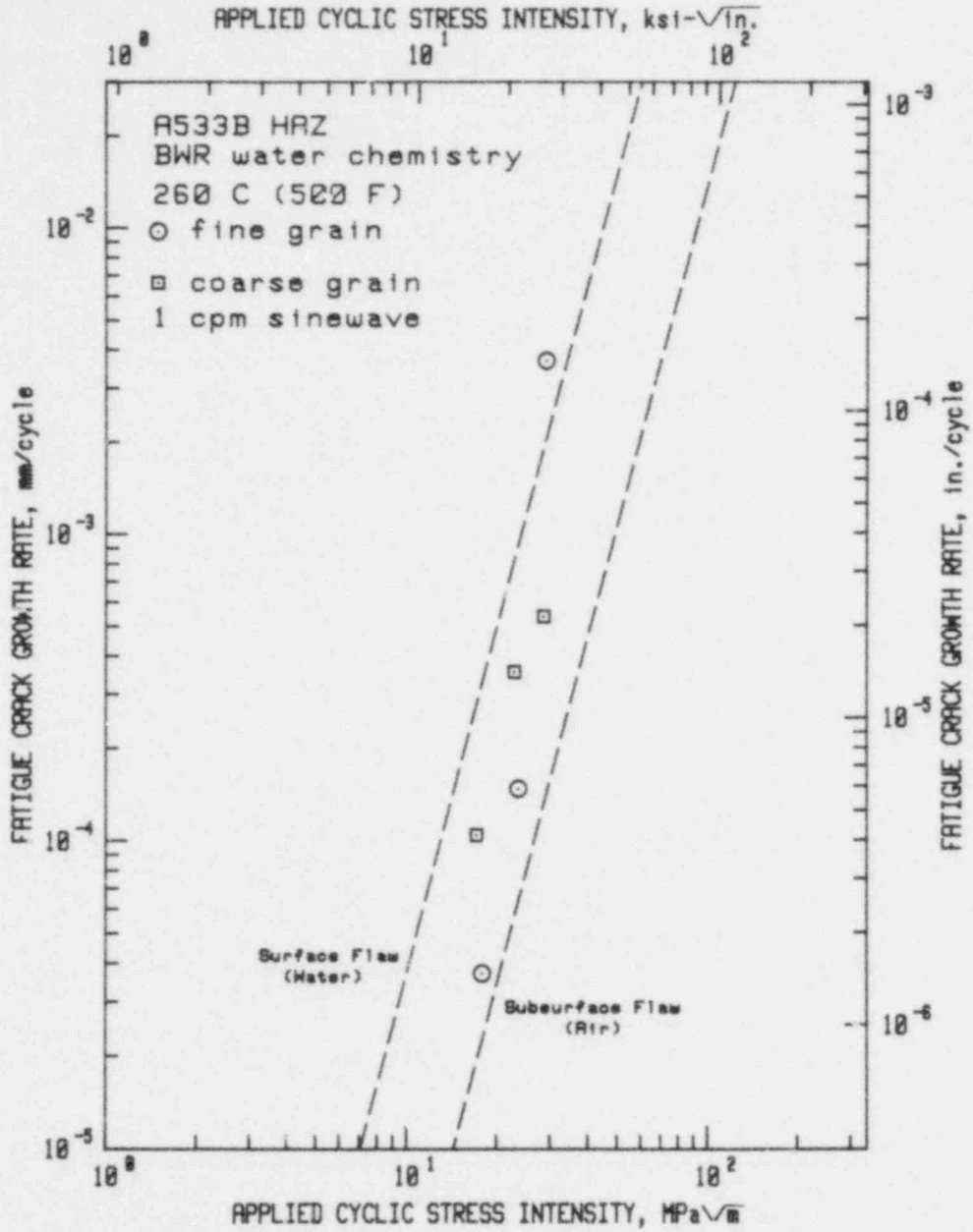

Fig. 88. Fatigue crack growth rate vs applied cyclic stress intensity factor for heat-affected zone material of A533B parent plate, in the high-temperature, pressurized reactor-grade water-BWR conditions. This data indicates a cross-over behavior of the fine and coarse grained materials. Reference 7.

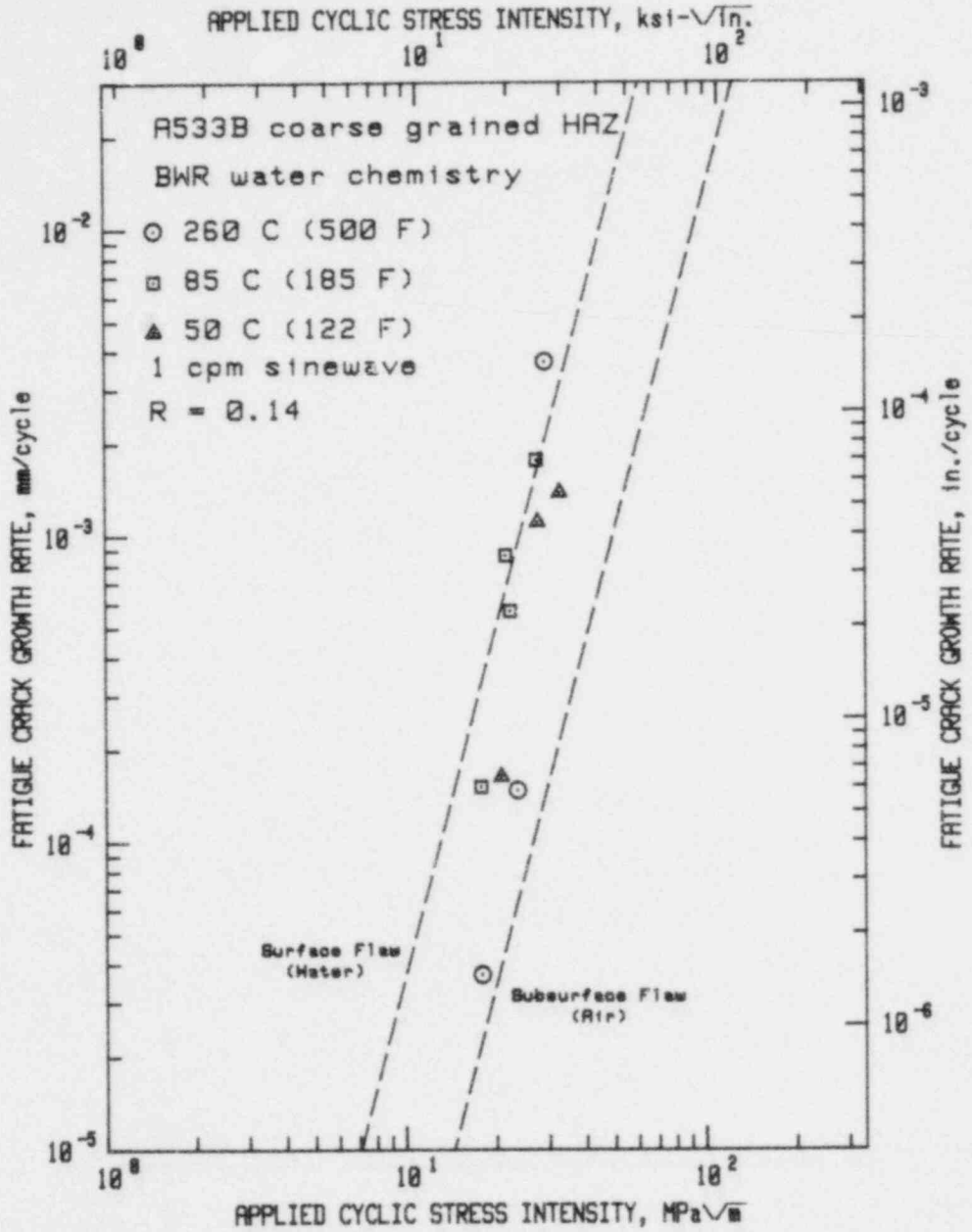

Fig. 89. Fatigue crack growth rate vs applied cyclic stress intensity factor for coarse-grained, heat-affected zone material of A533B parent plate in high-temperature, pressurized, and lower temperature, reactor-grade water--BWR conditions. At least for the higher ΔK values, the higher temperature environments result in higher crack growth rates. Reference 7.

REFERENCES:

1. M. L. Vanderglas and B. Mukherjee, "Fatigue Threshold Stress Intensity and Life Estimation of ASTM-A106B Piping Steel", ASME Publication 79-PVP-86, American Society of Mechanical Engineers, New York, NY, 10017 (1979).

2. T. Kondo, T. Kikuyama, H. Nakajima, M. Shindo and R. Nagasaki, "Corrosion Fatigue of ASTM A302B Steel in High Temperature Water, the Simulated Nuclear Reactor Environment" in Corrosion Fatigue: Chemistry, Mechanics and Microstructure, NACE-2, eds. O. Devereux et al, National Association of Corrosion Engineers, Houston, TX 77027, pp. 539-556 (1973).

3. T. Kondo, T. Kikuyama, H. Nakajima and M. Shindo, "Fatigue Crack Propagation Behavior of ASTM A533B and A302B Steels in High Temperature Aqueous Environment", Paper No. 6, Heavy Section Steel Technology Program, 6th Annual Information Meeting, Oak ridge National Laboratory, Oak Ridge, TN 37830, (Apr. 1972).

4. T. Kondo, "Fatigue-Crack-Growth Study of Nuclear Pressure Vessel Materials in Simulated Reactor Environment", in HSST Semiannual Progess Report for Period Ending Feb. 1972, ORNL-4816, pp. 56-64 (1972).

5. T. Kondo, T. Kikuyama, H. Nakajima and M. Shindo, "Fatigue of Low-Alloy Steels in Aqueous Environment at Elevated Temperatures", Proc. of the 1971 Int. Conf. on Mechanical Behavior of Materials, Vol. III, pp. 319-327 (1972).

6. T. Kondo, Y. Ogawa and H. Nakajima, "Stress Corrosion Failure of Stainless Steel Components in a BWR and the Effect of Cyclic Loading on the Crack Propagation", in Corrosion Problems in Energy Conversion, ed. C. S. Tedmon, Jr., Electrochemical Society, Princeton, NY, pp. 346-358 (1974).

7. M. Suzuki, H. Takahashi, T. Shoji, T. Kondo and H. Nakajima, "The Environment Enhanced Crack Growth Effects in Structural Steels for Water Cooled Reactors", in The Influence of Environment on Fatigue, Institution of Mechanical Engineers, London, pp. 161-169 (1977).

8. H. Nakajima, T. Shoji, M. Kikuchi, H. Niizuma and M. Shindo, "Detecting Acoustic Emission During Cyclic Crack Growth in Simulated BWR Environment", in Fatigue Crack Growth Measurement and Data Analysis, a forthcoming STP, American Society for Testing and Materials, Philadelphia, PA 19103.

9. K. Gott, "Corrosion Fatigue of Pressure Vessel Steel A533B, Part I: Survey of Experience up to mid 1978, Final Report", Studsvik/MS-78/239, Studsvik Energiteknik AB, Nykoping (1978).

10. J. D. Atkinson and T. C. Lindley, "The Effect of Frequency and Temperature on Environmentally Assisted Fatigue Crack Growth Below K_{ISCC} in Steels", in The Influence of Environment on Fatigue, Institution of Mechanical Engineers, London, pp. 65-74 (1977).

11. J. D. Atkinson and T. C. Lindley, "Effect of Stress Waveform and Hold-time on Environmentally Assisted Fatigue Crack Propagation in C-Mn Structural Steel", Metal Science, 13,pp. 444-448 (1979).

12. P. M. Scott, "The Use of Corrosion Fatigue Data in The Assessment of Crack Growth in Large Nuclear Pressure Vessels", in Tolerance of Flaws for Pressurized Components, Institution of Mechanical Engineers, London, pp. 77-86 (1978).

13. P. M. Scott, "Effects of Environment on Crack Propagation", in Developments in Fracture Mechanics-1, ed. C. G. Chell, Applied Science Publ., Barking, pp. 221-257 (1979).

14. P. M. Scott, "Corrosion Fatigue in Pressure Vessel Steels for Light Water Reactors", Metal Science 13, pp. 396-401 (1979).

15. B. Tomkins, "The Role of Crack Tip Opening in Corrosion Fatigue for the Ductile Ferritic Steel-Water System", in The Influence of Environment on Fatigue, Institution of Mechanical Engineers, London, pp. 111-116 (1977).

16. B. Tomkins, "Role of Mechanics in Corrosion Fatigue", Metal Science 13, pp. 387-395 (1979).

17. C. Gee, International Cyclic Crack Growth Rate Group Meeting, Unieux, France (Aug. 1979).

18. W. A. Van Der Sluys (ed), "Corrosion Fatigue Characterization of Reactor Pressure Vessel Steels", First Semiannual Report for EPRI Project No. RP 1325-1, Babcock & Wilcox, Alliance, OH 44601 (Sept. 1979).

19. T. L. Gerber, J. D. Heald and E. Kiss, "Fatigue Crack Growth in SA508-Cl2 Steel in a High Temperature, High Purity Water Environment", Trans. ASME, ser. H, J. Eng. Mat. and Technology, 96, pp. 255-261 (1974).

20. E. Kiss, T. L. Gerber and J. D. Heald, "Evaluation of Fatigue Crack Growth in a Simulated Light Water Reactor Environment", Closed Loop, 4, pp. 3-9 (1974).

21. D. A. Hale, J. Gallego, W. Briggs, and I. M. Coussers, "Task K-Effect of BWR Environment", in Reactor Primary Coolant System Pipe Rupture Study Progress Report No. 32, July-December 1974, GEAP-10207-32 (March 1975).

22. D. A. Hale, J. Gallego, W. Briggs and I. M. Coussers, "Task K-Effect of BWR Environment", in Reactor Primary Coolant System Pipe Rupture Study Progress Report No. 34, July-December 1974, GEAP-10207-34 (Feb. 1976).

23. D. A. Hale and D. Vogelhuber, "Task K-Effect of BWR Environment", in Reactor Primary Coolant System Pipe Rupture Study Progress Report No. 35, January-March 1976, GEAP-10207-35 (May 1976).

24. D. A. Hale and D. Vogelhuber, "Task K-Effect of BWR Environment", in Reactor Primary Coolant System Pipe Rupture Study Progress Report No. 39, January-March 1977, GEAP-10207-39 (May 1977).

25. D. A. Hale and J. L. Yuen, "Task K-Effect of BWR Environment", in Reactor Primary Coolant System Pipe Rupture Study Progress Report No. 40, April-June 1977, GEAP-NUREG-10207-40 (Aug. 1977).

26. D. A. Hale, J. Yuen and T. Gerber, "Fatigue Crack Growth in Piping and RPV Steels in Simulated BWR Water Environment" GEAP-24098, General Electric Co., San Jose, CA, (Jan. 1978).

27. D. A. Hale and J. N. Kass, "Fatigue Crack Growth of Low Alloy Steel in a High Temperature, High Purity Oxygenated Water Environment", Corrosion 79, Atlanta, GA, National Association of Corrosion Engineers (1979).

28. D. A. Hale, C. W. Jewett and J. N. Kass, "Fatigue Crack Growth Behavior of Four Structural Alloys in High Temperature High Purity Oxygenated Water", ASME Publication 79-PVP-104, American Society of Mechanical Engineers, New York, NY 10017 (1979).

29. D. A. Hale, J. N. Kass and C. Jewett, "Environmental Fatigue Crack Growth", in BWR Environmental Cracking Margins for Carbon Steel Piping, First Semiannual Progress Report, July 1978 to December 1978 , NEDC-24625 (Jan. 1979).

30. D. A. Hale, J. N. Kass and C. Jewett, "Environmental Fatigue Crack Growth", in BWR Environmental Cracking Margins for Carbon Steel Piping, 2nd Semiannual Progress Report, January 1979 to June 1979, NEDC-25145 (July 1979).

31. T. A. Prater, H. M. Morgan and L. F. Coffin, "Crack Growth Rate Measurements" in BWR Environmental Cracking Margins for Carbon Steel Piping, First Semiannual Progress Report, July 1978 to December 1978, NEDC-24635 (Jan. 1979).

32. L. F. Coffin, "Fatigue Design Basis", in BWR Environmental Cracking Margins for Carbon Steel Piping, 2nd Semiannual Progress Report, January 1979 to June 1979, NEDC-25145 (July 1979).

33. H. E. Watson, B. H. Menke, and F. J. Loss, "Evaluation of Critical Factors in Crack Growth Rate Studies", in Structural Integrity of Water Reactor Pressure Boundary Components, ed. F. J. Loss, NRL Memorandum Report 3782 (May 1978).

34. W. H. Cullen, Jr., H. E. Watson, K. J. Torronen, V. Provenzano, F. J. Loss and G. Gabetta, "Evaluation of Critical Factors in Cyclic Crack Growth Rate Studies", in Structural Integrity of Water Reactor Pressure Boundary Components, ed. F. J. Loss, NUREG/CR 0943, NRL Memorandum Report 4064 (Sept. 1979).

35. W. H. Cullen, Jr., H. E. Watson, V. Provenzano, "Results of Cyclic Crack Growth Rate Studies in Pressure Vessel and Piping Steels", in Structural Integrity of Water Reactor Pressure Boundary Components, ed. F. J. Loss, NUREG/CR 1128, NRL Memorandum Report 4122 (Dec. 1979).

36. W. H. Cullen, Jr., et al., "Evaluation of Factors in Cyclic Crack Growth Rate Studies" in Structural Integrity of Water Reactor Pressure Boundary Components, ed. F. J. Loss, NUREG/CR 1268, NRL Memorandum Report 4174 (Jan. 1980).

37. W. H. Cullen, Jr., et al., "Evaluation of Starting [illegible] Phenomenon on Cyclic Crack Growth in A508 Pressure Vessel Steels", Report of NRL Progress, pp. 14-17 (July 1978).

38. D. K. Sturm, F. J. Loss and W. H. Cullen, Jr., "Qualification of Crack Growth Data Beyond ASTM Committee E-24 Criteria", Report of NRL Progress, pp. 4-9 (Sept. 1978).

39. W. H. Cullen, Jr., B. H. Menke, H. E. Watson and F. J. Loss, "A Computerized Data Acquisition for a High-Temperature, Pressurized Water Fatigue Test Facility" in Computer Automation of Materials Testing, ASTM STP 710, pp. 127-140, American Society for Testing and Materials, Philadelphia, PA 19103.

40. W. H. Cullen, Jr., V. Provenzano, K. J. Torronen, H. E. Watson and F. J. Loss, "Fatigue Crack Growth of A508 Steel in High-Temperature, Pressurized Reactor-Grade Water", NUREG/CR 0969, NRL Memorandum Report 4063, (Sept. 1979).

41. W. H. Cullen, Jr., V. Provenzano and K. Torronen, "A Hydrogen Assisted Fatigue Crack Growth Model for PWR Environments" Report of NRL Progress, pp.9-15 (December 1979).

42. T. R. Mager and V. J. McLoughlin, "The Influence of an Environment of High Temperature Primary Grade Nuclear Reactor Water on the Fatigue Crack Growth Characteristics of A533 Grade B Class 1 Plate and Weldment Material", Heavy Section Steel Technology Program Technical Report No. 16, HSST-TM-16 (Oct. 1971).

43. T. R. Mager, J. D. Landes, V. McLoughlin and D. M. Moon, "The Effect of Low Frequencies on the Fatigue Crack Growth Characteristics of A533B Class 1 Plate in an Environment of High Temperature Primary Grade Nuclear Reactor Water", Heavy Section Steel Technology Program Technical Report No. 35, HSST-TM-35 (Dec. 1973).

44. S. A. Legge and T. R. Mager, "Effects of High-Temperature Primary Reactor Water on the Subcritical Crack Growth of Reactor Vessel Steel", in HSST Semiannual Progress Report ORNL-4855, pp. 12-16 (Aug. 1972).

45. T. R. Mager, D. M. Moon, J. D. Landes and J. M. McLoughlin, "Effect of High-Temperature Primary Reactor Water on the Subcritical Crack Growth of Reactor Vessel Steel", in HSST Semiannual Progress Report ORNL-4971. pp. 25-29 (Aug. 1973).

46. T. R. Mager, "Effect of High-Temperature Primary Reactor Water on the Subcritical Crack Growth of Reactor Vessel Steel" in HSST Quarterly Progress Report for July-September 1974, ORNL-TM-4729, pp. 33-35 (Nov. 1974).

47. T. R. Mager, D. M. Moon and J. D. Landes, "Fatigue Crack Growth Characerisitics of A533B Class 1 Plate in an Environment of High-Temperature Primary Grade Nuclear Reactor Water", Trans. ASME ser. J., J. Pressure Vessel Technology, 99, pp. 1-12 (May 1977).

48. W. H. Bamford, "Effect of High-Temperature Primary Reactor-Grade Water on the Subcritical Crack Growth of Reactor Vessel Steel", in HSST Quarterly Progress Report for January-March 1975, ORNL-TM-4914, pp. 18-20 (June 1975).

49. W. H. Bamford, "Effect of High-Temperature Primary Reactor-Grade Water on the Subcritical Crack Growth of Reactor Vessel Steel", in HSST Quarterly Progress Report for October-December 1975, ORNL/NUREG/TM-3, pp. 26-29 (April 1976).

50. W. H. Bamford and K. V. Scott, "Effect of High-Temperature Primary Reactor-Grade Water on the Subcritical Crack Growth of Reactor Vessel Steel", in HSST Quarterly Progress Report for April-June 1976, ORNL/NUREG/TM-49, pp. 19-26 (Oct. 1976).

51. W. H. Bamford and K. V. Scott, "Effect of High-Temperature Primary Reactor-Grade Water on the Subcritical Crack Growth of Reactor Vessel Steel", in HSST Quarterly Progress Report for October-December 1976, ORNL/NUREG/TM-94, pp. 9-17 (April 1977).

52. W. H. Bamford, D. M. Moon and K. V. Scott, "Effect of High-Temperature Primary Reactor-Grade Water on the Subcritical Crack Growth of Reactor Vessel Steel", in HSST Quarterly Progress Report for January-March 1977, ORNL/NUREG/TM-120, pp. 15-30 (September 1977).

53. W. H. Bamford, D. M. Moon, L. J. Ceschini and K. V. Scott, "Effect of High-Temperature Primary Reactor-Grade Water on the Subcritical Crack Growth of Reactor Vessel Steel" in HSST Quarterly Progress Report for April-June 1977, ORNL/NUREG/TM-147, pp. 16-28 (December 1977).

54. W. H. Bamford and L. J. Ceschini, "Effect of High-Temperature Primary Reactor-Grade Water on the Subcritical Crack Growth of Reactor Vessel Steel" in HSST Quarterly Progress Report for July-September 1977, ORNL/NUREG/TM-166, pp. 38-45 (April 1978).

55. W. H. Bamford, D. M. Moon and L. J. Ceschini, "Effect of High-Temperature Primary Reactor-Grade Water on the Subcritical Crack Growth of Reactor Vessel Steel" in HSST Quarterly Progress Report for October-December 1977, ORNL/NUREG/TM-194, pp. 25-35 (May 1978).

56. W. H. Bamford and L. J. Ceschini, "Effect of High-Temperature Primary Reactor-Grade Water on the Subcritical Crack Growth of Reactor Vessel Steel", in HSST Quarterly Progress Report for January-March 1978, ORNL/NUREG/TM-209, pp. 6-11 (July 1978).

57. W. H. Bamford, D. M. Moon and L. J. Ceschini, "Effect of High-Temperature Primary Reactor-Grade Water on the Subcritical Crack Growth of Reactor Vessel Steel", in HSST Quarterly Progress Report for April-June 1978, ORNL/NUREG/TM-239, pp. 9-18 (Oct. 1978).

58. W. H. Bamford, D. M. Moon and L. J. Ceschini, "Effect of High-Temperature Primary Reactor-Grade Water on the Subcritical Crack Growth of Reactor Vessel Steel", in HSST Quarterly Progress Report for July-September 1978, ORNL/NUREG/TM-275, pp. 21-29 (Jan. 1979).

59. W. H. Bamford, D. M. Moon and L. J. Ceschini, "Effect of High-Temperature Primary Reactor-Grade Water on the Subcritical Crack Growth of Reactor Vessel Steel", in HSST Quarterly Progress Report for October-December 1978, ORNL/NUREG/TM-298, pp. 14-23 (Apr. 1979).

60. W. H. Bamford, D. M. Moon and L. J. Ceschini, "Effect of High-Temperature Primary Reactor-Grade Water on the Subcritical Crack Growth of Reactor Vessel Steel", in HSST Quarterly Progress Report for January-March 1979, ORNL/NUREG/TM-324, pp. 33-55 (Aug. 1979).

61. W. H. Bamford, D. M. Moon and L. J. Ceschini, "Effect of High-Temperature Primary Reactor-Grade Water on the Subcritical Crack Growth of Reactor Vessel Steel", in HSST Quarterly Progress Report for April-June 1979, ORNL/NUREG/TM-347, pp. 9-35 (October 1979).

62. W. H. Bamford, D. M. Moon and L. J. Ceschini, "Cyclic Crack Growth Rate Studies Conducted by Westinghouse Nuclear Energy Systems Under NRL Contract" in Structural Integrity of Water Reactor Pressure Boundary Components, ed. F. J. Loss. NUREG/CR 1268, NRL Memorandum Report 4174 (Jan. 1980).

63. W. H. Bamford, D. M. Moon and L. J. Ceschini, "Crack Growth Rate Testing in Reactor Pressure Vessel Steels", Proc. Fifth Water Reactor Safety Information Meeting, Gaithersburg, MD (Nov. 1977).

64. W. H. Bamford, "The Effect of Pressurized Water Reactor Environment on Fatigue Crack Propagation of Pressure Vessel Steels", in The Influence of Environment on Fatigue, Institution of Mechanical Engineers, London pp. 51-56 (1977).

65. W. H. Bamford, D. H. Shaffer and G. M. Jouris, "Statistical Methods for Interpreting Fatigue Crack Growth Data with Applications to Reactor Pressure Vessel Steels", in Proc. Third International Conference on Pressure Vessel Technology, Part II - Materials and Fabrication, American Society of Mechanical Engineers, New York, NY, 10017, pp. 815-823 (1977).

66. W. H. Bamford, "A Review of Fatigue Crack Growth Studies of Light Water Reactor Pressure Boundary Steels", in Time and Load Dependent Degradation of Pressure Boundary Materials, IWG-RRPC-79/2, IAEA, Innsbruck, pp. 5-15 (Nov. 1978).

67. W. H. Bamford and D. M. Moon, "Some Mechanistic Observations on the Crack Growth Characteristics of Pressure Vessel and Piping Steels in PWR Environment", Corrosion 79, Atlanta, GA, National Association of Corrosion Engineers (1979).

68. W. H. Bamford, "Application of Corrosion Fatigue Crack Growth Rate Data to Integrity Analyses of Nuclear Reactor Vessels", ASME Publication 79-PVP-116, American Society of Mechanical Engineers, New York, NY, 10017 (1979).

69. P. C. Paris, R. J. Bucci, E. T. Wessel, W. G. Clark and T. M. Mager, "Extensive Study of Low Fatigue Crack Growth Rates in A533 and A508 Steels" in Stress Analysis and Growth of Cracks, ASTM STP 513, American Society for Testing and Materials, Philadelphia, PA 19103, pp. 141-176 (1972).

70. P. H. Hutton, E. B. Schwenk and R. J. Kurtz, "Acoustic Emission - Flaw Relationship for In-Service Monitoring of Nuclear Pressure Vessels" in Reactor Safety Research Programs Quarterly Report, April 1 - June 30, NUREG/CR 0341, Pacific Northwest Laboratory PNL-2653-1 (1978).

71. G. C. Salivar and D. W. Hoeppner, "A Weibull Analysis of Fatigue-Crack Propagation Data", Engineering Fracture Mechanics, 12, pp. 181-184 (1979).

72. L. A. James, "Fatigue-Crack Propagation Behavior of Several Pressure Vessel Steels and Weldments", Welding Journal, 56, pp. 386-391 (Dec. 1977).

73. W. G. Clark, Jr., "Effect of Temperature and Section Size on Fatigue Crack Growth in Pressure Vessel Steel" Journal of Materials, 6, pp. 134-149 (1971).

74. A. Gerscha and E. Klausnitzer, "Crack Growth Investigation on 22NiMoCr37 at Room Temperature and 300°C", Paper No. 7, Heavy Section Steel Technology Program, 6th Annual Information Meeting, Oak Ridge National Laboratory, Oak Ridge, TN 37830 (Apr. 1972).

75. A. Gerscha and H. Munster, "Frequenzeinfluss auf das Risswachstumsverhalten des Stahles 22NiMoCr37", KWU/R 413/8/80, Kraftwerk Union, Erlangen (1980).

76. D. F. Mowbray, W. R. Andrews and A. J. Brothers, "Fatigue-Crack Growth-Rate Studies of Low-Alloy Pressure Vessel Steels", Trans. ASME ser. B, J. Engin. for Industry, 90, pp. 648-655 (Nov. 1968).

77. A. D. Wilson, "Fatigue Crack Propagation in A533B Steels", Trans. ASME, ser. J., J. Presure Vessel Technology, 99, pp. 459-469 (Aug. 1977).

78. G. Gabetta and V. Provenzano, "Fractographic and Microstructural Analysis of Fatigue Specimens of A302 Grade B Steel Tested in Air at Room Temperature", NUREG/CR 0968, NRL Memorandum Report 4062 (Sept. 1979).

79. J. Wiberg, "Investigation of Ageing of Pressure Vessel Steel during the Growth of a Fatigue Crack" in Time and Load Dependent Degradation of Pressure Boundary Materials, IWG-RRPC-79/2, IAEA, Innsbruck, pp. 119-128 (Nov. 1978).

80. K. Kussmaul, R. Schaefer, O. Blind, "The Effect of Fatigue Embrittlement on Crack Growth and Fracture Behavior" in Time and Load Dependent Degradation of Pressure Boundary Materials, IWG-RRPC-79/2, IAEA, Innsbruck, pp. 164-182 (Nov. 1978).

81. L. A. James, "Effects of Irradiation and Thermal Ageing Upon Fatigue-Crack Growth Behavior of Reactor Pressure Boundary Materials", in Time and Load Dependent Degradation of Pressure Boundary Materials, IWG-RRPC-79/2, IAEA, Innsbruck, pp. 129-149 (Nov. 1978).

82. L. A. James, "Fatigue-Crack Propagation in Neutron-Irradiated Ferritic Pressure-Vessel Steels", Nuclear Safety, 18, pp. 791-801 (1977).

83. J. F. Hall, "Fatigue Properties in Nonirradiated and Irradiated Low-Alloy Steels". Report WAPD-TM-1176, Bettis Atomic Power Laboratory (1975)

84. P. Shahinian, H. E. Watson and J. R. Hawthorne, "Fatigue Crack Growth Resistance of Several Neutron-Irradiated Pressure-Vessel Steels and Welds", Journal of Engineering Materials and Technology, 96, pp. 242-248 (1974).

85. L. A. James and J. A. Williams, "The Effect of Temperature and Neutron Irradiation Upon the Fatigue-Crack Propagation Behavior of ASTM A533B Steel", Journal of Nuclear Materials, 47, pp. 17-22 (1973).

86. H. E. Watson, L. E. Steele and P. Shahinian, "Effects of Irradiation and Temperature on the Fatigue Properties of A533B Sttel", Journal of Materials, 7, pp. 527-535 (1972).

87. L. A. James and J. A. Williams, "Fatigue-Crack Propagation in Unirradiated and Irradiated ASTM A533B Steel at Low Cyclic Frequence", Journal of Nuclear Materials, 49, pp. 241-243 (1973).

88. S. J. Hudak Jr., and R. P. Wei, "Consideration of Nonsteady State Crack Growth in Materials Evaluation and Design", 5th Int. Conf. on Structural Mechanics in Reactor Technology, (1979).

89. V. Provenzano, K. Torronen, D. Sturm and W. H. Cullen, Jr., "Fractographic and Microstructural Analysis of Stress Corrosion Cracking of A533 Grade B Class 1 Plate and A508 Class 2 Forging in Pressurized Reactor-Grade Water at 93°C", NUREG/CR 1127, NRL Memorandum Report 4121, (Jan. 1980); also in Fractography and Materials Science a forthcoming STP, American Society for Testing and Materials, Phildelphia, PA 19103.

90. B. F. Brown, C. T. Fujii, and E. P. Dahberg, "Methods for Studying the Solution Chemistry Within Stress Corrosion Cracks", J. Electrochem. Soc., 116, pp. 218-219 (1969).

91. B. F. Brown, "Concept of the Occluded Corrosion Cell", Corrosion 26, pp. 249-250 (1970).

92. J. A. Smith, M. H. Peterson and B. F. Brown, "Electrochemical Conditions at the Tip of an Advancing Stress Corrosion Crack in AISI 4340 Steel," Corrosion, 26, pp. 539-542 (1970).

93. J. M. Barsom, "Mechanisms of Corrosion Fatigue Below K_{ISCC}," Inst. J. Fracture Mech., 7, pp. 163-182 (1971).

94. J. P. Gallagher, "Corrosion Fatigue Crack Growth Rate Behavior Above and Below K_{ISCC} in Steels," Journal of Materials, 6, pp. 941-964 (1971). (Also Naval Research Laboratory Report No. 7064, Washingon, DC, May 28, 1970).

95. J. M. Barsom, "Effect of Cyclic Stess Form on Corrosion Fatigue Crack Propagation Below K_{ISCC} in a High Yield Strength Steel," in Corrosion Fatigue: Chemistry Mechanics and Microstructure, NACE-2, eds. O. Devereux et al, National Association of Corrosion Engineers, Houston, TX 77027, pp. 424-436 (1973).

96. O. Vosikovsky, "Fatigue-Crack Growth in an X-65 Line-Pipe Steel at Low Cyclic Frequencies in Aqueous Environments,"Trans. ASME, Ser. H., J. Eng. Mat. and Technology, 97, pp. 298-304 (1975).

97. J. P. Hirth and H. H. Johnson, "Hydrogen Problems in Energy Related Technology, "Corrosion, 32, pp. 3-15 (1976).

98. E. N. Pugh, "A Post Conference Evaluation of Our Understanding of the Failure Mechanics," in Stress Corrosion Cracking and Hydrogen Embrittlement of Iron Base Alloys, NACE-5, eds. R. W. Staehle et al, National Association of Corrosion Engineers, Houston, TX 77027, pp. 36-51 (1977).

99. A. W. Thompson, "Microstructural Factors in Hydrogen Embrittlement and Stress Corrosion Cracking," in Environmental Degradation of Engineering Materials, eds. M. R. Louthan and R. P. McNitt, Virginia Tech., Blacksburg, VA, p. 13-17 (1977).

100. M. Cornet and S. Talbot-Besnard, "Present Ideas About Mechanisms of Hydrogen Embrittlement of Iron and Ferrous alloys," Met. Sci., 12, pp. 335-339 (1978)

101. H. K. Birnbaum, "Hydrogen Related Failure Mechanisms in Metals", in Environment-Sensitive Fracture of Engineering Materials, ed. Z. A. Faroulis, The Mechanical Society of AIME, New York, NY, 10017, pp. 326-360 (1979).

102. M. R. Louthan, G. R. Caskey, J. A. Donavan and D. E. Rawl, "Hydrogen Embrittlement of Metals," Material Science Engineering, 10, pp. 357-368 (1972).

103. J. D. Frandsen and H. L. Marcus, "The Correlation Between Grain Size and Plastic Zone Size for Environmental Hydrogen Assisted Fatigue Crack Propagation," Scripta Met., 9, pp. 1089-1094 (1975).

104. D. L. Davidson and J. Lankford, "The Influence of Water Vapour on Fatigue Crack Plasticity in Low Carbon Steel" in Fracture 1977, ed. D. M. R. Taplin, ICF4, Waterloo, pp. 897-904 (1977).

105. W. L. Morris, J. D. Frandsen and H. L. Marcus, "Environmentally Induced Transitions in Fatigue Fracture Mode," in Fractography-Microscopic Cracking Processes, ASTM STP 600, eds. C. D. Beachem and W. R. Warke, American Society for Testing and Materials, Philadelphia, PA 19103, pp. 49-61 (1976).

106. A. J. McEvily, "Current Aspects of Fatigue", Metal Sci., 11, pp. 274-284 (1977).

107. C. D. Beachem, "A New Model for Hydrogen Assisted Cracking," Met. Trans., 3, pp. 437-451 (1972).

108. C. D. Beachem, "Electron Fractographic Support for a New Model for Hydrogen-Assisted Cracking," in Stress Corrosion Cracking and Hydrogen Embrittlement of Iron Base Alloys, NACE-5, eds. R. W. Staehle et al, National Association of Corrosion Engineers, Houston, TX 77027, pp. 376-389 (1977).

109. J. J. Gilman, "Stress-Corrosion Cracking in Plastic Solids Including the Role of Hydrogen, " Phil. Mag., 26, pp. 801-812 (1972).

110. J. J. Gilman, "The Role of Surface Hydrides in Stress-Corrosion Cracking," in Stress Corrosion Cracking and Hydrogen Embrittlement of Iron Base Alloys, NACE-5, eds. R. W. Staehle et al, National Association of Corrosion Engineers, Houston, TX 77027, pp. 326-331 (1977).

111. J. R. Rice and R. Thomson, "Ductile versus Brittle Behavior of Crystals," Phil. Mag., 29, pp. 73-97 (1974).

112. R. Thomson, "Brittle Fracture in a Ductile Material with Application to Hydrogen Embrittlement," J. Mater. Sci., 13, pp. 128-142 (1978).

113. R. A. Oriani, "A Mechanistic Theory of Hydrogen Embrittlement of Steels," Berich'e der Bunsen-Gesellschaft, 76, pp. 868-857 (1972).

114. R. A. Oriani, "A Decohesion Theory for Hydrogen-Induced Crack Propagation," in Stress Corrosion Cracking and Hydrogen Embrittlement of Iron Base Alloys, NACE-5 eds. R. W. Staehle et al, National Association of Corrosion Engineers, Houston, TX 77027 (1977).

115. R. A. Oriani and P. H. Josephic, "Equilibrium Aspects of Hydrogen-Induced Cracking of Steels, "Acta Met.,22, pp. 1065-1074 (1974).

116. R. A. Oriani and P. H. Josephic, "Equilibrium and Kinetics Studies of the Hydrogen-Assisted Cracking of Steel," Acta Met., 25, pp. 979-988 (1977).

117. R. N. Parkins, F. Mazza, J. J. Raynela and J. C. Scully, "Stress Corrosion Tests Methods. Report prepared for the European Federation of corrosion Working Party on Stress Corrosion Test Methods," Br. Corros. J., 7, pp. 154-167 (1972).

118. J. Kruger,"New Approaches to the Study of Localized Corrosion," in Passivity and Its Breakdown on Iron and Iron Base Alloys, eds. R. W. Staehle and H. Okada, National Association of Corrosion Engineers, Houston, TX 77027, pp. 35-41 (1976).

119. J. C. Scully, "Mechanism of Dissolution-Controlled Cracking," Metal Sci., 12, pp. 290-300 (1978).

120. M. R. Louthan, R. G. Derrick, J. A. Donovan and G. R. Caskey, "Hydrogen Transport in Iron and Steels", in Effect of Hydrogen on Behavior of Materials, eds. A. W. Thompson and I. M. Bernstein, Metallurgical Society of AIME, New York, NY 10017, pp. 337-347 (1976).

121. W. E. Ruther and R. K. Hart, "Influence of Oxygen on High Temperature Aqueous Corrosion of Iron," Corrosion, 19, pp. 127t-133t (1963).

122. P. J. E. Forsyth, "A Two Stage Process of Fatigue Crack Growth", in Proc. of the Crack Propagation Symp., Vol. 1, the College of Aeronautics, Cranfield, pp. 76-94 (1961).